Goldstone bosons in the universe: composite dark matter and the QCD axion in neutron stars

Reuven Balkin

Dissertation

Physik–Department T75
Technische Universität München

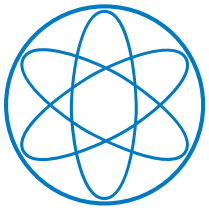

Technische Universität München

Goldstone bosons in the universe: composite dark matter and the QCD axion in neutron stars

Reuven Balkin

Vollständiger Abdruck der von der Fakultät für Physik der Technischen Universität München zur Erlangung des akademischen Grades eines

Doktors der Naturwissenschaften

genehmigten Dissertation.

Vorsitzender:		Prof. Dr. Elisa Resconi
Prüfer der Dissertation:	1.	Prof. Dr. Andreas Weiler
	2.	Prof. Dr. Björn Garbrecht

Diese Dissertation wurde am 15.06.2020 bei der Technischen Universität München eingereicht und durch die Fakultät für Physik am 14.07.2020 angenommen.

Goldstone bosons in the universe: composite dark matter and the QCD axion in neutron stars

Goldstone-Bosonen im Universum: zusammengesetzte dunkle Materie und das QCD-Axion in Neutronensternen

Reuven Balkin

Abstract

The hierarchy problem of the standard model can be naturally explained if the Higgs is a composite particle described as a Goldstone boson. In the first part of this thesis we explore the rich collider and dark matter phenomenology of composite Higgs models with extended composite sectors. The second part is dedicated to another Goldstone boson, the QCD axion, which solves the strong CP problem. We explore the effects of dense baryonic background on the QCD axion properties in nuclear densities, as well as in the color superconducting phase.

Zusammenfassung

Das Hierarchieproblem des Standardmodells lässt sich auf natürliche Art lösen, wenn das Higgs ein zusammengesetztes Teilchen ist, das als Goldstone-Boson beschrieben wird. Im ersten Teil dieser Arbeit untersuchen wir die vielfältige Collider- und dunkle Materie Phänomenologie von nicht-minimalen Composite-Higgs Modellen. Der zweite Teil ist einem weiteren Goldstone-Boson gewidmet, dem QCD-Axion, das das Strong CP Problem löst. Wir untersuchen die Auswirkungen einer Baryondichte auf die Eigenschaften des QCD-Axions sowohl bei nuklearer Dichte als auch in der farbsupraleitenden Phase.

Contents

Part I

Introduction

One of the crowning achievements of science, and perhaps even humanity, was the discovery of the Higgs particle in the Large Hadron Collider [1, 2]. The Higgs boson was the last piece needed in the mechanism which explains the origin of the short-range weak force and the long-range electromagnetic force, the mechanism of spontaneous symmetry breaking. Even prior to the Higgs discovery, a similar mechanism was used to explain the spectrum of the light mesons, e.g. pions, which we understand to be pseudo Nambu-Goldstone bosons of a broken global chiral symmetry. Importantly, the Higgs mechanism was conceived out of necessity, namely to address the unitarity violation in the perturbative scattering of massive gauge bosons [3, 4]. To the low energy observer, who knows nothing about the Higgs boson, the scattering cross section of longitudinal massive gauge bosons appears to increase uncontrollably with energy, until perturbative unitarity is violated is the theory becomes strongly coupled. The appearance of the Higgs at high energies prevents the violation of perturbative unitarity and effectively UV-completes the standard model as a weakly coupled gauge theory. With its last piece in place, the *standard model of particle physics* constitutes a consistent model which is able to accurately describe physics up to the highest terrestrially accessible scales. There is currently no similar obstruction limiting the validity of the standard model up to the Plank scale, where gravity must be included.

However, we have several reasons to assume that the standard model is not a complete description of Nature, namely that new physics must emerge at scales lower than the Plank scale. Some of these reasons are based on hard experimental evidence. A prime example of such a smoking gun is the observation of what appears to be large quantities of non-luminous matter in the universe. This additional matter, dubbed *dark matter*, cannot be conventionally explained using the particle content of the standard model (see Sec. 1.6 for an extended discussion). Other evidence for physics beyond the standard model are more circumstantial in nature. They are a result of a mismatch between the *measured* value of a standard model parameter and our *expectation* for its value. The expectation is not arbitrary but rather based on observations of similar phenomena in Nature. In this category we include the *Hierarchy problem* (see Sec. 1.1) and the *Strong CP problem* (see Sec. 4.1). All of the above-mentioned issues can be resolved by standard model extensions which are based on the spontaneous symmetry breaking mechanism. These extensions and the phenomenology of the corresponding Goldstone bosons are the main theme of this thesis.

In Part II we investigate the phenomenology of composite dark matter in non-minimal composite Higgs models. We start by presenting the motivation and framework for these models in Chapter 1. As mentioned above, we start by introducing in detail the Hierarchy problem in Sec. 1.1. In the composite Higgs framework, presented in Sec. 1.2, the Higgs is described as a pseudo Nambu Goldstone boson of a spontaneously broken symmetry $\mathcal{G} \to \mathcal{H}$. The lightness of the Higgs is than understood to be a consequence of an approximate shift symmetry. The compositeness scale f, above which the Higgs is no longer a relevant degree of freedom, is the natural cutoff scale of the theory. The phenomenon of dimensional transmutation can further explain the large scale separation between f and a much higher cutoff scale Λ. The formalism which describes the low energy theory that results from a symmetry breaking pattern $\mathcal{G} \to \mathcal{H}$ was developed by Callan, Coleman, Wess and Zumino (CCWZ) [5, 6] and is presented in Sec. 1.3. In this work we consider two non-minimal models based on the Little Higgs construction (Sec. 1.4) and on the minimal composite Higgs (Sec. 1.5). We conclude in Sec. 1.6 by presenting the dark matter problem and discussing the generic features of the composite dark matter.

The first model under consideration is the Little Higgs with T-Parity, whose phenomenology is the focus of Chapter 2. The original Little Higgs model does not contain the electroweak custodial group, and therefore in the original model unacceptably large contribution to electroweak precision observables are generated at tree level, forcing the compositeness scale to be above 10 TeV. Such a high compositeness scale effectively reintroduces the fine tuning of the Higgs mass. The original model was extended by an additional discrete symmetry dubbed T-Parity, which prohibits tree level contributions to the electroweak precision observables. We review the Little Higgs with T-Parity in Sec. 2.1, and in particular we discuss the difficulties in constructing such a theory without introducing a massless T-odd doublet. This difficulty is addressed by a minimal extension of the Little Higgs with T-Parity model, which we review for the remainder of this section. The detailed full Lagrangian is presented in App. 2.A. Importantly, this extension contains an additional singlet Goldstone boson, denoted by s. If s is the lightest T-odd particle, it is stable and therefore a viable dark matter candidate. In Sec. 2.2 we present the radiatively generated scalar potential, which is in general not calculable in this model. We provide supplemental information regarding the scalar potential in App. 2.B. The LHC phenomenology of the fermionic top partners, which are a generic prediction in composite Higgs models, is presented in Sec. 2.3. Next we review the model constraints due to electroweak precision observables in Sec. 2.4. Lastly we investigate the dark matter phenomenology of the composite dark matter in Sec. 2.5.

The second model, which we investigate in Chapter 3, is the $SO(7)/SO(6)$ extension of the minimal composite Higgs. The composite sector contains, in addition to the Higgs, a complex scalar, denoted by χ, which is charged under a $U(1)_{\rm DM}$ subgroup of $SO(6)$. This symmetry can be used to stabilize the complex scalar, thus making it a viable dark matter candidate. We start this chapter by reviewing the effective Lagrangian of the Higgs and χ in Sec. 3.1 and the composite dark matter phenomenology, which crucially depends on the manner in which the dark matter shift symmetry is broken. The shift symmetry in the minimal composite Higgs framework is broken by the linear couplings between the *elementary sector* (standard model fields) and the *composite sector*, under the partial compositeness hypothesis. After reviewing the $SO(7)/SO(6)$ model in Sec. 3 (for supplementary material see Apps. (3.A) - (3.C)), we investigate the dark matter phenomenology of several qualitatively different scenarios, where the shift symmetry breaking of dark matter originates from the top quark couplings in Sec. 3.3, the bottom quark couplings in Sec. 3.4 and lastly the gauging of $U(1)_{\rm DM}$ in Sec. 3.5. The latter scenario is of special interest due to addition of a dark photon, which leads to a rich dark matter phenomenology. The collider phenomenology of the heavy resonances, which is similar in all three scenarios, is presented in Sec. 3.3.4.

The focus of Part III of this thesis is another well motivated Goldstone boson : the QCD axion. The motivation behind the axion is the strong CP problem , namely the observation that the CP violating phase in the strong sector is extremely small $\theta < 10^{-10}$, in stark contradiction to the expected $O(1)$ value, like the one observed in the CP violating phase in the weak interaction. We present the origin on the strong CP problem and its relation to chiral anomalies in Sec. 4.1. The QCD axion is a consequence the Peccei-Quinn mechanism [7]: it is the Goldstone boson of an anomalous $U(1)$ symmetry, which allows the axion the dynamically relax the θ angle to 0. We present the Peccei-Quinn mechanism in Sec. 4.2, as well as the most notable realizations. First we discuss the so called *visible* axion due to Weinberg and Wilczek [8, 9]. Next, we discuss the so called *invisible* axion, which was developed after the exclusion of the Weinberg and Wilczek axion due to various experiments. In particular we

present the axion models formulated by Dine, Fischler, Srednicki and Zhitnitsky (DFSZ) [10, 11] and Kim, Shifman, Vainshtein and Zakharov (KSVZ) [12, 13]. The last part of the general introduction to the QCD axion is given in Sec. 4.3, where we discuss the axion potential in vacuum.

While the properties of the axion in finite temperature have been carefully studied [14], its properties in medium remained unexplored. Our goal in the remainder of Part III of this thesis is to investigate the $T = 0$ properties of the QCD axion in a dense background of baryons, such as the one found in neutron stars. Finite density is introduced in quantum field theory by introducing its canonical conjugate variable - the chemical potential. We review the relevant formalism in Sec. 4.4. In preparation to the next topic, we present the phenomenon of density-induced meson condensation in Sec. 4.5 and discussing its effect on the axion properties using a simple toy model.

As oppose to finite temperature effects which can be simulated on the lattice, realistic QCD at finite density cannot be simulated on the lattice due to the so called *sign problem*. Thus, we must rely on the available theoretical descriptions. For baryon densities $n \lesssim 2n_0$, with $n_0 = 0.16$ fm^{-3} being the nuclear saturation density, matter is described by nucleons and other baryons which experience the long-range electric force and the short-range nuclear force, the latter being mediated by the pions. This theory is described using chiral perturbation theory. We explore the axion properties within this framework in Part 5. In particular we single out the effects on the axion potential due to the density dependence of the quark condensates in Sec. 5.1, and due to the possible appearance of a kaon condensate at higher densities, which we discuss in Sec. 5.2. Supplemental material regarding the kaon condensed phase is given in Apps 5.A and 5.B. We conclude Part 5 by discussing the matter coupling of axion to nucleons inside dense matter in Sec. 5.3. These are of special importance due to the oft-quoted SN1987A cooling bounds [15], which are based on the cooling process of dense nuclear matter via axion emission.

At higher densities $n \gtrsim 2n_0$, nuclear matter becomes strongly coupled and the perturbative description begins to break down. Another perturbative regime reemerges only at ultra-high densities $n \gtrsim (10 - 100)n_0$, where it is postulated that matter is in a color superconducting phase, also known as the color-flavor locking (CFL) phase. Although this regime is somewhat denser than the expected density in the core of a neutron star $n \sim (3 - 6)n_0$, it is plausible that the description of matter in terms of the CFL phase is still *qualitatively* valid. We consider the properties of the axion in the CFL phase in Part 6. After reviewing the major ingredients of the theory, namely the kinetic terms (Sec. 6.1), the mass terms (Sec. 6.2) and the instanton induced terms (Sec. 6.3), we present the axion potential in the CFL phase in Sec. 6.4. Interestingly, we find the in both phases - nuclear and CFL - the axion may be destabilized around the origin, which could lead to a sourcing of axions inside large dense object i.e. neutron stars. We briefly discuss some of the potential observable effects of such sourcing in Part 7, before presenting our final conclusions in Part IV, pertaining to both Parts II and III of the thesis.

The thesis is largely based on the following publications

[16] Reuven Balkin, Gilad Perez, and Andreas Weiler. "Little composite dark matter". In: *Eur. Phys. J. C* 78.2 (2018), p. 104. DOI: 10.1140/epjc/s10052-018-5552-3. arXiv: 1707.09980 [hep-ph] ,

[17] Reuven Balkin, Maximilian Ruhdorfer, Ennio Salvioni, and Andreas Weiler. "Charged Composite Scalar Dark Matter". In: *JHEP* 11 (2017), p. 094. DOI: 10.1007/JHEP11(2017)094. arXiv: 1707.07685 [hep-ph] ,

[18] Reuven Balkin, Maximilian Ruhdorfer, Ennio Salvioni, and Andreas Weiler. "Dark matter shifts away from direct detection". In: *JCAP* 11 (2018), p. 050. DOI: 10.1088/1475-7516/2018/11/050. arXiv: 1809.09106 [hep-ph] ,

[19] Reuven Balkin, Javi Serra, Konstantin Springmann, and Andreas Weiler. "The QCD axion at finite density". In: *JHEP* 07 (2020), p. 221. DOI: 10.1007/JHEP07(2020)221. arXiv: 2003.04903 [hep-ph] .

In particular, some figures contained in this thesis have previously appeared in one of these articles.

Part II

Composite dark matter in composite Higgs models

1

Motivation and framework

1.1 The hierarchy problem

The Standard model (SM) is a renormalizable quantum field theory (QFT) written in terms of relevant and marginal operators. The SM has been incredibly successful in describing physics at small scales. The validity of the renormalizable theory is further reinforced by the experimental evidence, which demonstrate how well various charges, associated with global symmetries such as baryon and lepton numbers, are conserved [20].

However, the SM must be an effective field theory: we know that at some cutoff scale $\Lambda_{\rm NP}$, new physics beyond the SM (BSM) must emerge. For example, gravity becomes strongly coupled around the plank scale $M_{\rm PL} \sim 10^{19}$ GeV. This presents one clear upper bound on the cutoff scale. Moreover, there are already hints that a lower cutoff scale is required e.g. in order to unify the gauge couplings at $M_{\rm GUT} \sim 10^{16}$ GeV. The latter scale also appears to explain the origin of neutrino masses.

The usual argument used to demonstrate the Hierarchy problem involves the calculations of the quantum corrections to the Higgs mass, for example from the top quark loop

$$\frac{\delta m_h^2}{m_h^2} = \frac{3y_t^2}{8\pi^2}\left(\frac{\Lambda_{\rm NP}^2}{m_h^2}\right) \sim \left(\frac{\Lambda_{\rm NP}}{450\ \text{GeV}}\right)^2 , \tag{1.1}$$

where $y_t \sim 1$ is the top Yukawa and the calculation is regulated using a hard cut-off at the new physics (NP) scale $\Lambda_{\rm NP}$. For $\Lambda_{\rm NP} \gg 450$ GeV, the measured mass of $m_H^2 = 125$ GeV implies an *unnatural* large cancelation between the contribution of Eq. (1.1) and a counter term. This statement, while correct, obscures the physical argument which make the Hierarchy problem, well, a problem. This large cancellation between counter term and quantum correction might seem harmless to the naive IR observer, but the Hierarchy problem is in essence a UV problem. From a UV perspective, the above statement is reformulated in terms of the renormalization group equation (RGE) flow of the Higgs mass $m_H^2(\mu)$, given schematically by

$$m_h^2(\mu_{\rm IR}) \approx m_h^2(\Lambda_{\rm NP}) - \frac{3y_t^2}{8\pi^2}\Lambda_{\rm NP}^2 , \tag{1.2}$$

where the natural expectation is $m_h^2(\Lambda_{\rm NP}) \sim O(\Lambda_{\rm NP}^2)$. Hence we see that a UV theory at a scale much larger than m_h^2 can only account for the measured Higgs mass if two independent contributions are tuned.

If this tuning occurs in Nature, it has a very practical implications for the future of particle physics, namely our ability to resolve our parameters in terms of more fundamental constants. A known successful example is the fermi constant G_F which effectively describes the weak interaction strength between fermions at low energies. We know now that $G_F \sim g^2/M_W^2$, i.e. a combination of the more fundamental parameters g and M_W, the weak interaction coupling and the W-boson mass, respectively. If the measured m_h^2 is a result of a fine-tuned cancelation of fundamental parameters, the required experimental accuracy needed to resolve them might be beyond reach in the foreseeable future.

There are several possible solutions to the hierarchy problem. The first type of solutions is phrased in terms of anthropical reasoning [21, 22, 23], with similar arguments used to explain the smallness the cosmological constant [24]. A second type involves a dynamical relaxation mechanism which explains the large mass hierarchy [25]. The third type utilizes additional symmetries which protect the Higgs mass from large corrections, most notably supersymmetry [26] and composite Higgs models [27, 28]. We postpone the discussion about the latter as a solution to the Hierarchy problem to Sec. 1.2.

1.2 The composite Higgs

In this section we present the conceptual building blocks of composite Higgs models (for a detailed discussion see Ref. [29]) and present the mechanism which allows it to solve the Hierarchy problem. Let us assume that our UV theory is approximately conformal (hence scaleless and devoid of a Hierarchy problem) at some high scale e.g. $M_{\rm GUT}$. The theory has a large global symmetry $\mathcal{G}$ and gauged symmetries. As we flow to the IR, at some low scale the theory becomes strongly coupled, breaking the global symmetry $\mathcal{G} \to \mathcal{H}$. This dynamical generation of scale is known as dimensional transmutation, which was already presented to us by Nature. The $\Lambda_{\rm QCD}$ scale, where QCD becomes strong, is largely separated from the scale of weakly interacting $N_f = 3$ QCD at $\mu = m_Z$,

$$\log\left(\frac{m_Z}{\Lambda_{\rm QCD}}\right) = \frac{1}{18}\left(\frac{4\pi}{g_S(\mu = m_Z)}\right)^2 . \tag{1.3}$$

In direct analogy,

$$\log\left(\frac{m_*}{M_{\rm GUT}}\right) \sim \left(\frac{4\pi}{g(\mu = M_{\rm GUT})}\right)^2 . \tag{1.4}$$

where g denotes some gauge coupling of the new sector and m_* denotes the compositeness scale. Below m_*, similar to QCD, the theory contains resonances as well as the Goldstone-Nambu bosons (NGBs) that result from the global symmetry breaking $\mathcal{G} \to \mathcal{H}$. The Higgs doublet is assumed to be an NGB in the coset $\mathcal{G}/\mathcal{H}$, with some associated scale f. This implies that $\mathrm{Dim}(\mathcal{G}/\mathcal{H}) \geq 4$, and that the electroweak group $SU(2)_L \times U(1)_Y$ must be a subgroup of $\mathcal{H}$, with the Higgs transforming as a doublet.

In the limit where $\mathcal{G}$ is exact, the Higgs potential is protected by a shift symmetry and electroweak symmetry breaking (EWSB) is not possible. Therefore, some explicit breaking of $\mathcal{G}$ is required in order to generate a scalar potential, making the Higgs a pseudo Nambu-Goldstone boson (pNGB). The explicit breaking is introduced by tree level interactions with matter and gauge fields, which lead to a radiatively generated scalar potential à-la Coleman-Weinberg [30]. EWSB

can be interpreted geometrically as a misalignment between two directions in field space, one direction associated with the global symmetry breaking and the scale f, and another direction associated with EWSB and the measured vacuum expectation value (VEV) of the Higgs field $v = 246$ GeV. One usually defines the misalignment angle as

$$\xi^2 \sim \sin^2\left(\frac{\langle h\rangle}{f}\right) \equiv \frac{v^2}{f^2}\,. \tag{1.5}$$

A generic breaking of $\mathcal{G}$ naturally leads to a large misalignment angle $\xi \sim 1$. Such a scenario is equivalent to the disfavored minimal technicolor model (see e.g. Ref. [31]). Thus, some mechanism that can allow for $\xi \ll 1$ is required. As discussed below in Sec. 1.4, in little Higgs models it is achieved by a symmetry protection for the Higgs mass. For models based on the minimal composite Higgs of Sec. 1.5, some contributions to the Higgs potential must be fine-tuned to some extent in order to achieve $\xi \ll 1$.

1.3 CCWZ

The Callan, Coleman, Wess and Zumino (CCWZ) formalism [5, 6] provides the building blocks required in order to systematically write an effective field theory of NGB's and resonances below the confinement scale of a theory with a $\mathcal{G} \to \mathcal{H}$ symmetry breaking pattern. It has the advantage of allowing us to remain agnostic regarding the unknown physics above the confinement scale. The central object which parameterizes the vacuum fluctuations is

$$\xi(x) \equiv \exp\left[\frac{i\pi^{\hat{a}}(x)X^{\hat{a}}}{f}\right]\,. \tag{1.6}$$

with $\pi^{\hat{a}}$ the NGB's associated with the broken (global) symmetries and $X^{\hat{a}}$ the corresponding broken generators. The index $\hat{a}$ numerates the broken generators. Under a generic global transformation $g \in \mathcal{G}$

$$g \in \mathcal{G}\ :\ \xi(x) \to g\left[\frac{i\pi^{\hat{a}}(x)X^{\hat{a}}}{f}\right] h^{-1}(g,\pi^{\hat{a}}(x))\,, \tag{1.7}$$

where the non-linear transformation $h \in \mathcal{H}$ is an element of the unbroken subgroup which depends on g and $\pi(x)$. Due to the $\pi^{\hat{a}}(x)$ dependence, it is effectively a local transformation. The d and e symbols are decomposed from the Maurer-Cartan form

$$i\xi^\dagger(x)\partial_\mu\xi(x) \equiv d_\mu^{\hat{a}}X^{\hat{a}} + e_\mu^a T^a\,, \tag{1.8}$$

where T^a are the unbroken generators numerated by the index a. One can than show that under a global transformation

$$\begin{aligned} g \in \mathcal{G}\ &: d_\mu \to h(g,\pi^{\hat{a}}(x))\, d_\mu\, h^{-1}(g,\pi^{\hat{a}}(x))\,, \\ &\quad e_\mu \to h(g,\pi^{\hat{a}}(x))\,(e_\mu + i\partial_\mu)\, h^{-1}(g,\pi^{\hat{a}}(x))\,. \end{aligned} \tag{1.9}$$

The d symbol transforms *regularly* under h (still non-linearly) compared to the e_μ symbol, which transforms as a covariant derivative. The latter is used to construct $\mathcal{G}$-invariant kinetic terms for fields transforming non-linearly under $\mathcal{G}$ in some representation of $\mathcal{H}$. The d and e symbols carry one derivative such that $[d] = [e] = 1$, and a perturbative expansion in ∂/E is performed by writing higher order terms in d and e. For example, the leading order term in d is given by

$$\mathcal{L} \supset c\, f^2\, d_\mu^{\hat{a}} d^{\hat{a}\mu}\,. \tag{1.10}$$

This term contains the usual kinetic terms for the NGB's (c is chosen such that they are canonically normalized) as well the self-interactions. This formalism can be easily generalized to include a gauging of some subgroup of $\mathcal{G}$ by promoting the derivative of Eq. (1.8) to a covariant derivative

$$i\xi^\dagger(x)D_\mu\xi(x) \equiv d_\mu^{\hat{a}}X^{\hat{a}} + e_\mu^a T^a \,, \tag{1.11}$$

with $D_\mu = \partial_\mu - igA_\mu^{\hat{a}}X^{\hat{a}} - igA_\mu^a T^a$.

There are two interesting private cases worth noting regarding the transformation of the NGB's. In the first case, under a global transformation of the unbroken subgroup $\bar{h} \in \mathcal{H}$, the NGB's transform *linearly*

$$\bar{h} \in \mathcal{H} \;:\; \pi^{\hat{a}}(x)X^{\hat{a}} \;\to\; \bar{h}(\pi^{\hat{a}}(x)X^{\hat{a}})\bar{h}^{-1} \,, \tag{1.12}$$

namely $h(\bar{h}, \pi^{\hat{a}}(x)) = \bar{h}$ is a regular linear transformation. It is therefore often useful to decompose $\pi^{\hat{a}}$ to irreducible $\mathcal{H}$ representation[1]. In the second case, under a transformation $\bar{g} = \exp\left[\frac{i\alpha^{\hat{a}}X^{\hat{a}}}{f}\right]$ in $\mathcal{G}/\mathcal{H}$ associated with the broken generators, the NGB's *shift*

$$\bar{g} \in \mathcal{G}/\mathcal{H} \;:\pi^{\hat{a}}(x) \;\to\; \pi^{\hat{a}}(x) + \alpha^{\hat{a}} \,. \tag{1.13}$$

It is this shift symmetry that protects the NGB from non-derivative interactions.

Lastly let us address the inclusion of external fields, sometimes referred to as an elementary sector. These fields transform linearly under $\mathcal{G}$

$$g \in \mathcal{G}: \quad \psi_{\text{elem}} \to g\,\psi_{\text{elem}} \tag{1.14}$$

and can be dressed by $\xi^\dagger$ and projected into all the $\mathcal{H}$ representation contained within a specific $\mathcal{G}$ representation,

$$g \in \mathcal{G}: \quad \psi_{\text{comp}} \equiv \xi^{-1}\psi_{\text{elem}} \to h(g, \pi^{\hat{a}}(x))\,\xi^{-1}\psi_{\text{elem}} = h(g, \pi^{\hat{a}}(x))\psi_{\text{comp}} \,. \tag{1.15}$$

For example, for $SO(N)/SO(N-1)$, a fundamental representation of $SO(N)$ can be dressed with $\xi^\dagger$ and projected to a singlet and fundamental representation of $SO(N-1)$, since $\mathbf{N} = \mathbf{1}\oplus(\mathbf{N}-\mathbf{1})$. Equivalently, non-linearly transforming representations of $\mathcal{H}$ can be dressed by ξ and projected into all the $\mathcal{G}$ representations that contain them.

1.4 Littlest Higgs

One realization of the composite Higgs is the so-called Little Higgs, with its minimal realization denoted as the Littlest Higgs (LH) [32, 33, 34, 35, 36, 37, 38]. As shown below, the explicit breaking of the Higgs shift symmetry is realized in a non-trivial manner dubbed *Collective Breaking*. It relies on the shift symmetry of H being restored in the limit where either $g_1 \to 0$ or $g_2 \to 0$, with g_1, g_2 gauge or Yukawa couplings which partially break the Higgs shift symmetry. As a result, the Higgs potential $V(H) \propto g_1 \cdot g_2$. This restriction limits the divergence level of some operators that are generated radiatively. In particular, the Higgs mass is not quadratically sensitive to the cutoff scale at 1 loop, but only logarithmically.

[1] In practice it is more useful to decompose $\pi^{\hat{a}}$ to irreducible representations of the gauged subgroup of $\mathcal{H}$

The model is based on an $SU(5)/SO(5)$ coset. Σ is a linearly transforming field, in the **15** (symmetric) representation of $SU(5)$:

$$\Sigma \to U\Sigma U^T\,. \tag{1.16}$$

This field acquires a VEV which spontaneously breaks $SU(5) \to SO(5)$:

$$\langle\Sigma\rangle \equiv \Sigma_0 = \begin{pmatrix} & & \mathbb{1}_2 \\ & 1 & \\ \mathbb{1}_2 & & \end{pmatrix}\,. \tag{1.17}$$

The 10 unbroken SO(5) generators satisfy:

$$T^a\Sigma_0 + \Sigma_0(T^a)^T = 0\,, \tag{1.18}$$

While the 14 broken SU(5) generators satisfy:

$$X^{\hat{a}}\Sigma_0 - \Sigma_0(X^{\hat{a}})^T = 0\,. \tag{1.19}$$

We can reparameterize the Σ field using the non-linear realization of the NGB's, defining $\Pi_\Sigma = \pi^{\hat{a}}X^{\hat{a}}$:

$$\Sigma = e^{i\Pi_\Sigma/f}\Sigma_0 e^{i\Pi_\Sigma^T/f} = e^{2i\Pi_\Sigma/f}\Sigma_0\,. \tag{1.20}$$

The 14 Goldstone boson decompose under the EW group as $\mathbf{1}_0 \oplus \mathbf{3}_0 \oplus \mathbf{2}_{1/2} \oplus \mathbf{3}_1$ and can be written as

$$\Pi_\Sigma = \begin{pmatrix} \frac{\tau\cdot\sigma}{2} + \frac{\phi_0}{2\sqrt{5}}\mathbb{1}_2 & \frac{H}{\sqrt{2}} & \Phi \\ \frac{H^\dagger}{\sqrt{2}} & -\frac{2\phi_0}{\sqrt{5}} & \frac{H^T}{\sqrt{2}} \\ \Phi^\dagger & \frac{H^*}{\sqrt{2}} & \frac{\tau\cdot\sigma^*}{2} + \frac{\phi_0}{2\sqrt{5}}\mathbb{1}_2 \end{pmatrix}\,,\quad \Phi = \begin{pmatrix} \Phi^{++} & \Phi^+/\sqrt{2} \\ \Phi^+/\sqrt{2} & \Phi^0 \end{pmatrix}. \tag{1.21}$$

The ϕ_0 and τ (in the $\mathbf{1}_0$ and $\mathbf{3}_0$ representations, respectively) are associated with spontaneously broken gauged generators and are removed from the spectrum in the unitary gauge. H is the doublet ($\mathbf{2}_{1/2}$) that we identify as the SM Higgs and Φ is an SU(2) triplet ($\mathbf{3}_1$).
In order to realize the collective breaking scheme in the gauge sector, $\mathcal{G}$ must contain two copies of $SU(2) \times U(1)$. This implies that the group rank is at least 4, making $SU(5)$ the smallest $SU(n)$ group possible. The generators of these two copies are defined as:

$$Q_1^a = \begin{pmatrix} \sigma^a/2 & 0_{2\times2} \\ 0_{2\times2} & 0_{3\times3} \end{pmatrix}\,,\quad Y_1 = \mathrm{diag}(-3,-3,2,2,2)/10\,, \tag{1.22}$$

$$Q_2^a = \begin{pmatrix} 0_{3\times3} & 0_{2\times2} \\ 0_{2\times2} & -\sigma^{a*}/2 \end{pmatrix}\,,\quad Y_2 = \mathrm{diag}(-2,-2,-2,3,3)/10\,. \tag{1.23}$$

Both of these subgroups are gauged. One linear combination, $Q_1^a - Q_2^a$ is spontaneously broken. The other linear combination remains exact - it corresponds to the usual SM electroweak (EW) gauge group. The new gauge fields have masses $m_{W_H} \sim gf\,, m_{B_H} \sim g'f$, (with g, g' the SM gauge couplings) and they contribute at tree level to the electroweak oblique parameters, leading to strong constraints on the parameter space of the model, see discussion below regarding T-Parity.

Given the above gauge groups, let us examine how the collective breaking mechanism works. The

$SU(5)$ group in this model contains two custodial $SU(3)$'s spanned by the Gell-Mann matrices λ^i in the upper and lower 3-by-3 blocks

$$\lambda_1^i = \begin{pmatrix} \lambda^i & 0_{3\times 2} \\ 0_{2\times 3} & 0_{2\times 2} \end{pmatrix}, \qquad \lambda_2^i = \begin{pmatrix} 0_{2\times 2} & 0_{2\times 3} \\ 0_{3\times 2} & \lambda^i \end{pmatrix}. \tag{1.24}$$

It is clear from Eq. (1.21) that the generators associated with the shift symmetries of the Higgs field can be written as linear combination of $SU(3)_1$ and $SU(3)_2$ generators. Therefore, if any of these two $SU(3)$'s is exact, the Higgs field is protected by shift symmetry. In particular, in the limit $g_i \to 0$ for either $i = 1$ *or* $i = 2$ (with g_1, g_2 the gauge coupling associated with the gauge groups defined in Eq. (1.22) and Eq. (1.23), respectively), the group $SU(3)_i$ becomes exact and the Higgs potential vanishes. Therefore, the Higgs potential generated from the gauge interactions $V_{\rm V}(H) \propto g_1 \cdot g_2$.

The usual term which contains the kinetic terms and self-interactions of the NGB's is given by

$$\mathcal{L} \supset \frac{f^2}{8} Tr[D\Sigma (D\Sigma)^*] \tag{1.25}$$

with

$$D\Sigma \equiv \partial\Sigma - i \sum_{i=1,2} \left[\sum_{a=1,2,3} \left(g_i W_i^a (Q_i^a \Sigma + \Sigma Q_i^{aT}) \right) - {g'}_i B_i (Y_i \Sigma + \Sigma {Y_i}^T) \right]. \tag{1.26}$$

Now we turn out attention to the top sector. It is of special importance, as the top quark loop contributes the most to the Higgs mass. We introduce an incomplete $SU(5)$ representation of Weyl fermions[2]:

$$\Psi = \begin{pmatrix} \psi \\ \chi \\ 0_{2\times 1} \end{pmatrix}, \tag{1.27}$$

where ψ and χ are an EW doublet an EW singlet, respectively. We also introduce two EW singlet Weyl fermions τ and $\tilde{t}$, with the following interactions

$$\mathcal{L}_{\rm top} = \sum_{i,j,k=1,2,3} \sum_{x,y=4,5} \frac{\lambda_1 f}{2\sqrt{2}} \epsilon_{ijk} \epsilon_{xy} \bar{\Psi}_i \Sigma_{jx} \Sigma_{ky} \tilde{t}^c + \frac{\lambda_2 f}{\sqrt{2}} \bar{\chi} \tau^c + \text{h.c}\,. \tag{1.28}$$

Similarly to the gauge sector, the matter couplings break the Higgs shift symmetry *collectively*. In the limit $\lambda_2 \to 0$, the $SU(3)_1$ defined above in Eq. (1.24) is an exact symmetry which generates a shift in the Higgs field. In the limit $\lambda_1 \to 0$, the Higgs is completely decoupled from the matter sector and in particular, none of the Higgs shift symmetries are broken. Therefore, the Higgs potential generated from the Yukawa interactions $V_{\rm f}(H) \propto \lambda_1 \cdot \lambda_2$.

Let us see how the interaction of Eq. (1.28) lead to the usual SM Yukawa interaction. Expanding Eq. (1.28) to leading order in H,

$$\mathcal{L}_{\rm top} = -\lambda_1 \left(\bar{\psi} i H^* \right) \tilde{t}^c + \frac{f}{\sqrt{2}} \bar{\chi} \left(\lambda_2 \tau^c + \lambda_1 \tilde{t}^c \right) + \text{h.c}\,. \tag{1.29}$$

[2]Unless noted otherwise, Weyl fermions are left-handed. The superscript c denotes a conjugate field transforming as a right-handed field. When L and R subscripts are introduced they should be understood in the obvious way.

χ gets a Dirac mass term with one linear combination of $\tilde{t}$ and τ, with $m_{T^+} = \sqrt{\frac{\lambda_1^2+\lambda_2^2}{2}} f$. The orthogonal combination of $\tilde{t}$ and τ is identified as the right-handed top quark t_R, and after integrating out the heavy top partner one finds

$$\mathcal{L}_{\rm top} = y_t \left(\bar{q}_L \tilde{H}\right) t_R + \text{h.c}\,, \quad \tilde{H} \equiv i\sigma_2 H^*\,, \tag{1.30}$$

where

$$q_L = \begin{pmatrix} t_L \\ b_L \end{pmatrix} = \sigma_2 \psi \quad \text{and} \quad y_t = \frac{\lambda_1 \lambda_2}{\sqrt{\lambda_1^2+\lambda_2^2}}\,. \tag{1.31}$$

Note that we remain agnostic regarding the other Yukawa couplings, since their contribution to the Higgs mass is negligible compared to the top quark.

T-Parity

From a modern model building prospective, the Littlest Higgs lacks an essential component, namely the electroweak custodial group $SU(2)_L \times SU(2)_R \cong SO(4)$, under which the Higgs transforms in the bi-fundamental or fundamental representation, respectively. The explicit breaking of the custodial symmetry leads to sizable corrections to electroweak precision test (EWPT) observables, e.g. the ρ parameter [39, 40, 41, 42, 43, 44, 45, 46]. These constraints pushed the symmetry breaking scale f to be a few TeV, thus reintroducing considerable fine-tuning. T-Parity has been proposed in order to prevent tree-level exchanges of heavy states [47, 48, 49, 50], resulting in the so-called Little Higgs with $T-$Parity (LHT) model. The new heavy states are odd under a discrete T-parity, therefore contributions to electroweak observables are possible only at the 1-loop level. This allows the symmetry breaking scale f to be $O(1)$ TeV. As an added benefit, T-Parity can be used as a stabilizing symmetry for a DM candidate, as the lightest T-odd particle is guaranteed to be stable. Let us present how T-Parity is implemented in the Littlest Higgs model. It relies on an automorphism, under which the broken and unbroken generators are mapped to

$$T\text{-parity}: X^{\hat{a}} \to -\Omega X^{\hat{a}} \Omega\,, \quad T^a \to \Omega T^a \Omega\,, \tag{1.32}$$

with

$$\Omega = -\exp[2\pi i (Q_1^3 + Q_2^3)] = \text{diag}(1,1,-1,1,1)\,. \tag{1.33}$$

Note that Ω is a member of $SU(5)$, and its overall sign is arbitrarily chosen. From Eq. (1.32) we can immediately deduce the T-parity transformation of the NGBs, namely

$$T\text{-parity}: \Pi_\Sigma \to -\Omega \Pi_\Sigma \Omega\,, \tag{1.34}$$

$$\Sigma \to \Omega \Sigma_0 \Sigma^\dagger \Sigma_0 \Omega \equiv \tilde{\Sigma}\,. \tag{1.35}$$

The Ω matrix represents an $SU(2)_L$ rotation of 2π around the 3rd direction, and its effect is an extra minus sign for all half-integer representations of $SU(2)_L$. This insures that the Higgs field is T-even while all the other NGB's are T-odd.

The realization of T-Parity in the gauge sector is straight forward. T-Parity is realized as an exchange of the so-called sites $1 \leftrightarrow 2$:

$$T\text{-parity}: W_1^a \leftrightarrow W_2^a\,, \quad B_1 \leftrightarrow B_2\,. \tag{1.36}$$

Therefore, the heavy gauge Bosons associated with the odd combinations $Q_1^a - Q_2^a$ are T-odd, while the SM gauge boson associated with the even combination $Q_1^a + Q_2^a$ are T-even,

$$V_{\text{H}} = \frac{1}{\sqrt{2}}\left(V_1 - V_2\right), \; V_{\text{SM}} = \frac{1}{\sqrt{2}}\left(V_1 + V_2\right) \quad \text{for } V = W^1, W^2, W^3, B$$

The indistinguishability of the two sites implies that one must impose

$$g_1 = g_2 \equiv \sqrt{2} g_{\text{SM}}\,, \;\; g_1' = g_2' \equiv \sqrt{2} g_{\text{SM}}'\,. \tag{1.37}$$

We continue the detailed discussion about the realization of the Little Higgs with T-Parity (LHT) model, in particular in the matter sector in Sec. 2.1.

1.5 Minimal composite Higgs

In this section we discuss minimal composite Higgs models and their main features. The generic features discussed below are shared by extensions of the minimal composite Higgs, including the $SO(7)/SO(6)$ extension studied in Chapter 3. We start by presenting the general symmetry structure of the model. Next we review the NGB self- and gauge interactions. As part of the discussion on the matter sector, we present the *partial compositeness* hypothesis and discuss the inclusion of fermionic and gauge resonances in the theory. We conclude by discussing the calculation of the scalar potential and the Weinberg sum rules.

The minimal composite Higgs (MCH) [51] is based on the $SO(5)/SO(4)$ coset. The unbroken $SO(4)$ is identified as the custodial group $SO(4) \cong SU(2)_L \times SU(2)_R$, under which the 4 NGB's transform as a $\mathbf{4} = (\mathbf{2}, \mathbf{2})$. $SU(2)_L$ is identified as the SM gauge group. The symmetry group must be extended by an additional $U(1)_X$ factor in order to realize hypercharge symmetry with adjustable charges, as we demonstrate below. Hypercharge is than defined as the linear combination $Y = T_R^3 + X$. Since $U(1)_X$ commutes with $SO(5)$, the X-charge of the NGB's vanishes and after gauging $(\mathbf{2}, \mathbf{2}) \to \mathbf{2_{1/2}}$ under $SU(2)_L \times U(1)_Y$, as needed. MCH models benefit from the custodial symmetry and are therefore protected from dangerous EWPT constraints.

The gauge fields and the SM fermions in the MCH framework are *external* sources. They are considered as an *elementary* sector which furnishes linear representations of $SU(5)$. These linear representations are incomplete e.g. only a subgroup of $SO(4)$ is gauged, leading to an explicit breaking of the global symmetries. The SM fermions also come in incomplete representations of $SO(5)$, introducing another source of explicit symmetry breaking. The interactions of the Higgs with the SM fermions can be seen as a consequence of mixing between the SM elementary states and the resonant composite states. This is the mechanism behind the partial compositeness hypothesis, to be discussed below.

The MCH models enjoy an additional practical advantage, namely that the coset structure is simple enough to allow closed analytic forms. This greatly simplifies calculations, in comparison to the $SU(5)/SO(5)$, for which closed analytic forms are not available. The leading order term in the d symbol, which contains the Higgs-gauge interactions, is given in the unitary gauge $H = \frac{1}{\sqrt{2}}(0, \langle h \rangle + h)^T$ by

$$\frac{f^2}{4} d_\mu^i d^{\mu i} = \frac{1}{2}\,\partial_\mu h\,\partial^\mu h + \frac{1}{4} g^2 f^2 \sin^2\left(\frac{\langle h \rangle + h}{f}\right)\left(|W|^2 + \frac{1}{2c_w} Z_0^2\right) \tag{1.38}$$

where $c_w = \cos\theta_w$, $\tan\theta_w = \frac{g'}{g}$ and g, g' are the gauge couplings of $SU(2)_L \times U(1)_Y$, respectively. We identify $\sin^2\left(\frac{\langle h\rangle}{f}\right) \equiv \xi = \frac{v^2}{f^2}$. This calculation relies on the CCWZ construction for the $SO(5)/SO(4)$ coset which can be found in the literature (e.g. [29]). It can also be easily deduced from the $SO(7)/SO(6)$ CCWZ construction given in App. 3.A. The composite nature of the Higgs manifests itself, among other ways, through deformation of the gauge couplings. Expanding to linear order in h,

$$\frac{f^2}{4} d^i_\mu d^{\mu i} \supset \frac{1}{4} g^2 v^2 \left(|W|^2 + \frac{1}{2c_w} Z_0^2\right) \left[2\sqrt{1-\xi}\frac{h}{v} + O\left(\frac{h^2}{v^2}\right)\right] \tag{1.39}$$

The linear hVV coupling is reduced by a factor of $\sqrt{1-\xi}$ in comparison to the elementary Higgs coupling. In the limit $\xi \to 0$, taken as the limit $f \to \infty$ with fixed v, the Higgs is effectively reduced to an elementary particle. This is the generic expectation, since all the interactions that originate from the strong sector and are weighted by powers of $1/f$.

The top sector is constructed under the partial compositeness hypothesis [52]. Let us review the hypothesis and its implications. We assume that in the UV theory at some high scale Λ, the SM fermions have a *linear* interaction terms with composite fermion operators, given schematically by

$$\frac{\lambda_L}{\Lambda^{[\mathcal{O}^{\rm f}_L]-5/2}} \bar{Q}_L \mathcal{O}^{\rm f}_L + \frac{\lambda_R}{\Lambda^{[\mathcal{O}^{\rm f}_R]-5/2}} \bar{t}_R \mathcal{O}^{\rm f}_R \,. \tag{1.40}$$

For operators whose dimension is close to the critical value $\sim 5/2$, the RGE flow is slow (approaching logarithmic) and sizable couplings can survive deep in the IR around the compositeness scale m_*

$$\lambda(m_*) = \lambda(\Lambda)\left(\frac{m_*}{\Lambda}\right)^{[\mathcal{O}]-5/2} . \tag{1.41}$$

As a result, in the IR the elementary states linearly mix with composite states. The simplest toy model is given by [29]

$$\mathcal{L} \supset -m_* \bar{q} q - m_* \bar{T} T - \lambda_L f(\bar{Q}_L q + \text{h.c}) - \lambda_R f(\bar{t}_R T + \text{h.c}) \,. \tag{1.42}$$

The mixing angle is given schematically by

$$\theta_{L/R} = \frac{\lambda_{L/R}}{\sqrt{\lambda^2_{L/R} + g^2_*}} \,, \tag{1.43}$$

where $g_* \equiv m_*/f$. The resulting Yukawa coupling is given by

$$y_f = g_* \sin\theta_L \sin\theta_R \,. \tag{1.44}$$

This simple picture can be easily modified by introducing more resonances and more mixing angles. In order to write $SO(5)$ invariant terms, we first imbed the SM fermion in incomplete $SO(5) \times U(1)_X$ representations which reproduce the appropriate SM quantum numbers (this is equivalent to choosing the $SO(5)$ representations of the composite operators). For example, take the $\mathbf{5_{2/3}}$ of $SO(5) \times U(1)_X$. We can decompose it in two steps, according to the symmetry breaking pattern $SO(5) \times U(1) \to SU(4) \times U(1)_X \to SU(2)_L \times U(1)_Y$, namely

$$\mathbf{5_{2/3}} \to (\mathbf{2},\mathbf{2})_{\mathbf{2/3}} \oplus \mathbf{1_{2/3}} \to \mathbf{2_{7/6}} \oplus \mathbf{2_{1/6}} \oplus \mathbf{1_{2/3}} \,. \tag{1.45}$$

The last two representations contained in the $\mathbf{5_{2/3}}$ are the appropriate SM representations for the left-handed quark doublet and the right-handed quark singlet, respectively[3]. Equivalently, it indicates that the composite operators in these representations contain states which can mix with SM fermions. Once the SM fermions are imbedded in an $SO(5)$ representation, we have a finite set of $SO(4)$ representation for the fermion resonances for which $SO(5)$ invariant mixing terms can be written. This is achieved by dressing the $SO(4)$ representation with the NGB matrix denoted in Eq. (1.6) as ξ.

Let us briefly present on the parallel procedure for vector resonances, based on the hidden local symmetry formalism [53, 54]. Let us consider a simple example. A non-linearly transforming $(\mathbf{3},\mathbf{1})_\mathbf{0}$ of $SO(4)\times U(1)_X$ can in principle mix with the W_μ triplet. Let us denote this vector by $\rho_\mu \equiv \rho_\mu^a T_L^a$. It transforms non-linearly under $g\in\mathcal{G}$ as a gauge field

$$\rho_\mu \to h\,\rho_\mu\,h^{-1} + i(h\,\partial_\mu\,h^{-1})\,, \tag{1.46}$$

where the last term should be projected to the space of $SU(2)_L$ generators. The composite operator with the exact same transformation properties is found by decomposing the e symbol, which transform as a $\mathbf{6}$ of $SO(4)$, to its irreducible representations under $SU(2)_L\times SU(2)_R$, namely $\mathbf{6}=(\mathbf{3},\mathbf{1})\oplus(\mathbf{1},\mathbf{3})$

$$e_\mu^a T^a = (e_L)_\mu^a T_L^a + (e_R)_\mu^a T_R^a\,. \tag{1.47}$$

The interactions terms are therefore given by

$$\mathcal{L}\supset -\frac{1}{4g_\rho^2}\rho_{\mu\nu}\rho^{\mu\nu} + \frac{m_\rho^2}{2g_\rho^2}(\rho_\mu-(e_L)_\mu)^2 \tag{1.48}$$

Note that the combination $(\rho_\mu-(e_L)_\mu)$ transforms *regularly* (and non-linearly) under $\mathcal{G}$. Depending on the representations of the fermion resonances, this combination can be used to construct additional $SO(5)$ invariant interactions. The mixing between the gauge states implies that the effective gauge coupling g is a mixture of the elementary gauge coupling g_0 and g_ρ, namely $g^{-2}=g_0^{-2}+g_\rho^{-2}$. Analogously, one can add a $(\mathbf{3},\mathbf{1})$ vector resonance. This representation contains a state with the same quantum numbers of the hypercharge gauge field B_μ, inducing a similar mixing and redefinition of the effective hypercharge gauge coupling.

The introduction of resonances and their interactions with the elementary sector explicitly breaks the shift symmetry of the NGB's. This explicit generates a Coleman-Weinberg potential, which can be easily calculated at one loop. In the context of MCH models and their extensions, it is usually preformed as a two-step calculation. The first step involves integrating out the heavy resonances, resulting in form factors defined as

$$\mathcal{L}\subset \Pi_L\bar{t}_L\not{p}t_L + \Pi_R\bar{t}_R\not{p}t_R - \Pi_{LR}(\bar{t}_L t_R + \text{h.c})\,. \tag{1.49}$$

The form factors Π_L,Π_R,Π_{LR} are functions of the NGB's (only h in the MCH in the unitary gauge), the composite sector parameters i.e. the vector masses and mixing couplings $\{m_*,\lambda\}$ and momentum p^2 (remnant of the resonants' propagators). The second step is the calculation the Coleman-Weinberg potential, which in this case is given by

$$V(h) = -2N_c\int\frac{\mathrm{d}^4p}{(2\pi)^4}\log(p^2\Pi_L\Pi_R+|\Pi_{LR}|^2)\,. \tag{1.50}$$

[3]Note that $U(1)_X$ was necessary in order to recover the SM hypercharges.

The coefficient of the renormalizable operators can be extracted by taking the appropriate number of derivatives. Schematically this results in momentum integral of the following form, e.g. for the Higgs mass term

$$\mu_h^2 = \frac{\partial V(h)}{\partial h^2}\Big|_{h=0} = \int \mathrm{d}p^2\, p^2\, F(p^2, \{m_*, \lambda\}) \tag{1.51}$$

Lastly, the Weinberg sum rules [55] can be used the regulated the high momentum behavior of $F(p^2, \{m_*, \lambda\})$. This is achieved by imposing the following constraints on the resonant sector parameters $\{m_*, \lambda\}$, namely

$$\lim_{p^2\to\infty} p^2\, F(p^2, \{m_*, \lambda\}) = 0 \quad \text{(to remove quadratic divergence)}\,, \tag{1.52}$$

$$\lim_{p^2\to\infty} p^4\, F(p^2, \{m_*, \lambda\}) = 0 \quad \text{(to remove logarithmic divergence)}\,. \tag{1.53}$$

This renders the potential UV-independent, and therefore finite and calculable. The relations imposed on the parameters can be often understood in terms of enhanced symmetries in the UV e.g. restoration of the full $SO(5)$ symmetry, i.e. reemergence of the Higgs shift symmetry which prevents the generation of a non-derivative scalar interactions.

1.6 Dark matter

The gravitational effects of what appears to be non-baryonic matter were detected in various astrophysical and cosmological scales. Starting from the galactic scale, observed rotation curves of stars are inconsistent with the theoretically predicted curves [56, 57], suggesting there is additional matter in galaxies, known as dark matter (DM). The DM is electrically neutral (hence dark) and its dark halo is only detectable via its gravitational effects, e.g.. the flatting of rotation curves. From gravitational lensing around galaxy clusters one can deduce that considerable amount of DM exists in clusters of galaxies as well [58]. Lastly, at the cosmological scale, the cosmological model Λ-CDM, which contains a cosmological constant Λ and cold (i.e. non-relativistic) DM, is consistent with the observed Cosmic Microwave Background (CMB) [59, 60] and large-scale structure formation in the universe [61].

CMB measurements provide the most accurate determination of the present-day DM relic abundance [62]

$$\Omega_{\rm DM} h^2 = 0.1198 \pm 0.0012\,. \tag{1.54}$$

There have been numerous realizations of DM, spanning an enormous range of scales. Starting from ultra-heavy objects like primordial black holes [63, 64], all the way to ultra-light bosonic particles [65]. One of the best motivated realizations of DM is the weakly interacting massive particle (WIMP), which is the case we consider in this work. Initially, the active neutrinos were considered DM candidates as they are both stable and electrically neutral. This idea has been long excluded [66]. Moreover, with present day neutrino masses data, we know that they can only account for small amount of the universe energy budget $\Omega_\nu \sim 10^{-3}\,(\sum m_\nu/0.1\text{ eV})$, and that they are still fairly relativistic [67].

One therefore concludes that the SM does not contain a neutral and stable particle which could be a viable DM candidate. As a result, BSM physics is often required in order to provide

such a candidate. This fact has further motivated various extensions of the SM, which were originally intended to address other issues like the Hierarchy problem (see Sec. 1.1) or the strong CP problem (see Sec. 4.1). If a new particle predicted by some SM extension is electrically and color neutral, it could be a good DM candidate provided that it is stable in cosmological time scales. From our understanding of Nature, stable particles are a consequence of symmetries, whether it is the electron (electric charge conservation) or the proton (baryon number conservation). Since DM is not charged under any of the SM symmetries, in most cases an additional symmetry is needed in order to achieve the desired stability.

The stabilizing symmetry of DM can be a global symmetry, most simply a Z_2 discrete symmetry. This is the case in the little Higgs with T-Parity, as well as in non-minimal composite Higgs model such as the $SO(6)/SO(5)$ [68], where the symmetry is extended to $O(6)$ in order to include a parity operator making the additional NGB odd, and thus stable. There are two caveats regarding the use of a global symmetry for DM stabilization. First, it is conjectured that strong gravitational effects break all global symmetries (see Refs. [69, 70, 71] and further references therein)[4]. Second, global symmetry may be anomalous: respected at the classical level but broken at the quantum level. In fact, in QCD the π_0 is symmetric under a Z_2 symmetry and naively stable. This Z_2 is however anomalous, and the anomaly diagram mediates the main decay channel of π_0 to $\gamma\gamma$. In this respect, it is hard to imagine an anomalous symmetry as an efficient mean to stabile DM[5]. Note that while the first caveat is an open theoretical question, and the second caveat can be considered a model-building issue, neither of them is relevant in case the stabilizing symmetry is *local* i.e. gauged.

Once DM is stable, one must come up with a production mechanism which could explain its present-day abundance. A prominent (but certainly not the only) mechanism is the so-called freeze-out mechanism (e.g.. Ref. [72]), which successfully predicts the present-day abundance of neutrinos . The freeze-out mechanism could be easily understood by examining the Boltzmann equation which determines the time dependence of the DM density $n(t)$,

$$\dot{n} + 3H\, n = \langle \sigma_{\chi\chi\to \mathrm{SM}} v \rangle \, (n_\chi^2 - n_{\mathrm{eq}}^2)\,, \tag{1.55}$$

where H is the Hubble parameter and $\langle \sigma v \rangle$ is a thermally averaged annihilation cross section of DM to SM particles. Initially $H \ll \langle \sigma v \rangle\, n$ and the DM is in kinetic and chemical equilibrium with the SM heat bath. The dilution term $3Hn$ can be neglected and the abundance of DM closely follows the equilibrium abundance $n \approx n_{\mathrm{eq}}$. Freeze-out occurs when $H \sim \langle \sigma v \rangle\, n$, after which the dilution of DM is driven solely by the expansion of the universe. The Boltzmann equation can be solved numerically. An approximate solution predicts the final relic abundance (for self-conjugated DM) to be

$$\frac{\Omega_\chi h^2}{0.1198} \approx \frac{3 \cdot 10^{-26} \mathrm{cm}^3 \mathrm{s}^{-1}}{\langle \sigma_{\chi\chi\to \mathrm{SM}} v \rangle}\,. \tag{1.56}$$

The *WIMP miracle* is phrased as the coincidence that $\langle \sigma_{\chi\chi\to \mathrm{SM}} v \rangle \sim \frac{g^4}{m_\chi^2}$ produces the correct relic abundance for $m_\chi \sim O(100\ \mathrm{GeV})$ and $g \sim 0.1$. WIMP's are consequently one of the most popular and studied form of DM.

[4] The counter argument would be that the coefficients of the M_{PL}-suppressed breaking terms are unknown, which leaves the possibility that this effect does not jeopardize the stability of DM at cosmological time scales.

[5] The counter argument would be that given the correct matter content, global symmetries can be non-anomalous, like $B - L$ in the SM. Another possible approach to avoid anomalous global symmetries is to use groups which allow only real representations, e.g.. $SO(7)$.

Composite dark matter

In non-minimal composite Higgs models, additional stable NGB's in $\mathcal{G}/\mathcal{H}$ constitute compelling DM candidates. Let us assume $\{H, \chi\} \in \mathcal{G}/\mathcal{H}$, with χ being a complex (or real) scalar stabilized by a global $U(1)$ (or Z_2) symmetry. The non-renormalizable operators play a crucial role in the phenomenology of composite DM [73]. H and χ interact derivatively through the dim. 6 operator

$$\mathcal{L} \supset \frac{1}{f^2}\partial_\mu |H|^2 \partial^\mu |\chi|^2 \,. \tag{1.57}$$

As shown in Sec. 3.1, one can always find a basis where this is the only derivative interaction term at this order in the $1/f$ expansion. After EWSB, this interaction leads to s-channel annihilation of χ in the early universe. In the non-relativistic limit, the thermally averaged annihilation cross section $\langle \sigma v \rangle \propto \langle s \rangle / f^2 \approx 4m_\chi^2/f^2$ can be of the right size in order to account for the observed DM relic abundance with $m_\chi \sim 100$ GeV and $f \sim 1$ TeV. This is a fortunate (some might even say miraculous) coincident that the correct relic abundance is produced with the naturally expected values for m_χ and f. As an added benefit, this interaction is extremely suppressed in scattering processes probed by direct detection experiments: the cross section for the elastic scattering scales like $|t|/f^2 \sim (100 \text{ MeV})^2/(1 \text{ TeV}) \sim 10^{-8}$, with t the usual Mandelstam variable associated with the momentum transfer. Thus, one concludes that if the only interaction between the Higgs and χ was the derivative interaction of Eq. (1.57), χ can account for all the DM while being virtually invisible to present day direct detection experiments.

However, the fact that H and χ are massive already implies that their shift symmetry is broken, and therefore one must also consider the so-called Higgs portal coupling,

$$\mathcal{L} \supset -\lambda |H|^2 |\chi|^2, \tag{1.58}$$

which is strongly constrained by direct detection experiments. If no other annihilation channels are available, one finds that the derivative terms and portal coupling destructively interfere [73], and the annihilation cross section scales like

$$\langle \sigma_{\chi\chi\to \text{SM}} v \rangle \propto \left(\frac{4m_\chi^2}{f^2} - 2\lambda \right)^2 . \tag{1.59}$$

If $\lambda \gg m_\chi^2/f^2$, the composite nature of DM is negligible compared to the explicit shift symmetry breaking effects and the model is reduced to the elementary singlet DM model. If $\lambda \sim m_\chi^2/f^2$, there are two compatible values for the portal coupling, $\{\lambda_-, \lambda_+\}$, which can reproduce the correct relic abundance. Couplings inside the interval $[\lambda_-, \lambda_+]$ lead to over-abundance of DM and are excluded. Couplings outside the interval lead to under-abundance DM and are in principle allowed. If $\lambda \ll m_\chi^2/f^2$, as stated above the observed relic abundance is produced for $m_\chi \sim 100$ GeV and $f \sim 1$ TeV.

We consider three possible sources for the DM shift symmetry breaking:

DM shift symmetry broken by top quark couplings - we explore this possibility in Chapter 2 in the LHT model and in Sec. 3.3 in the $SO(7)/SO(6)$ model. In this case, the portal coupling is generated by the same dynamics which generate the Higgs quartic λ_H. The naive expectation is $\lambda \sim \lambda_H \sim 0.1$, which is in tension with direct detection bounds. In the LHT model the scalar potential is not calculable due to the unknown UV contribution, but we confirm that

the IR contribution is indeed $O(\lambda_H)$. In the $SO(7)/SO(6)$ model, we verify this expectation numerically by scanning over the parameter model and calculating the scalar potential. The conclusion is the same for both models: a model in which the DM shift symmetry is broken by the top interactions can evade DM direct detection bounds if some cancellation takes place which reduces λ, at the price of fine tuning some of the model's parameters. In Sec. 3.3.2 we explicitly show how in the $SO(7)/SO(6)$ model, this cancellation can be achieved by adding more resonances and tuning their contribution. Let us note that the models differ in their prediction for the DM mass. In the LHT model, the DM mass is protected at 1 loop and is generated only at the 2-loop order. It is than reasonable to assume that the $m_\chi \sim m_h$. On the other hand, in the $SO(7)/SO(6)$ model the DM mass is again generated by the same dynamics as the Higgs mass, but in general would not enjoy the same cancellation which allows for the small misalignment angle $\xi \ll 1$. Thus, the naive expectation is $m_\chi \gg m_h$, which is confirmed by the numerical results. Lastly we note that for the determination of the relic abundance, the following dim. 5 operator

$$\mathcal{L} \supset -2c_{tt\chi\chi}\, m_t \bar{t}t \frac{|\chi|^2}{v^2}\,, \tag{1.60}$$

has to be considered as well. The coefficient $c_{tt\chi\chi} \sim O(\xi)$ such that the whole term scales like $1/f$, and the amplitude for the annihilation process to top quarks scales like $|\mathcal{M}_{\chi\chi\to\bar{t}t}| \propto m_\chi^2/f^2$. This leads to an irreducible annihilation cross section for $m_\chi > m_t$, which above some critical m_χ/f value leads to under-abundant DM for every value of λ.

DM shift symmetry broken by bottom quark couplings - this possibility is considered in Sec. 3.4 in the framework of the $SO(7)/SO(6)$ model. In this case the naive expectation for the portal coupling becomes $\lambda \sim (y_b^2/y_t^2)\lambda_H \ll 1$, making the portal coupling small enough such that it is irrelevant for direct detection. The dominant scattering process in this case is via the contact term $\bar{b}b|\chi|^2$, leading to a scattering cross section that is within reach of future direct detection experiments. Due to the smallness of the bottom Yukawa coupling, the DM mass can be comparable to the Higgs mass $m_\chi \sim \sqrt{g_* y_b} f \sim m_h$.

DM shift symmetry respected by SM gauge/fermion couplings - if all the couplings between the elementary sector and the composite sector respect the DM shift symmetry, a new BSM source of explicit symmetry breaking must be introduced. For a complex scalar DM, gauging the stabilizing $U(1)$ symmetry leads to an explicit breaking of the DM shift symmetry and the addition of a dark photon to the theory. χ and the dark photon form a minimal dark sector, leading to a rich DM phenomenology which we explore in Sec. 3.5. The dark sector heat bath can decouple from the SM heat bath once the rate of the interactions keeping the two baths in kinetic equilibrium becomes slower than Hubble. After decoupling both sectors have separately conserved entropy and independent temperature. In a dark sector, additional versatile annihilation channels may become accessible, leading to scenarios such as co-annihilations [74] and semi-annihilations [75]. If the dark photon is massless, its contribution to the energy budget of the universe can be indirectly probed through CMB measurements, which gives a bound on the relativistic degrees of freedom at recombination. A light mediator can lead to Boltzmann enhanced annihilation cross sections at low velocities and potentially strong indirect detection signatures. We consider the possibility of a massless dark photon in Sec. 3.5.1. If the dark photon itself massive and stable, it can serve as an additional source of cold DM. The number densities in this multicomponent DM scenario are determined via coupled Boltzmann equations which must be solved numerically. We consider the possibility of a massless dark photon in Sec. 3.5.2.

2

Composite dark matter in Little Higgs

2.1 Model

In Sec. 1.4 we review the littlest Higgs model and conclude with a discussion regarding the necessity of T-Parity. In this section we present the realization of T-Parity in LH model. We continue to discuss the challenge of realizing a spectrum compatible with the SM and some potential solutions. The remainder of the section specifies in detail the structure and content of the model in a minimal extension of the LHT model [76].

In the original littlest Higgs mode, the new heavy gauge states contribute at tree level to the electroweak oblique parameters. These contributions lead to stringent constraints from EWPT, pushing the symmetry breaking scale of the original LH model $f \sim$ a few TeV (e.g [39]). The corrections to electroweak observables from the heavy gauge states are made smaller by introducing a discrete symmetry which forbids tree level exchanges of heavy states. The addition of a discrete symmetry stabilizes the lightest odd particle, making it a viable DM candidate. This discrete symmetry, usually referred to as T-parity, is defined as [47]

$$T\text{-parity:} \quad T_i \to \Omega T_i \Omega\,, \quad X_j \to -\Omega X_j \Omega \tag{2.1}$$

with

$$\Omega = -\exp[2\pi i Q^3_{1+2}] = \mathrm{diag}(1,1,-1,1,1)\,, \tag{2.2}$$

which is an automorphism defined on the $SU(5)$ generators. This definition determines the T-parity of all the fields associated with the $SU(5)$ generators, namely the Goldstone and gauge fields. The Ω rotation is introduced to make the Higgs even under T-parity, while keeping the rest of the Goldstone fields odd. For the gauge fields, the T-parity transformation can be interpreted as an exchange symmetry between the gauge groups $1 \leftrightarrow 2$. Hence the diagonal combination is even, and the broken combination is odd.

Let us understand how linear representations of $SU(5)$ transform under T-parity. One can use Eq. (2.2) to show that each transformation $g = e^{i\alpha_j X_j + i\beta_i T_i} \in SU(5)$ is mapped under T-parity to

$$g \;\to\; \tilde{g} \equiv \Omega \Sigma_0 g^* \Sigma_0 \Omega\,. \tag{2.3}$$

Therefore, up to a constant matrix, fundamental and anti-fundamental indices of $SU(5)$ are mapped to each other

$$\underbrace{V_i}_{\mathbf{5}} \;\leftrightarrow\; (\Sigma_0\Omega)_{ij}\, \underbrace{U^j}_{\overline{\mathbf{5}}}\,. \tag{2.4}$$

The Σ field transforms with two fundamental $SU(5)$ indices, so under T-parity

$$\Sigma \;\rightarrow\; \tilde{\Sigma} \equiv \Omega\Sigma_0\Sigma^\dagger\Sigma_0\Omega\,. \tag{2.5}$$

2.1.1 A UV doubling problem, making the T-odd doublet massive

The coset structure of LH with T-parity is in tension with the SM matter content [77, 76]. The low energy theory must contain a T-even massless $SU(2)$ doublet, the left-handed quark doublet of the SM. Since T-parity can be understood as an exchange symmetry between the two gauged $SU(2)$ subgroups of $SU(5)$ (we omit the $U(1)$ factors for the following discussion), one must therefore introduce two doublets ψ_i, each transforming under a different $SU(2)_i$ with $i = 1, 2$. Under T-parity the two doublets are mapped into each other

$$\psi_1 \;\leftrightarrow\; \psi_2\,. \tag{2.6}$$

We would like to write a mass term for the T-odd combination $\psi_- \equiv (\psi_1 - \psi_2)$ that respects the SM gauge group. Let us introduce a right-handed field ψ^c transforming as a doublet under the SM gauge group $[SU(2)]_{1+2}$

$$\mathcal{L} \supset (\overline{\psi}_1 - \overline{\psi}_2)\psi^c\,. \tag{2.7}$$

This term respects the SM gauge group, however each term by itself breaks $SU(2)_1 \times SU(2)_2$ and cannot be generated by a reasonable UV theory which respects those gauge symmetries, unless they are spontaneously broken. Assuming that ψ^c cannot be a doublet of just one of the $SU(2)'s$, we expect the mass term to arise as a result of spontaneous symmetry breaking

$$\mathcal{L} \supset (\overline{\psi}_1 \langle\phi_1\rangle - \overline{\psi}_2 \langle\phi_2\rangle)\psi^c\,, \tag{2.8}$$

where we introduced two sources of spontaneous symmetry breaking, the VEV's $\langle\phi_1\rangle$ and $\langle\phi_2\rangle$. Let us examine now the VEV's which we can use to write this term in a gauge-invariant way. We first examine two different constructions presented in the literature that generate the mass term of Eq. (2.7): first by using a non-linear representation and second by adding a third $SU(2)\times U(1)$. We mention possible shortcomings of these constructions, which motivate the construction used in this thesis. This third and last construction, which involves the mirroring of the $1 \leftrightarrow 2$ exchange symmetry, is presented at the end of this section.

Non-linear formulation of a massive odd doublet

One construction commonly presented in the literature uses the CCWZ formalism [5, 6]. The main advantage of this approach is that no new sources of spontaneous symmetry breaking are needed.
First we have the linear representations of $SU(5)$ [48]

$$\Psi_1 = \begin{pmatrix} \psi_1 \\ 0 \\ 0 \end{pmatrix}_{\overline{\mathbf{5}}}\,, \quad \Psi_2 = \begin{pmatrix} 0 \\ 0 \\ \psi_2 \end{pmatrix}_{\mathbf{5}}\,, \tag{2.9}$$

with the following T-parity transformation

$$\Psi_1 \;\rightarrow\; \Omega\Sigma_0\Psi_2\,. \tag{2.10}$$

A mass term for the T-odd combination is constructed using a non-linearly transforming field

$$\tilde{\Psi}^c = \begin{pmatrix} \psi_1^c \\ \chi^c \\ \psi_2^c \end{pmatrix}, \quad \text{a } \mathbf{5} \text{ of } SO(5)\,. \tag{2.11}$$

Under a transformation $g \in SU(5)$

$$\tilde{\Psi}^c \;\to\; h(\Pi_\Sigma, g)\tilde{\Psi}^c\,, \quad h \in SO(5)\,. \tag{2.12}$$

$e^{i\Pi_\Sigma/f}$ transforms under a transformation $g \in SU(5)$ in the following way

$$e^{i\Pi_\Sigma/f} \;\to\; g e^{i\Pi_\Sigma/f} h^\dagger = h e^{i\Pi_\Sigma/f}(\Sigma_0 g^T \Sigma_0)\,. \tag{2.13}$$

The kinetic term for $\tilde{\Psi}^c$ contains the e_μ symbol defined by [5, 6]

$$ie^{-i\Pi_\Sigma/f}(\partial_\mu e^{i\Pi_\Sigma/f}) \equiv d_\mu^j X^j + e_\mu^i T^i\,. \tag{2.14}$$

Using the automorphism defined in Eq. (2.2) we can write $e_\mu \equiv e_\mu^i T^i$ in a T-parity symmetric form

$$e_\mu = \frac{i}{2}\left(e^{-i\Pi_\Sigma/f}\partial_\mu e^{i\Pi_\Sigma/f} + e^{i\Pi_\Sigma/f}\partial_\mu e^{-i\Pi_\Sigma/f}\right)\,. \tag{2.15}$$

The e_μ symbol transform as a covariant derivative

$$(\partial_\mu + e_\mu) \;\to\; h(\partial_\mu + e_\mu)h^\dagger\,, \tag{2.16}$$

which allows us to write an invariant kinetic term for $\tilde{\Psi}^c$. Note that under T-parity

$$e_\mu \to \Omega e_\mu \Omega\,, \tag{2.17}$$

therefore the transformation of $\tilde{\Psi}^c$ under T-parity is

$$\tilde{\Psi}^c \to -\Omega\tilde{\Psi}^c\,. \tag{2.18}$$

The benefit of the CCWZ formalism is that the pion matrix can be used to dress the field $\tilde{\Psi}^c$ as linear representations of $SU(5)$, e.g $\mathbf{5}$ and $\bar{\mathbf{5}}$

$$e^{i\Pi_\Sigma/f}\tilde{\Psi}^c \;\to\; g(e^{i\Pi_\Sigma/f}\tilde{\Psi}^c)\,, \tag{2.19}$$

and

$$\Sigma_0 e^{-i\Pi_\Sigma/f}\tilde{\Psi}^c \;\to\; g^*(\Sigma_0 e^{-i\Pi_\Sigma/f}\tilde{\Psi}^c)\,, \tag{2.20}$$

with $g \in SU(5)$. Finally the mass term is given by [48]

$$\begin{aligned}\mathcal{L} \supset & \frac{\kappa f}{\sqrt{2}}(\overline{\Psi}_1\Sigma_0 e^{-i\Pi_\Sigma/f} - \overline{\Psi}_2 e^{i\Pi_\Sigma/f})\tilde{\Psi}^c + \text{h.c} \\ = & \frac{\kappa f}{\sqrt{2}}\left(\overline{\psi}_1 - \overline{\psi}_2\right)\psi_2^c + \dots\,.\end{aligned} \tag{2.21}$$

The field $\tilde{\Psi}^c$ must be a complete $SO(5)$ representation, otherwise the kinetic term for $\tilde{\Psi}^c$ would explicitly break the global symmetry protecting the Higgs mass [48]. The field ψ_1^c is still massless at this point. One could formally introduce an additional doublet η and write a mass term

$$\mathcal{L} \supset M(\bar{\eta}\psi_1^c + \text{h.c})\,. \tag{2.22}$$

This term breaks the global symmetries protecting the Higgs mass, generating $O(M^2)$ contributions to the Higgs mass.

Adding a third $SU(2) \times\ U(1)$

We conclude that the model requires additional structure in order to give mass to the T-odd combination without explicit breaking of the global symmetry.
One possible solution is to add an additional gauge group [77, 78], denoted by $[SU(2) \times U(1)]_3$. Now ψ^c of Eq. (2.8) transforms as a doublet under $[SU(2) \times U(1)]_3$ and the scalars ϕ_i transform as a bi-fundamentals of $[SU(2) \times U(1)]_i \times [SU(2) \times\ U(1)]_3$ with $i = 1, 2$. This solution introduces new heavy T-even gauge fields. The new T-even gauge fields can be made heavy by making the coupling constant of the third $SU(2)\ \times\ U(1)$ gauge group large, effectively decoupling them from the theory without spoiling the naturalness of the model. One has the choice of how to enlarge the global symmetry to incorporate this additional gauge group. The most naive extension is

$$SU(5) \to SU(5)\ \times\ [SU(2)\ \times\ U(1)]_3 \tag{2.23}$$

We introduce additional scalars Φ_1 and Φ_2 transform under the enlarged group as $(\bar{\mathbf{5}}, \bar{\mathbf{2}})$ and $(\mathbf{5}, \bar{\mathbf{2}})$ respectively (disregarding the $U(1)$ charges), namely

$$\begin{aligned} \Phi_1 \to & g^* \Phi_1 g_3^\dagger\,, \quad \Phi_2 \to g \Phi_2 g_3^\dagger\,, \\ & g \in SU(5)\,, \quad g_3 \in [SU(2)\ \times\ U(1)]_3\,. \end{aligned} \tag{2.24}$$

Under T-parity

$$\Phi_1 \to \Sigma_0 \Omega \Phi_2\,, \quad \psi^c \to -\psi^c\,. \tag{2.25}$$

The T-odd doublet gets a mass

$$\begin{aligned} \mathcal{L} \supset & \frac{\kappa}{\sqrt{2}} \left(\overline{\Psi}_1 \langle \Phi_1 \rangle - \overline{\Psi}_2 \langle \Phi_2 \rangle \right) \psi^c \\ = & \frac{\kappa f}{\sqrt{2}} \left(\overline{\psi}_1 - \overline{\psi}_2 \right) \psi^c + \ldots\,, \end{aligned} \tag{2.26}$$

after Φ_1 and Φ_2 acquire VEV's given by

$$\langle \Phi_1 \rangle = f \begin{pmatrix} \mathbb{1}_{2\ \times\ 2} \\ 0_{1\ \times\ 2} \\ 0_{2\ \times\ 2} \end{pmatrix} = \Sigma_0 \Omega \langle \Phi_2 \rangle\ . \tag{2.27}$$

The appearance of Φ_1, Φ_2 results in a deviation from the original coset structure of the LH, with the altered coset structure

$$\frac{SU(5)\ \times\ SU(2)\ \times\ U(1)}{[SU(2)\ \times\ U(1)]_{1+2+3}}\,. \tag{2.28}$$

We now identify $[SU(2)\ \times\ U(1)]_{1+2+3}$ as the SM gauge group. This coset contains in the original 14 NGB's of the LH coset, and additional 10 NGB's from the spontaneously broken $SO(5)$. These 10 additional states decompose under the SM gauge group as

$$\mathbf{1}_0 \oplus \mathbf{3}_0 \oplus \mathbf{2}_{1/2} \oplus \mathbf{1}_{1/2}\,. \tag{2.29}$$

The additional neutral singlet $\mathbf{1}_0$ and triplet $\mathbf{3}_0$ are eaten by the additional T-even gauge fields. This naive approach unavoidably introduces additional physical NGB's in the form of a T-odd doublet $\mathbf{2}_{1/2}$ and a T-even complex scalar $\mathbf{1}_{1/2}$. These states must be made massive without spoiling the symmetry protection of the SM Higgs. Additional NGB's are a generic result of the enlarged global symmetry structure, even more so when the additional $SU(2)$ is a gauged subgroup of a larger global symmetry [77].

Mirroring the $1 \leftrightarrow 2$ exchange symmetry

In this thesis we consider a concrete solution suggested in [76]. We extend the global symmetry

$$SU(5) \to SU(5) \times [SU(2) \times U(1)]_L \times [SU(2) \times U(1)]_R. \tag{2.30}$$

We introduce a scalar field, X, which transforms linearly under $[SU(2)\times U(1)]_L \times [SU(2)\times U(1)]_R$

$$X \to g_L X g_R^\dagger \,. \tag{2.31}$$

When the Σ and X acquire VEV's, $\langle \Sigma \rangle = \Sigma_0$ and $\langle X \rangle = \mathbb{1}_2$, the symmetry is spontaneously broken to

$$\frac{SU(5)}{SO(5)} \times \frac{[SU(2) \times U(1)]_L \times [SU(2) \times U(1)]_R}{[SU(2) \times \ U(1)]_V} \,. \tag{2.32}$$

We gauge two $SU(2) \ \times \ U(1)$ subgroups defined as the combinations $[SU(2) \ \times \ U(1)]_{1+L}$ and $[SU(2) \ \times \ U(1)]_{2+R}$. The residual gauge symmetry $[SU(2) \ \times \ U(1)]_{1+2+L+R}$ is identified as the SM gauge group. We can parametrise X using the non-linearly transforming Goldstone fields associated with this symmetry breaking,

$$X \equiv e^{\frac{i}{f'}\Pi_X} \langle X \rangle \, e^{\frac{i}{f'}\Pi_X} = e^{\frac{2i}{f'}\Pi_X} \,, \quad \Pi_X = \frac{1}{2}\left(\pi_i \sigma^i + \pi_0 \mathbb{1}_2\right) . \tag{2.33}$$

Note that the symmetry breaking scale f' may be different than f, the symmetry breaking scale of the original coset defined in Eq. (1.21). T-parity in the additional coset is realized as an $L \ \leftrightarrow \ R$ exchange, mirroring the $1 \leftrightarrow 2$ exchange symmetry of the original coset. Under T-parity,

$$\Pi_X \to -\Pi_X \,, \tag{2.34}$$

We introduce a non-linear representation of

$$[SU(2) \times U(1)]_L \times [SU(2) \times U(1)]_R \,.$$

ψ^c is a doublet of the unbroken subgroup $[SU(2) \ \times \ U(1)]_{L+R}$, transforming non-linearly under $g_L, g_R \in [SU(2) \times U(1)]_L \times [SU(2) \times U(1)]_R$

$$\begin{aligned} &\psi^c \to V(\Pi_X, g_L, g_R)\psi^c \,, \\ &V \in [SU(2) \times U(1)]_{L+R} \,. \end{aligned} \tag{2.35}$$

The transformation properties under $[SU(2) \times U(1)]_L \times [SU(2) \times U(1)]_R$ of $e^{i\Pi_X/f'}$ in this case are

$$e^{i\Pi_X/f'} \to g_L e^{i\Pi_X/f'} V^\dagger = V e^{i\Pi_X/f'} g_R^\dagger \,. \tag{2.36}$$

This object can be used to dress ψ^c as linear representations

$$e^{i\Pi_X/f'}\psi^c \to g_L(e^{i\Pi_X/f'}\psi^c) \,, \tag{2.37}$$

$$e^{-i\Pi_X/f'}\psi^c \to g_R(e^{i\Pi_X/f'}\psi^c) \,. \tag{2.38}$$

Finally the mass term can be written as [76]

$$\mathcal{L} \ni (\overline{\psi}_1 e^{i\Pi_X/f'} - \overline{\psi}_2 \Sigma_0 e^{-i\Pi_X/f'})\psi^c + \text{h.c} \,. \tag{2.39}$$

This extension allows us to add a single $SU(2)$ doublet to the spectrum, ψ^c, and write a mass term for the T-odd doublet, without any explicit breaking of the global symmetry. In additional to the 14 original NGB's of Eq. (1.21), our spectrum includes now an additional NGB's, a real singlet $\mathbf{1}_0$ and a real triplet $\mathbf{3}_0$.

2.1.2 Gauge sector

We write the Lagrangian for the non-linear σ model

$$\mathcal{L}_{nl\sigma} = \frac{f^2}{8}\mathrm{Tr}[(D_\mu\Sigma)(D^\mu\Sigma^*)] + \frac{f'}{4}\mathrm{Tr}[(D_\mu X)(D^\mu X^\dagger)]\,. \tag{2.40}$$

We parameterize Σ, X using the NGB's as defined in Eq. (1.21) and Eq. (2.33). The exact form of the covariant derivatives can be found in App. 2.A.
Once we set Σ, X to their respected VEV's, we find that the following linear combinations,

$$W_H^a = \frac{1}{\sqrt{2}}(W_1^a - W_2^a)\,,\quad B_H = \frac{1}{\sqrt{2}}(B_1 - B_2)\,, \tag{2.41}$$

acquire a mass

$$M_{W_H}^2 = g^2 f^2(1+r^2)\,, M_{B_H}^2 = \frac{1}{5}g'^2 f^2\left(1+\frac{1}{5}r^2\right), \tag{2.42}$$

with

$$r \equiv \frac{f'}{f}\,. \tag{2.43}$$

We recognize the orthogonal linear combinations,

$$W^a = \frac{1}{\sqrt{2}}(W_1^a + W_2^a)\,,\quad B = \frac{1}{\sqrt{2}}(B_1 + B_2)\,, \tag{2.44}$$

as the SM gauge fields.

2.1.3 Goldstone sector

In addition to the complex Higgs doublet H and the charged triplet Φ, the Goldstone sector includes additional physical states: a real singlet s and a real triplet $\varphi \equiv \frac{1}{2}\varphi_a\sigma^a$, defined as the following linear combinations

$$s = c_0\pi_0 + s_0\phi_0\,,\quad \varphi_a = c_3\tau_a - s_3\pi_a\,, \tag{2.45}$$

with the mixing angles

$$s_0 = \sqrt{1-c_0^2} \equiv \frac{r}{\sqrt{5+r^2}}\,, \tag{2.46a}$$

$$c_3 = \sqrt{1-s_3^2} \equiv \frac{r}{\sqrt{1+r^2}}\,. \tag{2.46b}$$

The orthogonal linear combinations,

$$G_0 = -s_0\pi_0 + c_0\phi_0\,,\quad G^a = s_3\tau_a + c_3\pi_a\,, \tag{2.47}$$

are eaten by the heavy gauge fields and removed from the spectrum in the unitary gauge.

2.1.4 Matter sector

The top Yukawa generates the largest quadratically divergent contribution to the Higgs mass, therefore we limit our discussion to the third quark family. The terms in the top sector must respect enough of the global symmetries in order for the Higgs mass to be protected from 1-loop quadratically divergent contributions. This mechanism is usually referred to as *collective breaking*. In order to respect these symmetries we enlarge the multiplets introduced in Eq. (2.9) and introduce top partners. The quadratically divergent contribution to the Higgs mass from these top partners would eventually cancel out with the top contribution. We start by introducing left-handed Weyl fermions. We embed the doublets $\psi_{1,2}$ with the singlets $\chi_{1,2}$ (the top partners) in incomplete $SU(5)$ multiplets

$$\Psi_1 = \begin{pmatrix} \psi_1 \\ \chi_1 \\ 0 \end{pmatrix}_{\overline{\mathbf{5}}} , \quad \Psi_2 = \begin{pmatrix} 0 \\ \chi_2 \\ \psi_2 \end{pmatrix}_{\mathbf{5}} . \tag{2.48}$$

Under T-parity,

$$\Psi_1 \to \Omega\Sigma_0\Psi_2 \,, \tag{2.49}$$

or equivalently

$$\psi_1 \leftrightarrow \psi_2 \,, \quad \chi_1 \leftrightarrow -\chi_2 \,. \tag{2.50}$$

We introduce 3 right-handed singlets denoted by $\tilde{t}_R, \tau_{1,2}$. Under T-parity,

$$\tilde{t}_R \leftrightarrow \tilde{t}_R \,, \quad \tau_1 \leftrightarrow \tau_2 \,. \tag{2.51}$$

The top Yukawa is given by [32, 49]

$$\begin{aligned} \mathcal{L}_{\text{top}} =& \frac{\lambda_1 f}{2}\left(\overline{\Psi}_{1i} O_i + (\overline{\Psi}_2\Omega\Sigma_0)_i \tilde{O}_i\right)\tilde{t}_R + \frac{\lambda_2 f}{\sqrt{2}}\left(\overline{\chi}_1\tau_1 - \overline{\chi}_2\tau_2\right) + \text{h.c}\,, \\ O_i \equiv& \epsilon_{ijk}\Sigma_{j4}\Sigma_{k5} \,, \quad \tilde{O}_i \equiv \epsilon_{ijk}\tilde{\Sigma}_{j4}\tilde{\Sigma}_{k5} \,. \end{aligned} \tag{2.52}$$

$\tilde{\Sigma}$ is defined in Eq. (2.5). The indices i, j, k are summed over $1, 2, 3$. We define the T-parity eigenstates

$$\Psi_+ = \frac{1}{\sqrt{2}}\left(\Psi_1 + \Omega\Sigma_0\Psi_2\right) \equiv \begin{pmatrix} \sigma_2 q_L \\ \chi_+ \\ 0 \end{pmatrix} , \tag{2.53}$$

$$\Psi_- = \frac{1}{\sqrt{2}}\left(\Psi_1 - \Omega\Sigma_0\Psi_2\right) \equiv \begin{pmatrix} \sigma_2 \psi_L^- \\ T_L^- \\ 0 \end{pmatrix} , \tag{2.54}$$

with

$$q_L = \begin{pmatrix} \tilde{t}_L \\ b_L \end{pmatrix} = \frac{1}{\sqrt{2}}\sigma_2(\psi_1 + \psi_2) \,, \tag{2.55}$$

$$\psi_L^- = \frac{1}{\sqrt{2}}\sigma_2(\psi_1 - \psi_2) \,. \tag{2.56}$$

The singlet T-parity eigenstates are defined as

$$\chi_+ = \frac{1}{\sqrt{2}}(\chi_1 - \chi_2)\,, \quad \tau_+ = \frac{1}{\sqrt{2}}(\tau_1 + \tau_2)\,, \tag{2.57}$$

$$T_L^- = \frac{1}{\sqrt{2}}(\chi_1 + \chi_2)\,, \quad T_R^- = \frac{1}{\sqrt{2}}(\tau_1 - \tau_2)\,. \tag{2.58}$$

Note that the T-even fields, and in particular $\tilde{t}_L, \tilde{t}_R$, are not the mass eigenstates (hence the tilde). After the Higgs field acquires its VEV, $\langle H \rangle = \frac{1}{\sqrt{2}}(0, v)^T$, we find the following mass matrix for the T-even fermions

$$\mathcal{L}_{\text{top}} \ni f \begin{pmatrix} \bar{\tilde{t}}_L & \bar{\chi}_+ \end{pmatrix} \begin{pmatrix} \frac{\lambda_1 s_v}{2} & 0 \\ \frac{\lambda_1(1+c_v)}{2\sqrt{2}} & \frac{\lambda_2}{\sqrt{2}} \end{pmatrix} \begin{pmatrix} \tilde{t}_R \\ \tau_+ \end{pmatrix} + \text{h.c}\,. \tag{2.59}$$

We denoted

$$s_v = \sin\sqrt{2\xi}\,, \quad c_v = \cos\sqrt{2\xi}\,, \quad \xi \equiv \frac{v^2}{f^2}\,. \tag{2.60}$$

The physical basis is given by

$$\begin{pmatrix} t_L \\ T_L^+ \end{pmatrix} = \begin{pmatrix} c_L & -s_L \\ s_L & c_L \end{pmatrix} \begin{pmatrix} \tilde{t}_L \\ \chi_+ \end{pmatrix}\,, \tag{2.61}$$

$$\begin{pmatrix} t_R \\ T_R^+ \end{pmatrix} = \begin{pmatrix} c_R & -s_R \\ s_R & c_R \end{pmatrix} \begin{pmatrix} \tilde{t}_R \\ \tau_+ \end{pmatrix}\,, \tag{2.62}$$

with $\sin\theta_{L/R} \equiv s_{L/R}$ and $\cos\theta_{L/R} \equiv c_{L/R}$. The mixing angles are given by [50]

$$\theta_L = \frac{1}{2}\tan^{-1}\left(\frac{2\sqrt{2}\lambda_1^2 s_v(1+c_v)}{4\lambda_2^2 + (1+c_v)^2\lambda_1^2 - 2\lambda_1^2 s_v}\right)\,, \tag{2.63}$$

$$\theta_R = \frac{1}{2}\tan^{-1}\left(\frac{4\lambda_1\lambda_2(1+c_v)}{4\lambda_2^2 - \lambda_1^2(2s_v^2 + (1+c_v)^2)}\right)\,. \tag{2.64}$$

The masses at leading order in ξ are

$$m_t^2 = \frac{1}{\sqrt{2}}\left(\frac{\lambda_1\lambda_2}{\sqrt{\lambda_1^2+\lambda_2^2}}\right)\sqrt{\xi} f\,, \tag{2.65}$$

$$m_{T^+} = \frac{\sqrt{\lambda_1^2+\lambda_2^2}}{\sqrt{2}} f\,. \tag{2.66}$$

The top Yukawa coupling at leading order in ξ is therefore

$$y_t = \frac{\lambda_1\lambda_2}{\sqrt{\lambda_1^2+\lambda_2^2}}\,. \tag{2.67}$$

We shall keep λ_2 as a free parameter and fix λ_1 to produce the correct top Yukawa $y_t \approx 1$. The mixing angles at leading order in ξ are

$$s_L = \frac{\lambda_1^2}{\lambda_1^2+\lambda_2^2}\sqrt{\xi} = \left(\frac{y_t}{\lambda_2}\right)^2\sqrt{\xi}\,, \tag{2.68}$$

$$s_R = \frac{\lambda_1}{\sqrt{\lambda_1^2+\lambda_2^2}} = \frac{y_t}{\lambda_2}\,. \tag{2.69}$$

For the T-odd sector we must introduce a mass term for the doublet similar to the term in Eq. (2.39). To this end, we introduce a RH doublet ψ_R^- transforming non-linearly under $[SU(2)\times U(1)]_L \times [SU(2)\times U(1)]_R$ according to the CCWZ formalism. ψ_R^- is odd under T-parity

$$\psi_R^- \to -\psi_R^- \,. \tag{2.70}$$

The mass term is given by [76]

$$\mathcal{L}_\kappa = \frac{\kappa f}{\sqrt{2}} \left(\overline{\psi}_1 \sigma_2 e^{\frac{i}{f'}\Pi_X} - \overline{\psi}_2 \sigma_2 e^{-\frac{i}{f'}\Pi_X} \right) \psi_R^- + \text{h.c}\,. \tag{2.71}$$

Our spectrum contains a T-odd singlet T^- and a T-odd doublet ψ^- with the following masses

$$m_{T^-} = \frac{\lambda_2}{\sqrt{2}} f\,, \quad m_{\psi^-} = \kappa f\,. \tag{2.72}$$

Lastly, the explicit form of the kinetic terms can be found in App. 2.A.

2.2 Scalar potential

At tree level, the pNBG's interact only through derivative interactions and their classical potential vanishes. The gauge and top sector couplings explicitly break the global symmetry. The classical scalar potential is radiatively generated from fermion and gauge loops. At 1-loop the UV-dependent fermion and gauge loops contributions are given by [30]

$$\begin{aligned} &V_f(H,\Phi,s,\varphi) \\ &= -\frac{N_c}{8\pi^2}\Lambda^2 a_1 \,\text{Tr}\left[M_f M_f^\dagger\right] - \frac{N_c}{16\pi^2} a_2 \text{Tr}\left[\left(M_f M_f^\dagger\right)^2 \log\left(\frac{M_f M_f^\dagger}{\Lambda^2}\right)\right], \end{aligned} \tag{2.73}$$

$$\begin{aligned} &V_{\text{V}}(H,\Phi,s,\varphi) \\ &= \frac{3}{32\pi^2}\Lambda^2 a_3 \,\text{Tr}\left[M_{\text{V}}^2\right] + \frac{3}{64\pi^2} a_4 \text{Tr}\left[M_{\text{V}}^4 \log\left(\frac{M_{\text{V}}^2}{\Lambda^2}\right)\right], \end{aligned} \tag{2.74}$$

respectively. $M_f(H,\Phi,s,\varphi)$ and $M_{\text{V}}^2(H,\Phi,s,\varphi)$ are the fermion and gauge bosons mass matrices in the background of the pNGB's. The a_i parameters with $i = 1,..,4$ are $O(1)$ numbers originating from unknown UV contributions to these operators. $\Lambda \sim 4\pi f$ is the cutoff scale of the theory. Expanding the scalar potential $V = V_f + V_{\text{V}}$ in the NGB fields, we find that

$$V \;=\; m_\Phi^2 \text{Tr}[\Phi^\dagger\Phi] - \mu_h^2 |H|^2 + m_\varphi^2 \text{Tr}[\varphi^2] + \lambda_h |H|^4 + \lambda\, s^2 |H|^2 + \lambda_\varphi s H^\dagger \varphi H + \dots\,. \tag{2.75}$$

We have omitted additional radiatively generated operators that are inconsequential for the upcoming discussions. A detailed analysis of the symmetries of the scalar potential of this model can be found in App. 2.B. In this section we summarize the most important features of the scalar potential.

The mass of the charged triplet Φ is quadratically divergent, $m_\Phi \sim$ a few TeV. We consider energy scales well below m_Φ. We remove Φ from our spectrum by integrating it out. Due to T-parity, integrating out Φ at tree-level does not influence any of the couplings explicitly written in the scalar potential of Eq. (2.75). Like m_Φ^2, the Higgs quartic λ is generated by 1-loop quadratically divergent diagrams.

The rest of the operators in Eq. (2.75), including the Higgs mass term μ_h^2, are generated through logarithmically divergent loops, and as such they exhibit a mild dependence on the UV cutoff scale. The explicit calculations, found in App. 2.B, give us an order of magnitude estimation for the IR contribution to these operators at 1-loop. However quadratically divergent 2-loop diagrams as well as UV contributions can have comparable effects on these operators. Therefore we do not presume to be able to predict these couplings accurately in terms of the fundamental parameters of this model. In this thesis we treat the couplings in Eq. (2.75) as free parameters, except μ_h^2 and λ_h which are fixed to their measured values. Our goal is to allow the free parameters to take values that are reasonable in light of the approximation given by the 1-loop IR contribution, and state explicitly when this is not the case.

In addition to m_φ^2, λ and λ_φ, we must introduce a mass term for the singlet s. The singlet remains massless at 1-loop, and a mass for s is generated at the 2-loop level. We take the pre-EWSB mass term of the singlet, denoted as $\tilde{m}_s^2$, as a free parameter as well. The sizes and ranges of $m_\varphi^2, \lambda_\varphi, \tilde{m}_s^2, \lambda$ are dictated by the DM phenomenology and are discussed in Sec. 2.5.

2.3 LHC phenomenology

2.3.1 T-even singlet T^+

The T-even singlet is responsible for cancelling the quadratically divergent top loop contribution to the Higgs mass, hence it is the standard top partner predicted by composite Higgs models. It can be doubly produced at the LHC via QCD processes, as well as singly produced with an associated third generation quark through the following EW interactions

$$\mathcal{L} \ni \frac{g}{2} C_{bW} \bar{T}_L^+ \not{W} b_L + \frac{g}{2} C_{tZ} \bar{T}_L^+ \not{Z} t_L + \text{h.c}\,. \tag{2.76}$$

In this model,

$$\begin{aligned} C_{bW} =& \sqrt{2} s_L \approx \frac{\sqrt{2\xi}}{\lambda_2^2} \approx 0.35 \left(\frac{1}{\lambda_2}\right)^2 \left(\frac{1\text{ TeV}}{f}\right), \\ C_{tZ} =& \frac{s_L c_L}{c_W} \approx \frac{\sqrt{\xi}}{c_W \lambda_2^2} \approx 0.28 \left(\frac{1}{\lambda_2}\right)^2 \left(\frac{1\text{ TeV}}{f}\right). \end{aligned} \tag{2.77}$$

Decay modes

We consider the limit $m_{T^+} \gg m_H, m_W, m_Z$. In this regime EWSB effects are negligible and we can formally take $\xi \to 0$. The dominant decays of T^+ are to the physical Higgs or to the longitudinal components of the SM gauge bosons with an associated third generation quark, in accordance with the equivalence theorem. We can parameterize the Higgs field in a general R_ξ gauge using these would-be longitudinal components as

$$H = \begin{pmatrix} \phi^+ \\ \frac{1}{\sqrt{2}}(v + h + i\phi_0) \end{pmatrix}. \tag{2.78}$$

The relevant interactions between the Higgs doublet and T^+ are

$$\mathcal{L}_{\text{top}} \ni -\frac{1}{\sqrt{2}} \lambda_1 s_R \left(\bar{t}_L (v + h + i\phi_0) - \sqrt{2} \bar{b}_L \phi^+ \right) T_R^+, \tag{2.79}$$

predicting that in the high energy limit,

$$\text{Br}[T_+ \to h\, t] : \text{Br}[T_+ \to Z\, t] : \text{Br}[T_+ \to W^+ b] = 1 : 1 : 2\,. \tag{2.80}$$

LHC searches

Single production: T_+ can be singly produced at the LHC in association with a third generation quark. A recent search from CMS [79] looked for $(T^+ \to Z\, t)bq$ with a fully leptonic Z decay. The search places a lower bound on the mass of the singlet LH Top partner at 1.2 TeV, assuming negligible width and BR$[T^+ \to Zt] = 0.25$. The bound strongly relies on a model-dependent production cross-section, which in term depends on the coefficients of Eq. (2.77). In the CMS search the coupling is fixed at $C_{bW} = 0.5$. Conservatively we consider the $m_{T^+} > 1.2$ TeV bound at face value, although we expect a smaller value for C_{bW}, as can be seen in Eq. (2.77). C_{bW} is further suppressed for $\lambda_2 > 1$, which is the region in parameters space that, as we later show, is consistent with the LHC constraints on the T-odd top partners masses. The mass of the T-odd singlet is bound from below to be $m_{T^+} > \sqrt{2}f$. The lower bound of 1.2 TeV can be trivially satisfied by taking $f > 850$ GeV.
Double production: T_+ can also be doubly-produced via QCD processes. A recent search from ATLAS [80] looked for a pair produced top partners in a range of final states, assuming that at least one of the top partner decays to th. The quoted nominal bound of the singlet top partner is

$$m_{T^+} > 1.02 \text{ TeV}\,. \tag{2.81}$$

This bound can be satisfied by taking $f > 700$ GeV.

2.3.2 T-odd singlet T^-

The phenomenology of the T-odd singlet resembles that of a stop squark with conserved R-parity. It can be doubly produced at the LHC via QCD processes, and consequently decay to tops and missing energy.

Decay modes

We consider the limit $m_{T^-} \gg m_s, m_{B_H}, m_t$. T^- couples to the singlet ϕ_0 of the original $SU(5)/SO(5)$ coset. In a general R_ξ gauge, ϕ_0 is composed of the physical singlet and the would-be longitudinal component of B_H,

$$\phi_0 = s_0 s + c_0 G_0\,. \tag{2.82}$$

The relevant interactions are

$$\begin{aligned}\mathcal{L}_{\text{top}} &\ni i\lambda_1\sqrt{\frac{2}{5}}\left(\phi_0 \bar{T}^- t_R\right) + \text{h.c} \\ &= i\lambda_1\sqrt{\frac{2}{5}}\left(s_0\, s\, \bar{T}^- t_R + c_0\, G_0\, \bar{T}^- t_R\right) + \text{h.c}\,.\end{aligned} \tag{2.83}$$

Leading to the simple prediction in the high energy limit

$$\Gamma(T^- \to s\, t) : \Gamma(T^- \to B_H t) = \left(\frac{s_0}{c_0}\right)^2 = \frac{r^2}{5}\,. \tag{2.84}$$

LHC searches

We performed a simple recast of recent stop bounds by accounting for the enhanced production cross section of the fermionic T^- relative to the scalar stop squark case. We would like to account for the presence of the T-odd doublet, which contributes to the same final states as T^-. We postpone the derivation of these bounds to Sec. 2.3.3.

2.3.3 T-odd doublet ψ^-

The phenomenology of the T-odd doublet resembles that of a mass-degenerate stop and sbottom squarks with conserved R-parity. The upper (lower) component up ψ^- can be doubly produced at the LHC via QCD processes, and consequently decay to tops (bottoms) and missing energy.

Decay modes

We consider the limit where $m_{\psi^-} \gg m_{B_H}, m_{W_H}, m_s, m_\varphi$. In a general R_ξ gauge, we can express our original pNGB's in terms of the physical pNGB's and the would-be longitudinal modes of the heavy gauge fields defined in Eqs. (2.45) and (2.47),

$$\begin{pmatrix} \tau^a \\ \pi^a \end{pmatrix} = \begin{pmatrix} c_3 & s_3 \\ -s_3 & c_3 \end{pmatrix} \begin{pmatrix} \varphi^a \\ G^a \end{pmatrix} , \tag{2.85}$$

$$\begin{pmatrix} \pi^0 \\ \phi_0 \end{pmatrix} = \begin{pmatrix} c_0 & -s_0 \\ s_0 & c_0 \end{pmatrix} \begin{pmatrix} s \\ G^0 \end{pmatrix} . \tag{2.86}$$

with the mixing angles c_0, c_3, s_0, s_3 defined in Eq. (2.46). The relevant interaction in the $\xi \to 0$ limit originate from $\mathcal{L}_\kappa$. For $(\psi_R^-)^1$,

$$\mathcal{L}_\kappa \ni \frac{i\kappa}{2}\frac{1}{r}\left[(c_0 s - s_0 G_0)\bar{t}_L + (-s_3\varphi_3 + c_3 G_3)\bar{t}_L + \sqrt{2}(-s_3\varphi^- + c_3 G^-)\bar{b}_L\right](\psi_R^-)^1 , \tag{2.87}$$

and similarly for $(\psi_-^R)^2$,

$$\mathcal{L}_\kappa \ni \frac{i\kappa}{2}\frac{1}{r}\left[(c_0 s - s_0 G_0)\bar{b}_L - (-s_3\varphi_3 + c_3 G_3)\bar{b}_L + \sqrt{2}(-s_3\varphi^+ + c_3 G^+)\bar{t}_L\right](\psi_R^-)^2 . \tag{2.88}$$

In the high energy limit

$$\mathrm{Br}[\psi^- \to q\ s] = \frac{c_0^2}{4} , \quad \mathrm{Br}[\psi^- \to q\ G_0] = \frac{s_0^2}{4} , \tag{2.89}$$

$$\mathrm{Br}[\psi^- \to q\ \varphi_3] = \frac{1}{2}[\psi^- \to q\ \varphi_\pm] = \frac{s_3^2}{4} , \tag{2.90}$$

$$\mathrm{Br}[\psi^- \to q\ G_3] = \frac{1}{2}[\psi^- \to q\ G_\pm] = \frac{c_3^2}{4} . \tag{2.91}$$

with the final state with $q = \{b, t\}$ depending on the electric charge of the initial state. The exact branching ratios for ψ^- including EWSB and phase space effects can be found in Fig. 2.1.

LHC searches

The T-odd sector contains two top-like and one bottom-like fermions. We perform a recast of recent bounds on stop and sbottom masses by accounting for the enhanced production cross section of a fermionic colored top partner, along the lines of [81] and [82]. The quoted bounds in Ref. [83] for the stop and sbottom masses are

$$m_{\tilde{t}} \geq 1070\ \mathrm{GeV} , \quad m_{\tilde{b}} \geq 1175\ \mathrm{GeV} , \tag{2.92}$$

respectively. We denote the QCD pair production cross section at $\sqrt{s} = 13$ TeV for a spin s coloured particle with mass M as $\sigma^s_{\mathrm{pair}}(M)$. We require that

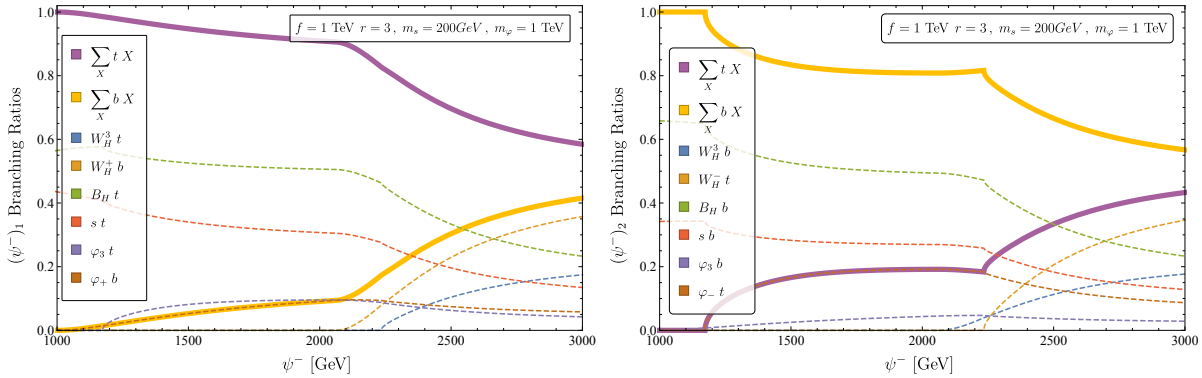

Figure 2.1: *Numeric results for the branching ratios of the upper (lower) component of ψ_- presented in the left (right) panel, with $f = 1$ TeV, $r = 3, m_s = 200$ GeV, $m_\varphi = 1$ TeV and $\lambda_2 = 2.5$. The masses of the heavy gauge boson are fixed at $m_{B_H} = 270$ GeV and $m_{W_H} = 2.1$ TeV. The dashed colored lines indicate the branching ratios to the different exclusive final states. The solid thick lines indicate the sum of branching ratios with either a top (purple curve) or a bottom (yellow curve) at the final state.*

$$\sigma^0_{\text{pair}}(1070\text{ GeV}) \geq \sigma^{1/2}_{\text{pair}}(m_{T^-}) + \sigma^{1/2}_{\text{pair}}(m_{\psi^-}) \times \text{BR}[(\psi_-)_1 \to t + \text{MET}] \tag{2.93}$$

and

$$\sigma^0_{\text{pair}}(1175\text{ GeV}) \geq \sigma^{1/2}_{\text{pair}}(m_{\psi^-}) \times \text{BR}[(\psi_-)_2 \to b + \text{MET}]\,, \tag{2.94}$$

with $m_{\psi^-} = \kappa f$ and $m_{T^-} = \frac{\lambda_2 f}{\sqrt{2}}$ the masses of the T-odd doublet and T-odd singlet top partners respectively. We use $\sigma^0_{\text{pair}}(M)$ reported by the CMS collaboration [84] and $\sigma^{1/2}_{\text{pair}}(M)$ calculated using HATHOR [85]. We conservatively assume all the branching ratios to be 100%. We thus obtain the following lower bounds on the T-odd fermion masses

$$m_{\psi^-}, m_{T_-} > 1.6\text{ TeV}\,. \tag{2.95}$$

The combination of all LHC constrains in the (f, λ_2) plane is shown in the right panel of Fig. 2.2. We summarize the constraints for the couplings for a for a given f,

$$\frac{1.6\text{ TeV}}{f} < \kappa < 4\pi\,, \tag{2.96}$$

$$\text{Max}\left[1, \frac{2.3\text{ TeV}}{f}\right] < \lambda_2 < 4\pi\,. \tag{2.97}$$

2.4 Electroweak precision tests

The main contributions to electroweak precision observables are unaffected by the extended coset structure. The mixing in the left-handed sector generates a correction to the T oblique parameter due to loops of the T-even singlet T^+ [50]

$$T_{T^+} = T_{\text{SM}}\, {s_L}^2 \left[\frac{{s_L}^2}{x_t} - 2 + {s_L}^2 - \frac{2{s_L}^2}{1 - x_t}\log x_t\right], \tag{2.98}$$

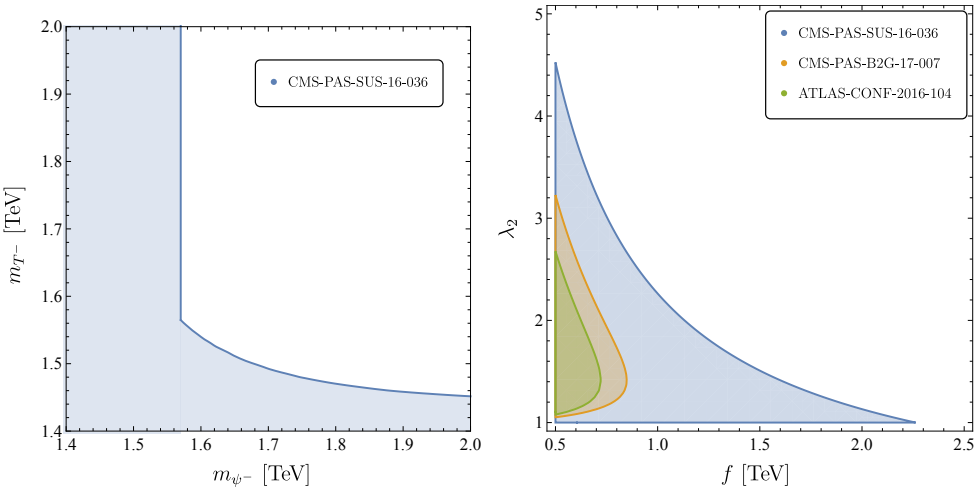

Figure 2.2: *Left Panel: Exclusion limits (blue region) in the (m_{ψ^-}, m_{T^-}) plane, using recasted limits from the CMS SUSY search of Ref. [83]. We impose the condition of Eqs. (2.93) and (2.94), assuming branching ratios of 100%. Right Panel: Exclusion limits in the (f, λ_2) plane using Ref. [83] (blue region, using the bound from Eq. (2.96)), Ref. [79] (orange region) and Ref. [80] (green region).*

with

$$T_{\rm SM} = \frac{3}{16\pi}\,\frac{1}{s_w^2 c_w^2}\,\frac{m_t^2}{m_Z^2} \approx 1.24\,, \quad x_t \equiv \frac{m_t^2}{m_{T^+}^2} \approx \left(\frac{\lambda_2^2-1}{\lambda_2^4}\right)\xi\,, \tag{2.99}$$

and

$$s_L \equiv \sin\theta_L \approxeq \sqrt{\frac{x_t}{\lambda_2^2-1}}\,. \tag{2.100}$$

We express T_{T^+} in terms of x_t using Eq. (2.100). In light of the LHC constrains on the T-even top partner mass of Eq. (2.81), we expect $x_t \leq 0.03 \ll 1$. We therefore expand Eq. (2.98) to leading order in x_t:

$$\begin{aligned}\frac{T_{T^+}}{T_{\rm SM}} &\approx \left(\frac{x_t}{\lambda_2^2-1}\right)\left(2\log\frac{1}{x_t} + \left[\frac{1}{\lambda_2^2-1}\right] - 2\right) \\ &= \left(\frac{\xi}{\lambda_2^4}\right)\left(2\log\left[\frac{\lambda_2^4}{(\lambda_2^2-1)\xi}\right] + \left[\frac{1}{\lambda_2^2-1}\right] - 2\right)\,.\end{aligned} \tag{2.101}$$

An additional contribution to the T parameter is due to loops of T-odd heavy gauge bosons. The correction is proportional to the mass splitting after EWSB,

$$\Delta m_{W_H}^2 \equiv m_{W_H^3}^2 - m_{W_H^\pm}^2 = \frac{1}{2} f^2 g^2 \sin^4\left(\sqrt{\frac{\xi}{2}}\right)\,, \tag{2.102}$$

neglecting corrections of order $O(g'^2)$. The T-odd gauge loops generate the following correction to the T parameter [50]

$$\begin{aligned}T_{W_H} &= -\frac{9}{16\pi c_w^2 s_w^2 M_Z^2}\Delta m_{W_H}^2 \log\left(\frac{\Lambda^2}{f^2 g^2(1+r^2)}\right) \\ &= -\frac{9}{16\pi s_w^2}\xi\log\left(\frac{\Lambda}{fg\sqrt{1+r^2}}\right)\,.\end{aligned} \tag{2.103}$$

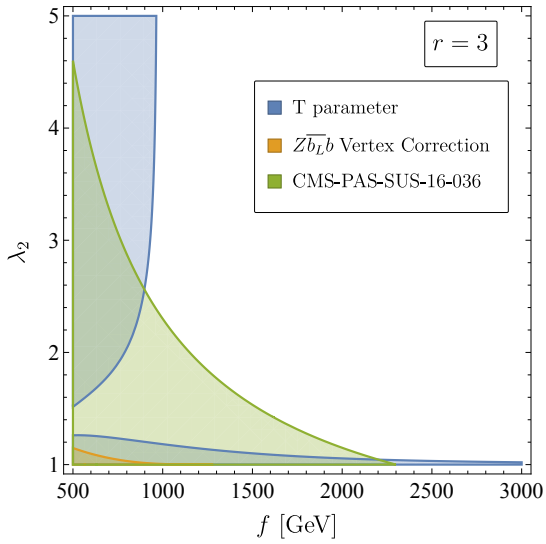

Figure 2.3: *Combined EWPT and LHC exclusion regions in the (f, λ_2) plane, for $r = 3$ and $\Lambda = 4\pi f$. The EWPT exclusion regions due to T-parameter (blue region) and $\delta g_L^{Z\bar{b}b}$ (orange region) are plotted at the 3σ level using the results of Ref. [86], $T = 0.12 \pm 0.07$ and $\delta g_L^{b\bar{b}} = 0.002 \pm 0.001$. The LHC exclusion (green region) is due to Ref. [83] using the lower bound of Eq. (2.96).*

This correction is λ_2 independent, and becomes the dominant one for higher values of λ_2 as $T_{T^+} \to 0$. We assume that the UV contributions to these loop processes are sub-leading with respect to the log-enhanced IR contribution.

Let us mention that the oblique S and U parameters also receive corrections due to the mixing the LH fermion sector. As noted in Ref. [50], the size of these corrections are an order of magnitude smaller than the correction to the T parameter and are therefore sub-leading. Additionally, the $Z\bar{b}_L b_L$ vertex receives corrections due to T_+ loops [50]

$$\delta g_L^{Z\bar{b}b} = \frac{g}{c_w}\frac{\alpha}{8\pi s_w^2}\frac{m_t^4}{m_W^2 m_{T^+}^2}\left(\frac{1}{\lambda_2^2 - 1}\right)\log\frac{m_{T^+}^2}{m_t^2}\,, \tag{2.104}$$

with $\delta g_L^{Z\bar{b}b} \equiv g_L^{Z\bar{b}b} - g_{L\,\mathrm{SM}}^{Z\bar{b}b}$ and $g_{L\,\mathrm{SM}}^{Z\bar{b}b} = -\frac{1}{2} + \frac{s_w^2}{3}$. We constrain the parameters of the model using the results of Ref. [86], namely

$$T = 0.12 \pm 0.07\,, \quad \delta g_L^{Z\bar{b}b} = 0.002 \pm 0.001\,. \tag{2.105}$$

The combinations of the EWPT and LHC constraints are plotted in Fig. 2.3. For $f \lesssim 1.5$ TeV, values of $\lambda_2 < 1.5$ are excluded by LHC. The correction T_{T^+} decreases as λ_2 increases, and in the allowed regions we find that $T_{W_H} \gg T_{T^+}$. We conclude that the correction from T-odd gauge loops to the T-parameter is the dominant constraint in the allowed region where λ_2 is large. We find the following lower bound on f from Eq. (2.103) at 3σ after taking $\Lambda = 4\pi f$

$$\begin{aligned} f >& (1240\ \mathrm{GeV}) \times \sqrt{1 - \frac{1}{6}\log(1 + r^2)} \\ &\approx (970\ \mathrm{GeV}) \ \times \ (1 - 0.08(r - 3)))\,. \end{aligned} \tag{2.106}$$

Therefore we set the lower bound on the symmetry breaking scale to be $f > 1$ TeV.

2.5 DM phenomenology

2.5.1 Spectrum

The lightest T-odd particle (LTP) in the spectrum is stable and therefore a natural DM candidate. One possible LTP is the gauge field B_H. This possibility has been considered in the past in the context of the original LHT model [87]. In this thesis we explore the possibility of DM being part of the composite scalar sector, in particular the singlet s. The singlet mass m_s is a free parameter in our model. The mass m_{B_H}, given in Eq. (2.42), is of order $O(200)$ GeV. The region in which s is the LTP corresponds to $r \sim 2-3$ and thus would be the focus of our study. In this region we may safely neglect co-annihilation effects of s with B_H. Since larger values of r correspond to heavier T-odd gauge bosons, one might be concerned that the gauge contribution to the Higgs mass suffers from larger tuning. However, by comparing the logarithmically divergent contributions to the Higgs mass from the gauge and top sector

$$\frac{\mu^2_{\text{gauge}}}{\mu^2_{\text{top}}} \sim \frac{g^4(1+r^2)}{\lambda_1^2\lambda_2^2} \sim \left(\frac{g^4}{\lambda_2^2}\right)(1+r^2) \sim \text{a few precent} \times (1+r^2)\,, \tag{2.107}$$

one finds that the gauge contributions is in any case negligible compared to the dominant contribution of the top sector, which remain the dominant source of tuning in the model.

2.5.2 Singlet-triplet mixing

The last term of the scalar potential in Eq. (2.75) induces mixing between the singlet s and the neutral component of the triplet φ_3 after EWSB. The effects of singlet-triplet mixing on the DM phenomenology have been considered in Ref. [88]. We focus on the composite nature of the singlet DM. For simplicity, we limit ourselves to the region in parameter space where we may neglect the mixing effects. The mixing angle is given by

$$\sin^2\theta_{s\varphi} = \frac{1}{2}\left[1-\sqrt{\frac{1}{1+t^2}}\right] = \frac{t^2}{4}+O(t^4)\,, \tag{2.108a}$$

$$t \equiv \frac{1}{2}\frac{\lambda_\varphi v^2}{|m_\varphi^2 - m_s^2|}\,. \tag{2.108b}$$

Assuming for simplicity that $m_s \sim v, \lambda_\varphi \sim 1$ and demanding conservatively that $\sin\theta_{s\varphi} < 5\%$, we find the following lower bound

$$\frac{m_\varphi}{m_s} \gtrsim 2.5\,, \tag{2.109}$$

which implies $m_\varphi \gtrsim 600$ GeV, consistent with current collider bounds. [1] We note that the assumption $\lambda_\varphi \sim 1$ as well as the lower bound on m_φ are consistent with the IR contribution of Eq. (2.75) to these operators. We find that the operator corresponding to λ_φ enjoys an accidental factor ~ 5 enhancement to its coefficient in the CW potential. The IR contributions can be found in App. 2.B in Eqs. (2.180) and (2.181). We conclude that a moderate mass separation is sufficient in order to neglect the singlet-triplet mixing effects.

[1] The LHC phenomenology of φ resembles that of the Wino, which implies that the charged components can be doubly produced via electroweak processes and decay to $W^\pm$ and missing energy. However, the relevant SUSY searches, e.g [89, 90] , do not pose strong constraints on m_φ, especially in light of the reduced production cross section of the scalar triplet in comparison to the fermionic Wino.

2.5.3 Annihilation cross section

The DM relic abundance is calculated by solving the Boltzmann equation for the particle density [72]

$$\dot{n}_s + 3Hn_s = -\langle\sigma v\rangle \left[n_s^2 - (n_s^{\rm EQ})^2\right] . \tag{2.110}$$

The thermally averaged cross section for a non-relativistic gas at temperature T is given by [91]

$$\langle\sigma v\rangle = \frac{\int_{4m_s^2}^{\infty} {\rm d}s\ \sigma(s-4m_s^2)\sqrt{s}K_1(\sqrt{s}/T)}{8m_s^4 T K_2^2(m/T)} , \tag{2.111}$$

and the usual approximation yields [72]

$$\frac{\Omega_s h^2}{0.12} \approx \left(\frac{3\ \times\ 10^{-26}\ {\rm cm}^3\ {\rm s}^{-1}}{\langle\sigma v\rangle}\right) = \left(\frac{1\ {\rm pb\ c}}{\langle\sigma v\rangle}\right) . \tag{2.112}$$

The measured DM relic abundance is [92]

$$\Omega_{\rm DM} h^2 = 0.1199 \pm 0.0027 . \tag{2.113}$$

In the following we consider three types of interactions relevant to our model that determine the annihilation cross section, the Higgs portal, the derivative couplings and the contact term [73, 93].

Higgs portal

Due to the explicit breaking of the global symmetry, the scalar potential of Eq. (2.75) is generated radiatively, and in particular the following operators are present in the theory

$$\mathcal{L} \supset -\frac{1}{2}\tilde{m}_s^2 s^2 - \lambda\, s^2 H^\dagger H . \tag{2.114}$$

λ is the usual Higgs portal coupling of the singlet DM model [94, 95, 96]. The Higgs mediates s-channel annihilation to SM gauge fields and fermions. The annihilation channel $ss \to hh$ is also possible via the s,t and u channels as well as directly via the dimension 4 operator s^2h^2. We assume that freeze-out occurs after the EW phase transition. In unitary gauge, we can rewrite Eq. (2.114) as

$$\mathcal{L} \supset -\frac{1}{2}\left(\tilde{m}_s^2 + \lambda v^2\right) s^2 - \lambda v\ s^2 h - \frac{\lambda}{2} s^2 h^2 . \tag{2.115}$$

We define the physical mass of the singlet

$$m_s^2 \equiv \tilde{m}_s^2 + \lambda v^2 . \tag{2.116}$$

As discussed in Sec. 2.2, we take m_s, λ to be free parameters. We note a posteriori that the phenomenologically viable regions not excluded by direct detection have $\lambda \lesssim 1\%$. The naive IR contribution to λ is $O(10\%)$. To obtain a viable model we assume that additional contributions generate cancellations of order a few in order for the Higgs portal coupling to take smaller values. These additional contributions can originate from UV physics, e.g loops of heavier resonances, and higher loop order diagrams containing the lightest top partners . The latter can be quadratically dependent on the UV scale, since we expect the collective breaking mechanism to break down at higher loop order. These additional contributions are expected to be comparable to the leading logarithmic contributions, allowing a substantial cancelation with the leading order contributions to take place in some parts of parameter space.

Goldstone derivative interaction

The kinetic term of the non linear sigma model of Eq. (2.40) contains derivative interactions among the Goldstone fields, in particular in the unitary gauge (before EWSB)

$$\mathcal{L}_{nl\sigma} \supset \frac{1}{2}(\partial_\mu h)^2 + \frac{1}{2}(\partial_\mu s)^2 - \frac{5s_0^2}{24f^2}(s\partial_\mu h - h\partial_\mu s)^2 \,. \tag{2.117}$$

We can remove the derivative terms that contribute to the direct detection cross-sections (namely $h^2(\partial_\mu s)^2$ and $s^2(\partial_\mu h)^2$) by the non-linear transformation

$$h \to h\left(1 + \frac{5s_0^2}{24f^2}s^2\right) \,, \quad s \to s\left(1 + \frac{5s_0^2}{24f^2}h^2\right) \,. \tag{2.118}$$

In this new basis the leading order derivative interactions are

$$\mathcal{L}_{nl\sigma} \supset \frac{1}{2}(\partial_\mu h)^2 + \frac{1}{2}(\partial_\mu s)^2 + \frac{5s_0^2}{16f^2}\partial_\mu h^2 \partial^\mu s^2 \,, \tag{2.119}$$

The transformation of Eq. (2.118) changes the form of the scalar potential, in particular it generates a shift in the portal coupling

$$\lambda \to \lambda + \frac{5s_0^2\,(m_h^2 + m_s^2)}{12f^2} \,. \tag{2.120}$$

In this new basis, the effect of the derivative interactions are disentangled: the term in Eq. (2.119) contributes to the s-channel annihilation of DM after EWSB, and its contribution scales like m_s^2/f^2. As discussed below, the derivative interaction interferes with the portal coupling λ. The λ in the old basis is effectively larger, as seen in Eq. (2.120). This is is due to the derivative interactions of the old basis, and the effective portal coupling has an additional contribution proportional to $s_0^2 m_s^2/f^2, s_0^2 m_h^2/f^2 \sim 10^{-3}$ for $f \sim 1$ TeV and $r = 3$. Importantly , the derivative interaction term of Eq. (2.119) is suppressed in the elastic scattering probed by direct detection experiments.

Contact term

The non-renormalizable nature of the theory and the mixing in the top sector leads to the appearance of the following contact term,

$$\mathcal{L}_{\rm top} \supset -c_{tt\,ss}\, m_t \bar{t}t \frac{s^2}{v^2} \tag{2.121}$$

with

$$c_{tt\,ss} = s_0^2\left[c_L\left(\frac{7\xi}{15}\right) + \frac{4}{5}s_L\sqrt{\xi}\right] \,. \tag{2.122}$$

As opposed to the standard singlet DM which interacts with the SM only through the Higgs portal, this dimension 5 operator allows the singlet to annihilate directly into tops without the mediation of the Higgs. Similarly to the derivative interactions, the contact term becomes increasingly important at higher energies. At leading order in ξ, we obtain

$$c_{s^2\bar{t}t} = \frac{7s_0^2}{15}\left(1 + \frac{12}{7\lambda_2^2}\right)\xi + O(\xi^2) \,. \tag{2.123}$$

Note that both the derivative interactions and the dim. 5 contact term scale with s_0^2. The $r \to \infty$ limit correspond for $f' \gg f$. In this limit $s \approx \phi_0$ (with ϕ_0 the singlet that belongs to the $SU(5)/SO(5)$ coset) and the derivative interactions are at the maximal value as $s_0 \to 1$. In the opposite regime, $r \to 0$, which corresponds to $f' \ll f$, the DM is comprised almost entirely of $s \approx \pi_0$ (with π_0 the singlet that belongs to the $[SO(2) \times U(1)]^2/[SU(2) \times U(1)]$ coset). h and π_0 are decoupled since they belong to different cosets, and the derivative interactions between h and s are effectively shut down as $s_0 \to 0$.

2.5.4 Relic abundance

We can characterize the DM phenomenology in 3 distinct mass regions, see also [97]. In the first region where $m_s \ll \sqrt{\lambda_{\rm DM}} f$, all the effects of the interactions originating from higher dimensional operators, namely the derivative interactions and contact term, are negligible compared to the portal coupling interaction. The DM phenomenology in this region coincides with the standard singlet DM [94, 95, 96]. In regions where $m_s \sim \sqrt{\lambda_{\rm DM}} f$, the effect of higher dimensional operators becomes comparable with the marginal portal coupling operator. In particular we find a destructive interference between the Higgs portal coupling and the derivative interactions. Lastly, for heavy DM masses $m_s \gg \sqrt{\lambda_{\rm DM}} f$, the higher dimensional derivative operators dominate. For the following discussion it would be useful to parameterize the thermal cross section as

$$\begin{aligned} \langle \sigma v \rangle &= \sigma_0(x) \left[(\lambda - f_1(x))^2 + f_2(x) \Theta(m_s - m_t) \right], \\ x &\equiv \frac{m_s}{f}. \end{aligned} \tag{2.124}$$

σ_0, f_1, f_2 are monotonically increasing functions of x. Furthermore, σ_0, f_1, f_2 depend in general on f, r, λ_2. $f_1(x)$ parametrizes the destructive effects of the dimension 6 operator of Eq. (2.117), hence we expect $f_1 \sim x^2$. $f_2(x)$ accounts for the dimension 5 operator of Eq. (2.121), which allows the singlet to annihilate into two tops independently of the Higgs interactions, therefore we expect $f_2 \sim x$.

Portal coupling dominance

In regions of parameter space where

$$m_s \ll \sqrt{\lambda_{\rm DM}} f, \tag{2.125}$$

the composite features of the DM are negligible, and the phenomenology is that of the standard singlet DM [94, 95, 96], where irrelevant operators are irrelevant. In this area of parameter space, the thermally averaged cross section is approximately

$$\langle \sigma v \rangle \approx \sigma_0(x) \lambda^2, \tag{2.126}$$

and the observed relic abundance is produced for

$$\lambda^+(x) \approx \sqrt{\frac{1 \text{ pb}}{\sigma_0(x)}}. \tag{2.127}$$

For $\lambda < \lambda^+$ the singlet is over-abundant. These regions are experimentally excluded. In the range $\lambda > \lambda^+$ the singlet is under-abundant. In this region an additional source of DM must be present in order to account for the observed relic abundance. For a fixed value of f, this region is characterized by a large portal couplings or small DM masses. The mass region $m_s < m_h/2$ is severely constrained by the LHC due to the Higgs invisible width to singlets. For $m_s \approx m_h/2$,

the Higgs mediator is resonantly produced and $\lambda_{\rm DM}$ must be extremely suppressed in order to produce the correct relic abundance, making this finely tuned region hard to probe experimentally. We shall focus on DM masses above $m_h/2$ the avoid the above-mentioned issues.

This region can be seen in the left panel of Fig. 2.4 where $m_s < 150$ GeV. In this region the total annihilation cross section for a fixed portal coupling decreases with m_s, as expected in the standard singlet DM scenario for $m_s > m_h/2$. In the right panel of Fig. 2.4, the portal coupling dominance region is to the right of the minima of the curves. In this region, for a fixed value of the mass, the total annihilation cross section increases with λ.

Contact term dominance

In region of masses where

$$m_s \sim \sqrt{\lambda_{\rm DM}} f \,, \tag{2.128}$$

the derivative interactions and Higgs portal are comparable. In this region $\lambda \sim x^2 \sim f_1(x)$ such that the portal coupling and derivative interactions interfere destructively, implying that

$$\langle \sigma v \rangle \approx \sigma_0 f_2(x) \Theta(m_s - m_t) \,. \tag{2.129}$$

In regions where $x < m_t/f$, $\langle \sigma v \rangle$ becomes arbitrarily small and the singlet is over-abundant. This parameter space is experimentally excluded. In the range where $x > m_t/f$ we find that $\langle \sigma v \rangle$ is positive since the singlet is kinematically allowed to decay into tops. For a particular value $x = x_{\rm max}$ defined by

$$\sigma_0(x_{\rm max}) f_2(x_{\rm max}) = 1 \text{ pb} \,, \tag{2.130}$$

the observed relic abundance is produced. In the parameter space where $m_t/f < x < x_{\rm max}$ we find that $\langle \sigma v \rangle < 1$ pb and the singlet is over-abundant. This range is also experimentally excluded. For coupling and masses such that $x_{\rm max} < x$ we find that $\langle \sigma v \rangle > 1$ pb and the singlet is under-abundant. In this region an additional source of DM must be present in order to account for the observed relic abundance. We conclude that for a given point in (λ_2, r, f) parameter space, the largest DM mass for which the singlet can account for the entire DM relic abundance is therefore given by $m_s^{\rm max} = \sqrt{x_{\rm max}} f$.

The relevant parameter space in the left panel of Fig. 2.4 corresponds to the region where $m_s \sim 220$ GeV, close to the minimal value of the cross section. The annihilation to the Higgs and gauge bosons is effectively suppressed by the destructive interference between the portal coupling and the derivative interactions. As this suppression occurs where $m_s > m_t$, the remaining annihilation cross section is exclusively to tops. In the right panel of Fig. 2.4, the minima of the different curves are precisely mapped to this area of maximal interference. For the fixed mass $m_s = 150$ GeV, the singlet is not allowed kinematically to decay into tops and the annihilation cross section vanishes. Conversely, for $m_s = 200$ GeV the decay into tops is allowed and the annihilation cross section is dominated by the contact term. Lastly, the minimum of the curve corresponding to $m_s = 250$ GeV is approximately 1 pb, meaning that for this particular point in the (λ_2, r, f) parameter space, $x_{\rm max} \approx 250/1000 = 1/4$.

Derivative interaction dominance

In the regions of parameters space where

$$m_s \gg \sqrt{\lambda_{\rm DM}} f \,, \tag{2.131}$$

the irrelevant operators, namely the dimension 6 operators corresponding to the derivative interactions, are dominating, and the annihilation cross section grows with the singlet mass. The observed relic abundance is produced for

$$\lambda^- \approx f_1(x) - \sqrt{\frac{1\text{ pb}}{\sigma_0(x)} - f_2(x)\Theta(m_s - m_t)} \tag{2.132}$$

for $x > x_{\min}$, with $x_{\min}$ defined by

$$f_1(x_{\min}) = \sqrt{\frac{1\text{ pb}}{\sigma_0(x_{\min})} - f_2(x_{\min})\Theta(x_{\min} - \frac{m_t}{f})}\,. \tag{2.133}$$

For $x \sim x_{\min}$ the correct relic abundance is recovered with $\lambda^- \ll 1$ and with DM mass $m_s^{\min} \equiv \sqrt{x_{\min}} f$. The nuclear cross section is typically $\sim 10^{-11}$ pb, beyond the reach of current direct detection experiments. For $\lambda > \lambda^-$ the singlet is over-abundant. This regions are experimentally excluded. In the region $\lambda < \lambda^-$ the singlet is under-abundant. In this region an additional source of DM must be present in order to account for the observed relic abundance.

In the left panel of Fig. 2.4, the derivative interactions become dominant at $m_s > 225$ GeV. The total annihilation cross section increases with m_s for a fixed λ, and the annihilation channels to the Higgs and gauge bosons become dominant compared to the annihilation channel to tops. In the right panel of Fig. 2.4 the derivative interactions dominance region can be identified to the left of the minima, where λ is small. The annihilation cross section increases as λ decreases. In this region smaller values of λ correspond to smaller destructive interference between the portal coupling and the derivative interactions, and therefore an increased overall annihilation cross section. For the curve corresponding to $m_s = 150$ GeV, we see that $\lambda^+ \approx 0.065$ and $\lambda^- \ll 1$, meaning that for this particular point in the (λ_2, r, f) parameter space, $x_{\min} \approx 150/1000 = 0.15$.

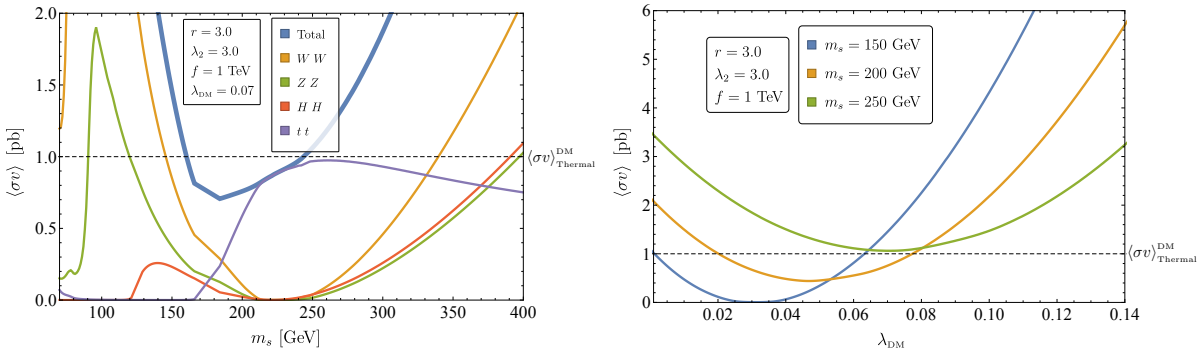

Figure 2.4: Left panel: *The thermally averaged cross section as a function of the DM mass m_s for $\lambda = 0.07$, $f = 1000$ GeV, $r = 3$ and $\lambda_2 = 3$. The dashed line at $\langle\sigma v\rangle = 1$ pb represents the cross section that produces the correct relic abundance according to Eq. (2.112).* Right panel: *The thermally averaged cross section as a function of λ for different values of m_s with $f = 1000$ GeV, $r = 3$ and $\lambda_2 = 3$. The dashed line at $\langle\sigma v\rangle = 1$ pb represents the cross section that produces the correct relic abundance according to Eq. (2.112).*

2.5.5 Direct detection

The model was implemented using FeynRules [98] and exported to `micrOMEGAs` [99]. The strongest direct detection bounds are due to XENON1T [100] after 34.2 live days. Scan results for this model can be seen in Fig. 2.5. The two branches appearing in each panel represent the

two possible solutions for λ for each mass value which produce the observed relic abundance. The branches meet at some maximal DM mass, above which the singlet is always under-abundant. The upper branch is ruled out by direct detection. Some of the lower branch is still consistent with experimental bounds. In the region where $m_s \approx \sqrt{x_{\min}} f$, λ can be arbitrarily small, thus avoiding direct detection. In this regions, the theory gives a sharp prediction for the DM mass. At mentioned previously, the naive IR contribution to λ is too big and of $O(10\%)$. We therefore assume that additional contributions from UV physics and higher loops generate mild cancellations, allowing this coupling to take the allowed $O(1\%)$ values.
Note that the 34.2 live days XENON1T bounds are sensitive to $\lambda \sim 10^{-2} \gg s_0^2 m_s^2/f^2 \sim 10^{-3}$, therefore the bounds are insensitive to the value of m_s (except for a slight mass-dependence coming the Xenon bound itself, which becomes less sensitivity for higher DM masses). The 1.1 yrs $\times$ Ton live days XENON1T bounds, on the other hand, are sensitive to much lower values $\lambda \sim 10^{-3}$, which becomes comparable to the $s_0^2 m_s^2/f^2$ contribution of the derivative interactions shown in Eq. (2.120). As expected, this effect is clearly more visible for lower values of f, and the direct detection bounds become stronger for higher values of m_s, see left panel of Fig. 2.5.

The impact of varying λ_2, r for a fixed value of f can be seen in Fig. 2.6. The largest effect is seen for increasing r, which in turn raises the importance of the non-renormalizable interactions at lower DM masses. A smaller effect due to the increase of λ_2 can be seen in the meeting point of the two branches. Larger values of λ_2 decrease the contact term, pushing $m_s^{\max} = \sqrt{x_{\max}} f$ to higher values.

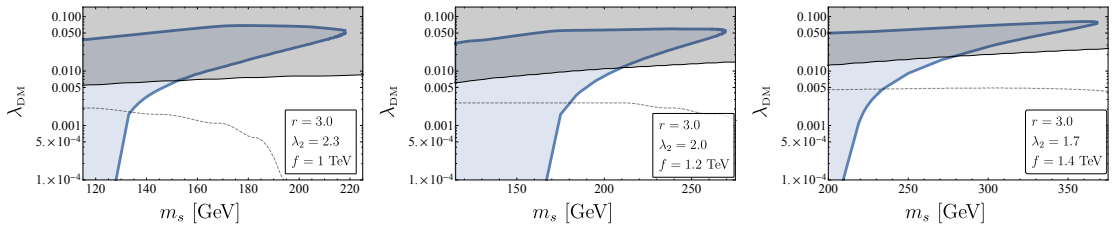

Figure 2.5: *Singlet relic abundance in the $\{m_s, \lambda = \lambda_{DM}\}$ plane for $f = 1$ TeV (left), $f = 1.2$ TeV (middle) and $f = 1.4$ TeV (right), for fixed $r = 3$ and minimal $\lambda_2 \sim \frac{2300\ GeV}{f}$. The solid blue lines represent areas where $\Omega_s = \Omega_{DM}$. The blue areas are regions where $\Omega_s > \Omega_{DM}$, and therefore are excluded. The grey regions are excluded by XENON1T [100] after 34.2 live days. The Dashed lines are the projected sensitivities for XENON1T at 1.1 yrs $\times$ Ton [101].*

2.A The complete Lagrangian

The model is defined by the global symmetry

$$\mathcal{G} \;=\; SU(5) \times [SU(2)_L \times U(1)_L] \times [SU(2)_R \times U(1)_R] \times U(1)_Q \,. \tag{2.134}$$

A global unbroken $U(1)_Q$ is added in order to fix the hyper charges of the matter fields. $SU(5)$ contains two $SU(2) \times U(1)$ subgroups defined in Eqs. (1.22) and (1.23), denoted by $[SU(2) \times U(1)]_{1/2}$. We gauge the following subgroup

$$SU(2)_{1+L} \times U(1)_{1+L+Q} \times SU(2)_{2+R} \times U(1)_{2+R+Q} \,. \tag{2.135}$$

We implicitly include $SU(3)_c$ as an external gauge symmetry. We introduce fields in representations of $\mathcal{G}$ denoted by $(\mathcal{R}, \mathcal{R}_L, \mathcal{R}_R)_{q_L, q_R, q_Q}$. A generic representation of Eq. (2.134) is mapped

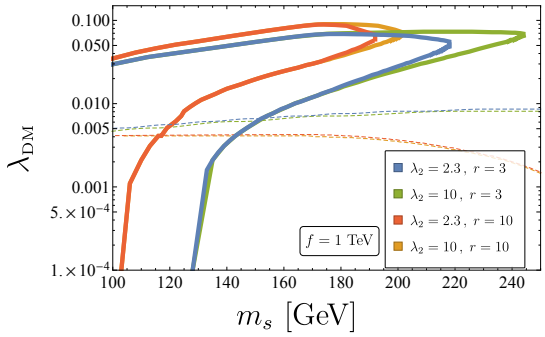

Figure 2.6: *The effects of changing r and λ_2 on the relic abundance curves, shown as solid curves. The dashed curves represent the XENON1T [100] bounds after 34.2 live days. Increasing r has similar effects to lowering f - the coefficients of the non-renormalizable terms increase and their effect is noticeable at lower DM masses. Increasing λ_2 reduces the size of the coefficient of the dimension 5 contact term, therefore increasing $m_s^{max} = \sqrt{x_{max}} f$.*

under T-parity to

$$(\mathcal{R}, \mathcal{R}_L, \mathcal{R}_R)_{q_L, q_R, q_Q} \to (\overline{\mathcal{R}}, \mathcal{R}_R, \mathcal{R}_L)_{q_R, q_L, q_Q} \,. \tag{2.136}$$

The representation $\overline{\mathcal{R}}$ is defined by the automorphism of Eq. (2.2). The Lagrangian is described by the following sum

$$\mathcal{L} = \mathcal{L}_{\text{gauge}} + \mathcal{L}_{\text{kin}} + \mathcal{L}_{\text{top}} + \mathcal{L}_{\kappa} \,. \tag{2.137}$$

The gauge kinetic terms are given as usual by

$$\mathcal{L}_{\text{gauge}} = \; - \; \frac{1}{4} \sum_{i=1,2} W_{ia}^{\mu\nu} W_{\mu\nu}^{ia} - \frac{1}{4} \sum_{i=1,2} B_i^{\mu\nu} B_{\mu\nu}^i - \frac{1}{4} G_a^{\mu\nu} G_{\mu\nu}^a \,. \tag{2.138}$$

We introduce two scalar fields with the following $\mathcal{G}$ representation

$$\Sigma : (\mathbf{15}, \mathbf{1}, \mathbf{1})_{0,0,0} \,, \quad X : (\mathbf{1}, \mathbf{2}, \overline{\mathbf{2}})_{q_X, -q_X, 0} \,. \tag{2.139}$$

The charges of X under $U(1)_L \times U(1)_R$ are constrained by the requirement to preserve the T-even combination $U(1)_{R+L}$. We determine the value of q_X in Eq. (2.154). The global symmetry is spontaneously broken by the VEV's of Σ and X with the following coset structure

$$\frac{SU(5)}{SO(5)} \times \frac{[SU(2) \times U(1)]_L \times [SU(2) \times U(1)]_R \times U(1)_Q}{[SU(2) \times U(1)]_{L+R} \times U(1)_Q} \,. \tag{2.140}$$

We parametrize Σ and X following Eqs. (1.21) and (2.33) and write down the kinetic terms of the non-linear sigma model

$$\mathcal{L}_{\text{nl}\sigma} = \quad \frac{f^2}{8} \text{Tr}[(D_\mu \Sigma)(D^\mu \Sigma^*)] + \frac{f'^2}{4} \text{Tr}[(D_\mu X)(D^\mu X^\dagger)] \,, \tag{2.141}$$

with

$$D\Sigma \;\; = \;\; \partial \Sigma - i \sum_{i=1,2} g_i W_i^a (Q_i^a \Sigma + \Sigma Q_i^{aT}) - i \sum_{i=1,2} g_i' B_i (Y_i \Sigma + \Sigma Y_i^T) \,, \tag{2.142}$$

$$DX \;\; = \;\; \partial X - \frac{i}{2} (g_1 W_1^a \sigma^a X - g_2 W_2^a X \sigma^a) - i q_X (g_1' B_1 - g_2' B_2) \,. \tag{2.143}$$

T-parity dictates that

$$g_1 = g_2 = \sqrt{2}g\,, \quad g_1' = g_2' = \sqrt{2}g'\,, \tag{2.144}$$

with g, g' the SM gauge couplings.
The matter sector contains the following linearly transforming fields

$$\Psi_1 = \begin{pmatrix}\psi_1\\ \chi_1\\ 0\end{pmatrix} : (\overline{\mathbf{5}}, \mathbf{1}, \mathbf{1})_{0,0,\frac{1}{3}}\,, \quad \Psi_2 = \begin{pmatrix}0\\ \chi_2\\ \psi_2\end{pmatrix} : (\mathbf{5}, \mathbf{1}, \mathbf{1})_{0,0,\frac{1}{3}}\,, \tag{2.145}$$

as well as the singlets

$$\tau_1 : (\mathbf{1}, \mathbf{1}, \mathbf{1})_{\frac{8}{15},\frac{2}{15},0}\,, \quad \tau_2 : (\mathbf{1}, \mathbf{1}, \mathbf{1})_{\frac{2}{15},\frac{8}{15},0}\,, \quad \tilde{t}_R : (\mathbf{1}, \mathbf{1}, \mathbf{1})_{0,0,\frac{1}{3}}\,. \tag{2.146}$$

We introduce a non linearly transforming doublet ψ_R^-. Non-linear representations are described in terms of representations of the unbroken subgroup

$$\mathcal{H} = SO(5) \times SU(2)_{L+R} \times U(1)_{L+R} \times U(1)_Q\,. \tag{2.147}$$

ψ_R^- transforms non-linearly under the full global group $\mathcal{G}$ using the CCWZ formalism. In our case

$$\psi_R^- : (\mathbf{1}, \mathbf{2})_{q_X, q_\psi} \text{ under } \mathcal{H}\,. \tag{2.148}$$

The $U(1)_Q$ charge of ψ_R^- , denoted here by q_ψ, is determined in Eq. (2.154). q_X is the same charge appearing in Eq. (2.143). Under T-parity,

$$\Psi_1 \to \Omega\Sigma_0\Psi_2\,, \quad \tau_1 \leftrightarrow \tau_2\,, \tag{2.149a}$$
$$\tilde{t}_R \to \tilde{t}_R\,, \quad \psi_R^- \to -\psi_R^-\,. \tag{2.149b}$$

The $U(1)$ charge assignments are fixed by matching the required SM hyper charges and requiring that all the gauged $U(1)$ symmetries are conserved. The SM hyper charge is given by

$$Y_{\rm SM} = Y_1 + Y_2 + q_L + q_R + 2q_Q\,. \tag{2.150}$$

e.g for ψ_1,

$$Y_{\rm SM} = -\frac{3}{10} - \frac{2}{10} + 0 + 0 + 2 \times \frac{1}{3} = \frac{1}{6}\,. \tag{2.151}$$

Let us determine the q_X and q_ψ charges.
Defining $U \equiv e^{\frac{i\Pi_X}{f'}}$, the combinations $U\psi_R^-$ and $U^\dagger\psi_R^-$ transform linearly under the global group

$$U\psi_R^- : (\mathbf{1}, \mathbf{2}, \mathbf{1})_{q_X,0,q_\psi}\,, \quad U^\dagger\psi_R^- : (\mathbf{1}, \mathbf{1}, \mathbf{2})_{0,q_X,q_\psi}\,. \tag{2.152}$$

Using these identifications as linear representations, it is clear that conservation of $U(1)_{1+L+Q}$ and $U(1)_{2+R+Q}$, e.g in the first term of Eq. (2.71), requires

$$-\left(-\frac{3}{10} + \frac{1}{3}\right) + q_X + q_\psi = 0 \tag{2.153}$$

and

$$-\left(-\frac{1}{5} + \frac{1}{3}\right) + q_\psi = 0 \to q_\psi = \frac{2}{15}\,,\ q_X = -\frac{1}{10}\,. \tag{2.154}$$

We introduce the kinetic terms

$$\begin{aligned}\mathcal{L}_{\rm kin} &= i\sum_{i=1,2}\overline{\Psi}_i \not{D}\Psi_i + i\sum_{i=1,2}\overline{\tau}_i\not{D}\tau_i \\ &\quad + i\overline{\tilde{t}_R}\not{D}\tilde{t}_R + i\overline{\psi_R^-}\not{D}\psi_R^- \,. \end{aligned} \tag{2.155}$$

The kinetic term for the non-linearly transforming doublet ψ_R^- is given by

$$D_\mu\psi_R^- = (\partial_\mu + e_\mu - iq_\psi(g_1'B_{1\mu} + g_2'B_{2\mu}))\psi_R^- \,. \tag{2.156}$$

The $e_\mu \equiv e_\mu^i T^i$ symbol of the CCWZ formalism connects the non-linearly transforming field and the NGB's via the matrix U [5, 6]

$$U^\dagger(D_\mu U) \equiv d_\mu^j X^j + e_\mu^i T^i \,, \tag{2.157a}$$

$$D_\mu U = \left(\partial_\mu - ig_1 W_1^a \frac{\sigma^a}{2} - iq_X g_1' B_1\right) . \tag{2.157b}$$

Using the automorphism defined by T-parity we can also write

$$U(D_\mu U^\dagger) \equiv -d_\mu^j X^j + e_\mu^i T^i \,, \tag{2.158a}$$

$$D_\mu U^\dagger = \left(\partial_\mu - ig_2 W_2^a \frac{\sigma^a}{2} - iq_X g_2' B_2\right) . \tag{2.158b}$$

This automorphism allows us to write the e_μ symbol in terms of the pion matrix U and the gauge fields

$$e_\mu = \frac{1}{2}\left(U^\dagger D_\mu U + U D_\mu U^\dagger\right) . \tag{2.159}$$

The covariant derivatives of Ψ_1 and Ψ_2 are

$$\begin{aligned} D_\mu\Psi_1 &= (\partial_\mu + i\sum_{i=1,2}[g_i W_{i\mu}^a Q_i^{a*} + g_i' B_{i\mu} Y_i^*] \\ &\quad - \frac{i}{3}(g_1'B_{1\mu} + g_2'B_{2\mu}))\Psi_1 \,, \end{aligned} \tag{2.160}$$

$$\begin{aligned} D_\mu\Psi_2 &= (\partial_\mu - i\sum_{i=1,2}[g_i W_{i\mu}^a Q_i^{a} + g_i' B_{i\mu} Y_i] \\ &\quad - \frac{i}{3}(g_1'B_{1\mu} + g_2'B_{2\mu}))\Psi_2 \,. \end{aligned} \tag{2.161}$$

The covariant derivative of a singlet field χ transforming as $(\mathbf{1},\mathbf{1},\mathbf{1})_{q_L,q_R,q_Q}$ is given by

$$D_\mu\chi = (\partial_\mu - i(q_L+q_Q)g_1'B_{1\mu} - i(q_R+q_Q)g_2'B_{2\mu})\chi \,. \tag{2.162}$$

For completeness we report the top sector Lagrangian

$$\begin{aligned}\mathcal{L}_{\rm top} &= \frac{\lambda_1 f}{2}\left(\overline{\Psi}_{1i}O_i + (\overline{\Psi}_2\Omega\Sigma_0)_i\tilde{O}_i\right)\tilde{t}_R \\ &\quad + \frac{\lambda_2 f}{\sqrt{2}}\left(\overline{\chi}_1\tau_1 - \overline{\chi}_2\tau_2\right) + \text{h.c}\,, \end{aligned} \tag{2.163a}$$

$$O_i \equiv \epsilon_{ijk}\Sigma_{j4}\Sigma_{k5} \,,\quad \tilde{O}_i \equiv 2\epsilon_{ijk}\tilde{\Sigma}_{j4}\tilde{\Sigma}_{k5} \,, \tag{2.163b}$$

and the terms that gives the T-odd doublet combination a mass

$$\mathcal{L}_\kappa = \frac{\kappa f}{\sqrt{2}}\left(\overline{\psi}_1\sigma_2 U - \overline{\psi}_2\sigma_2 U^\dagger\right)\psi_R^- + \text{h.c}\,. \tag{2.164}$$

Ψ_1	Ψ_2	t	τ_1	τ_2	ψ_R^-	λ_1	$\tilde{\lambda}_1$	λ_2	$\tilde{\lambda}_2$	κ	$\tilde{\kappa}$
a	b	c	d	e	f	$a-c$	$b-c$	$a-d$	$b-e$	$a-f$	$b-f$

Table 2.1: *Spurionic $U(1)$ assignment for the fields and couplings.*

2.B The scalar potential and its symmetries

In this appendix we discuss in detail the symmetry structure of the model and the scalar potential. The Higgs doublet is protected by two different shift symmetries. Each of the shift symmetries is contained inside a different $SU(3)$ subgroup of $SU(5)$

$$\exp\left[\frac{i}{\sqrt{2}f}\begin{pmatrix} & & \vec{\epsilon} \\ & & \\ \vec{\epsilon}^T & & \end{pmatrix}\right] \in [SU(3)]_1\,, \tag{2.165a}$$

$$\exp\left[\frac{i}{\sqrt{2}f}\begin{pmatrix} & & \\ & & \vec{\epsilon}^T \\ & \vec{\epsilon} & \end{pmatrix}\right] \in [SU(3)]_2\,. \tag{2.165b}$$

All the couplings that explicitly break the global symmetry in this model, namely the gauge couplings and the top sector couplings, preserve at least one of the $SU(3)$ subgroups. A Higgs potential is generated only when at least two couplings are non zero, such that all the shift symmetries are broken. This so-called collective breaking mechanism insures the absence of quadratically divergent contributions to the Higgs mass. The couplings and their T-parity conjugate respect different symmetries, therefore it is useful to denote the T-conjugate couplings with a tilde

$$\begin{aligned}\mathcal{L}_{\text{top}} &= \frac{f}{4}\left(\lambda_1\overline{\Psi}_{1i}O_i + \tilde{\lambda}_1(\overline{\Psi}_2\Omega\Sigma_0)_i\tilde{O}_i\right)\tilde{t}_R \\ &\quad + \frac{f}{\sqrt{2}}\left(\lambda_2\overline{\chi}_1\tau_1 - \tilde{\lambda}_2\overline{\chi}_2\tau_2\right) + \text{h.c}\,, \end{aligned}\tag{2.166}$$

$$\mathcal{L}_\kappa = \frac{f}{\sqrt{2}}\left(\kappa\overline{\psi}_1\sigma_2 U - \tilde{\kappa}\overline{\psi}_2\sigma_2 U^\dagger\right)\psi_R^- + \text{h.c}\,. \tag{2.167}$$

In order to better understand the structure of the generated scalar potential, we assign spurionic $U(1)$ charges to our fields and couplings, which can be found in Table 2.1. The combinations of couplings appearing in the quadratically divergent contribution to the scalar potential must be of the form $gg^\dagger$ or $\tilde{g}\tilde{g}^\dagger$. We can deduce from the residual symmetries a generic form for the quadratically divergent potential. For concreteness let us consider the coupling λ_1 and set all the other explicit symmetry breaking couplings to zero. The original coset in Eq. (2.140) contains $(24-10)+(9-5) = 18$ NGB's, out of which 4 are eaten, leaving us with 14 physical NGB's with the following $SU_L(2)\times U_Y(1)$ representations

$$\mathbf{3}_{\pm1} \oplus \mathbf{2}_{\pm1/2} \oplus \mathbf{3}_0 \oplus \mathbf{1}_0\,. \tag{2.168}$$

Turning on only λ_1 breaks the global symmetry and changes the coset structure

$$\begin{aligned}&\frac{SU(3)\times[SU(2)\times U(1)]_2}{[SU(2)\times U(1)]_{1+2}} \\ &\times\frac{[SU(2)\times U(1)]_L\times[SU(2)\times U(1)]_R\times U(1)_Q}{[SU(2)\times U(1)]_{L+R}\times U(1)_Q}\,,\end{aligned}\tag{2.169}$$

This coset contains $(8+4)-4+(9-5)=12$ NGB's, out of which 4 are eaten, leaving us with 8 physical NGB's with the following $SU_L(2)\times U_Y(1)$ representations

$$\mathbf{2}_{\pm 1/2}\oplus\mathbf{3}_0\oplus\mathbf{1}_0\,. \tag{2.170}$$

There must exist a non-linear combination of the goldstone fields

$$\begin{aligned}\tilde{\Phi}_{ij} \;\equiv\; & f_1\left(1,\frac{s}{f},\frac{s^2}{f^2},\frac{\varphi^2}{f^2},\frac{|H|^2}{f^2},...\right)\Phi_{ij}\\ & +f_2\left(1,\frac{s}{f},\frac{s^2}{f^2},\frac{\varphi^2}{f^2},\frac{|H|^2}{f^2},...\right)\frac{H_iH_j}{f}\end{aligned} \tag{2.171}$$

with f_1, f_2 some functions of gauge-invariants, such that the quadratically divergent potential can be written as gauge-invariant function of only $\tilde{\Phi}$

$$V(\Phi,H,s,\varphi)=V(\tilde{\Phi})\,. \tag{2.172}$$

This constraint limits the form of the quadratically divergent scalar potential. E.g the mass term in the RHS of Eq. (2.172) would appear in the original NGB basis as

$$\begin{aligned}&\Lambda^2|\lambda_1|^2\mathrm{Tr}[\tilde{\Phi}\tilde{\Phi}^*]=\\ &\Lambda^2|\lambda_1|^2(|f_1|^2\mathrm{Tr}[\Phi\Phi^*]+\frac{1}{f}f_1f_2^*\mathrm{Tr}[H^\dagger\Phi H^*]\\ &+\frac{1}{f}f_1^*f_2\mathrm{Tr}[H^T\Phi^*H]+\frac{1}{f^2}|f_2|^2(H^\dagger H)^2)\,.\end{aligned} \tag{2.173}$$

This argument can be repeated for every coupling $c\in\{\tilde{\lambda}_1,g_1,g_2,g_1',g_2'\}$ which generates a scalar potential proportional to $|c|^2\Lambda^2$. We can immediately see that the symmetry structure allows a quadratically divergent mass term for Φ. The collective breaking structure prevents the appearance of $|H|^2$ in the quadratically divergent potential, as well other operators, such as

$$s^2,\varphi^2,s^2|H|^2\;\text{ and }\;sH^\dagger\varphi H\,. \tag{2.174}$$

Logarithmically divergent 1-loop contributions to the scalar potential contain four couplings. Possible combinations are trivial combination like $|c|^2|c'|^2$, and non trivial combinations like

$$\lambda_1\tilde{\lambda}_1^\dagger\tilde{\kappa}\kappa^\dagger\,,\;\tilde{\lambda}_1\lambda_1^\dagger\kappa\tilde{\kappa}^\dagger+\text{T-conjugates}\,. \tag{2.175}$$

At this level all scalar operators can be generated except the singlet mass. The singlet remains exactly massless at 1-loop and must acquire a mass from higher order loops, e.g 2-loop diagram by closing the Higgs loop in the 1-loop induced $s^2|H|^2$ interaction. We report the radiatively generated couplings calculated from Eq. (2.73) after setting all the T-conjugate couplings to their respective values $\tilde{c}=c$. We neglect the gauge contributions which generate $O(1\%)$ corrections to the fermion loops contribution. We define $C\equiv\frac{N_c}{16\pi^2}a_2\log\left(\frac{\Lambda^2}{f^2}\right)$. Note that $C\sim 0.1$ for $a_2=1$

and $\Lambda = 4\pi f$.

$$m_\Phi^2 = \frac{N_c}{4\pi^2} a_1 |\lambda_1|^2 \Lambda^2 \,, \tag{2.176}$$

$$\lambda_h = \frac{N_c}{16\pi^2} a_1 |\lambda_1|^2 \left(\frac{\Lambda}{f}\right)^2 \,, \tag{2.177}$$

$$\lambda = \frac{C|\lambda_1|^2 r^2 \left(25|\lambda_2|^2 + 6|\kappa|^2 (r+5)^2\right)}{30\,(r^2+5)} > 2.3C \,, \tag{2.178}$$

$$\mu_h^2 = -Cf^2 |\lambda_1|^2 |\lambda_2|^2 < -4Cf^2 \,, \tag{2.179}$$

$$\lambda_\varphi = \frac{C|\lambda_1|^2 r^2 \left(5|\lambda_2|^2 + 6\kappa^2 (r+1)(r+5)\right)}{3\sqrt{5}\sqrt{r^4+6r^2+5}} > 5.2C \,, \tag{2.180}$$

The bounds are calculated assuming $\kappa, r > 1$. We find the minimal/maximal value with respect to λ_1, λ_2 under the top Yukawa constraint. The triplet mass is generated only from gauge loops. We define $D \equiv \frac{3}{64\pi^2} a_4 \log\left(\frac{\Lambda^2}{f^2}\right) = \frac{C}{4}\frac{a_4}{a_2} \sim 0.025$. The triplet mass is given by

$$\begin{aligned} m_\varphi^2 &= Df^2 \left(\frac{8g^4 r^2 (1+r)^2}{1+r^2}\right) \\ &\approx \left(\frac{D}{0.025}\right)\left(\frac{f}{1200\ \text{GeV}}\right)^2 (850\ \text{GeV})^2 \,, \end{aligned} \tag{2.181}$$

where we used $r = 3$. Lastly, we report the Higgs potential. The Higgs potential in the unitary gauge up to order $O(\sin^4 h)$

$$\begin{aligned} V_h &= \frac{N_c}{16\pi^2} f^2 \Lambda^2 a_1 \left(|\lambda_1|^2 + |\tilde{\lambda}_1|^2\right) s_h^4 \\ &+ Cf^4 \left(|\tilde{\lambda}_1|^2 |\tilde{\kappa}|^2 - \tilde{\lambda}_1 \lambda_1^\dagger \kappa \tilde{\kappa}^\dagger - |\tilde{\lambda}_1|^2 |\tilde{\lambda}_2|^2 + [g \leftrightarrow \tilde{g}]\right) s_h^2 \\ &+ \frac{1}{4} Cf^4 \left(-|\lambda_1|^2 |\tilde{\lambda}_1|^2 - |\lambda_1|^2 |\lambda_1|^2 + 2|\tilde{\lambda}_1|^2 |\tilde{\lambda}_2|^2\right. \\ &\left. + 4\left(\lambda_1^\dagger \tilde{\lambda}_1 \kappa \tilde{\kappa}^\dagger - |\tilde{\lambda}_1|^2 |\tilde{\kappa}|^2\right) + [g \leftrightarrow \tilde{g}]\right) s_h^4 \left(\frac{h}{\sqrt{2}f}\right) . \end{aligned} \tag{2.182}$$

where we defined $s_h^n \equiv \sin^n\left(\frac{h}{\sqrt{2}f}\right)$. After setting $\tilde{g} = g$, we find

$$\begin{aligned} V_h &= -2Cf^4 |\lambda_1|^2 |\lambda_2|^2 s_h^2 \\ &+ \left[\frac{N_c}{8\pi^2}\Lambda^2 a_1 + Cf^2\left(|\lambda_2|^2 - |\lambda_1|^2\right)\right] f^2 |\lambda_1|^2 s_h^4 \,. \end{aligned} \tag{2.183}$$

Although terms proportional to $|\lambda_1|^2|\kappa|^2$ could have appeared a priori in the Higgs potential, they vanish due to T-parity. Clearly if we were to set $\tilde{\kappa} = -\kappa$, which is equivalent to flipping the parity of ψ_R^- and coupling it to the T-even combination $\frac{1}{\sqrt{2}}(\psi_1 + \psi_2)$, the κ coupling would have appeared in the Higgs potential. Since κ does not appear in the Higgs potential, taking large values of κ would have no influence on the tuning of the Higgs potential at one loop.

3

Composite dark matter in $SO(7)/SO(6)$

3.1 Effective Lagrangian for Higgs and DM pNGBs

The low-energy effective Lagrangian for the pNGBs, namely the Higgs doublet H and the SM-singlet DM, taken to be a complex scalar χ stabilized by a $U(1)_{\rm DM}$ symmetry,[1] has the form

$$\mathcal{L}_{\rm eff} = \mathcal{L}_{\rm GB} + \mathcal{L}_f - V_{\rm eff}\,, \tag{3.1}$$

where $\mathcal{L}_{\rm GB}$ contains only derivative interactions, whose structure is determined by the non-linearly realized global symmetry. $\mathcal{L}_f$ contains the couplings to the SM fermions, which originate from elementary-composite mixing couplings that break $\mathcal{G}$ explicitly. These elementary-composite mixings, together with the gauging of a subgroup of $\mathcal{G}$ that includes the SM electroweak symmetry, generate the radiative potential $V_{\rm eff}$. We discuss first the leading order Lagrangian $\mathcal{L}_{\rm GB}$, and then turn to the effects of the explicit symmetry breaking, contained in $\mathcal{L}_f - V_{\rm eff}$.

3.1.1 Two-derivative Lagrangian

The most general two-derivative, $SU(2)_L \times SU(2)_R \times U(1)_{\rm DM} \subset \mathcal{H}$ invariant Lagrangian[2] that arises from the nonlinear sigma model kinetic term is[3]

$$\mathcal{L}_{\rm GB} \;=\; |D^\mu H|^2 + |\partial^\mu \chi|^2 + \frac{c_H}{2f^2}\partial_\mu |H|^2 \partial^\mu |H|^2 + \frac{c_d}{f^2}\partial_\mu |H|^2 \partial^\mu |\chi|^2 + \frac{c_\chi}{2f^2}\partial_\mu |\chi|^2 \partial^\mu |\chi|^2. \tag{3.2}$$

We could have written four additional operators,

$$\frac{c_1}{f^2}|D_\mu H|^2|H|^2\,, \qquad \frac{c_2}{f^2}|D_\mu H|^2|\chi|^2\,, \qquad \frac{c_3}{f^2}|\partial_\mu \chi|^2|H|^2\,, \qquad \frac{c_4}{f^2}|\partial_\mu \chi|^2|\chi|^2\,, \tag{3.3}$$

but these can be removed through the $O(1/f^2)$ field redefinition

$$H \to \Big(1 - \frac{c_1}{2f^2}|H|^2 - \frac{c_2}{2f^2}|\chi|^2\Big)H\,, \qquad \chi \to \Big(1 - \frac{c_3}{2f^2}|H|^2 - \frac{c_4}{2f^2}|\chi|^2\Big)\chi\,. \tag{3.4}$$

[1] For real DM η that is stable due to a Z_2 symmetry, we simply replace $\chi \to \eta/\sqrt{2}$ in $\mathcal{L}_{\rm eff}$.

[2] More precisely, this is the most general $SU(2)_L \times SU(2)_R \times U(1)_{\rm DM}$ invariant Lagrangian where $SU(2)_R$ is only broken by the gauging of hypercharge.

[3] We do not include in $\mathcal{L}_{\rm GB}$ operators containing $\chi^* \overset{\leftrightarrow}{\partial_\mu} \chi \equiv \chi^* \partial_\mu \chi - \partial_\mu \chi^* \chi$, which vanish trivially in the $SO(6)/SO(5)$ model where $\chi \to \eta/\sqrt{2}$ with real η, and are forbidden in the $SO(7)/SO(6)$ model by custodial $SO(4) \simeq SU(2)_L \times SU(2)_R$ invariance, since H and χ belong to the same irreducible representation of $\mathcal{H} = SO(6)$. Notice also that $\chi^* \overset{\leftrightarrow}{\partial_\mu} \chi$ is odd under the charge conjugation associated to $U(1)_{\rm DM}$.

Notice that for $c_1 = c_2 = c_3 = c_4 = -2/3$ these are the leading terms of

$$\frac{\sin(\pi/f)}{\pi}\,\pi^a \to \frac{\pi^a}{f}\,, \qquad \pi = \sqrt{\vec{\pi}^T\vec{\pi}}\,, \tag{3.5}$$

where $\vec{\pi}$ is the GB vector [68]. This redefinition has customarily been adopted in studies of the $SO(6)/SO(5)$ and $SO(7)/SO(6)$ models, see App. 3.A. In the basis of Eq. (3.2), which also coincides with the SILH basis [102] when restricted to Higgs interactions, the scalar potential reduces to a simple polynomial and the vacuum expectation value (VEV) of the Higgs is equal to $v \simeq 246$ GeV. In those models the coefficients take the values $c_H = c_d = c_\chi = 1$, which we often adopt as reference in the following.

The "derivative Higgs portal" operator parametrized by c_d, which constitutes the only interaction between the DM and the SM contained in $\mathcal{L}_{\rm GB}$, allows the DM to annihilate to SM particles via s-channel Higgs exchange, and the observed DM relic density to be produced via the freeze-out mechanism. This fixes the interaction strength c_d/f^2 as a function of the DM mass, as shown by the blue curve in Fig. 3.1, which was obtained by solving the Boltzmann equation for the χ number density using micrOMEGAs [103]. For $m_\chi > m_h$ the relation is very simple, being approximately determined by

$$1 = \frac{\Omega_{\chi+\chi^*}}{\Omega_{\rm DM}} \simeq \frac{\langle\sigma v_{\rm rel}\rangle_{\rm can}}{\frac{1}{2}\langle\sigma v_{\rm rel}\rangle}\,, \qquad \langle\sigma v_{\rm rel}\rangle \simeq \frac{c_d^2 m_\chi^2}{\pi f^4} \tag{3.6}$$

hence

$$\frac{f}{c_d^{1/2}} \approx 1.1\ {\rm TeV}\left(\frac{m_\chi}{130\ {\rm GeV}}\right)^{1/2}, \tag{3.7}$$

where $\langle\,\cdot\,\rangle$ denotes thermal average, $\Omega_{\rm DM} = 0.1198\,h^{-2}$ [62], $\langle\sigma v_{\rm rel}\rangle_{\rm can} \approx 2\times10^{-26}\,{\rm cm}^3\,{\rm s}^{-1}$ is the canonical value of the thermal cross section [104], and the dominant $\chi\chi^* \to WW, ZZ, hh$ channels were included in the annihilation.[4]

Crucially, the derivative Higgs portal also leads to negligibly small cross sections for the scattering of DM with heavy nuclei: the amplitude for $q\chi \to q\chi$ scattering mediated by Higgs exchange is proportional to $|t|/f^2 \lesssim (100\ {\rm MeV})^2/(1\ {\rm TeV})^2 \sim 10^{-8}$, where we took 100 MeV as a rough estimate of the maximum momentum transfer. The expected strength of the direct detection signal is then set by the interactions contained in $\mathcal{L}_f - V_{\rm eff}$, which depend on the explicit breaking of the global symmetry.

The other important effect encapsulated in $\mathcal{L}_{\rm GB}$ is that h, due to its pNGB nature, has all its couplings rescaled by a universal factor with respect to their SM values: writing in unitary gauge $H = (0\,,\,\tilde{h}/\sqrt{2})^T$ we have

$$\tilde{h} = v + \Big(1 - \frac{c_H}{2}\frac{v^2}{f^2}\Big)\,h\,. \tag{3.8}$$

A robust and model-independent probe of this effect is the measurement of the hVV couplings ($V = W, Z$). In Fig. 3.1 we compare the projected sensitivity on this observable of current and future colliders [105] with the pNGB DM parameter space, under the assumption that $c_H = c_d$.

[4] The cross section for annihilation to $t\bar{t}$ scales as $\sigma_{t\bar{t}}\,v_{\rm rel} \sim N_c m_t^2/(\pi f^4)$, as opposed to $\sigma_{WW,ZZ,hh}\,v_{\rm rel} \sim m_\chi^2/(\pi f^4)$, therefore $t\bar{t}$ is important only for m_χ not much larger than m_t. See the right panel of Fig. 3.1.

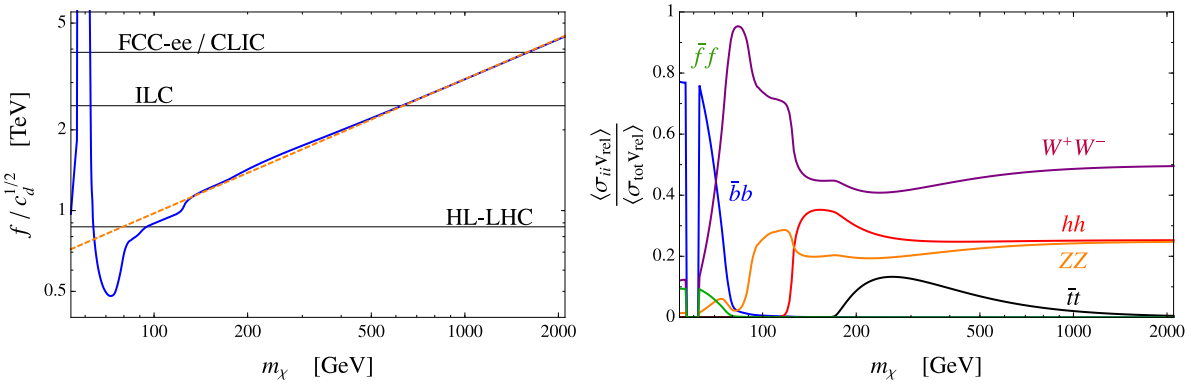

Figure 3.1: *Left panel: value of the global symmetry breaking scale f that allows to reproduce the observed DM relic density via the derivative Higgs portal, as function of the DM mass. In solid blue the full Boltzmann solution, in dashed orange the approximate relation given in Eq. (3.7). The gray lines show the 95% CL lower bounds achievable from the measurement of the hVV couplings at current and future colliders, assuming $c_H = c_d$. Right panel: fractions for annihilation to the different SM final states. $\bar{f}f$ denotes the sum over all light quarks and leptons.*

3.1.2 Explicit symmetry breaking effects

The most general effective Lagrangian coupling the pNGBs to the third generation quarks is

$$\mathcal{L}_f = -y_t \bar{q}_L \widetilde{H} t_R \left(1 - \frac{c_t}{f^2}|H|^2 - \frac{c_t^\chi}{f^2}|\chi|^2\right) - y_b \bar{q}_L H b_R \left(1 - \frac{c_b}{f^2}|H|^2 - \frac{c_b^\chi}{f^2}|\chi|^2\right) + \text{h.c.}\,. \quad (3.9)$$

The general form of the one-loop scalar potential generated by the explicit symmetry breaking is, up to quartic order in the fields,

$$V_{\rm eff} = \mu_h^2|H|^2 + \lambda_h|H|^4 + \mu_{\rm DM}^2|\chi|^2 + \lambda_{\rm DM}|\chi|^4 + 2\lambda|H|^2|\chi|^2\,. \quad (3.10)$$

The parameters μ_h^2 and λ_h^2 are fixed by requiring the observed mass and VEV for the SM-like Higgs. We only consider regions of parameters where $\langle\chi\rangle = 0$, so that $U(1)_{\rm DM}$ is not spontaneously broken and χ is stable. This imposes a mild constraint on the parameter space of the fermionic sector (see App. 3.C for a concrete example), whereas the gauging of $U(1)_{\rm DM}$ automatically yields $\mu_{\rm DM}^2 > 0$.

In addition to providing the DM with a mass $m_\chi^2 = \mu_{\rm DM}^2 + \lambda v^2$, the explicit symmetry breaking can affect its phenomenology in important ways. The annihilation to SM particles is still dominated by s-channel Higgs exchange, but now the $\chi^*\chi h$ coupling has both a derivative and a non-derivative component,

$$\mathcal{M}(\chi\chi^* \to \text{SM}) \propto \left(c_d \frac{s}{f^2} - 2\lambda\right) v \simeq \left(c_d \frac{4m_\chi^2}{f^2} - 2\lambda\right) v\,. \quad (3.11)$$

A priori, for $m_\chi > m_t$ the $\chi^*\chi\bar{t}t$ interaction proportional to c_t^χ can also give an important contribution to $\chi^*\chi \to t\bar{t}$. This is the case when the shift symmetry is broken by the top quark, considered in Sec. 3.3. In case the top quark couplings respect the DM shift symmetry, as in Secs. 3.4 and 3.5, c_t^χ is suppressed or altogether absent, hence Eq. (3.11) is a good approximation of the strength for annihilation to SM particles.

DM scattering with nuclei proceeds via t-channel Higgs exchange and through the contact interactions parametrized by c_q^χ. The effective interactions with the SM quarks q have the form

$$2m_q a_q\, \bar{q}q\chi^*\chi\,, \qquad a_q \approx \frac{\lambda}{m_h^2} + \frac{c_q^\chi}{2f^2}\,. \tag{3.12}$$

As already emphasized, the contribution of the derivative Higgs portal is negligible.

Note that, for any relevant values of the parameters, the DM self-interactions mediated by c_χ and $\lambda_{\rm DM}$ are far too small to have any effects on cosmological scales.

3.1.3 Origins of explicit breaking and DM scenarios

Two irreducible sources of explicit symmetry breaking, which generate at least some of the interactions contained in Eqs. (3.9) and (3.10), are the gauging of the SM electroweak subgroup $SU(2)_L \times U(1)_Y \subset \mathcal{H}$ and the Yukawa couplings for the SM fermions. The SM gauging only contributes to the scalar potential and, under our assumption that the DM is a SM singlet, at one-loop level generates only μ_h^2 and λ_h. In the fermion sector, Yukawas are assumed to arise via the partial compositeness mechanism [52]: the elementary fermions couple linearly to operators of the strong sector,

$$\mathcal{L}_{\rm mix}^{\rm UV} \sim \lambda_q f\, \bar{q}_L \mathcal{O}_q + \lambda_t f\, \bar{t}_R \mathcal{O}_t + \lambda_{q'} f\, \bar{q}_L \mathcal{O}_{q'} + \lambda_b f\, \bar{b}_R \mathcal{O}_b + \text{h.c.}, \tag{3.13}$$

where we have ignored the flavor structure and put our focus on the masses of the third generation of quarks [106]. We have included mixings of the left-handed quark doublet with two distinct operators, as it is in general required to generate both the top and bottom Yukawa couplings. For example, in the $SO(6)/SO(5)$ and $SO(7)/SO(6)$ models the global symmetry is extended by an unbroken $U(1)_X$, hence if t_R and b_R are coupled to operators with different X charge, two distinct embeddings of q_L are needed in order to generate both y_t and y_b. At low energies Eq. (3.13) leads to mass mixing between the elementary fermions and the composite resonances, and as a result the physical SM fields are linear combinations of elementary and composite degrees of freedom. Their compositeness fractions are defined schematically as $\epsilon_{L,R}^t \sim \lambda_{q,\,t} f/\sqrt{m_{*q,\,t}^2 + \lambda_{q,\,t}^2 f^2}$ and $\epsilon_{L,R}^b \sim \lambda_{q',\,b} f/\sqrt{m_{*q',\,b}^2 + \lambda_{q',\,b}^2 f^2}$, where $m_{*q,\,t,\,q',\,b}$ are the relevant masses of the resonances in the top and bottom sectors. The Yukawas have the form

$$y_\psi \simeq \frac{M_{*\psi}}{f}\, \epsilon_L^\psi\, \epsilon_R^\psi\,, \qquad (\psi = t, b) \tag{3.14}$$

where $M_{*\psi}$ is a combination of the resonance mass parameters.

Since the elementary fermions do not fill complete $\mathcal{G}$ representations, Eq. (3.13) breaks explicitly at least part of the global symmetry. The Higgs shift symmetry must be broken by the couplings of both the top and bottom, in order to generate the observed values of $y_{t,b}$, v and m_h. However, whether each of these couplings breaks or preserves the χ shift symmetry is a priori unknown, and all possibilities deserve close scrutiny. The three scenarios discussed in this thesis are listed in Fig. 3.2, along with the Feynman diagrams that dominate the annihilation and direct detection of DM in each case. In Sec. 3.3 we consider the scenarios where the leading breaking of the DM shift symmetry originates from the top quark. In Sec. 3.4 we consider the case of DM shift symmetry breaking due to the bottom quark couplings. Then, in Sec. 3.5 we study the scenario where the fermion sector is fully symmetric, and the leading explicit breaking arises from the gauging of the $U(1)_{\rm DM}$ symmetry that stabilizes the DM. Before considering all these cases, let us first present the framework in which these were studied, namely the $SO(7)/SO(6)$ model.

Leading source of DM shift symmetry breaking		*DM annihilation*	*DM direct detection*
t_R	Sec. 3.3	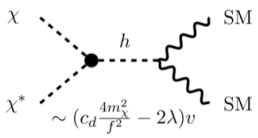	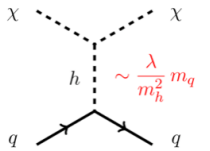
b_R	Sec. 3.4	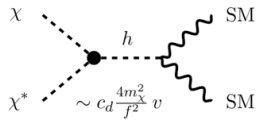	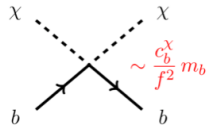
γ_D	$m_{\gamma_D} = 0$ Sec. 3.5.1	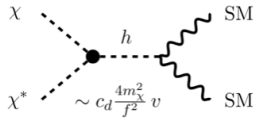 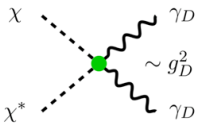	*negligible*
	$m_\chi < m_{\gamma_D}$ Sec. 3.5.2	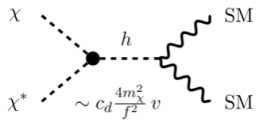 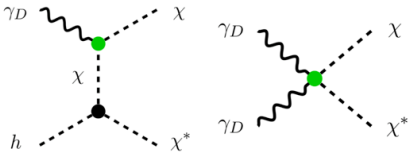	

Figure 3.2: *Schematic summary of the three scenarios discussed in this thesis. The EFT coefficients c_d, c_b^χ and λ were defined in Eqs. (3.2), (3.9) and (3.10), respectively. In the third scenario we denote with γ_D the dark photon associated to the gauging of $U(1)_{\rm DM}$ with coupling g_D, and mark the gauge interactions in green.*

3.2 $SO(7)/SO(6)$ model

We assume that the strong sector possesses an $SO(7)$ global symmetry, spontaneously broken to $SO(6)$ at the scale f. The six Goldstone bosons (GBs) π^a, $a = 1, \ldots, 6$ transform in the fundamental representation of the unbroken $SO(6)$, which under $SO(4)$ decomposes into $H \sim \mathbf{4}$, identified with the Higgs doublet, and two real singlets η, κ. Following the Callan-Coleman-Wess-Zumino (CCWZ) construction [5, 6], whose details are given in App. 3.A, the GBs are parameterized by the matrix $U = \exp\left(i\sqrt{2}\pi^a X^a / f\right)$, where the X^a are the broken generators. At the leading order in derivatives, the Goldstone Lagrangian is given by

$$\mathcal{L}_\pi = \frac{f^2}{4} d_\mu^a d^{a\,\mu}, \tag{3.15}$$

where the CCWZ d_μ symbol is constructed out of U and its $SU(2)_L \times U(1)_Y$ covariant derivative. In the unitary gauge the vector of GBs can be written as

$$\vec{\pi} = \Big(0,\ 0,\ 0,\ \tilde{h},\ \eta,\ \kappa\Big)^T, \tag{3.16}$$

with $\tilde{h}$ denoting the field whose physical excitation will be identified with the observed Higgs boson. After performing a convenient field redefinition (see Eq. (3.85)), the Goldstone Lagrangian reads

$$\mathcal{L}_\pi = \frac{1}{2}\Big[(\partial_\mu \tilde{h})^2 + (\partial_\mu \eta)^2 + (\partial_\mu \kappa)^2\Big] + \frac{1}{2}\frac{\left(\tilde{h}\partial_\mu \tilde{h} + \eta \partial_\mu \eta + \kappa \partial_\mu \kappa\right)^2}{f^2 - \tilde{h}^2 - \eta^2 - \kappa^2} + \frac{\tilde{h}^2}{4}\Big[\bar{g}^2 |\bar{W}^+_\mu|^2 + \frac{1}{2}(\bar{g}\bar{W}^3_\mu - \bar{g}'\bar{B}_\mu)^2\Big]. \tag{3.17}$$

The bar on the gauge fields (and their associated couplings) indicates that these are elementary states. In analogy to photon-rho mixing in QCD, the gauge fields couple linearly to resonances of the strong sector. The resulting mass mixing is diagonalized, for example for the charged fields, by $\bar{g}\bar{W}^\pm_\mu \to g W^\pm_\mu + \ldots$, where g and $W^\pm_\mu$ are the SM gauge coupling and field, respectively, and the dots stand for terms containing the vector resonances (see Eq. (3.96)). Hence we identify $\langle \tilde{h} \rangle = v \simeq 246$ GeV. Assuming furthermore $\langle \eta \rangle = \langle \kappa \rangle = 0$ and expanding around the vacuum, we find that the singlets have canonical kinetic terms, whereas for the Higgs the canonical normalization is achieved with

$$\tilde{h} = v + \sqrt{1-\xi}\, h\,, \qquad \xi \equiv \frac{v^2}{f^2}\,, \tag{3.18}$$

where h is the physical excitation.

Coupling to elementary fermions and dark matter stability

To examine the different options for the embedding of the SM fields, it is convenient to consider the decomposition of the representations of $SO(7)$ under its subgroup $SO(4) \times SO(3)$, which we can write as $SU(2)_L \times SU(2)_R \times SU(2)'$, where $SO(4) \cong SU(2)_L \times SU(2)_R$ while $SO(3) \cong SU(2)'$ is generated by the broken generators under which the two singlets shift, $X^\eta \equiv X^5$ and $X^\kappa \equiv X^6$, together with

$$T^{\rm DM} \equiv T^{56} = \frac{1}{\sqrt{2}}\,\mathrm{diag}(\mathbf{0}_{4\times 4}, \sigma^2, 0) \ \in\ SO(6), \tag{3.19}$$

where we used block notation. The label given to this generator anticipates its role in the dark matter stabilization, which will be discussed momentarily. For the first few irreducible $SO(7)$ representations we have the following $(SU(2)_L, SU(2)_R, SU(2)')$ decompositions (see for example Ref. [107]),

$$\begin{aligned}
\mathbf{1} &= (\mathbf{1},\mathbf{1},\mathbf{1}),\\
\mathbf{7} &= (\mathbf{2},\mathbf{2},\mathbf{1}) \oplus (\mathbf{1},\mathbf{1},\mathbf{3}),\\
\mathbf{8} &= (\mathbf{2},\mathbf{1},\mathbf{2}) \oplus (\mathbf{1},\mathbf{2},\mathbf{2}),\\
\mathbf{21} &= (\mathbf{2},\mathbf{2},\mathbf{3}) \oplus (\mathbf{3},\mathbf{1},\mathbf{1}) \oplus (\mathbf{1},\mathbf{3},\mathbf{1}) \oplus (\mathbf{1},\mathbf{1},\mathbf{3}),\\
\mathbf{27} &= (\mathbf{3},\mathbf{3},\mathbf{1}) \oplus (\mathbf{2},\mathbf{2},\mathbf{3}) \oplus (\mathbf{1},\mathbf{1},\mathbf{5}) \oplus (\mathbf{1},\mathbf{1},\mathbf{1}).
\end{aligned} \tag{3.20}$$

For the top Yukawa, we imbed q_L in the $(\mathbf{2},\mathbf{2})_{2/3}$ representation of $(SU(2)_L,\ SU(2)_R)_X$. This guarantees custodial protection against zero-momentum corrections to the $Zb_L\bar{b}_L$ vertex, which

would conflict with LEP measurements [108]. Hence a natural and minimal possibility is $\mathcal{O}_q \sim \mathbf{7}_{2/3}$. In this case the coupling of q_L preserves the entire $SU(2)'$. The requirement of $U(1)_X$-invariance of the top mass term fixes then the X charge of $\mathcal{O}_t$ to be 2/3, but several options are available for its transformation under $SO(7)$. Additionally, once the top quark couplings respect the DM shift symmetry, additional embeddings might be needed in order to break the shift symmetry i.e for the right handed bottom quark. We summarize the embeddings used throughout this thesis in Table 3.1.

Section	Embeddings	DM shift sym.	$Z\bar{b}b$ cust. sym.
Secs. 3.3-3.5	$\xi_L^{(t)} \sim \mathbf{7}_{2/3} \supset (\mathbf{2},\mathbf{2},\mathbf{1})_{2/3} = (\mathbf{2})^0_{7/6} \oplus \color{red}{(\mathbf{2})^0_{1/6}}$	✓	✓
Sec. 3.3	$\xi_R^{(t)} \sim \mathbf{7}_{2/3} \supset (\mathbf{1},\mathbf{1},\mathbf{3})_{2/3} = (\mathbf{1})^{+1}_{2/3} \oplus \color{red}{(\mathbf{1})^0_{2/3}} \oplus (\mathbf{1})^{-1}_{2/3}$	X	-
Sec. 3.4	$\xi_R^{(t)} \sim \mathbf{21}_{2/3} \supset (\mathbf{1},\mathbf{3},\mathbf{1})_{2/3} = (\mathbf{1})^0_{5/3} \oplus \color{red}{(\mathbf{1})^0_{2/3}} \oplus (\mathbf{1})^0_{-1/3}$	✓	-
	$\xi_L^{(b)} \sim \mathbf{7}_{-1/3} \supset (\mathbf{2},\mathbf{2},\mathbf{1})_{-1/3} = \color{red}{(\mathbf{2})^0_{1/6}} \oplus (\mathbf{2})^0_{-5/6}$	✓	X
	$\xi_R^{(b)} \sim \mathbf{7}_{-1/3} \supset (\mathbf{1},\mathbf{1},\mathbf{3})_{-1/3} = (\mathbf{1})^{+1}_{-1/3} \oplus \color{red}{(\mathbf{1})^0_{-1/3}} \oplus (\mathbf{1})^{-1}_{-1/3}$	X	✓
Sec. 3.5	$\xi_R^{(t)} \sim \mathbf{21}_{2/3}$ (as in Sec. 3.4)	✓	-
	$\xi_R^{(b)} \sim \mathbf{21}_{2/3} \supset (\mathbf{1},\mathbf{3},\mathbf{1})_{2/3} = (\mathbf{1})^0_{5/3} \oplus (\mathbf{1})^0_{2/3} \oplus \color{red}{(\mathbf{1})^0_{-1/3}}$	✓	X

Table 3.1: *The various SM fermion embeddings used in the thesis. We specify the used $SO(7) \times U(1)_X$ representation and focus on the relevant $(SU(2)_L, SU(2)_R, SU(2)')_X$ representation, which we subsequently decompose to its $(SU(2)_L)^{DM}_Y$ representations. We highlight in red the relevant SM representation. In Sec. 3.3 only the right handed top breaks the DM shift symmetry. In Secs. 3.4 and 3.5 the right handed top coupling preserves the DM shift symmetry. The DM shift symmetry is eventually broken in those cases by the right handed bottom (Sec. 3.4) and the $U(1)_{DM}$ gauging (Sec. 3.5). Note that in Sec. 3.4, a second embedding of q_L is needed in order to produce the bottom Yukawa, which introduces a $X = -1/3$ sector and the accompanying resonances, see App. 3.C*

As an example, let us consider the embedding used in Sec. 3.3,

$$t_R \sim (\mathbf{1},\mathbf{1},\mathbf{3}) \subset \mathbf{7}\,. \tag{3.21}$$

In this case the $SU(2)'$ is explicitly broken, but the embedding can be chosen as to preserve a residual $U(1)$, generated by one among $\{X^\eta, X^\kappa, T^{\rm DM}\}$. Therefore we can either leave the shift-symmetry of one of the singlets intact, thus keeping it massless, or preserve the $U(1)$ symmetry acting on η and κ that is generated by $T^{\rm DM}$. We choose the latter, hence η and κ are combined into a complex scalar field

$$\chi \equiv (\kappa + i\eta)/\sqrt{2}\,, \tag{3.22}$$

that is an eigenstate of $U(1)_{\rm DM}$ with charge $+1$, while t_R is uncharged under this symmetry. The complex scalar χ is our DM candidate, and the unbroken $U(1)_{\rm DM}$ ensures its stability. This setup is represented schematically in Fig. 3.3.

Under $(SU(2)_L, SU(2)_R)^{\rm DM}_X$ the $\mathbf{7}_{2/3}$ decomposes as

$$\mathbf{7}_{2/3} = (\mathbf{2},\mathbf{2})^0_{2/3} \oplus (\mathbf{1},\mathbf{1})^0_{2/3} \oplus (\mathbf{1},\mathbf{1})^{\pm 1}_{2/3}\,, \tag{3.23}$$

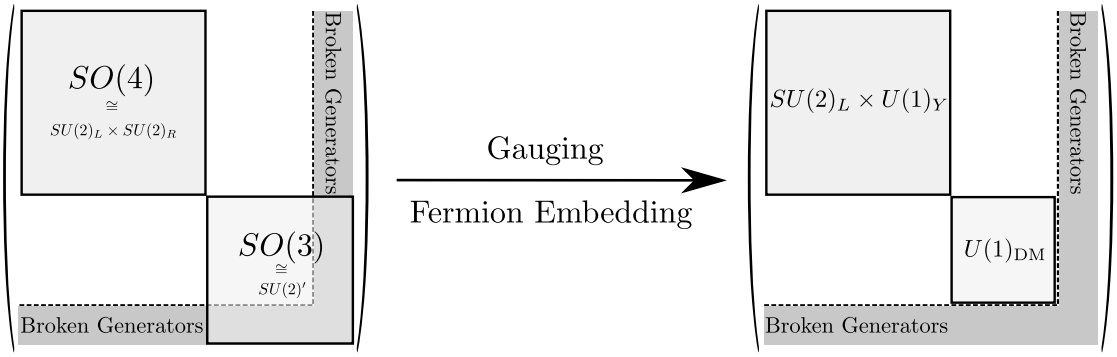

Figure 3.3: *Schematic overview of the $SO(7)$ algebra. In the left drawing the structure of the $SU(2)_L \times SU(2)_R \times SU(2)'$ subgroup is displayed, whereas the right drawing shows the symmetries that remain unbroken after the weak gauging of the SM electroweak group and the coupling of q_L, t_R to operators $\mathcal{O}_q, \mathcal{O}_t \sim \mathbf{7}_{2/3}$ of $SO(7)_X$.*

where the t_R is embedded in the $(\mathbf{1},\mathbf{1})^0_{2/3}$, while the q_L is embedded in the $(\mathbf{2},\mathbf{2})^0_{2/3}$. In Sec. 3.3, the coupling of t_R to the strong sector explicitly breaks the shift symmetry for χ, which will acquire a potential, and in particular a mass, of the same parametric size as the Higgs. The explicit form of the embeddings is

$$\xi_L = \frac{1}{\sqrt{2}}\Big(ib_L, \quad b_L, \quad it_L, \quad -t_L, \quad 0, \quad 0, \quad 0\Big)^T, \qquad \xi_R = \Big(0, \quad 0, \quad 0, \quad 0, \quad 0, \quad 0, \quad t_R\Big)^T. \tag{3.24}$$

A different phenomenological scenario is realized if the embedding of t_R preserves $SU(2)'$. Glancing at Eq. (3.20), this can be obtained in several ways: for example, $t_R \sim (\mathbf{1},\mathbf{3},\mathbf{1}) \subset \mathbf{21}$ (antisymmetric tensor) or $t_R \sim (\mathbf{1},\mathbf{1},\mathbf{1}) \subset \mathbf{27}$ (symmetric traceless tensor). Alternatively, we may assume that t_R is a fully composite $SO(7)$ singlet. In all these cases the couplings of the top quark do not break the symmetries under which χ shifts, hence the leading contributions to its potential come from the couplings of the light fermions, from the weak gauging of $U(1)_{\rm DM}$, or from both. As a consequence, the DM is naturally much lighter than the Higgs. This intriguing possibility is considered in Secs. 3.4 and 3.5. For $m_\chi < m_h/2$, an important constraint comes from the invisible decay width of the Higgs, mediated by the derivative interactions in Eq. (3.17). The decay width is

$$\Gamma(h \to \chi^*\chi) = \frac{m_h^3 v^2}{16\pi f^4(1-\xi)}\sqrt{1-\frac{4m_\chi^2}{m_h^2}}\,, \tag{3.25}$$

where we neglected the contribution of the radiative portal coupling λ (see Eq. (3.29) below), which is expected to be very small in the light χ scenario. The current 95% CL lower bound of $\mathrm{BR}(h \to \chi^*\chi) < 0.24$ [109] translates into $f \gtrsim 1.2$ TeV.

One further comment about the DM stability is in order. In the above discussion we have assumed that each elementary fermion multiplet couples, in a $U(1)_{\rm DM}$-invariant way, to only one operator of the strong sector. However, in general additional, subleading couplings to other operators could be present. If any of these break the $U(1)_{\rm DM}$, the DM stability may be compromised. Therefore we need to make the assumption that the $U(1)_{\rm DM}$ is either a global symmetry respected by all elementary-composite mixing couplings, or an unbroken gauge symmetry.

3.3 Breaking of the DM shift symmetry by top quark couplings

3.3.1 Resonances

The strong sector resonances fill multiplets of the unbroken $SO(6)$ and can be consistently described in the CCWZ framework. We begin with the fermion sector, which plays a dominant role in our discussion. Since we have chosen to embed the top quark in the fundamental of $SO(7)$, which decomposes as $\mathbf{7}_{2/3} = \mathbf{6}_{2/3} \oplus \mathbf{1}_{2/3}$ under $SO(6) \times U(1)_X$, we consider top partners in the fundamental Q and singlet S representations of $SO(6)$. The explicit expression of the fundamental is

$$Q = \frac{1}{\sqrt{2}} \Big(iB - iX_{5/3}, \quad B + X_{5/3}, \quad iT + iX_{2/3}, \quad -T + X_{2/3}, \quad -i\mathcal{Y} + i\mathcal{Z}, \quad \mathcal{Y} + \mathcal{Z} \Big)^T . \tag{3.26}$$

The doublet $(T, B)^T$ transforms as $\mathbf{2}^0_{1/6}$ under $(SU(2)_L)^{\rm DM}_Y$, and therefore has the same quantum numbers as q_L, whereas the exotic doublet $(X_{5/3}, X_{2/3})^T \sim \mathbf{2}^0_{7/6}$ contains an exotic fermion with electric charge equal to 5/3. The two states $\mathcal{Y}, \mathcal{Z} \sim \mathbf{1}^{\pm 1}_{2/3}$ share the SM quantum numbers of the t_R, but are additionally charged under $U(1)_{\rm DM}$. The latter symmetry, being exact, strongly constrains their couplings. Finally, the quantum numbers of the $SO(6)$ singlet are $S \sim \mathbf{1}^0_{2/3}$. The leading order Lagrangian describing the fermion sector is

$$\begin{aligned} \mathcal{L}_f \;=\; & i\bar{q}_L \not{D} q_L + i\bar{t}_R \not{D} t_R + \sum_{i=1}^{N_Q} \bar{Q}_i \left(i\not{D} + \not{e} - m_{Q_i} \right) Q_i + \sum_{j=1}^{N_S} \bar{S}_j \left(i\not{D} - m_{S_j} \right) S_j \\ & + \sum_{i=1}^{N_Q} \left(\epsilon^i_{tQ} \bar{\xi}^A_R U_{Aa} Q^a_{iL} + \epsilon^i_{qQ} \bar{\xi}^A_L U_{Aa} Q^a_{iR} \right) + \sum_{j=1}^{N_S} \left(\epsilon^j_{tS} \bar{\xi}^A_R U_{A7} S_{jL} + \epsilon^j_{qS} \bar{\xi}^A_L U_{A7} S_{jR} \right) + \text{h.c.}, \end{aligned} \tag{3.27}$$

where N_Q and N_S denote the number of copies of each species of resonance that lie below the cutoff of the low-energy theory, and $A\,(a)$ is an index in the fundamental of $SO(7)\,(SO(6))$. The second line of Eq. (3.27) is the low-energy interpolation of Eq. (3.13): the embeddings $\xi_{L,R}$ defined in Eq. (3.24), which transform linearly under $SO(7)$, have been 'dressed' into reducible $SO(6)$ representations via insertions of the Goldstone matrix U. Also notice that the kinetic term of the Q_i includes the e_μ symbol, which is necessary to respect the nonlinearly realized $SO(7)$. In general the following term should also be added to the Lagrangian,

$$\mathcal{L}_d = \sum_{i=1}^{N_Q} \sum_{j=1}^{N_S} c^L_{ji} \bar{S}_{jL} \not{d}^a Q^a_{iL} + \text{h.c.} + (L \to R), \tag{3.28}$$

where $c^{L,R}_{ji}$ are coefficients of $O(1)$. The operators in Eq. (3.28) arise purely from the strong dynamics, and as a consequence they do not contribute to the scalar potential. At leading order in the $1/f$ expansion, they give rise to derivative interactions of one GB and two fermions, which scale as $\sim c^{L,R}\, p/f$, where p is the relevant energy. In the processes relevant for DM phenomenology, namely annihilation and scattering with heavy nuclei, we have $p/f \lesssim m_\chi/f \ll 1$, hence these interactions are suppressed compared to the $\mathcal{G}$-breaking couplings that arise from Eq. (3.27), which scale as $\sim \epsilon/f$. For this reason, the interactions in Eq. (3.28) will be neglected in the remainder of this thesis, unless otherwise noted. Nevertheless, since they can be important in hadron collider processes [110], where $p/f \sim m_*/f \sim O(1)$ with m_* the mass of a resonance, we will return to them in the discussion of the LHC and future collider prospects in Sec. 3.3.4.

3.3.2 Scalar potential and realistic EWSB

Resonances in the gauge sector are assumed to follow the generalized hidden local symmetry approach [54], where given a $\mathcal{G}/\mathcal{H}$ sigma model, the vector resonances are introduced as gauge fields of a local $\mathcal{G}$ symmetry. In our case $\mathcal{G} = SO(7)$, whose adjoint representation decomposes as $\mathbf{21} = \mathbf{15} \oplus \mathbf{6}$ under $SO(6)$. Thus we introduce vector resonances in the adjoint $\rho_\mu \sim \mathbf{15}$ and in the fundamental $a_\mu \sim \mathbf{6}$ of $SO(6)$. Their Lagrangian is given in App. 3.A. The explicit $SO(7)$ breakings introduced by the weak gauging of $SU(2)_L \times U(1)_Y$ and by the fermionic elementary-composite mixing parameters in Eq. (3.27), which we will often collectively denote by ϵ, generate a radiative potential for the GBs. This can be computed at 1-loop using the standard Coleman-Weinberg (CW) technique [30]. In the unitary gauge and expanded to quartic order in the fields, the effective potential takes the form

$$V(\tilde{h}, \chi) = \frac{1}{2}\mu_h^2 \tilde{h}^2 + \frac{\lambda_h}{4}\tilde{h}^4 + \mu_{\rm DM}^2 \chi^*\chi + \lambda_{\rm DM}(\chi^*\chi)^2 + \lambda \tilde{h}^2 \chi^*\chi \,. \tag{3.29}$$

This potential must, first of all, yield a correct EWSB VEV, $\langle \tilde{h} \rangle = v \ll f$. Even though $U(1)_{\rm DM}$ is exactly preserved by the Lagrangian, in general it may still be broken spontaneously. Since this would spoil the DM stability, in the following we only consider parameter choices that satisfy $\langle \chi \rangle = 0$. Then the masses of the physical scalars are

$$m_h^2 = (1-\xi)\left.\frac{\partial^2 V}{\partial \tilde{h}^2}\right|_{\tilde{h}=v,\,\chi=0} = (1-\xi)2\lambda_h v^2 \,, \qquad m_\chi^2 = \left.\frac{\partial^2 V}{\partial \chi \partial \chi^*}\right|_{\tilde{h}=v,\,\chi=0} = \mu_{\rm DM}^2 + \lambda v^2 \,, \tag{3.30}$$

where the $(1-\xi)$ factor in the expression of m_h^2 is due to Eq. (3.18). In general, the mass parameters $\mu_h^2, \mu_{\rm DM}^2$ and couplings $\lambda_h, \lambda_{\rm DM}, \lambda$ are quadratically and logarithmically sensitive, respectively, to the UV cutoff $\Lambda \lesssim 4\pi f$ of the effective theory.[5] However, to retain predictivity we assume that they are fully saturated by the contribution of the SM fields plus the first few vector and fermion resonances that we introduced in Sec. 3.3.1. This is achieved by imposing a set of generalized WSRs [55], which ensure that the form factors determining the parameters of the CW potential vanish sufficiently fast at large momenta [111, 112]. In addition, we assume that further explicit breakings of $SO(7)$ originating from the UV dynamics, if present, give a subleading contribution to the scalar potential.[6]

Beginning with the gauge sector, we recall that the gauging of $SU(2)_L \times U(1)_Y$ preserves $U(1)_{\rm DM}$ (see e.g. Fig. 3.3), hence the associated loops only yield a contribution to the Higgs mass parameter, denoted $\mu_{h,g}^2$, and one to the quartic coupling, $\lambda_{h,g}$. The UV-finiteness of these coefficients can be obtained by introducing one multiplet of vector resonances in the adjoint of $SO(6)$, ρ_μ, and one in the fundamental, a_μ, and imposing two WSRs that translate into the

[5] Notice that by naive power counting, the quartic couplings can also be quadratically divergent. However, the structure of the field-dependent mass matrices leads to a quadratically divergent term $\sim \Lambda^2 {\rm STr}\, m^2(h,\chi) = \Lambda^2(k_0 + k_h h^2 + k_\chi \chi^*\chi)$ with $k_{0,h,\chi}$ field-independent constants. Thus the leading degree of divergence of the quartics is only logarithmic.

[6] Notice also that, due to the contribution of top quark and SM gauge boson loops, the expression of λ_h in Eq. (3.29) is infrared (IR) divergent. To retain full predictivity, this issue is resolved by adding to $V(\tilde{h}, \chi)$ an additional quartic for $\tilde{h}$ that is non-analytic at $\tilde{h} = 0$. See App. 3.C for further details.

conditions

$$2f_\rho^2 - 2f_a^2 = f^2\,, \qquad f_\rho^2 m_\rho^2 = f_a^2 m_a^2\,, \qquad (\text{WSR } 1+2)_g \tag{3.31}$$

where $f_{\rho,\,a}$ are the decay constants of the resonances, and $m_{\rho,\,a}$ their masses. The first relation removes the quadratic divergence in $\mu_{h,g}^2$ and makes $\lambda_{h,g}$ finite, whereas the second ensures the cancellation of the residual logarithmic divergence in $\mu_{h,g}^2$. Equations (3.31) allow us to express f_a and m_a in terms of f_ρ, m_ρ and f; the first one also requires $f_\rho > f/\sqrt{2}$. The contribution to the Higgs mass parameter reads, at leading order in $g^2/g_\rho^2 \ll 1$ (where $g_\rho = m_\rho/f_\rho$) and neglecting the subleading hypercharge coupling,

$$\mu_{h,\,g}^2 \approx \frac{9\,g^2}{32\pi^2} m_\rho^2 \frac{f_\rho^2}{f^2} \log\left(\frac{2f_\rho^2/f^2}{2f_\rho^2/f^2 - 1}\right). \tag{3.32}$$

Since this is strictly positive, the gauge loops alone do not lead to EWSB. However, a negative contribution to μ_h^2 can easily arise from the fermionic sector, and $\mu_{h,\,g}^2$ will be tuned against it to obtain a realistic Higgs VEV $v \ll f$. On the other hand, the gauge contribution to the Higgs quartic is small, and plays a subleading role.

In the fermionic sector, the elementary-composite mixing parameters ϵ explicitly break the shift symmetries protecting both $\tilde{h}$ and χ, therefore in general fermion loops yield contributions to all the coefficients in the effective potential of Eq. (3.29). To ensure their UV finiteness, we impose two sets of WSRs, which translate into the relations

$$\sum_{i=1}^{N_Q} \left|\epsilon_{qQ}^i\right|^2 = \sum_{j=1}^{N_S} \left|\epsilon_{qS}^j\right|^2, \qquad \sum_{i=1}^{N_Q} \left|\epsilon_{tQ}^i\right|^2 = \sum_{j=1}^{N_S} \left|\epsilon_{tS}^j\right|^2, \qquad (\text{WSR } 1)_f \tag{3.33}$$

$$\sum_{i=1}^{N_Q} \left|\epsilon_{qQ}^i\right|^2 m_{Q_i}^2 = \sum_{j=1}^{N_S} \left|\epsilon_{qS}^j\right|^2 m_{S_j}^2\,, \qquad \sum_{i=1}^{N_Q} \left|\epsilon_{tQ}^i\right|^2 m_{Q_i}^2 = \sum_{j=1}^{N_S} \left|\epsilon_{tS}^j\right|^2 m_{S_j}^2\,. \qquad (\text{WSR } 2)_f \tag{3.34}$$

The first set of WSRs reduce the 1-loop degree of divergence of the mass parameters $\mu_{h,f}^2$ and $\mu_{\mathrm{DM},f}^2$ (where the "f" subscript indicates the fermionic piece) from quadratic to logarithmic and make the dimensionless couplings finite, whereas the second set remove the residual logarithmic divergences in $\mu_{h,f}^2$ and $\mu_{\mathrm{DM},f}^2$. The minimal set of resonances compatible with Eqs. (3.33, 3.34) consists of one $SO(6)$ fundamental Q and one singlet S. This 'one-layer' setup is very predictive, but, as discussed in Sec. 3.3.2, it leads to a DM candidate that is phenomenologically ruled out. Nevertheless, thanks to the simplicity of the one-layer model, we obtain some analytical results and thus gain valuable insight. We then turn to an enlarged setup where two copies of each species of resonance are present below the cutoff. As shown in Sec. 3.3.2, this "two-layer" construction gives sufficient freedom to accommodate a fully viable DM candidate, leading us to concentrate on this model for our phenomenological analysis.

One layer of fermionic resonances

We consider the fermionic Lagrangian of Eq. (3.27) with $N_Q = N_S = 1$. In this case the WSRs in Eqs. (3.33, 3.34) give

$$\epsilon_{qQ}^2 = \epsilon_{qS}^2\,, \qquad \epsilon_{tQ}^2 = \epsilon_{tS}^2\,, \qquad m_Q^2 = m_S^2\,, \tag{3.35}$$

where we have assumed all the parameters to be real, so that CP is conserved. In the following we take, without loss of generality, positive masses $m_Q = m_S \equiv m > 0$. Then the conditions in

Eq. (3.35) do not fix the relative signs of the mixing parameters, $\epsilon_{qQ} = \pm\,\epsilon_{qS}$ and $\epsilon_{tQ} = \pm\,\epsilon_{tS}$. If these two signs are equal, then the non-derivative part of Eq. (3.27) has an additional $SO(7)$ symmetry that allows the Goldstone matrix to be removed by means of a field redefinition (see for example Ref. [113]), hence the scalar potential vanishes. If instead the mixings have opposite sign, the potential does not vanish. Taking for definiteness $\epsilon_{qQ} = -\epsilon_{qS} \equiv -\epsilon_q$ and $\epsilon_{tQ} = \epsilon_{tS} \equiv \epsilon_t$,[7] we find

$$\mu^2_{\mathrm{DM},f} = \lambda_{\mathrm{DM},f} = 0\,, \qquad \lambda_f = -\frac{\mu^2_{h,f}}{f^2} = \frac{N_c \epsilon_q^2 \epsilon_t^2 m^2 \log(M_T^2/M_S^2)}{2\pi^2 f^4 (M_T^2 - M_S^2)}\,, \tag{3.36}$$

where $M^2_{T,S} = m^2 + \epsilon^2_{q,t}$ are the squared masses of the top partners that mix with the q_L and t_R, respectively, neglecting small corrections due to EWSB. Equation (3.36) gives the complete expressions of $\mu^2_{\mathrm{DM}}, \lambda_{\mathrm{DM}}$ and λ, which do not receive any contribution from the gauge sector. In addition, we find the following approximate expression for the Higgs quartic,

$$\lambda_h \approx \frac{N_c \epsilon_q^2 \epsilon_t^2 m^2 \log(M_T^2/M_S^2)}{\pi^2 f^4 (M_T^2 - M_S^2)}\,, \tag{3.37}$$

obtained by neglecting the gauge contribution to the potential. Equations (3.36) and (3.37) suggest the relation $\lambda \approx \lambda_h/2$, which is indeed verified within 20% in our numerical scan of the parameter space. Therefore both the portal coupling and the DM mass are fixed in terms of v and the Higgs mass,

$$\lambda \approx \frac{\lambda_h}{2} \simeq \frac{m_h^2}{4v^2} \simeq 0.065\,, \qquad m_\chi^2 = \lambda v^2 \approx \frac{\lambda_h v^2}{2} \simeq \frac{m_h^2}{4} \simeq (63\ \mathrm{GeV})^2\,. \tag{3.38}$$

Unfortunately, this combination of DM mass and coupling has already been ruled out experimentally: since the DM is light and the portal coupling is not very suppressed, the derivative interactions in Eq. (3.17) have negligible effects, and the phenomenology of χ can be approximately described with a renormalizable Higgs portal model [94, 95, 96]. In this model, the region $\lambda \sim \lambda_h/2$, $m_\chi \sim m_h/2$ has been ruled out by direct detection experiments and, for $m_\chi < m_h/2$, also by LHC bounds on the Higgs invisible width, see e.g. Ref. [115] for a recent assessment.

The problematic values in Eq. (3.38) arose because in the presence of only one layer of resonances, the second set of WSRs in Eq. (3.34) imply that the form factors Π_{L_1} and Π_{R_1} in Eqs. (3.110, 3.111) vanish, and as a consequence we find a non-generic form of the potential, whose structure is entirely determined by the top mass form factor Π_{LR}. Thus it seems plausible that a viable phenomenological scenario may be obtained by extending the model to include a second layer of resonances, which provides additional parametric freedom and should allow for significant departures from Eq. (3.38) while preserving full calculability via WSRs. This hypothesis is supported by a test on the one-layer model, where we lift the second set of WSRs and instead cut off the residual logarithmic divergences in $\mu^2_{h,f}$ and $\mu^2_{\mathrm{DM},f}$ at the scale $\Lambda = 4\pi f$. In this case the potential has a generic form, and accordingly we find that large deviations from Eq. (3.38) are realized. Therefore, in the next subsection we will analyze the model where two layers of fermionic resonances lie below the cutoff. Before doing so, however, we point out a few additional properties of the case $N_Q = N_S = 1$, which apply at least at the qualitative level also in the extended model. Combining Eq. (3.37) with the expression of the top mass at leading order in $\xi \ll 1$, $m_t \simeq \sqrt{2}\epsilon_q \epsilon_t v/(M_T M_S f)$, we obtain

$$\frac{m_h^2}{m_t^2} \approx \frac{N_c}{\pi^2 f^2} \frac{M_T^2 M_S^2}{M_T^2 - M_S^2} \log(M_T^2/M_S^2)\,. \tag{3.39}$$

[7] Notice that by redefining the phases of the resonances, we can equivalently choose a field basis with same-sign mixings and $m_Q + m_S = 0$. This is a realization of the "maximal symmetry" of Ref. [114]. Accordingly, the tuning of the model is minimal, see Eq. (3.41) below.

This relation, which was already obtained in the context of the MCHM based on $SO(5)/SO(4)$ [116, 112], shows that realizing a light Higgs requires at least one of the top partners to be relatively light, with mass roughly comparable to f. Equation (3.39) is verified numerically to good accuracy, with minor corrections arising due to the presence of the gauge contribution in the potential, which was neglected in the derivation of Eq. (3.37). The fine-tuning needed to obtain $v \ll f$ can be estimated using the standard measure [117]

$$\Delta = \Delta_\xi = \max_i \left| \frac{\partial \log \xi}{\partial \log c_i} \right| , \tag{3.40}$$

where c_i denotes the input parameters. In the one-layer model we have $c_i = \{\epsilon_q, \epsilon_t, m, f_\rho, m_\rho\}$, but an immediate estimate of the tuning can be obtained by noticing that if the gauge contribution to V is neglected, Eqs. (3.36)-(3.38) give $\xi \approx 1/2$. Thus $\mu^2_{h,g}$ must be adjusted to give $\xi \ll 1$, leading to a fine-tuning

$$\Delta^{-1} \sim 2\xi \, . \tag{3.41}$$

This is in fact the minimal (or irreducible) amount of tuning characteristic of models where the Higgs potential is entirely generated at the radiative level. A numerical estimate obtained using Eq. (3.40) agrees well with this result.

To conclude, we remark that very similar results, including the prediction of Eq. (3.38), were previously found in Ref. [93] for the realization of the $SO(6)/SO(5)$ model with minimal fermion content.

Two layers of fermionic resonances

We consider the fermionic Lagrangian of Eq. (3.27) with $N_Q = N_S = 2$. In this case the conditions imposed by the first set of WSRs, Eq. (3.33), can be solved in terms of two mixings $\epsilon_{q,t}$ and four angles α, θ, β and ϕ,

$$\frac{\epsilon^1_{qQ}}{\cos\alpha} = \frac{\epsilon^2_{qQ}}{\sin\alpha} = \frac{\epsilon^1_{qS}}{\cos\theta} = \frac{\epsilon^2_{qS}}{\sin\theta} = \epsilon_q \, , \qquad \frac{\epsilon^1_{tQ}}{\cos\beta} = \frac{\epsilon^2_{tQ}}{\sin\beta} = \frac{\epsilon^1_{tS}}{\cos\phi} = \frac{\epsilon^2_{tS}}{\sin\phi} = \epsilon_t \, . \tag{3.42}$$

The second set of WSRs in Eq. (3.34) fixes two of the angles, modulo discrete ambiguities. We choose

$$s^2_{\theta,\phi} = \frac{m^2_{Q_1} - m^2_{S_1} + \left(m^2_{Q_2} - m^2_{Q_1}\right) s^2_{\alpha,\beta}}{m^2_{S_2} - m^2_{S_1}} \qquad (s^2_x \equiv \sin^2 x), \tag{3.43}$$

and without loss of generality we assume $m_{S_2} > m_{S_1}$ and $m_{Q_2} > m_{Q_1}$. The resulting parameter space[8] is scanned numerically, see App. 3.C for details. Figure 3.4 shows the resulting distribution in the (m_χ, λ) plane for two values of f, namely 1 TeV and 1.4 TeV. As expected, large deviations from the predictions of 1-loop-finite one-layer model are generic. First of all, χ is typically much heavier than $m_h/2 \sim 63$ GeV. In particular, its mass populates the 100 - 400 GeV range where, as will be shown in Sec. 3.3.3, we find that the DM relic abundance is around the observed value. In addition, the portal coupling λ can be smaller than $\lambda_h/2 \sim 0.065$. This is crucial because, as will also be discussed in detail in Sec. 3.3.3, direct detection bounds require smaller values of this coupling. In Fig. 3.4 we also observe that a reduction of the portal coupling is correlated with the appearance of light top partners, which can run into tension with the current lower

[8] Note that for special values of the parameters, the model can be realized via a three-site construction [118].

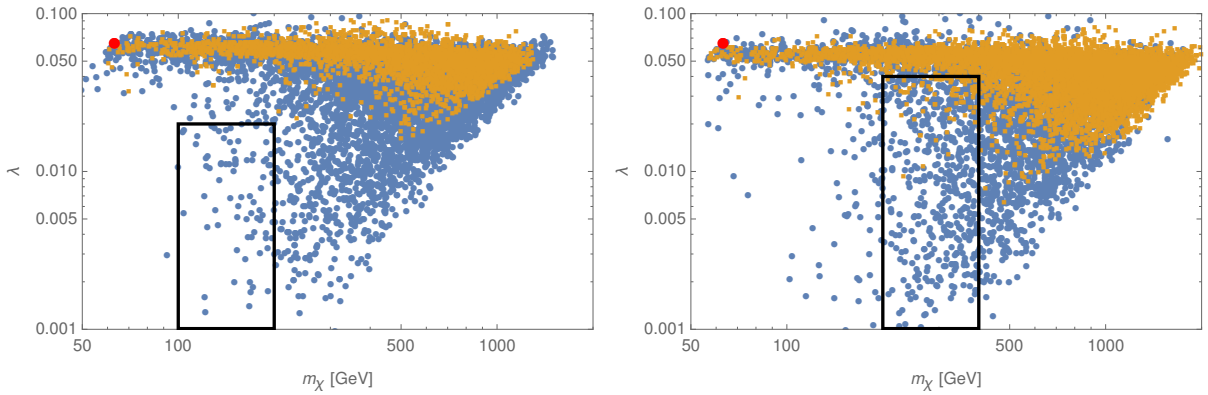

Figure 3.4: *Distribution in the (m_χ, λ) plane for the parameter scan of the two-layer model. The left panel corresponds to $f = 1$ TeV, the right panel to $f = 1.4$ TeV. The black boxes roughly indicate the viable regions of parameters for DM. The red dot shows the approximate prediction of the one-layer model, Eq.* (3.38)*. For orange (blue) points, the lightest fermionic resonance is heavier (lighter) than the approximate LHC lower bound of* 1 *TeV.*

bound of approximately 1 TeV set by LHC searches. (We will discuss the LHC constraints in detail in Sec. 3.3.4, but this rough estimate suffices for the scope of the present discussion.) In fact, for $f = 1$ TeV we do not find any points that have viable DM parameters, i.e. roughly 100 GeV $\lesssim m_\chi \lesssim$ 200 GeV and $\lambda \lesssim 0.02$ (indicated by the black box in the left panel of Fig. 3.4), without running into conflict with top partner bounds. Increasing f relaxes this tension, because it allows the top partners to be naturally heavier and it shifts the viable DM mass region to higher values, where the constraints on λ from direct detection are less stringent. The minimal f that yields a sizable region of allowed parameter space is 1.4 TeV, which we will therefore use as our primary benchmark for the remainder of this subsection. The corresponding viable ranges for the DM mass and portal coupling are 200 GeV $\lesssim m_\chi \lesssim$ 400 GeV and $\lambda \lesssim 0.04$, respectively, shown by the black box in the right panel of Fig. 3.4.

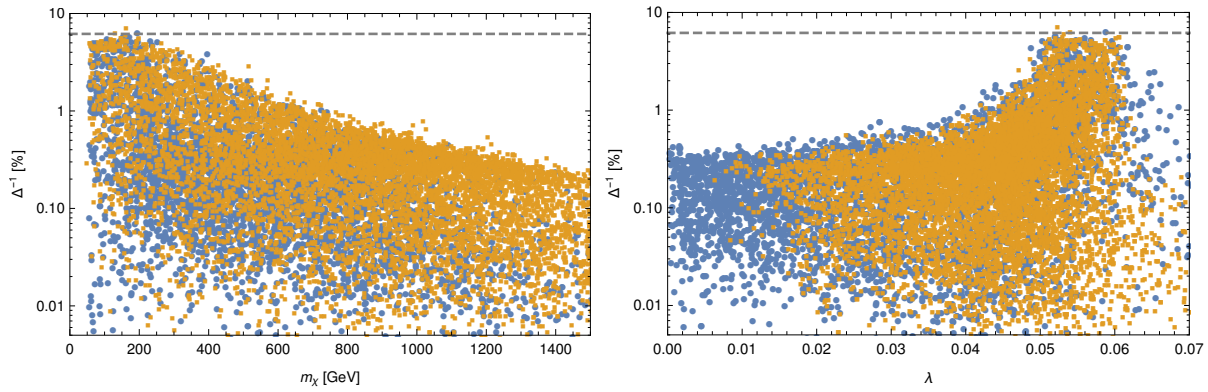

Figure 3.5: *Fine-tuning of the two-layer model, shown versus the DM mass (left panel) and versus the portal coupling (right panel). For orange (blue) points, the lightest fermionic resonance is heavier (lighter) than the approximate LHC lower bound of* 1 *TeV. The scale f is fixed to* 1.4 *TeV.*

The irreducible tuning associated to $f = 1.4$ TeV is, according to Eq. (3.41), $\Delta^{-1} \sim 2\xi \simeq 6\%$. A more precise, point-by-point estimate is obtained by applying the general definition of Eq. (3.40), and shown in Fig. 3.5. We see that as the departure from the predictions of the one-layer model

becomes larger, namely as the χ mass is raised to $m_\chi \gg m_h/2$ and the portal coupling is suppressed to $\lambda \ll \lambda_h/2$, the minimum tuning required increases. The worsening of the tuning for larger m_χ, observed in the left panel of Fig. 3.5, can be explained by noticing that a heavier χ can only be obtained by increasing the size of the form factor Π_{R_1}, which vanishes in the one-layer model (see Eq. (3.113)). This in turn requires a more severe cancellation in the Higgs mass parameter in order to achieve a small ξ. Nevertheless, a phenomenologically viable DM mass, 200 GeV $\lesssim m_\chi \lesssim$ 400 GeV, can be obtained without significantly exacerbating the tuning compared to irreducible contribution of $2\xi \sim 6\%$. On the other hand, from the right panel of Fig. 3.5 we read that a portal coupling that is small enough to satisfy the current direct detection bounds, $\lambda \lesssim 0.04$, requires $\Delta^{-1} \lesssim 1\%$. We have also checked that once the Higgs VEV and mass are fixed to the observed values, no additional tuning is needed in the DM mass: replacing ξ with $\mu^2_{\rm DM}$ in Eq. (3.40), for the points shown in Fig. 3.5 we found that $\Delta^{-1}_{\mu^2_{\rm DM}}$ can be of $O(1)$ even for DM mass as low as 200 GeV. In summary, we estimate that in this model the level of fine-tuning required to solve both the Higgs naturalness and DM puzzles is 1% or slightly worse. This is primarily a consequence of the experimental pressure from direct detection experiments and LHC direct searches for top partners.

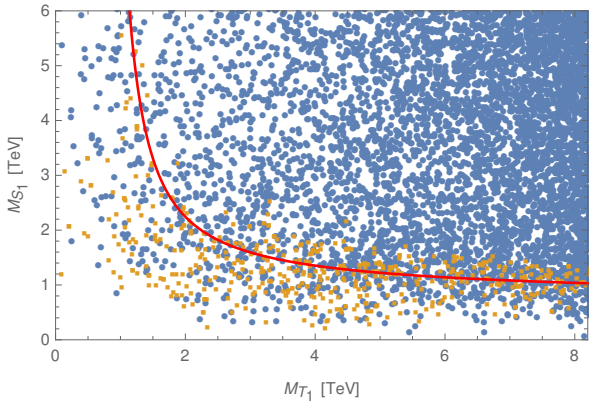

Figure 3.6: *Mass of the lightest top partner mixing with the t_R (M_{S_1}) versus mass of the lightest top partner mixing with the q_L (M_{T_1}), neglecting EWSB corrections, in the two-layer model. Orange (blue) points have a Higgs mass within (outside) the range* 120 GeV $< m_h <$ 130 *GeV. The red line shows the approximate prediction of the one-layer model, Eq.* (3.39)*. We set $f = 1.4$ TeV.*

Figure 3.6 shows that the correlation between a light Higgs and light top partners, which in the one-layer model was expressed by Eq. (3.39), holds in the two-layer setup as well. Furthermore, Eq. (3.39) still yields a reasonable quantitative first approximation, provided we identify M_T and M_S with the masses of the lightest top partners mixing with q_L and t_R, respectively.

Having qualitatively characterized the viable parameter space, we are now ready to present its phenomenology. We begin in Sec. 3.3.3 with DM physics, and then discuss the collider aspects in Sec. 3.3.4.

3.3.3 Dark matter phenomenology

In this section we present the phenomenology of our DM candidate χ. We focus on two main observables, namely the DM relic abundance and the DM-nucleus scattering cross section, which is relevant for direct detection experiments. We conclude the section with a brief comment on the constraints from indirect detection.

Effective theory for DM annihilation

The DM relic abundance is set by the annihilation rate in the early universe, which takes place at an energy scale $\sqrt{s} \sim 2m_\chi \ll m_*$, where m_* denotes the mass of the strong sector resonances ($m_* \sim g_* f$, with g_* some strong sector coupling). The relic abundance can therefore be calculated in an effective theory where the resonances have been integrated out, and only the pNGB scalars χ, h, the SM gauge bosons and the SM fermions are included as propagating degrees of freedom. Assuming that the freeze-out temperature satisfies $T_f \ll v$, which is generically the case for DM with a weak-scale mass, the Lagrangian can be written in the broken electroweak phase. Additionally, we will consider operators which are at most quadratic in the DM field, since higher-order terms do not contribute to the annihilation processes. The effective Lagrangian has the structure

$$\mathcal{L}_{\rm eff} \;=\; \underbrace{\mathcal{L}_{\rm GB} \,+\, \mathcal{L}_t}_{\text{tree}} \underbrace{-\, V_{\rm eff}}_{\text{1-loop}} . \tag{3.44}$$

The first piece originates from the sigma model Lagrangian in Eq. (3.17), expanded in terms of the physical fields

$$\begin{aligned}\mathcal{L}_{\rm GB} \;=\; & \frac{1}{2}(\partial_\mu h)^2\Big(1 + 2\,a_{hhh}\frac{h}{v} + 2\,a_{hh\chi\chi}\frac{\chi^*\chi}{v^2}\Big) + \partial_\mu\chi\partial^\mu\chi^* + \frac{1}{v}\partial_\mu h\,\partial^\mu(\chi^*\chi)\Big(b_{h\chi\chi} + b_{hh\chi\chi}\frac{h}{v}\Big) \\ & + 2\,a_{hVV}\frac{h}{v}\Big(m_W^2 W_\mu^+ W^{-\,\mu} + \frac{m_Z^2}{2} Z_\mu Z^\mu\Big).\end{aligned} \tag{3.45}$$

$V_{\rm eff}$ arises instead from the radiative scalar potential, Eq. (3.29), and reads

$$V_{\rm eff} = \frac{1}{2}m_h^2 h^2 + d_{hhh}\,\frac{m_h^2}{2v}\,h^3 + m_\chi^2\chi^*\chi + 2\,d_{h\chi\chi}v\lambda h\chi^*\chi + d_{hh\chi\chi}\lambda h^2\chi^*\chi\,. \tag{3.46}$$

The scalar couplings in Eq. (3.46), despite being loop-suppressed, can have effects comparable to those of the tree-level interactions in $\mathcal{L}_{\rm GB}$, whose derivative structure leads to a suppression $\sim s/f^2 \ll 1$ (see Eq. (3.51) below) [73]. With the exception of λ, all the dimensionless coefficients in Eqs. (3.45, 3.46) are functions of ξ only and are given in Eq. (3.130).

Finally, the Lagrangian containing the couplings of the top quark relevant to DM annihilation is

$$\mathcal{L}_t = i\bar{t}\not{\partial}t - m_t\bar{t}t\Big(1 + c_{tth}\frac{h}{v} + 2\,c_{tt\chi\chi}\frac{\chi^*\chi}{v^2}\Big), \tag{3.47}$$

where the dimensionless coefficients have the form

$$c_k = c_k^{\rm nl\sigma m}(\xi) + O\Big(\xi\frac{\epsilon^2}{m_*^2}\Big), \qquad k = \{tth, tt\chi\chi\}. \tag{3.48}$$

The functions $c_k^{\rm nl\sigma m}(\xi)$ encode the nonlinearity of the sigma model and read

$$c_{tth}^{\rm nl\sigma m} = \frac{1-2\xi}{\sqrt{1-\xi}}\,, \qquad c_{tt\chi\chi}^{\rm nl\sigma m} = -\frac{\xi}{2(1-\xi)}\,. \tag{3.49}$$

The additional terms in the RHS of Eq. (3.48) come instead from the mixing of the top with the top partners. These terms are suppressed unless one of the chiralities of the top is largely composite, in which case $\epsilon \sim m_*$, and were neglected in the previous studies of composite pNGB DM of Refs. [73, 93]. In our analysis, however, we find that these corrections play a very important role, as can be seen in Fig. 3.7, where the full numerical value of the c_k coefficients

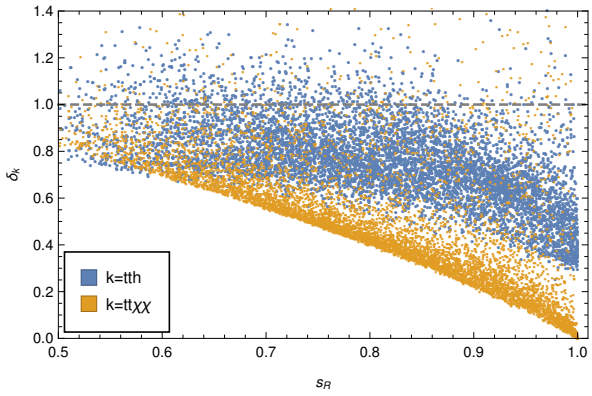

Figure 3.7: *Corrections from top partner mixing to the effective $t\bar{t}h$ and $t\bar{t}\chi^*\chi$ couplings, defined as $\delta_{tt\chi\chi} \equiv c_{tt\chi\chi}/c^{\mathrm{nl}\sigma\mathrm{m}}_{tt\chi\chi}$ and $\delta_{tth} \equiv (c_{tth}-1)/(c^{\mathrm{nl}\sigma\mathrm{m}}_{tth}-1)$, as functions of the compositeness fraction s_R of the right handed top (see Eq. (3.117) for its definition). The gray dashed line indicates the pure sigma model result, where top partner mixing is neglected. The points shown are obtained from a parameter scan of the two-layer model with $f = 1.4$ TeV, requiring all fermionic resonances to be heavier than the approximate LHC bound of 1 TeV.*

is compared to the $c^{\mathrm{nl}\sigma\mathrm{m}}_k(\xi)$. In particular, the coefficient $c_{tt\chi\chi}$ is strongly suppressed by top partner mixing even for moderate t_R compositeness, and in the limit of fully composite t_R the top partner contribution exactly cancels $c^{\mathrm{nl}\sigma\mathrm{m}}_{tt\chi\chi}(\xi)$, leading to a vanishing $c_{tt\chi\chi}$. This can be understood as follows: With our choice of embeddings, the shift symmetry of the DM pNGB χ is automatically preserved by the couplings of the elementary q_L to the strong sector resonances, whereas the couplings of the elementary t_R break it (see Eq. (3.24)). However, in the limit where the physical RH top is a fully composite field (whose overlap with the elementary fermion is zero), its couplings also preserve the χ shift symmetry, hence a non-derivative $t\bar{t}\chi^*\chi$ coupling is forbidden. On the other hand, the $t\bar{t}h$ coupling receives smaller, but still important, corrections from top partner mixing.[9]

DM relic abundance

The present abundance of DM, which arises from its freeze-out in the early Universe, is computed by solving the corresponding Boltzmann equation. A useful approximate solution is given by

$$\frac{\Omega_{\mathrm{DM}}h^2}{0.1198} \simeq \frac{3\cdot 10^{-26}\mathrm{cm}^3\,\mathrm{s}^{-1}}{\frac{1}{2}\langle\sigma v_{\mathrm{rel}}\rangle(T_f)}\,. \tag{3.50}$$

On the LHS of this equation, Ω_{DM} is the ratio between the energy density of DM and the critical energy density of the Universe, $h = H_0/(100\ \mathrm{km/s/Mpc})$ is the reduced value of the present Hubble parameter, and $(\Omega_{\mathrm{DM}}h^2)_{\mathrm{exp}} = 0.1198 \pm 0.0015$ is the experimental value as measured by the Planck collaboration [119]. On the RHS, $\langle\sigma v_{\mathrm{rel}}\rangle(T_f)$ is the thermally averaged annihilation cross section times the relative velocity of two DM particles, computed at the freeze-out temperature $T_f \approx m_\chi/20$. The factor 1/2 in the denominator of the RHS accounts for the fact that the DM is not self-conjugate.

DM annihilation proceeds dominantly via $\chi\chi^* \to t\bar{t}, WW, ZZ$ and hh. All these processes are mediated by diagrams where a Higgs is exchanged in the s-channel. Even though the $\chi\chi^* \to hh, t\bar{t}$ amplitudes receive additional contributions, it is nevertheless useful to assume in

[9] Notice that the $t\bar{t}h$ coupling does not vanish at full RH top compositeness, because even in that limit the coupling of q_L to the strong sector breaks the h shift symmetry.

first approximation that annihilation proceeds entirely through s-channel Higgs exchange. In this case the cross section is proportional to the square of the $\chi\chi^* h$ vertex, which from the effective Lagrangian of Eq. (3.44) reads

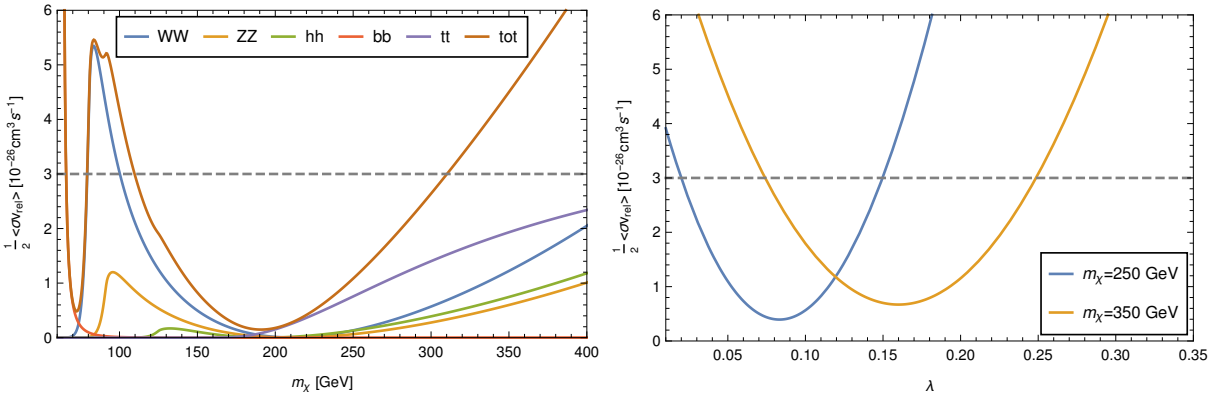

Figure 3.8: *Thermally averaged cross section for DM annihilation. The gray dashed line shows the value required to reproduce the present relic abundance according to the approximate relation in Eq.* (3.50)*. The scale f was fixed to* 1.4 *TeV. In the left panel we set the portal coupling to the representative value $\lambda = 0.05$, in the right panel we chose two representative values of the DM mass. In both panels the $t\bar{t}h$ and $t\bar{t}\chi^*\chi$ couplings were set to their sigma model values (Eq.* (3.49)*), thus neglecting top partner mixing. With this simplification, $\langle\sigma v_{\rm rel}\rangle$ is completely determined by f, m_χ and λ.*

$$\sigma v_{\rm rel} \propto \left(\frac{b_{h\chi\chi}}{v} s - 2\, d_{h\chi\chi}\lambda v\right)^2 \approx v^2\left(\frac{s}{f^2} - 2\lambda\right)^2, \tag{3.51}$$

where the first term comes from the derivative interactions in Eq. (3.45) and the second term from the radiative scalar potential in Eq. (3.46). Neglecting relativistic corrections we have $s \approx 4m_\chi^2$, therefore the two contributions cancel out for $m_\chi^2 \sim \lambda f^2/2$, leading to a strong suppression of the annihilation cross section [73, 93, 120]. This feature can be clearly observed in the cross sections for annihilation into WW, ZZ and also hh, see the left panel of Fig. 3.8. The structure in Eq. (3.51) also implies that for given f and m_χ, there are two values of the portal coupling λ that reproduce the observed DM relic density, see the right panel of Fig. 3.8. As will be shown below, however, the branch with larger λ is excluded by direct detection, whereas the one with smaller portal coupling provides a viable scenario.

For $m_\chi > m_t$, the simple scaling in Eq. (3.51) is violated by the $\chi\chi^* \to t\bar{t}$ amplitude, where the $t\bar{t}\chi^*\chi$ contact interaction plays an important role. This is illustrated in Fig. 3.9, where we show the effect on the total annihilation cross section of varying the $t\bar{t}\chi^*\chi$ coupling within the range $c_{tt\chi\chi}^{\rm nl\sigma m} < c_{tt\chi\chi} < 0$, which contains all phenomenologically interesting points (recall Fig. 3.7). The effect of top partner mixing is to suppress $|c_{tt\chi\chi}|$, which in turn shifts the DM relic abundance contour to larger m_χ for fixed λ, or conversely, to smaller λ for fixed DM mass. As can be seen in the right panel of Fig. 3.9, at fixed m_χ the shift is larger for the branch with smaller λ. This can be explained by noticing that the size of the amplitude containing the $t\bar{t}\chi^*\chi$ contact interaction, relative to the one that couples $\chi\chi^*$ to an s-channel virtual Higgs via the portal coupling, is parametrically $2m_\chi^2/(\lambda f^2)$ (for $m_\chi \gg m_h/2$). On the branch with larger λ this ratio is smaller than 1, so the corrections to the $t\bar{t}\chi^*\chi$ coupling play a subleading role. Conversely, on the branch with smaller λ the ratio is larger than 1, hence the reduction of the portal coupling caused by top partner mixing is sizable. As it will be shown below, this effect is crucial to evade direct detection bounds.

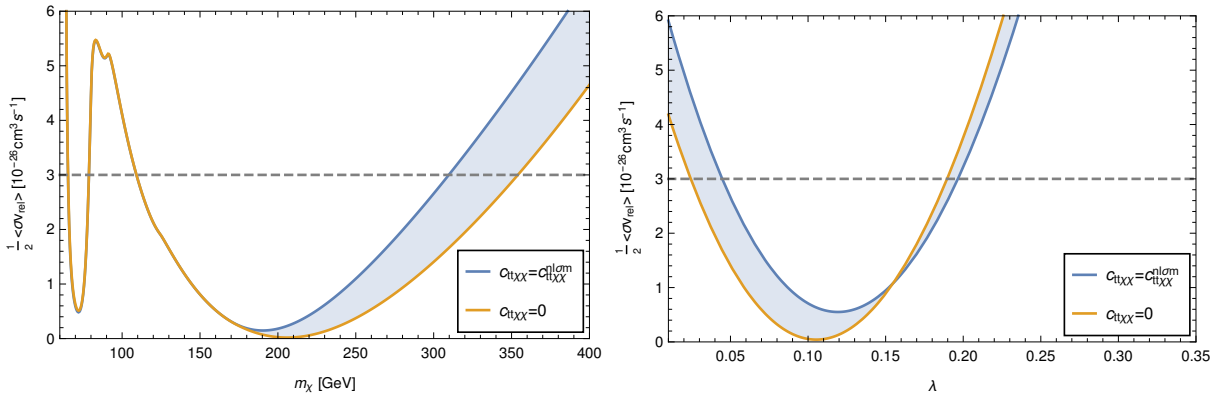

Figure 3.9: *Impact on the total annihilation cross section of varying the strength of the $t\bar{t}\chi^*\chi$ contact interaction in the range $c_{tt\chi\chi} \in [c_{tt\chi\chi}^{\rm nl\sigma m}, 0]$. The lower value corresponds to the pure sigma model, where top partner mixing is neglected, whereas the upper value corresponds to a setup with fully composite t_R, where top partner mixing is maximal. The realistic parameter points lie within this range, i.e. they fall within the band shaded in blue. The gray dashed line shows the value required to reproduce the present relic abundance according to the approximate relation in Eq.* (3.50)*. In the left panel we set $\lambda = 0.05$, whereas in the right panel the DM mass was fixed to $m_\chi = 300$ GeV. We took $f = 1.4$ TeV in both panels.*

Radiative corrections to pNGB derivative interactions

Throughout our discussion thus far, the effects of gauge and fermionic loops were taken into account via the CW effective potential. In particular, for the computation of the annihilation cross sections we made use of Eq. (3.44), where the tree-level couplings were supplemented by the 1-loop CW term. The effective potential, however, only captures the radiative corrections in the approximation of vanishing external momenta. This is not appropriate for DM annihilation, where the relevant external momentum scale is $p \sim m_\chi$, and 1-loop corrections to derivative operators of $O(p^2)$ are expected to be also important. As an illustrative example, let us consider the $\chi\chi^* hh$ interaction at high energies, where EWSB effects can be neglected. From Eq. (3.45), the tree-level (derivative) coupling reads simply

$$\mathcal{L}_{\rm GB} \supset \frac{1}{f^2} h\partial_\mu h(\chi^*\partial^\mu\chi + \chi\partial^\mu\chi^*). \tag{3.52}$$

Radiative corrections to this interaction arise only from the fermion sector. The $O(p^0)$ 1-loop contribution is proportional to the $SO(7)$-breaking parameters ϵ and is just given by the portal coupling, $V_{\rm eff} \supset \lambda h^2\chi^*\chi$. It is in general logarithmically UV-divergent, but it is rendered finite by the set of WSRs in Eq. (3.33). The $O(p^2)$ 1-loop term must also be proportional to the ϵ parameters, because in the limit of vanishing explicit breaking, $\epsilon \to 0$, the $O(p^2)$ scalar Lagrangian is simply given by the sigma model kinetic term, Eq. (3.15), whose coefficient is fixed by f. Then the radiatively corrected form of the two-derivative coupling can be estimated as

$$i(c_{\rm tree} + c_{1-\rm loop})\frac{p^2}{f^2}\,, \qquad c_{\rm tree} \sim 1\,, \qquad c_{1-\rm loop} \sim \frac{N_c\epsilon^2}{16\pi^2 f^2}\log\Lambda^2\,. \tag{3.53}$$

Notice that $c_{1-\rm loop}$ is expected to be logarithmically divergent, since the WSRs in Eqs. (3.33, 3.34) do not soften its UV behavior. The log enhancement, together with the fact that in general the ratio ϵ/f is of $O(1)$ or even somewhat larger, make this 1-loop correction potentially very important and thus warrant a detailed calculation. We find four classes of diagrams that

renormalize the operator in Eq. (3.52), depicted in Fig. 3.10. Two types of fermion-scalar vertices appear in the diagrams: the non-derivative couplings arising from elementary-composite mixing terms, as well as the derivative couplings originating from the e_μ symbol that are contained in the kinetic terms of the resonances in the $SO(6)$ fundamental, $\sum_i \bar{Q}_i \not{e} Q_i$.[10] Neglecting external masses, so that $s + t + u \simeq 0$, we find for the $O(p^2)$ piece of the $\chi^*\chi \to hh$ amplitude (see App. 3.D for details)

$$i(c_{\rm tree} + c_{1-\rm loop})\frac{s}{f^2}\,, \qquad c_{\rm tree} = 1\,, \qquad c_{1-\rm loop} = \frac{N_c}{2\pi^2 f^2}\Big(\epsilon_t^2 - \frac{\epsilon_q^2}{8}\Big)\log\frac{\Lambda^2}{m_*^2}\,, \tag{3.54}$$

where we have imposed the WSRs, and m_* stands for the mass of some fermionic resonance. Notice the mild loop suppression factor $N_c/(2\pi^2)$, and the log enhancement. After EWSB, this interaction contributes to the trilinear $\chi^*\chi h$ derivative coupling, which as we discussed in

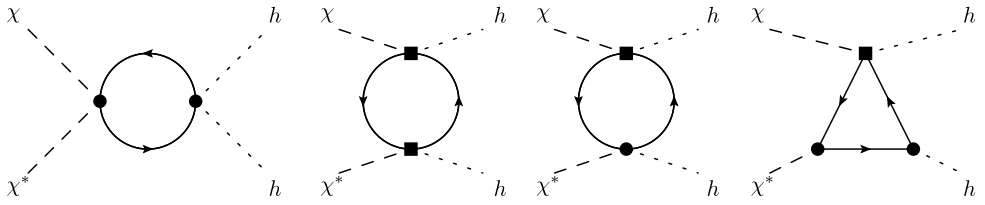

Figure 3.10: *Representative set of* 1*-loop diagrams that contribute to the renormalization of the* $\chi^*\chi hh$ *interaction at* $O(p^2)$*. The circles indicate non-derivative interactions arising from elementary-composite mixing terms, whereas the squares denote derivative couplings originating from the* e_μ *symbol (see Eq.* (3.27)*).*

Sec. 3.3.3 enters all annihilation cross section amplitudes, and in fact dominates in the viable region of parameters, where λ is suppressed. Therefore in order to retain predictivity, we must keep the size of the radiative correction under control. We find an irreducible uncertainty of about 50% at the cross section level, which corresponds to

$$0.5 < \Big(1 + \frac{c_{1-\rm loop}}{c_{\rm tree}}\Big)^2 < 1.5 \qquad \longrightarrow \qquad -0.4 < \frac{1}{f^2}\Big(\epsilon_t^2 - \frac{\epsilon_q^2}{8}\Big) < 0.3\,, \tag{3.55}$$

where we have estimated $\Lambda \sim 10$ TeV and $m_* \sim 1$ TeV. Barring a cancellation $\epsilon_q^2 \approx 8\,\epsilon_t^2$, which may be regarded as a tuning unless it can be enforced by a symmetry, a further reduction of the uncertainty would lead to values of $\epsilon_{q,t}$ that are too small to reproduce the measured top mass. In conclusion, we will require that Eq. (3.55) is satisfied throughout our phenomenological analysis, and we will correspondingly assign a 50% theoretical uncertainty on the total DM annihilation cross section.

Constraints from DM direct detection

Direct detection experiments aim at revealing DM-nucleus scattering events by measuring the nuclear recoil energy. Currently, the strongest constraints on the spin-independent (SI) DM-nucleon elastic cross-section come from the Xenon-based XENON1T [100] and LUX [121] experiments, with the former providing a slightly tighter bound. In our model, the elastic scattering of DM with a quark q is mediated by three types of diagrams: Higgs exchange in the t-channel, the $\chi^*\chi\bar{q}q$ contact interaction, and diagrams involving the exchange of the

[10] Notice that in general the couplings containing the d_μ symbol that appear in Eq. (3.28) also contribute. However, for simplicity we set their coefficients to zero in the computation.

$U(1)_{\rm DM}$-charged top partners $\mathcal{Y}, \mathcal{Z}$. The first two classes mediate scattering with all quarks, whereas the exchange of $\mathcal{Y}, \mathcal{Z}$ only affects the scattering with (virtual) tops. Importantly, in Higgs exchange diagrams the contribution of the derivative coupling $\sim (v/f^2)\partial h \partial(\chi^*\chi)$ is suppressed by $-q^2/f^2 \ll 1$, where $\sqrt{-q^2} \lesssim 100$ MeV is the small momentum transfer. Therefore these diagrams are effectively proportional to the portal coupling λ. Furthermore, throughout the realistic parameter space the Higgs exchange amplitude dominates, being enhanced by $2\lambda f^2/m_h^2 \gg 1$ with respect to the sum of the other two terms. Hence the SI DM-nucleon cross section is well approximated by the simple expression familiar from the renormalizable Higgs portal model (see e.g. Ref. [122]),

$$\sigma_{\rm SI}^{\chi N} \simeq \frac{f_N^2}{\pi}\frac{m_N^4\lambda^2}{m_\chi^2 m_h^4} \sim 4\cdot 10^{-46}\,{\rm cm}^2 \left(\frac{\lambda}{0.03}\right)^2\left(\frac{300\ {\rm GeV}}{m_\chi}\right)^2, \tag{3.56}$$

where m_N is the nucleon mass, and $f_N \simeq 0.30$ contains the dependence on the nucleon matrix elements. The exact expression of $\sigma_{\rm SI}^{\chi N}$ is reported in App. 3.D. The cross section value $4\cdot 10^{-46}$ cm^2 corresponds to the current 90% CL upper bound at $m_{\rm DM} = 300$ GeV from XENON1T [100], showing that direct detection constraints require λ to be suppressed by about a factor 2 with respect to the most natural value $\lambda \sim \lambda_h/2 \sim 0.065$. Notice that to calculate the excluded regions in the (m_χ, λ) plane of Fig. 3.11 below, the local DM density was assumed to take the standard value $\rho_0 = 0.3$ GeV cm^{-3}, independently of the predicted thermal value. All direct detection constraints are given at 90% CL.

Results

The main results of our phenomenological analysis are shown in Fig. 3.11. We set $f = 1.4$ TeV and perform a parameter scan, imposing that v, m_h and m_t match the experimental values. We also require each point to be compatible with detailed LHC constraints on top partners, which are discussed in Sec. 3.3.4 below and summarized in Eq. (3.60). In addition, the parameter space is restricted by the condition of Eq. (3.55), thus ensuring that the theoretical uncertainty on the annihilation cross section due to missing radiative corrections is within 50%. The points are projected onto the plane (m_χ, λ), using three different colors depending on whether the relic abundance is compatible with (green), exceeds (red) or undershoots (purple) the observed value. To compute the relic abundance we implemented the effective Lagrangian of Eq. (3.44) in FeynRules [98] and used micrOMEGAs [123] to solve the Boltzmann equation (see App. 3.D for details) for the DM density.[11] Notice that the couplings involving the top quark depend on the elementary-composite mixings and top partner masses, hence the relic abundance is not a function only of f, m_χ and λ, but must be separately evaluated at each point in parameter space. By contrast, the bounds from direct detection experiments, namely LUX (brown) and XENON1T (gray), are insensitive to the top partner parameters.

In the upper panel of Fig. 3.11, we illustrate the effect of neglecting the 50% theoretical uncertainty on $\langle\sigma v_{\rm rel}\rangle$, and show in green color the points that yield a relic abundance within 5% of the observed value. For reference we also show, as thick blue lines, the 3σ relic abundance contours that are obtained by setting the $t\bar{t}h$ and $t\bar{t}\chi^*\chi$ couplings to their sigma model values. In this limit the annihilation cross section is completely fixed by $\{f, m_\chi, \lambda\}$. The "two-branch" structure discussed in Sec. 3.3.3 is clearly visible: for each value of $m_\chi \gtrsim 180$ GeV there are two values of λ that reproduce the correct relic abundance. In the upper branch DM annihilation proceeds dominantly through the portal coupling, whereas in the lower branch it is controlled

[11] This treatment includes annihilation into light quarks and leptons, as well as into the three-body final states WW^* or ZZ^*, which become important for lighter DM.

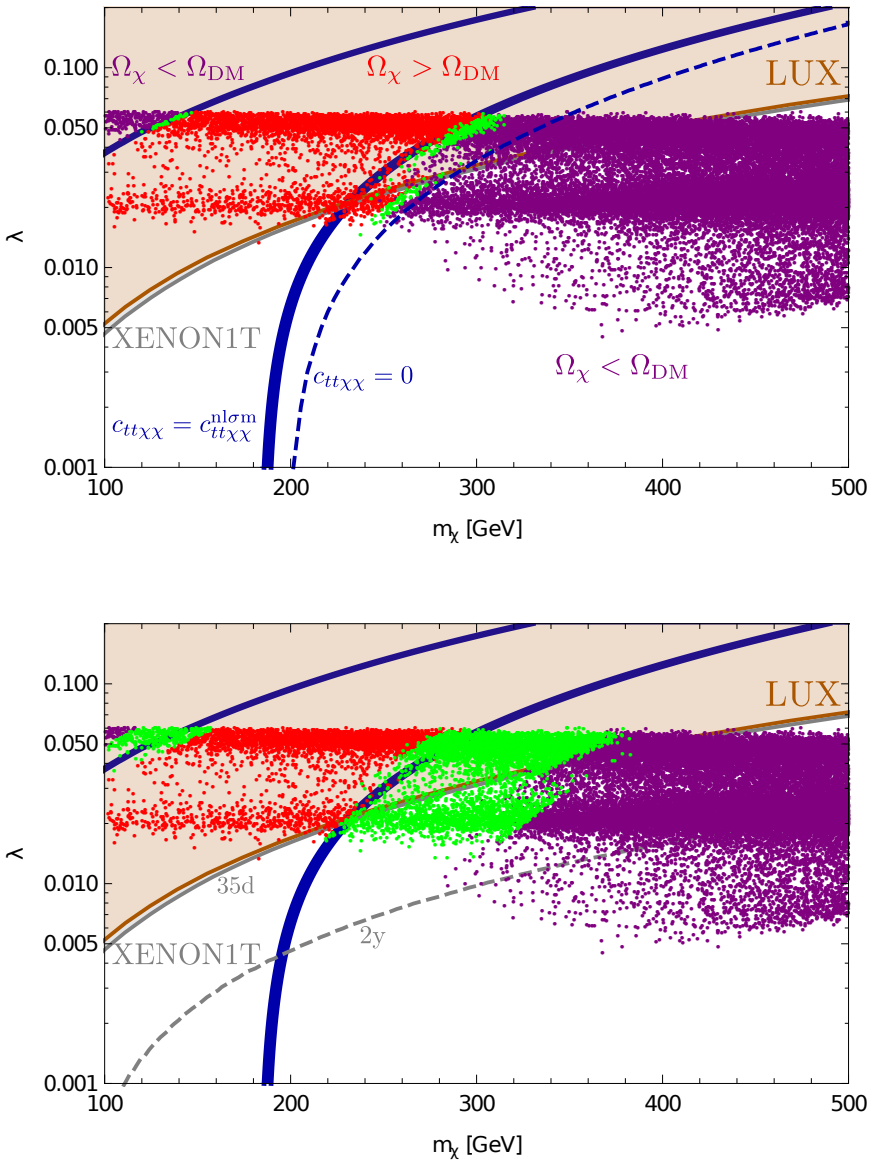

Figure 3.11: *Distributions in the (m_χ, λ) plane that summarize our analysis of DM phenomenology. The points have different colors depending on whether they are compatible with (green), exceed (red) or undershoot (purple) the observed value of the DM relic abundance. In the upper (lower) panel, the theoretical uncertainty of 50% on the annihilation cross section is neglected (included). See the main text for further explanations on the meaning of the different curves.*

primarily by the derivative interactions. In between the branches the two effects strongly cancel (see the discussion below Eq. (3.51)), leading to a suppressed annihilation cross section and therefore to over-abundant DM. On the contrary, outside of the two branches one of the two couplings becomes too strong, and as a consequence the DM is under-abundant. The upper branch is robustly ruled out by direct detection, and we therefore focus on the lower branch. Here the green points fall between the two relic abundance contours obtained setting $c_{tt\chi\chi} = c_{tt\chi\chi}^{\rm nl\sigma m}$ (solid blue) and $c_{tt\chi\chi} = 0$ (dashed blue). The latter corresponds to maximal t_R compositeness. For fixed m_χ, a suppressed $|c_{tt\chi\chi}|$ reduces the portal coupling required for the correct relic abundance, and this in turn relaxes the direct detection constraints. Indeed, the subset of viable

points that are compatible with direct detection limits lies close to the $c_{tt\chi\chi} = 0$ curve. Had we not included top partner mixing, we would have wrongly concluded that all these points are ruled out by LUX and XENON1T data. This highlights the importance of carefully taking into account the effects of the fermionic resonances.

In the lower panel of Fig. 3.11 we show the complete picture. The theoretical uncertainty is now included, so the green points reproduce the experimental value of the relic abundance within 50%. We find a large set of points that reproduce the relic abundance within the uncertainty, and at the same time evade the current direct detection bounds. The DM mass is in the range 200 GeV $\lesssim m_\chi \lesssim$ 400 GeV and the portal coupling between roughly $0.01 \lesssim \lambda \lesssim 0.04$. We also show, as a dashed gray curve, the projected XENON1T sensitivity after two years of data taking [101] (whereas the "35d" label on the solid dashed curve refers to the current exposure of 35 days [100]). All the currently viable points lie well within the ultimate reach of XENON1T, which will thus be able to test the entire parameter space of the model for $f = 1.4$ TeV.

Indirect detection

Indirect detection experiments, which search for signals of DM annihilation in the galaxy halo, constitute an additional probe of the model discussed here. Detailed constraints from the antiproton spectrum measured by PAMELA [124] were presented, for the real singlet pNGB DM in the $SO(6)/SO(5)$ model, in Ref. [93]. Since the annihilation pattern of our complex DM is very similar, we were able to check that the viable region of our parameter space is safely compatible with PAMELA antiproton data. It is important to observe that changing the assumptions on the systematic uncertainties that affect the astrophysical backgrounds can have a very large impact on the antiproton limits. For example, the more conservative approach taken in Ref. [125] resulted in bounds on the DM annihilation cross section at present time, $\langle\sigma v_{\rm rel}\rangle_0$, that were an order of magnitude weaker than those quoted in Ref. [93]. Very recently, Refs. [126, 127] used the new AMS-02 antiproton measurement [128] to set very strong constraints. For example, assuming annihilation into $b\bar{b}$ the thermal value of the cross section $\langle\sigma v_{\rm rel}\rangle_0 \sim 3 \times 10^{-26}$ cm^3 s^{-1} was excluded for DM masses in the range 150 GeV $\lesssim m_{\rm DM} \lesssim$ 500 GeV [126]. A detailed scrutiny of the AMS-02 constraints on pNGB DM, including the aforementioned large impact of the assumptions on systematic uncertainties, is an interesting direction for future work. Finally, we note that gamma ray observations of nearby dwarf spheroidal galaxies also set competitive bounds on DM annihilation, while being affected by smaller systematics compared to the antiproton channel. The current limits are roughly $\langle\sigma v_{\rm rel}\rangle_0 \lesssim 10^{-25}$ cm^3 s^{-1} for DM mass in the few hundred GeV range [129].[12]

3.3.4 Collider phenomenology

In this section the collider phenomenology of the model is outlined, focusing on the signals of fermionic top partners at hadron colliders, which constitute the most sensitive probe. Nevertheless, before discussing this aspect in more detail we briefly touch upon other observables. Due to its pNGB nature, the Higgs boson couples to the other SM particles with strength that deviates at $O(v^2/f^2)$ from the SM predictions. In particular, the hVV coupling ($V = W, Z$) is rescaled by a factor $c_V = \sqrt{1-\xi}$. For our benchmark value $f = 1.4$ TeV, the deviation is of $\approx 1.5\%$, which is unaccessible at the LHC, but will be tested at future e^+e^- colliders (see Ref. [130] for a recent overview). Parametrically similar deviations affect other SM couplings, such as $h\bar{t}t$, $hgg/h\gamma\gamma$ and $Z\bar{t}t$, which however will be tested with less accuracy than hVV. In addition, monojet searches only provide subleading constraints, because the coupling of χ to the proton

[12] We thank A. Urbano for illuminating discussions about indirect detection constraints.

constituents is very weak. In particular the contact interactions $\bar{q}q\chi^*\chi$, where q is a light quark, are Yukawa-suppressed (if present at all).

LHC constraints on top partners

A rather generic feature of pNGB Higgs models with partial compositeness is that the lightness of the Higgs requires at least some of the top partners to be light, $m_* = g_* f$ with $g_* \sim 1$ (see Ref. [131] for an extensive discussion). In our model, this is illustrated by Fig. 3.6. Since the top partners are colored, the searches for their signals at hadron colliders, in particular at the LHC, are among the most important experimental tests of the composite Higgs framework [132, 133, 134, 110]. In the following discussion we adopt a simplified model where only one layer of resonances, containing one $SO(6)$ fundamental Q and one singlet S, is included. This captures the main phenomenological features of the complete model, provided the second layer of resonances is somewhat heavier than the first, as it is the case in most of the parameter space.

We start from the fermionic Lagrangian in Eq. (3.27) with $N_Q = N_S = 1$. Notice that, as consistently done throughout our analysis, the coefficients of the derivative interactions in Eq. (3.28) are set to zero, $c^{L,R} = 0$. We will return to the possible role of these interactions in LHC physics in Sec. 3.3.4. Neglecting EWSB effects, the elementary-composite mixings are diagonalized by the rotations

$$\begin{pmatrix} t_R \\ S_R \end{pmatrix} \to \begin{pmatrix} \cos\phi_R & -\sin\phi_R \\ \sin\phi_R & \cos\phi_R \end{pmatrix} \begin{pmatrix} t_R \\ S_R \end{pmatrix}, \qquad \begin{pmatrix} q_L \\ Q_L \end{pmatrix} \to \begin{pmatrix} \cos\phi_L & -\sin\phi_L \\ \sin\phi_L & \cos\phi_L \end{pmatrix} \begin{pmatrix} q_L \\ Q_L \end{pmatrix}, \tag{3.57}$$

where $Q \equiv (T, B)^T$ and the mixing angles are $\tan\phi_R = \epsilon_{tS}/m_S$ and $\tan\phi_L = \epsilon_{qQ}/m_Q$. On the other hand, the remaining fermions contained in Q, namely the exotic doublet $(X_{5/3}, X_{2/3})^T$ and the $U(1)_{\rm DM}$-charged SM singlets $\mathcal{Y}, \mathcal{Z}$, do not mix with the elementary fermions. In summary, the top partner masses are

$$M_S = \sqrt{m_S^2 + \epsilon_{tS}^2}\,, \qquad M_{T,B} = \sqrt{m_Q^2 + \epsilon_{qQ}^2}\,, \qquad M_{X_{5/3},\, X_{2/3},\, \mathcal{Y},\, \mathcal{Z}} = m_Q\,. \tag{3.58}$$

Hence at the bottom of the spectrum we find either a singlet S, or four approximately degenerate states $X_{2/3}, X_{5/3}, \mathcal{Y}$ and $\mathcal{Z}$.[13] The scan of the complete two-layer model, shown in the left panel of Fig. 3.12, demonstrates that the lightest top partner is typically a singlet, although the alternative configuration is also possible. The decay patterns of the resonances can be immediately understood using the Goldstone equivalence theorem. Expanding the U matrix to $O(1/f)$ and diagonalizing the elementary-composite mixings via Eq. (3.57), one immediately finds the leading order results

$$\begin{aligned} \mathrm{BR}(S \to W^+ b) &= 2\,\mathrm{BR}(S \to Zt) = 2\,\mathrm{BR}(S \to ht) = \frac{1}{2}\,, \\ \mathrm{BR}(T \to ht) &= \mathrm{BR}(T \to Zt) = \mathrm{BR}(X_{2/3} \to ht) = \mathrm{BR}(X_{2/3} \to Zt) = \frac{1}{2}\,, \\ \mathrm{BR}(X_{5/3} \to W^+ t) &= \mathrm{BR}(B \to W^- t) = \mathrm{BR}(\mathcal{Y} \to \chi t) = \mathrm{BR}(\mathcal{Z} \to \chi^* t) = 1\,. \end{aligned} \tag{3.59}$$

In particular, as a consequence of $U(1)_{\rm DM}$ conservation, $\mathcal{Y}\,(\mathcal{Z})$ always decays into a top quark and a $\chi\,(\chi^*)$ particle (see Refs. [135, 81, 82] for recent studies of top partner decays into additional Goldstone scalars). The above predictions are well respected in the complete model. For example, in the right panel of Fig. 3.12 the exact branching ratios of the singlet are shown, for the parameter points where it is the lightest fermionic resonance. We find good agreement with Eq. (3.59).

[13] EWSB effects do not alter the masses of $X_{5/3}, \mathcal{Y}$ and $\mathcal{Z}$, which remain exactly degenerate, but they do shift $M_{X_{2/3}}$ slightly. The correction can have either sign depending on the parameter point.

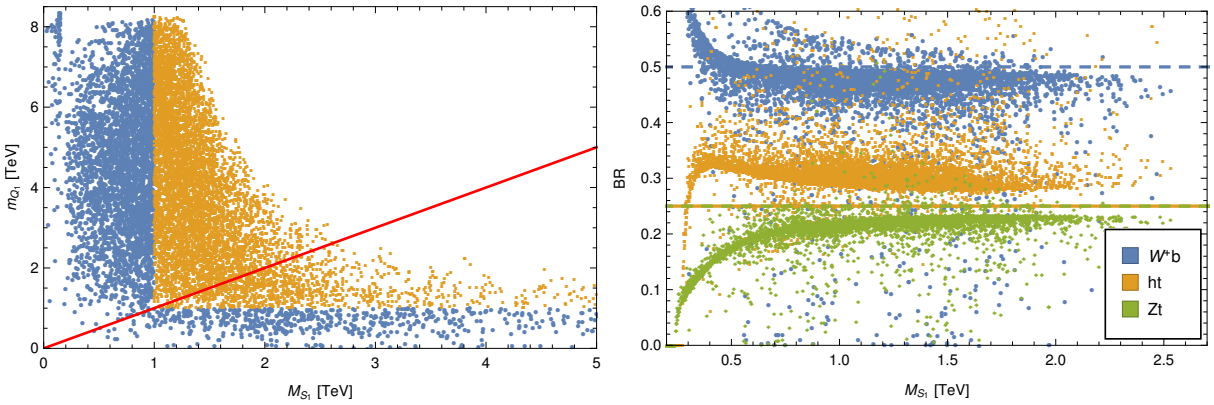

Figure 3.12: *Distributions in the model with two fermionic resonance layers. Left: mass of the lightest exotic top partner (m_{Q_1}) versus the mass of the lightest singlet top partner (M_{S_1}). For orange (blue) points, the lightest fermionic resonance is heavier (lighter) than the approximate LHC lower bound of 1 TeV. The red line corresponds to $m_{Q_1} = M_{S_1}$. Right: branching ratios of the lightest singlet S_1, for the parameter points where it is the lightest fermionic resonance. The dashed lines indicate the leading order predictions, see Eq.* (3.59).

The LHC searches for top partners target two distinct production mechanisms: pair production via the QCD interactions, namely $pp \to \bar{\psi}\psi$ where ψ is a generic top partner, and single production in association with a top or bottom via the electroweak interactions, for example for a singlet S the leading process is $pp \to S\bar{b}j$ via the $\bar{b}W^-S$ vertex. Notice that the $U(1)_{\rm DM}$-charged top partners $\mathcal{Y}$ and $\mathcal{Z}$ cannot be singly produced. We have verified that under our assumption $c_{ji}^{L,R} = 0$, the bounds from single production [79] are weaker than those coming from QCD pair production [80, 136], hence we only discuss the latter. For simplicity, in the following we set the branching ratios to the approximate values of Eq. (3.59). The search of Ref. [80] focuses on the $\bar{\psi}\psi \to t(h \to b\bar{b})+X$ process in 1- and 0-lepton final states, yielding the 95% CL constraints $M_S > 1.02$ TeV and $M_{X_{2/3}} > 1.16$ TeV (henceforth, LHC limits will always be quoted at 95% CL). The bound on $X_{2/3}$ is stronger due to the larger branching ratio into th. The search of Ref. [136] instead specifically targets the $X_{5/3}$ in the same-sign-dileptons final state, and gives $M_{X_{5/3}} > 1.16$ TeV.[14] In addition to these "standard" constraints, we must account for those on $\mathcal{Y}$ and $\mathcal{Z}$, which are mass-degenerate and always decay into a top quark and a DM particle, giving rise to $t\bar{t}$ + missing transverse energy (MET) signatures. The corresponding constraint depends on the DM mass. As motivated by the results of our phenomenological analysis (see Fig. 3.11), we choose the representative value $m_\chi = 300$ GeV. To estimate the current bound on $M_\mathcal{Y} = M_\mathcal{Z}$, we start from the result obtained in the dedicated 8 TeV analysis of Ref. [137], $m_\psi > 0.85$ TeV based on ~ 20 fb^{-1} of data. Using the Collider Reach [138] method, we rescale this bound to the current luminosity and energy, ~ 36 fb^{-1} at 13 TeV, obtaining $m_\psi > 1.30$ TeV. Finally, to take into account that $\mathcal{Y}$ and $\mathcal{Z}$ are *two* degenerate Dirac fermions that contribute to the signal, we solve the following equation for $M_\mathcal{Y}$: $\sigma_{pp\to\bar{\psi}\psi,\,13\text{ TeV}}(m_\psi = 1.30\text{ TeV}) = 2\,\sigma_{pp\to\bar{\psi}\psi,\,13\text{ TeV}}(M_\mathcal{Y})$, arriving to $M_\mathcal{Y} > 1.42$ TeV.[15] In summary, the current LHC constraints on the top partner

[14] This is the bound obtained for a purely right-handed $\bar{t}W^-X_{5/3}$ coupling, as appropriate since in this model the left-handed coupling is suppressed by one extra power of v.

[15] As an independent cross-check, we have recast the constraint on the stop mass extracted from Ref. [139], $m_{\tilde{t}} > 1.04$ TeV with ~ 36 fb^{-1}, by solving for $M_\mathcal{Y}$ the equation $\sigma_{pp\to\tilde{t}^*\tilde{t},\,13\text{ TeV}}(m_{\tilde{t}} = 1.04\text{ TeV}) = 2\,\sigma_{pp\to\bar{\psi}\psi,\,13\text{ TeV}}(M_\mathcal{Y})$, obtaining a consistent bound $M_\mathcal{Y} > 1.47$ TeV.

masses are, at 95% CL,

$$M_S > 1 \text{ TeV}, \qquad M_{X_{5/3},\, X_{2/3}} > 1.2 \text{ TeV}, \qquad M_{\mathcal{Y},\, \mathcal{Z}} > 1.4 \text{ TeV}. \tag{3.60}$$

These conditions are imposed at every point in the parameter scan presented in Fig. 3.11.

Beyond the lightest top partner(s)

As discussed in Sec. 3.3.4, the first experimental manifestation of the model at colliders would most likely be the discovery of the lightest top partner. We now turn to a brief discussion of the opportunities to probe the heavier fermionic resonances at the LHC and future colliders. If the lightest top partner is a singlet S, the connection with the DM problem could not be made until the $U(1)_{\rm DM}$-charged top partners $\mathcal{Y}$ and $\mathcal{Z}$, which belong to the heavier multiplet Q, can be accessed. For large enough splitting $m_Q - M_S$, the direct decay to $\chi^{(*)}t$ and the cascade decay to $\chi^{(*)}S$ are both unsuppressed. The branching fraction is, assuming $\epsilon_{tQ}, M_S \ll m_Q$ and in the limit of full t_R compositeness $\sin\phi_R \to 1$,

$$\text{BR}(\mathcal{Y} \to \chi t) = \text{BR}(\mathcal{Z} \to \chi^* t) \simeq \frac{c_R^2}{c_L^2 + c_R^2}\,, \tag{3.61}$$

where to keep the discussion general we took nonzero coefficients for the derivative interactions in Eq. (3.28), setting $c^{L,R} = i\, c_{L,R}$ so that CP is conserved. Equation (3.61) suggests that $\mathcal{Y}$ and $\mathcal{Z}$ decay rather democratically into the two available channels. Therefore the QCD pair production of $\mathcal{Y}$ and $\mathcal{Z}$, either at the LHC or at a future FCC-hh, can generate cascades where the decay of an intermediate S yields a Z or h in addition to the "stop-like" $bW\bar{b}W\chi\chi^*$ signature, potentially providing an additional handle to characterize the exotic top partners.

In the opposite scenario $m_Q < M_S$, since the $\mathcal{Y}$ and $\mathcal{Z}$ are at the bottom of the spectrum, their discovery in the $t\bar{t}$ + MET final state would happen early on, hinting to a connection with DM physics. The heavier singlet may then be accessed via single production $pp \to S\bar{b}j$, whose rate can be enhanced by the derivative interactions proportional to $c_{L,R}$ [110]. Of special interest is the decay into the $U(1)_{\rm DM}$-charged top partners, $S \to \chi^*\mathcal{Y}, \chi\mathcal{Z}$, leading at the end of the cascade to the final state $t\chi\chi^*\bar{b}j$, i.e. a monotop signature. The branching ratio for these decays is, assuming $\epsilon_{tQ}, m_Q \ll M_S$ and in the limit of full t_R compositeness,

$$\text{BR}(S \to \chi^*\mathcal{Y}) = \text{BR}(S \to \chi\mathcal{Z}) \simeq \frac{1}{6}\,. \tag{3.62}$$

Notice that this result holds for arbitrary c_L and c_R. Hence $\approx 1/3$ of the singly-produced singlets yield the monotop final state. This promising signature deserves a dedicated analysis, which is however beyond the scope of this work.

3.4 Breaking of the DM shift symmetry by bottom quark couplings

A different scenario is obtained if the DM shift symmetry is fully preserved by the interactions of the top quark, but it is broken by those of the bottom. As a concrete example we take $\mathcal{O}_q \sim \mathbf{7}_{2/3}, \mathcal{O}_t \sim \mathbf{21}_{2/3}$ and $\mathcal{O}_{q',b} \sim \mathbf{7}_{-1/3}$ under $SO(7) \times U(1)_X$, in which case only the couplings of b_R to the strong sector break the χ shift symmetries. Only the essential features of the setup are presented here, while a detailed discussion is provided in Appendix 3.C. We focus on the region of parameter space where $\epsilon_L^b \sim \epsilon_R^b \sim \sqrt{y_b f / M_{*b}}$, which in turn lead to the scalings

$$\lambda \propto y_b^2 \qquad \text{and} \qquad m_\chi \propto (y_b g_*)^{1/2} f\,, \tag{3.63}$$

with $g_* \sim M_{*b}/f$. As a result, the χ mass can be of $O(100)$ GeV while the portal coupling remains very suppressed. Quantitatively, we estimate

$$m_\chi \simeq \sqrt{\mu^2_{\rm DM}} \approx 120\ {\rm GeV} \left(\frac{M_{*b}}{8\ {\rm TeV}}\right)^{3/2} \left(\frac{1\ {\rm TeV}}{f}\right)^{1/2}, \tag{3.64a}$$

$$\lambda \approx 3 \times 10^{-4} \left(\frac{M_{*b}}{8\ {\rm TeV}}\right)^{2} \left(\frac{1\ {\rm TeV}}{f}\right)^{2}. \tag{3.64b}$$

The above parametrics have been confirmed by a numerical scan of the $SO(7)/SO(6)$ model whose results are reported in Appendix 3.C. The important message contained in Eq. (3.64) is that since $\lambda f^2 \ll m_\chi^2$, χ annihilation proceeds dominantly via the derivative portal, and the DM is heavy enough that the correct relic density can be reproduced for $f \sim$ TeV, see Fig. 3.1. In addition, we have $c_b^\chi \simeq 1$ and $\lambda f^2 \ll m_h^2$ in Eq. (3.12), so the scattering with nuclei is dominated by the $\chi^* \chi b\bar{b}$ contact interaction. The DM-nucleon scattering cross section is

$$\begin{aligned}\sigma^{\chi N}_{\rm SI} &\simeq \frac{\tilde{f}_N^2}{\pi} \frac{m_N^4}{4 f^4 m_\chi^2} \\ &\approx 1.0\text{-}5.6 \times 10^{-47}\,{\rm cm}^2 \left(\frac{1\ {\rm TeV}}{f}\right)^4 \left(\frac{100\ {\rm GeV}}{m_\chi}\right)^2, \quad (b_R \text{ breaking})\end{aligned} \tag{3.65}$$

where the range of values accounts for the theory uncertainty on the couplings of the first and second generation quarks. The lower estimate corresponds to breaking of the DM shift symmetry only by the bottom quark ($c_b^\chi = 1$ and $c_q^\chi = 0$ for all $q \neq b$, case I), yielding a nucleon form factor $\tilde{f}_N \simeq 0.066$. The higher estimate corresponds to breaking by all down-type quarks ($c^\chi_{d,s,b} = 1$ and $c^\chi_{u,c,t} = 0$, case II),[16] yielding $\tilde{f}_N \simeq 0.15$. The extremely suppressed cross sections in Eq. (3.65) will be probed by next-generation experiments such as LZ [140], for which they constitute a very motivated target.

A summary of the current constraints and future reach on the (m_χ, f) parameter space is shown in Fig. 3.13, where we have set $c_d = c_b^\chi = 1$, $c_t^\chi = \lambda = 0$. Points lying on the blue curve reproduce the observed DM relic density. The red-shaded region is ruled out by current XENON1T results [141] assuming case I for the DM-nucleon cross section, whereas the dashed red line corresponds to the exclusion for case II. The solid gray (dashed gray) lines show the expected sensitivity achieved by LZ [140] for case I (case II). The region $m_\chi < m_h/2$ is also constrained by LHC searches for invisibly-decaying Higgses. The current 95% CL bound ${\rm BR}(h \to \chi^* \chi) < 0.24$ [142] rules out the region shaded in orange, which extends up to $f \simeq 1.2$ TeV for very light χ. The projected HL-LHC limit ${\rm BR}(h \to \chi^* \chi) < 0.08$ [143], corresponding to the dotted orange curve, will extend the reach to $f \simeq 1.6$ TeV. Finally, the region shaded in purple is excluded by searches for present-day DM annihilations from dwarf spheroidal galaxies (dSphs) performed at Fermi-LAT [144]. This bound was derived by comparing the total cross section for DM annihilation in our model to the limit reported by Fermi for the $b\bar{b}$ final state, and should therefore be taken as approximate. Additional indirect detection constraints [126, 127] arise from the measurement of the antiproton spectrum by AMS-02 [128]. These are, however, affected by systematic uncertainties whose sizes are under active debate. We have therefore chosen to quote only the more conservative bounds from dSphs. Figure 3.13 shows that most of the best-motivated parameter space, with 80 GeV $\lesssim m_\chi \lesssim$ 200 GeV and 0.8 TeV $\lesssim f \lesssim$ 1.4 TeV, is currently untested but within reach of LZ.

[16] This is the pattern obtained by extending the embeddings $\mathcal{O}_q \sim \mathbf{7}_{2/3}$, $\mathcal{O}_t \sim \mathbf{21}_{2/3}$ and $\mathcal{O}_{q',b} \sim \mathbf{7}_{-1/3}$ to all three generations.

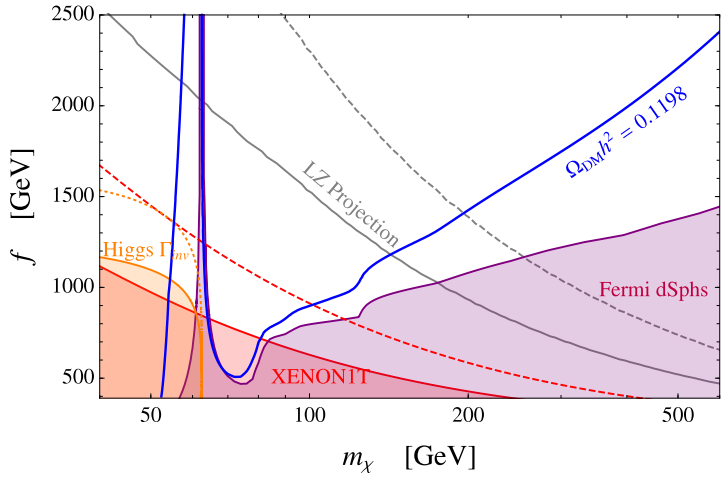

Figure 3.13: *Parameter space of the model where the bottom quark gives the leading breaking of the DM shift symmetry. The coefficients of the effective Lagrangian are set to $c_d = c_b^\chi = 1$, $c_t^\chi = \lambda = 0$. To draw the exclusions from direct and indirect detection we have assumed that all of the observed DM is composed of χ particles, irrespective of the thermal value of the χ density predicted at each (m_χ, f) point.*

3.5 Breaking of the DM shift symmetry by $U(1)_{\rm DM}$ gauging

It is possible to couple all the elementary quarks to the strong sector in a way that preserves the DM shift symmetry [73, 17]. For example, in the $SO(7)/SO(6)$ model this is achieved with $\mathcal{O}_q \sim \mathbf{7}_{2/3}$, $\mathcal{O}_{u,d} \sim \mathbf{21}_{2/3}$ for all three generations. This setup gives $c_q^\chi = 0$ in Eq. (3.9) and no contribution to $\mu^2_{\rm DM}, \lambda_{\rm DM}$ and λ in Eq. (3.46) from the fermion sector, while at the same time top loops easily produce a realistic Higgs potential. In this case, some additional explicit breaking should be responsible for generating the DM mass. If χ is a complex scalar, a natural possibility is that the explicit breaking originates from the gauging of $U(1)_{\rm DM}$. In the $SO(7)/SO(6)$ coset the generators associated with the real and imaginary parts of χ together with the $U(1)_{\rm DM}$ generator form an $SU(2)' \sim \{X^{\rm Re}, X^{\rm Im}, T^{\rm DM}\}$, hence gauging $U(1)_{\rm DM}$ generates a radiative mass for χ in very similar fashion to the contribution of photon loops to the charged pion mass in the SM.

From the effective theory point of view, the effects of gauging $U(1)_{\rm DM}$ with coupling g_D can be taken into account by replacing in $\mathcal{L}_{\rm GB}$ in Eq. (3.2),

$$|\partial^\mu \chi|^2 \quad \to \quad |(\partial^\mu - i g_D A_D^\mu)\chi|^2 - \frac{1}{4} F_D^{\mu\nu} F_{D\mu\nu} + \frac{1}{2} m^2_{\gamma_D} A_{D\mu} A_D^\mu \,, \tag{3.66}$$

where we took χ to have unit charge. Note that to be general we have included a mass term for the dark photon γ_D, which can arise via the Stückelberg mechanism without spontaneous breaking of $U(1)_{\rm DM}$. The one-loop DM mass and marginal portal coupling are

$$m_\chi = \sqrt{\mu^2_{\rm DM}} \simeq \sqrt{\frac{3\alpha_D}{2\pi}}\, m_\rho \approx 100 \text{ GeV} \left(\frac{\alpha_D}{10^{-3}}\right)^{1/2} \left(\frac{m_\rho}{5 \text{ TeV}}\right), \qquad \lambda = 0 \,, \tag{3.67}$$

where $\alpha_D \equiv g_D^2/(4\pi)$ and the loop that generates m_χ was cut off at m_ρ, the mass of vector resonances (in the $SO(7)/SO(6)$ model, this is the mass of the **15** multiplet of $SO(6)$). The estimate for the DM mass in Eq. (3.67) is valid as long as $m_{\gamma_D} \ll m_\rho$, which we assume. Importantly, since the Higgs is uncharged under $U(1)_{\rm DM}$ the marginal portal coupling is not

generated at one loop, leading from Eq. (3.12) to an extremely suppressed DM-nucleon cross section. We find it remarkable that such a simple model is effectively inaccessible to direct detection experiments.

The introduction of the dark photon has significant impact on the phenomenology. It is important to stress that in Eq. (3.66) we have not included the operator $\varepsilon B_{\mu\nu}F_D^{\mu\nu}/2$ that mixes kinetically $U(1)_{\rm DM}$ and the SM hypercharge. The choice to set $\varepsilon = 0$ in the EFT is motivated by the $SO(7)/SO(6)$ model, where the kinetic mixing is forbidden by C_D, the charge conjugation of $U(1)_{\rm DM}$, which is an accidental symmetry (provided it is respected by subleading spurionic embeddings of the SM fermions, see Appendix 3.E). In particular, in the low-energy theory C_D transforms $A_D^\mu \to -A_D^\mu$ and $\chi \to -\chi^*$, whereas all SM fields are left unchanged. An additional, important consequence of this discrete symmetry is that the dark photon is stable if $m_{\gamma_D} < 2m_\chi$, when the $\gamma_D \to \chi\chi^*$ decay is kinematically forbidden. The complete discussion of kinetic mixing, as well as the details on the implementation of C_D as an $O(6)$ transformation that we call P_6, are contained in Appendix 3.E.

The dark sector, composed of the DM and the dark photon, is thus characterized by the four parameters $\{m_\chi, f, \alpha_D, m_{\gamma_D}\}$. In the remainder of this section we analyze its phenomenology in detail, beginning in Sec. 3.5.1 with the simplest setup where the dark photon is massless, and later moving to the massive case in Sec. 3.5.2.

3.5.1 Phenomenology for massless dark photon

Setting $m_{\gamma_D} = 0$ leaves the three-dimensional parameter space $\{m_\chi, f, \alpha_D\}$. We begin the discussion with a summary of the thermal history of the model. At early times the dark sector, composed of χ and γ_D, and the visible sector are kept in kinetic equilibrium by elastic $\chi f \to \chi f$ scatterings mediated by Higgs exchange, where f denotes the still-relativistic SM fermions. These processes are effective down to temperatures $T \ll m_\chi$, but eventually they become slower than the Hubble expansion rate and the dark and visible sectors decouple. The corresponding decoupling temperature $T_{\rm dec}$ is defined through [145] $H(T_{\rm dec}) = \gamma(T_{\rm dec})/2$, where $H(T) = \pi\sqrt{g_*(T)}\,T^2/(3\sqrt{10}M_{\rm Pl})$ is the Hubble parameter for a radiation-dominated Universe ($g_*(T)$ is the total number of relativistic degrees of freedom including both the visible and dark sectors, and $M_{\rm Pl}$ is the reduced Planck mass), whereas $\gamma(T)$ is the momentum relaxation rate, which scales as $\gamma \sim (T/m_\chi)n_f\langle\sigma_{\chi f}v_{\rm rel}\rangle$. Using the exact expression of $\gamma(T)$ given in Ref. [145] we calculate[17] $T_{\rm dec}$ as a function of m_χ and f, finding that it is typically between 1 and 3 GeV as shown in the left panel of Fig. 3.14.

The massless dark photon behaves as radiation at all temperatures. The strongest constraint on new relativistic degrees of freedom arises from Cosmic Microwave Background (CMB) measurements of the Hubble parameter, usually formulated in terms of the effective number of light neutrino species $N_{\rm eff}$. In our model the dark photon gives a contribution [146]

$$\Delta N_{\rm eff} = N_{\rm eff} - 3.046 = \frac{8}{7}\frac{g_{\rm dark}(T)}{2}\left(\frac{T}{T_\nu}\right)^4\left(\frac{g_{\rm dark}(T_{\rm dec})}{g_{\rm dark}(T)}\frac{g_{*s,{\rm vis}}(T)}{g_{*s,{\rm vis}}(T_{\rm dec})}\right)^{4/3}, \tag{3.68}$$

where $T \sim 0.3$ eV is the photon temperature at decoupling, $N_{\rm eff} = 3.046$ is the SM prediction, $T/T_\nu = (11/4)^{1/3}$ and $g_{*s,{\rm vis}}(T) = 3.91$. To obtain Eq. (3.68) we have used the fact that below $T_{\rm dec}$ the entropies of the dark and visible sectors are separately conserved. Since χ is already non-relativistic at kinetic decoupling, we have $g_{\rm dark}(T_{\rm dec}) = g_{\rm dark}(T) = 2$ and $\Delta N_{\rm eff}$ is determined by the number of SM relativistic degrees of freedom at $T_{\rm dec}$. As shown in the right panel of

[17] For simplicity, in deriving $T_{\rm dec}$ the total number of relativistic degrees of freedom was set to the approximate constant value $g_* = g_{*,{\rm vis}} + g_{\rm dark} = 75.75 + 2 = 77.75$, which corresponds to $m_\tau < T < m_b$.

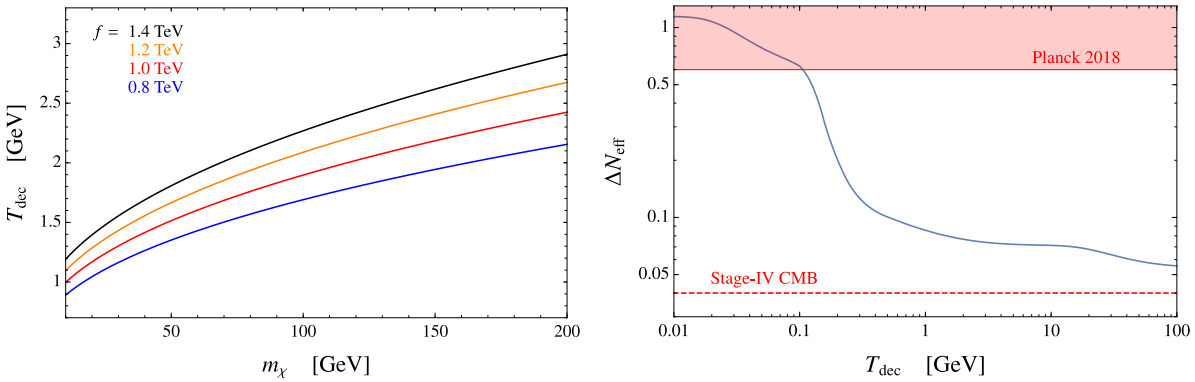

Figure 3.14: *Left panel: temperature of kinetic decoupling between the dark and visible sectors. Right panel: contribution of the dark photon to* $\Delta N_{\rm eff}$ *at photon decoupling, calculated from Eq.* (3.68)*. In the evaluation of* $g_{*s,\rm vis}(T_{\rm dec})$ *we assumed* 150 MeV *as temperature of the QCD phase transition. The region shaded in red corresponds to the current CMB constraint* $\Delta N_{\rm eff} \lesssim 0.6$*, while the dashed red line shows the projected Stage-IV CMB bound* $\Delta N_{\rm eff} \lesssim 0.04$*.*

Fig. 3.14, as long as $T_{\rm dec} \gg 100$ MeV the current bound $\Delta N_{\rm eff} \lesssim 0.6$ [62] (95% CL) is easily satisfied. As we have seen, the typical decoupling temperature is 1 - 3 GeV, corresponding to $\Delta N_{\rm eff} \approx 0.07$ - 0.09. Such values could be probed in future Stage-IV CMB measurements, which are expected to constrain $\Delta N_{\rm eff} \lesssim 0.04$ at 95% CL [147]. A similar, but slightly weaker, current bound is obtained from Big-Bang nucleosynthesis [148].

In addition, the Compton scattering process $\chi\gamma_D \to \chi\gamma_D$ delays kinetic decoupling of the DM compared to the standard WIMP scenario [146, 149], suppressing the matter power spectrum on small scales and leading to a minimum expected DM halo mass. For weak-scale DM and typical coupling $\alpha_D \sim 10^{-3}$, though, χ - γ_D kinetic decoupling takes place at temperature of O(MeV) and the minimum halo mass is too small to be testable with current observations [149].

Having established that the massless dark photon does not conflict with cosmological observations, we turn to the DM phenomenology. The $\chi\chi^*$ pairs undergo s-wave annihilation both to SM particles via the derivative Higgs portal, and to $\gamma_D\gamma_D$ with amplitude mediated by the scalar QED interactions in Eq. (3.66). The cross section for the latter is

$$\langle \sigma_{\gamma_D\gamma_D} v_{\rm rel} \rangle = \frac{2\pi\alpha_D^2}{m_\chi^2}\,, \tag{3.69}$$

where we took the leading term in the velocity expansion. Notice that the "mixed" dark-visible annihilation $\chi\chi^* \to \gamma_D h$ is instead p-wave suppressed: the amplitude vanishes at threshold, because spin cannot be conserved for $m_{\gamma_D} = 0$.[18] Therefore this process has only a very small impact on the freeze-out. The requirement to obtain the observed relic density yields a two-dimensional manifold in the parameter space, whose features are best understood by considering slices with fixed f.

As discussed in Sec. 3.1.1, there exists then only one value of the DM mass which gives the correct relic density by annihilation only through the derivative Higgs portal: for example, for $f = 1\,(1.4)$ TeV this is $m_\chi^{(f)} \approx 122\,(194)$ GeV. For $m_\chi > m_\chi^{(f)}$ the derivative portal coupling strength $\sim m_\chi^2/f^2$ is too large, yielding DM underdensity for any value of α_D. Conversely, for

[18] The p-wave suppression applies also for $m_{\gamma_D} \neq 0$, since the longitudinal polarization does not contribute to the amplitude due to $U(1)_{\rm DM}$ invariance.

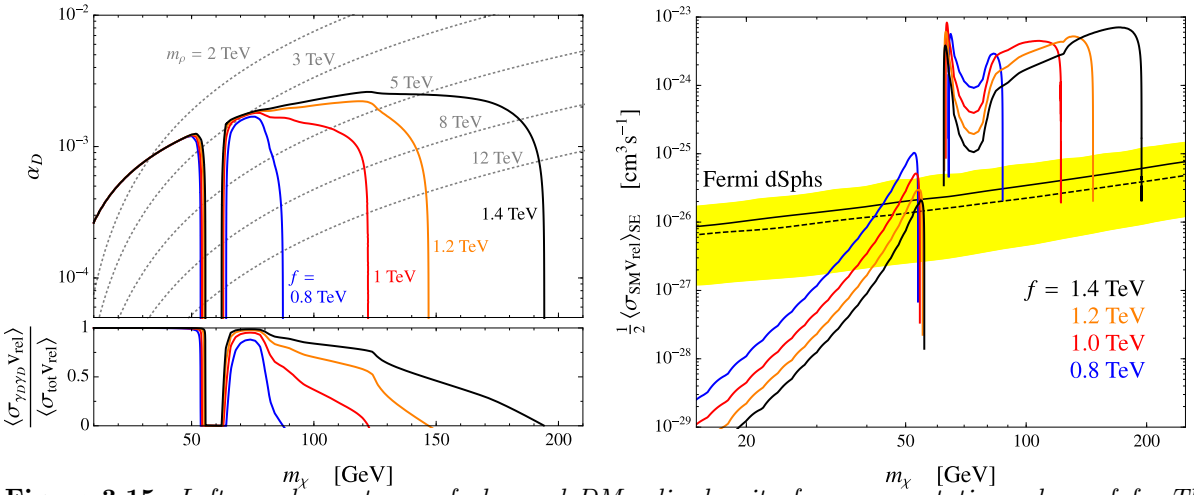

Figure 3.15: *Left panel: contours of observed DM relic density for representative values of f. The inset shows the fraction of annihilations to dark photons. Contours of constant vector resonance mass m_ρ are also shown, as dashed grey lines. Right panel: the colored curves show $\langle\sigma_{\rm SM} v_{\rm rel}\rangle_{\rm SE}$, the present-day annihilation cross section to SM particles including Sommerfeld enhancement, calculated along the relic density contours shown in the left panel. The black line is the observed 95% CL upper limit from the dSphs analysis in Ref. [129]. The yellow band corresponds to 95% uncertainty on the expected limit in the same analysis. We also show, as dashed black line, the observed limit from the analysis of a smaller dSphs sample [144]. The quoted experimental limits were obtained assuming DM annihilation to $b\bar{b}$.*

$m_\chi < m_\chi^{(f)}$ the $\chi\chi^* \to \gamma_D\gamma_D$ annihilation compensates for the reduced derivative portal for an appropriate value of α_D. Comparing Eqs. (3.6) and (3.69), the two annihilation channels have equal strength when $\alpha_D^2 \sim m_\chi^4/(2\pi^2 f^4)$, which since $m_\chi/f \sim 1/10$ corresponds to $\alpha_D \sim 2\times 10^{-3}$. For very light DM, $m_\chi \ll m_h/2$, only annihilation to dark photons is relevant and the coupling is fixed to $\alpha_D \approx 7\times 10^{-4}\,(m_\chi/30\text{ GeV})$ by the analog of Eq. (3.6). These features are illustrated by the left panel of Fig. 3.15, where contours of the observed relic abundance in the (m_χ, α_D) plane are shown. Notice that in the window 55 GeV $\lesssim m_\chi \lesssim$ 62.5 GeV the DM is always underdense, because the annihilation to SM particles is too strongly enhanced by the Higgs resonance. To help identify the most plausible parameter space we also show contours of constant vector resonance mass m_ρ, as obtained from the one-loop expression of the χ mass in Eq. (3.67).[19] We expect $1 \lesssim m_\rho/f \lesssim 4\pi$, although stronger lower bounds can arise from electroweak precision tests and from direct searches for the ρ particles at colliders.

The massless dark photon mediates a long-range force between DM particles, which leads to the non-perturbative Sommerfeld enhancement (SE) [150] of the annihilation cross section. For s-wave annihilation the cross section times relative velocity including SE is

$$(\sigma v_{\rm rel})_{\rm SE} = (\sigma v_{\rm rel})_0\, S(\alpha_D/v_{\rm rel}), \qquad S(\zeta) = \frac{2\pi\zeta}{1-e^{-2\pi\zeta}}\,, \tag{3.70}$$

where $(\sigma v_{\rm rel})_0$ is the perturbative result, e.g. $(\sigma v_{\rm rel})_0 = 2\pi\alpha_D^2/m_\chi^2$ for $\chi\chi^* \to \gamma_D\gamma_D$. The SE is important when the ratio $\alpha_D/v_{\rm rel}$ is not too small, and scales as $S \simeq 2\pi\alpha_D/v_{\rm rel}$ for $\alpha_D/v_{\rm rel} \gtrsim 1/2$. Assuming a Maxwell-Boltzmann distribution for the DM velocity, the thermally averaged cross

[19] Precisely, we employed Eq. (3.107) with $f_\rho = f$.

section times relative velocity including SE can be written in the approximate form [151]

$$\langle\sigma v_{\rm rel}\rangle_{\rm SE} = (\sigma v_{\rm rel})_0\, \overline{S}_{\rm ann}\,, \qquad \overline{S}_{\rm ann} = \sqrt{\frac{2}{\pi}}\frac{1}{v_0^3 N}\int_0^{v_{\rm max}} dv_{\rm rel}\, S(\alpha_D/v_{\rm rel}) v_{\rm rel}^2\, e^{-\frac{v_{\rm rel}^2}{2v_0^2}} \tag{3.71}$$

where v_0 is the most probable velocity. The maximal relative velocity $v_{\rm max}$ and the normalization constant N depend on whether we consider early-Universe annihilation around the time of freeze-out, in which case $v_{\rm max} = \infty$ and $N = 1$, or present-day annihilation in a galaxy halo, where $v_{\rm max} = 2\, v_{\rm esc}$ with $v_{\rm esc}$ the escape velocity, and $N = {\rm erf}(z/\sqrt{2}) - \sqrt{2/\pi}\, z\, e^{-z^2/2}$, $z \equiv v_{\rm max}/v_0$. We have checked that Eq. (3.71) agrees within a few percent with the full numerical treatment. At DM freeze-out the typical DM speed is $v_0 = \sqrt{2/x_{\rm fo}} \sim 0.3$ since $x_{\rm fo} \equiv m_\chi/T_{\rm fo} \sim 25$, so for the typical coupling $\alpha_D \sim 10^{-3}$ the SE enhancement is negligible. Today, however, DM particles are much slower, with typical relative velocities of 10^{-3} in the Milky Way (MW), and $\lesssim 10^{-4}$ in dwarf galaxies. For the MW we take $v_0 = 220\,{\rm km/s}$ and $v_{\rm esc} = 533\,{\rm km/s}$ [152], obtaining a typical SE of $\overline{S}_{\rm ann} \approx 6.9$ for $\alpha_D = 10^{-3}$. For a dwarf galaxy with representative parameters $v_0 = 10\,{\rm km/s}$ and $v_{\rm esc} = 15\,{\rm km/s}$ [153] we find $\overline{S}_{\rm ann} \approx 150$, again for $\alpha_D = 10^{-3}$. If the DM has a sizeable annihilation to SM particles, these large enhancements lead to conflict with bounds from indirect detection of DM.

The strongest constraint comes from the non-observation by the Fermi-LAT [144, 129] of excess gamma ray emission from dSphs, which are the most DM-dominated galaxies known. For $m_\chi \sim 100$ GeV the current exclusion on $\langle\sigma v_{\rm rel}\rangle$ is about the thermal relic value. In the right panel of Fig. 3.15 we show the total cross section for χ annihilation to SM particles, including the SE, calculated along contours in the $\{m_\chi, f, \alpha_D\}$ parameter space where the observed relic density is reproduced. Due to the large SE the region $m_\chi > m_h/2$, where an $O(1)$ fraction of DM annihilations produce SM particles, is ruled out by dSphs analyses. Notice that the experimental limits shown in Fig. 3.15 were obtained assuming DM annihilates to $b\bar{b}$ only, whereas our χ annihilates to a combination of SM final states (see the right panel of Fig. 3.1), but the uncertainty due to this approximation is mild and cannot change the conclusion that the region $m_\chi > m_h/2$ is excluded. Furthermore, in our analysis we have neglected the effects of bound state formation, which has the same parametric dependence on $\alpha_D/v_{\rm rel}$ as the SE and is expected to further enhance the signal from dSphs by an $O(1)$ factor (see Ref. [153] for a comprehensive analysis). On the other hand, bound state formation has negligible impact on freeze-out for the relatively light DM we consider in this work, $m_\chi \sim 100$ GeV [154].

Additional, important constraints on the DM self-interaction mediated by the dark photon arise from observations of DM halos. The strongest such bounds come from the triaxial structure of galaxy halos, in particular from the well-measured nonzero ellipticity of the halo of NGC720 [155]. This disfavors strong self interactions, which would have reduced the anisotropy in the DM velocity distribution via the cumulative effect of many soft scatterings [149]. In the nonrelativistic limit the scattering of two DM particles is dominated by dark photon exchange. The differential cross section in the center of mass frame is

$$\frac{d\sigma}{d\Omega} \simeq \frac{\alpha_D^2}{4m_\chi^2 v_{\rm cm}^4 (1-\cos\theta_{\rm cm})^2} \tag{3.72}$$

where we only retained the leading singular behavior at small $\theta_{\rm cm}$, which is the same for same-charge $\chi\chi \to \chi\chi$ and opposite-charge $\chi\chi^* \to \chi\chi^*$ scattering. Notice the very strong velocity dependence $\propto v_{\rm cm}^{-4}$, which implies that constraints from galaxies are much stronger than those from clusters. The authors of Ref. [149] obtained a constraint by requiring that the relaxation time to obtain an isotropic DM velocity distribution be longer than the age of the Universe,

$$\tau_{\rm iso} \equiv \langle E_k\rangle/\langle\dot{E}_k\rangle = \mathcal{N} m_\chi^3 v_0^3 (\log\Lambda)^{-1}/(\sqrt{\pi}\alpha_D^2\rho_\chi) > 10^{10}\,{\rm years} \tag{3.73}$$

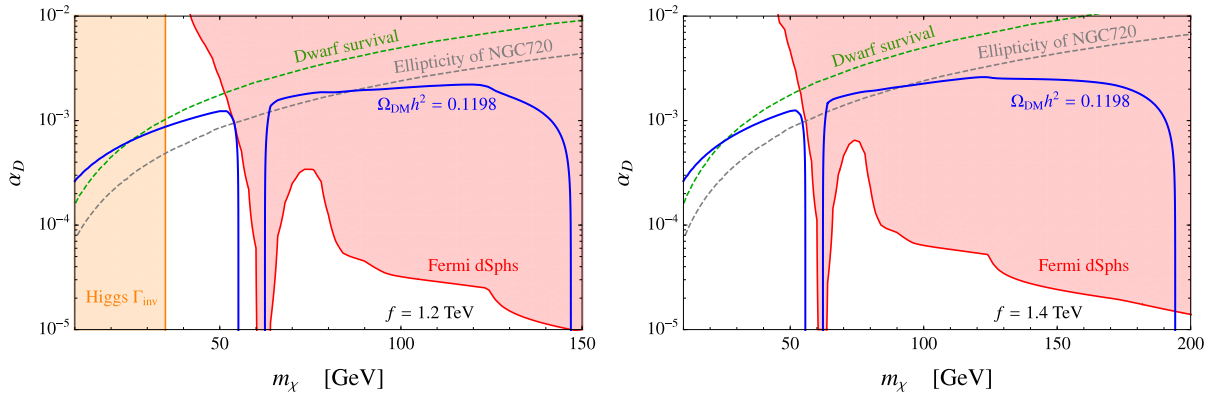

Figure 3.16: *Parameter space of the model where the gauging of $U(1)_{\rm DM}$ gives the leading breaking of the DM shift symmetry, for $f = 1.2$ TeV (left panel) and $f = 1.4$ TeV (right panel). The coefficients of the effective Lagrangian are set to $c_d = 1$, $c_t^\chi = c_b^\chi = \lambda = 0$, $m_{\gamma_D} = 0$. The exclusions from Fermi dwarfs were drawn assuming that all of the observed DM is composed of χ particles, irrespective of the thermal value of the χ density predicted at each point in parameter space.*

where $E_k = m_\chi v^2/2$, $\dot{E}_k$ is the rate of energy transfer proportional to $d\sigma/d\Omega$, $\mathcal{N}$ is an $O(1)$ numerical factor, v_0 is the velocity dispersion (very roughly 250 km/s in NGC720), $\rho_\chi = m_\chi n_\chi$ is the χ energy density and the "Coulomb logarithm" $\log\Lambda$ originates from cutting off the infrared divergence arising from Eq. (3.72). The ellipticity bound was recently reconsidered by the authors of Ref. [156], who found it to be significantly relaxed compared to the original calculation of Ref. [149]. We do not review their thorough analysis here, but simply quote the result

$$\alpha_D < 2.4 \times 10^{-3} \left(\frac{m_\chi}{100\ \text{GeV}}\right)^{3/2}. \qquad \text{(ellipticity)} \tag{3.74}$$

Although Ref. [156] considered Dirac fermion DM, their ellipticity bound directly applies to our model, because the leading term of the self-scattering cross section in Eq. (3.72) is the same for fermions and scalars.[20] Furthermore, there exist several reasons [156] to take even the bound in Eq. (3.74) with some caution, including the fact that it relies on a single galaxy, and that the measured ellipticity is sensitive to unobservable initial conditions (for example, a galaxy that recently experienced a merger may show a sizeable ellipticity even in the presence of strong DM self-interactions). Therefore we also quote the next most stringent constraint, obtained by requiring that the MW satellite dSphs have not evaporated until the present day as they traveled through the Galactic DM halo [157]. This yields

$$\alpha_D < 5 \times 10^{-3} \left(\frac{m_\chi}{100\ \text{GeV}}\right)^{3/2}, \qquad \text{(dwarf survival)} \tag{3.75}$$

which stands on a somewhat more robust footing than ellipticity, but is not free from caveats either [156].

A summary of all constraints on our parameter space is shown in Fig. 3.16, for the choices $f = 1.2$ and 1.4 TeV. While the region $m_\chi > m_h/2$ is ruled out by gamma ray observations from dSphs, for $m_\chi < m_h/2$ the strongest bounds arise from ellipticity and dwarf evaporation.

[20] Notice that Fig. 4 in Ref. [156] was drawn requiring $\Omega_X = 0.265$ for the DM density, instead of the correct $2\,\Omega_X = 0.265$. As a result, for $m_X < 200$ GeV (where the SE is negligible) their relic density contour should be multiplied by $\sqrt{2}$. We thank P. Agrawal for clarifications about this point.

In light of the previous discussion, however, we do not interpret these as strict exclusions, but rather note that they constitute an important class of probes of our setup, which may in the near future provide important evidence in favor of, or against, DM self-interactions mediated by a massless dark photon. Such self-interactions could also have interesting implications [156] for the small-scale issues of the collisionless cold DM paradigm [158]. A complementary test of the light DM mass region is the search for invisible $h \to \chi^*\chi$ decays at the LHC,[21] which will be sensitive to $f \lesssim 1.6$ TeV by the end of the high-luminosity phase (see Fig. 3.13).

3.5.2 Phenomenology for massive dark photon

We regard the mass of the dark photon as a free parameter of our model. Having extensively discussed the simplest possibility $m_{\gamma_D} = 0$ in Sec. 3.5.1, we turn here to the study of the massive case. The physics is qualitatively different if $m_{\gamma_D} < m_\chi$ or $m_\chi < m_{\gamma_D}$, so we analyze these two regions separately. Our main findings are that (1) the region $m_{\gamma_D} < m_\chi$ is ruled out, unless γ_D is so light that it still behaves as radiation today, and (2) for $m_\chi \lesssim m_{\gamma_D} < 2m_\chi$ we obtain a two-component DM setup with novel properties. Table 3.2 summarizes the mileposts in the m_{γ_D} parameter space.

$m_{\gamma_D} < 6 \times 10^{-4}$ eV	✓ / X	γ_D is dark radiation today, strong constraints from SE of $\chi\chi^* \to$ SM
6×10^{-4} eV $< m_{\gamma_D} \lesssim 3m_\chi/25$	X	γ_D is relativistic at freeze-out, ruled out by warm DM bounds/overabundant
$3m_\chi/25 < m_{\gamma_D} < m_\chi$	X	γ_D is non-relativistic at freeze-out, overabundant
$m_\chi \lesssim m_{\gamma_D} < 2m_\chi$	✓	both γ_D and χ are cold DM
$2m_\chi < m_{\gamma_D}$	✓	γ_D is unstable

Table 3.2: *Overview of the different regions in the dark photon mass space. The second column indicates whether each region satisfies (✓) or conflicts with (X) experimental constraints, while the third column summarizes the key features.*

Light dark photon: $m_{\gamma_D} < m_\chi$

If $m_{\gamma_D} < m_\chi$, the dark photon abundance freezes out almost simultaneously with the χ abundance. Assuming γ_D is still relativistic at freeze-out, i.e. $m_{\gamma_D} \lesssim 3T_{\rm fo}^\chi \approx 3m_\chi/25$, the ratio of its number density to the SM entropy density $s_{\rm SM} = (2\pi^2/45)g_{*s,\rm vis}T^3$ is $r_{\gamma_D} = n_{\gamma_D}/s_{\rm SM} = 45\,\zeta(3)g_{\gamma_D}/(2\pi^4 g_{*s,\rm vis}) \approx 0.01$, where we assumed that the dark and visible sectors are still in kinetic equilibrium at freeze-out, and took $g_{\gamma_D} = 3$, $g_{*s,\rm vis} \sim 80$. Since after freeze-out there are no γ_D-number-changing interactions in equilibrium (the scattering $\gamma_D\chi \to (h^* \to f\bar{f})\chi$ is extremely suppressed), r_{γ_D} is conserved.[22] As the Universe cools the dark photon becomes non relativistic, its energy density being $\Omega_{\gamma_D} = m_{\gamma_D} r_{\gamma_D} s_{\rm SM}$. Requiring that today this does not

[21] The Higgs can also decay to $\gamma_D\gamma_D$ via a χ loop. The decay width for $m_{\gamma_D} = 0$ is $\Gamma(h \to \gamma_D\gamma_D) = m_h^3 \alpha_D^2 c_d^2 v^2 |F\big(\frac{m_h^2}{4m_\chi^2}\big)|^2/(64\pi^3 f^4)$, where $F(\tau)$ is given in Eq. (3.148). Numerically, for $m_\chi < m_h/2$ this is negligible compared to $\Gamma(h \to \chi^*\chi)$, while for $m_\chi > m_h/2$ it is too small to be observable: e.g. for $m_\chi = 100$ GeV and $f = 1$ TeV we have $\Gamma(h \to \gamma_D\gamma_D) \sim 10^{-12}$ GeV.

[22] Before kinetic decoupling of the dark and visible sectors only $n_{\gamma_D}/s_{\rm tot}$ is conserved, where $s_{\rm tot}$ is the total entropy, but $s_{\rm tot} \approx s_{\rm SM}$ since $g_{\gamma_D} \ll g_{*s,\rm vis}$.

exceed the observed DM density yields

$$\Omega_{\gamma_D} < \Omega_{\rm DM} \qquad \to \qquad m_{\gamma_D} < 40 \text{ eV} \qquad \text{(dark photon over-abundance)} \tag{3.76}$$

where we used $g_{*s,\rm vis}(T_0) = 3.91$.

Stronger constraints are derived from studies of "mixed DM" models, where the DM consists of an admixture of cold and non-cold particles. Recently, Ref. [159] obtained bounds on the fraction $f_{\rm ncdm}$ of the non-cold DM component, assumed to be a thermal relic, for a wide range of masses, by combining observations of the CMB, baryon acoustic oscillations (BAO) and the number of dwarf satellite galaxies of the MW. In our model, if the dark photon freezes out when relativistic it constitutes a hot DM component. Its temperature at late times is obtained from entropy conservation, $T_{\gamma_D}/T = [g_{*s,\rm vis}(T)/g_{*s,\rm vis}(T_{\rm dec})]^{1/3} \approx 0.37$, where T is the SM photon temperature and we took $g_{*s,\rm vis}(T_{\rm dec}) = 75.75$. The fraction of non-cold DM is

$$f_{\rm ncdm} \simeq \frac{\Omega_{\rm ncdm}}{\Omega_{\rm DM}} = \frac{\rho_{\gamma_D,0}}{\rho_0^c \Omega_{\rm DM}} = \frac{r_{\gamma_D} s_{\rm SM,0}}{\rho_0^c \Omega_{\rm DM}} \begin{cases} \frac{\pi^4 T_{\gamma_D,0}}{30\,\zeta(3)} \\ m_{\gamma_D} \end{cases} \approx \begin{cases} 5.8 \times 10^{-6} & m_{\gamma_D} \lesssim 3\,T_{\gamma_D,0} \\ 0.024 \left(\frac{m_{\gamma_D}}{1\text{ eV}}\right) & m_{\gamma_D} \gtrsim 3\,T_{\gamma_D,0} \end{cases} \tag{3.77}$$

where the first (second) expression applies to the case where the dark photon is still relativistic (non-relativistic) today, with $3\,T_{\gamma_D,0} \approx 2.6 \times 10^{-4}$ eV. In the first equality we assumed $\Omega_{\rm ncdm} \ll \Omega_{\rm DM}$ since the non-cold component is in practice constrained to be small, while $\rho^c = 3H^2 M_{\rm Pl}^2$ is the critical density. The prediction in Eq. (3.77) can be compared with the bounds given in Ref. [159], after correcting for the fact that there the non-cold relic was assumed to have temperature equal to that of the SM neutrinos, hence the mass needs to be rescaled by a factor $T_{\gamma_D}/T_\nu \approx 0.52$. The result is shown in Fig. 3.17, from which we read a 95% CL bound

$$m_{\gamma_D} < 6 \times 10^{-4} \text{ eV}, \qquad (\text{CMB} + \text{BAO} + \text{MW satellites}) \tag{3.78}$$

roughly equivalent to the requirement that γ_D be still relativistic today. For dark photon masses that satisfy the overclosure bound of Eq. (3.76) the relevant observables are CMB and BAO measurements, while the MW satellite count becomes important at higher masses, of order keV [159]. In the region $m_{\gamma_D} \lesssim 1$ eV, where the dark photon behaved as radiation at photon decoupling, the constraints shown in Fig. 3.17 are stronger than those derived purely from $\Delta N_{\rm eff}$. This is due to the inclusion of BAO, which are sensitive to the suppression of the matter power spectrum on small scales caused by the free-streaming of the hot DM component.

For dark photon masses satisfying Eq. (3.78), the phenomenology for $m_{\gamma_D} = 0$ discussed in Sec. 3.5.1 still applies. The χ annihilation is unaffected, including the SE, as the dark photon mediates an effectively long-range force: its wavelength is much larger than the Bohr radius of the $(\chi^*\chi)$ bound state, $m_{\gamma_D} \ll \alpha_D m_\chi/2$. In addition, the Coulomb limit of Eq. (3.70) is still appropriate, since the average momentum transfer is much larger than the mediator mass, $m_{\gamma_D} \ll m_\chi v_{\rm rel}/2$ [160]. In the calculation of the ellipticity bound for massless dark photon [156] the infrared divergence that arises from integrating Eq. (3.72) over angles was cut off at the inter-particle distance, $\lambda_P = (m_\chi/\rho_\chi)^{1/3} \sim 5$ cm, where the numerical value was estimated for a representative DM mass $m_\chi = 100$ GeV and density $\rho_\chi \sim 1$ GeV/cm^3 in the DM-dominated outer region (r ≥ 6 kpc) of NGC720 [161]. When $m_{\gamma_D} > 1/\lambda_P \sim 4 \times 10^{-6}$ eV, it is $1/m_{\gamma_D}$ that must be taken as IR cutoff. However, since the cutoff only enters logarithmically in the expression of the timescale for velocity isotropization, the ellipticity bound discussed for $m_{\gamma_D} = 0$ applies essentially unchanged to the whole region defined by Eq. (3.78). The same holds for the bound from dwarf galaxy survival.[23]

For $3T_{\rm fo}^\chi \approx 3m_\chi/25 \lesssim m_{\gamma_D} < m_\chi$ the dark photon freezes out non-relativistically, but is nevertheless over-abundant.

[23]The small dark photon masses in Eq. (3.78) are legitimate from an EFT standpoint. Still, it has recently been

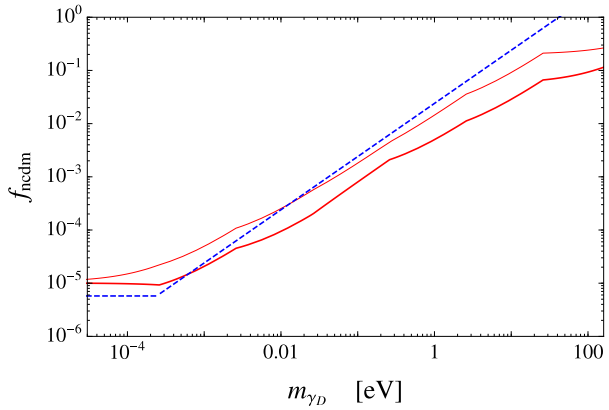

Figure 3.17: *The fraction of non-cold DM embodied by the dark photon as predicted by our model (dashed blue), compared to the 2σ (thick red) and 3σ (thin red) upper bounds from Ref. [159].*

Heavy dark photon: $m_\chi < m_{\gamma_D}$

In the region $m_\chi \lesssim m_{\gamma_D} < 2m_\chi$ both γ_D and χ are stable and freeze out when non-relativistic, naturally giving rise to a two-component cold DM model. The features of this region are best explained by fixing f and $m_\chi > m_\chi^{(f)}$, so that χ would be under-abundant in isolation, owing to its too strong annihilation to SM particles via the derivative Higgs portal. Requiring that the heavier dark photon provides the remaining DM fraction then gives a contour in the $(m_{\gamma_D}/m_\chi, \alpha_D)$ plane, shown in the left panel of Fig. 3.18 for $f = 1$ TeV and some representative choices of m_χ. The relic densities of χ and γ_D were computed solving the coupled Boltzmann equations with micrOMEGAs [164]. To understand the basic features of Fig. 3.18-left, a useful first approximation is to treat the freeze-outs of χ and γ_D as decoupled processes, since in this limit the relic density of χ is simply fixed by the freeze-out of $\chi\chi^* \to$ SM and therefore completely determined by f and m_χ. This simplified picture does receive important corrections in some regions of parameter space, as we discuss below. Focusing first on the $m_\chi = 300$ GeV case, four qualitatively different regions arise in our analysis:

1. The non-degenerate region, $2m_\chi - m_h \approx 1.6\, m_\chi < m_{\gamma_D} < 2m_\chi$. The dark photon freeze-out is determined by the semi-annihilation process $\gamma_D h \to \chi\chi^*$, which is kinematically allowed at zero temperature. Hence the relic density contour is approximately given by $n_h^{\rm eq}\langle\sigma_{\gamma_D h\to\chi\chi^*} v_{\rm rel}\rangle =$ constant, where the LHS is evaluated at the γ_D freeze-out temperature, $T_{\gamma_D}^{\rm fo} \approx m_{\gamma_D}/25$, and the thermally averaged cross section is given in Eq. (3.151). As m_{γ_D}/m_χ decreases, the dark fine structure constant increases exponentially to compensate for the suppression of the Higgs number density, $\alpha_D \propto \exp\left(\frac{m_h}{m_\chi}\frac{25}{m_{\gamma_D}/m_\chi}\right)$, where we dropped subleading power corrections. The importance of semi-annihilation processes, which change the total DM number by one unit (rather than two units as for ordinary annihilation), was discussed for the first time in Ref. [75].

2. The intermediate region, $1.3\, m_\chi \lesssim m_{\gamma_D} \lesssim 1.6\, m_\chi \approx 2m_\chi - m_h$. The γ_D freeze-out

conjectured [162] that quantum gravity forbids arbitrarily small Stückelberg masses: local quantum field theory would break down at $\Lambda_{\rm UV} \sim (m_{\gamma_D} M_{\rm Pl}/g_D)^{1/2}$. Taking $g_D \sim 0.1$ as needed to obtain the observed relic density for χ, Eq. (3.78) corresponds then to a troublesome $\Lambda_{\rm UV} \lesssim 4$ TeV. The conjecture does not apply, however, if m_{γ_D} arises from a dynamical symmetry breaking [162]. This topic is currently under debate [163].

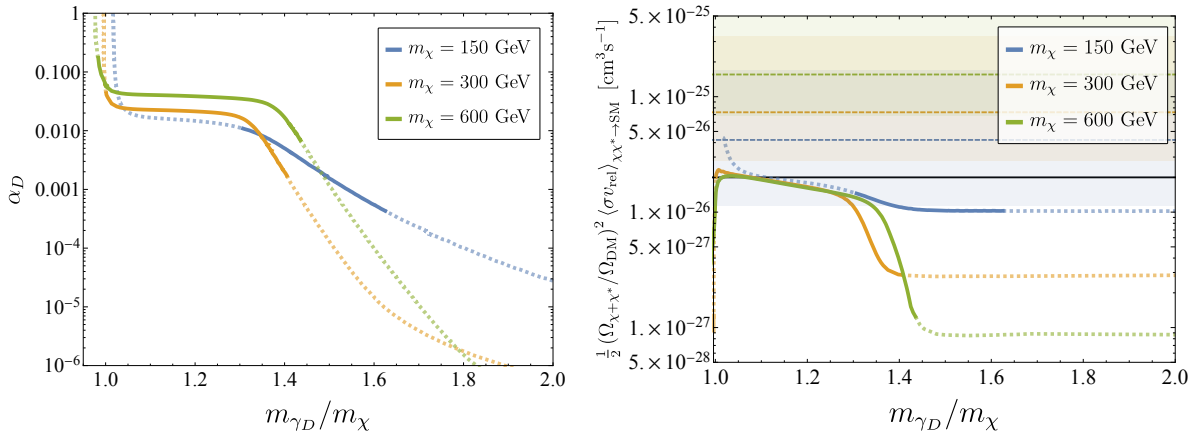

Figure 3.18: *Left panel: contours in the $(m_{\gamma_D}/m_\chi, \alpha_D)$ plane where the sum of the χ and γ_D densities matches the observed total DM density, $\Omega_{\chi+\chi^*} + \Omega_{\gamma_D} = \Omega_{\rm DM}$, assuming $f = 1$ TeV and for representative values of $m_\chi > m_\chi^{(f)} \approx 122$ GeV. The solid portions highlight the range of α_D where m_χ can be obtained from dark photon loops cut off at 2.5 TeV $< m_\rho < 4\pi f$ (see Eq. (3.107)), where the lower bound comes from the S parameter, $\widehat{S} \sim m_W^2/m_\rho^2 \lesssim 10^{-3}$ (see e.g. Ref. [102]). Right panel: effective cross section for present-day DM annihilation to SM particles, calculated along the relic density contours in the left panel. Also shown are the observed 95% CL limits from dSphs in the WW channel [144] (dashed lines), together with the 95% CL uncertainties on the expected limits (colored regions). For reference, the black solid line shows $\langle\sigma v_{\rm rel}\rangle_{\rm can}$, the cross section expected for a single thermal relic that annihilates entirely to SM particles.*

is still determined by $\gamma_D h \to \chi\chi^*$, which however is now forbidden at zero temperature. Using detailed balance, the relic density contour is given by $n_h^{\rm eq}\langle\sigma_{\gamma_D h\to\chi\chi^*} v_{\rm rel}\rangle = (n_\chi^{\rm eq\,2}/n_{\gamma_D}^{\rm eq})\langle\sigma_{\chi\chi^*\to\gamma_D h} v_{\rm rel}\rangle = $ constant, where the LHS is evaluated at $T_{\gamma_D}^{\rm fo} \approx m_{\gamma_D}/25$ and the cross section can be found in Eq. (3.152). The dependence of α_D on m_{γ_D}/m_χ is exponential and faster than in the non-degenerate region, $\alpha_D \propto \exp\left[(2 - \frac{m_{\gamma_D}}{m_\chi})\frac{25}{m_{\gamma_D}/m_\chi}\right]$, where power corrections were neglected.

3. The degenerate region, $m_\chi \lesssim m_{\gamma_D} \lesssim 1.3\, m_\chi$. As m_{γ_D}/m_χ decreases the semi-annihilation is increasingly Boltzmann suppressed, while the rate of the annihilation $\gamma_D\gamma_D \to \chi\chi^*$ increases as α_D^2. Therefore the dark photon freezes out when its annihilation to $\chi\chi^*$ goes out of equilibrium. The relic density contour is approximately described by $\langle\sigma_{\gamma_D\gamma_D\to\chi\chi^*} v_{\rm rel}\rangle = $ constant, where the cross section is given in Eq. (3.150). The resulting variation of α_D is slow in comparison to the regions dominated by semi-annihilation, thus explaining the nearly flat behavior of the contours. Importantly, in this region the evolutions of the χ and γ_D densities are tightly coupled, and the injection of χ particles due to the $\gamma_D\gamma_D \to \chi\chi^*$ process gives a larger χ abundance than the one expected based on the simplified decoupled picture. This interesting type of system was first studied numerically in Ref. [165], and we provide here analytical insight into its dynamics. After the yields Y_{χ,γ_D} become much larger than their equilibrium values, they obey the simplified Boltzmann equations ($x \equiv m_\chi/T$)

$$\widehat{\lambda}^{-1} x^2 \frac{dY_\chi}{dx} = -\langle\sigma v_{\rm rel}\rangle_{\rm SM} Y_\chi^2 + \tfrac{1}{2}\langle\sigma v_{\rm rel}\rangle_{\gamma_D\gamma_D} Y_{\gamma_D}^2 \tag{3.79a}$$

$$\widehat{\lambda}^{-1} x^2 \frac{dY_{\gamma_D}}{dx} = -\langle\sigma v_{\rm rel}\rangle_{\gamma_D\gamma_D} Y_{\gamma_D}^2 \tag{3.79b}$$

where $\widehat{\lambda} \equiv (2\sqrt{10}\,\pi/15)(g_{*s} m_\chi M_{\rm Pl}/\sqrt{g_*})$, while $\langle\sigma v_{\rm rel}\rangle_{\rm SM}$ refers to $\chi\chi^* \to$ SM and $\langle\sigma v_{\rm rel}\rangle_{\gamma_D\gamma_D}$

to $\gamma_D\gamma_D \to \chi\chi^*$. The analytical solution of this system gives at $x \gg 1$

$$\frac{1}{a_\sigma}\left(\frac{2Y_\chi}{Y_{\gamma_D}}\right)^2 \simeq 1 + \tfrac{1}{2}\left(a_\sigma + \sqrt{a_\sigma(a_\sigma+4)}\right), \qquad a_\sigma \equiv \frac{\langle\sigma v_{\rm rel}\rangle_{\gamma_D\gamma_D}}{\langle\sigma v_{\rm rel}\rangle_{\rm SM}/2}\,, \tag{3.80}$$

where a_σ goes to a constant since both processes are s-wave. This result is obtained by solving a quadratic equation, whose other root yields $dY_\chi/dx > 0$ and is therefore unphysical. For $a_\sigma \ll 1$, as verified in the $m_\chi = 300, 600$ GeV examples, the RHS of Eq. (3.80) goes to 1 and the formula expresses the equality of the fluxes that enter and leave the χ population, $Y_{\gamma_D}^2\langle\sigma v_{\rm rel}\rangle_{\gamma_D\gamma_D} = (2Y_\chi)^2\langle\sigma v_{\rm rel}\rangle_{\rm SM}/2$. Correspondingly, the relative χ density is suppressed (albeit still larger than in the simplified decoupled picture), $2n_\chi/n_{\gamma_D} \simeq a_\sigma^{1/2}$. In the $m_\chi = 150$ GeV example we have $a_\sigma = O(1)$ instead: in this regime the annihilation to the SM is not as efficient, leading to an accumulation of the χ particles injected by $\gamma_D\gamma_D$ annihilation and therefore to a large relative χ abundance, $2n_\chi/n_{\gamma_D} \simeq$ few.

4. The very degenerate and forbidden [74] region, $m_{\gamma_D} \lesssim m_\chi$. The dark photon freeze-out is determined by $\gamma_D\gamma_D \to \chi\chi^*$, but α_D increases very rapidly as m_{γ_D}/m_χ is decreased toward and eventually slightly below 1, in order to compensate for the kinematic suppression.

The previous discussion focused on the $m_\chi = 300$ GeV benchmark. The features of the relic density contour for $m_\chi = 600$ GeV are very similar. On the contrary, in the case $m_\chi = 150$ GeV we have $2m_\chi - m_h \approx 1.2\, m_\chi$ and as a consequence we observe a direct transition from the non-degenerate to the degenerate region, while the intermediate region is absent.

The right panel of Fig. 3.18 shows the effective cross section for DM annihilation to SM particles today, computed along the relic density contours. All processes that yield SM particles were included in the numerical evaluation, but we have checked that $\chi\chi^* \to$ SM is always dominant and the subleading channels (such as $\gamma_D\chi \to h\chi$ and $\gamma_D\gamma_D \to$ SM, the latter of which proceeds at one loop) contribute at the sub-percent level.[24] Two different regimes can be observed. In the non-degenerate region the freeze-outs of χ and γ_D can be treated as independent to a good approximation, hence from Eq. (3.6) the effective cross section is reduced compared to the standard thermal value $\langle\sigma v_{\rm rel}\rangle_{\rm can} \approx 2\times10^{-26}\,{\rm cm}^3\,{\rm s}^{-1}$ by a factor $\langle\sigma v_{\rm rel}\rangle_{\rm can}/(\frac{1}{2}\langle\sigma v_{\rm rel}\rangle_{\chi\chi^*\to\,\rm SM}) < 1$. For $m_\chi = 600$ GeV the suppression amounts to more than one order of magnitude. Conversely, in the degenerate region the already discussed injection of χ particles from $\gamma_D\gamma_D$ annihilations compensates the increased $\langle\sigma v_{\rm rel}\rangle_{\chi\chi^*\to\,\rm SM}$, resulting in effective cross sections that are numerically close to $\langle\sigma v_{\rm rel}\rangle_{\rm can}$.

Finally, if $2m_\chi < m_{\gamma_D}$ the dark photon is unstable, with decay width $\Gamma(\gamma_D \to \chi^*\chi) = (\alpha_D m_{\gamma_D}/12)(1-4m_\chi^2/m_{\gamma_D}^2)^{3/2}$. In the early Universe, the inverse decay process keeps the dark sector in chemical equilibrium until $H \sim \langle\Gamma\rangle\, n_{\gamma_D}/n_\chi$, when the ratio of the number densities is

$$\frac{n_{\gamma_D}}{n_\chi} \sim \frac{H}{\Gamma} \sim \frac{10\,T^2}{M_{\rm Pl}\alpha_D m_{\gamma_D}} < 10^{-12}\left(\frac{m_{\gamma_D}}{100\ {\rm GeV}}\right)\left(\frac{10^{-3}}{\alpha_D}\right), \tag{3.81}$$

where we assumed that $T < m_{\gamma_D}$ at this point, and neglected $O(1)$ factors. Thus, the subsequent decay of the remaining dark photons has negligible impact on the χ relic density, which can effectively be computed considering only the freeze-out of $\chi\chi^*$ annihilations to SM particles, with the results summarized in Fig. 3.1. In the region $2m_\chi < m_{\gamma_D}$ the only phenomenologically relevant imprint of the dark photon is the one-loop mass for χ, estimated in Eq. (3.67).

[24] Note that due to the large mass of the dark photon, in this case the Sommerfeld enhancement of the $\chi\chi^* \to$ SM annihilation is negligible.

3.A CCWZ construction for $SO(7)/SO(6)$

For the generators of the fundamental representation of $SO(7)$ we take

$$\begin{aligned}(T^{\alpha}_{L,R})_{IJ} &= -\frac{i}{2}\left[\frac{1}{2}\epsilon^{\alpha\beta\gamma}(\delta^{\beta}_{I}\delta^{\gamma}_{J}-\delta^{\beta}_{J}\delta^{\gamma}_{I})\pm(\delta^{\alpha}_{I}\delta^{4}_{J}-\delta^{\alpha}_{J}\delta^{4}_{I})\right], \qquad \alpha=1,2,3,\\ T^{ab}_{IJ} &= -\frac{i}{\sqrt{2}}(\delta^{a}_{I}\delta^{b}_{J}-\delta^{a}_{J}\delta^{b}_{I}), \qquad b=5,6;\ a=1,\dots,b-1,\\ X^{a}_{IJ} &= -\frac{i}{\sqrt{2}}(\delta^{a}_{I}\delta^{7}_{J}-\delta^{a}_{J}\delta^{7}_{I}), \qquad a=1,\dots,6,\end{aligned} \tag{3.82}$$

where the indices I,J take the values $1,\dots,7$. $T^{\alpha}_{L,R}$ and T^{ab} are the generators of $SO(6)$, collectively denoted by $T^{\hat{a}}$ ($\hat{a}=1,\dots,15$), with $T^{\alpha}_{L,R}$ spanning the custodial $SO(4)\cong SU(2)_L\times SU(2)_R$ subgroup, while X^a are the broken generators that parameterize the coset space $SO(7)/SO(6)$. Notice that the unbroken generators are block-diagonal in our basis,

$$T^{\hat{a}}=\begin{pmatrix} t^{\hat{a}} & 0\\ 0 & 0\end{pmatrix}, \qquad t^{\hat{a}}\in SO(6). \tag{3.83}$$

All generators T^A ($A=1,\dots,21$) are normalized such that $\mathrm{Tr}\left[T^AT^B\right]=\delta^{AB}$. Under the unbroken $SO(6)$, the six GBs π^a transform linearly and in the fundamental representation, whose decomposition under $SO(4)$ is $\mathbf{6}=\mathbf{4}\oplus\mathbf{1}\oplus\mathbf{1}$. The Higgs doublet $H=(h_u,h_d)^T$ is identified with the $\mathbf{4}$, so that

$$\vec{\pi}=\frac{1}{\sqrt{2}}\left(-i(h_u-h_u^*),\quad h_u+h_u^*,\quad i(h_d-h_d^*),\quad h_d+h_d^*,\quad \sqrt{2}\,\eta,\quad \sqrt{2}\,\kappa\right)^T. \tag{3.84}$$

In unitary gauge, i.e. $h_u=0$, $h_d=\tilde{h}/\sqrt{2}$, this has the expression in Eq. (3.16) and the Goldstone matrix $U(\vec{\pi})=\exp\left(i\sqrt{2}\pi^aX^a/f\right)$ can be written, after performing the convenient field redefinition [68]

$$\frac{\sin(\pi/f)}{\pi}\,\pi^a\to\frac{\pi^a}{f} \qquad \text{with} \qquad \pi=\sqrt{\vec{\pi}^{\,T}\vec{\pi}}\,, \tag{3.85}$$

in the following form

$$U=\begin{pmatrix} \mathbf{1}_{3\times3} & & & & \\ & 1-\frac{\tilde{h}^2}{f^2(1+\Omega)} & -\frac{\tilde{h}\eta}{f^2(1+\Omega)} & -\frac{\tilde{h}\kappa}{f^2(1+\Omega)} & \frac{\tilde{h}}{f}\\ & -\frac{\tilde{h}\eta}{f^2(1+\Omega)} & 1-\frac{\eta^2}{f^2(1+\Omega)} & -\frac{\eta\kappa}{f^2(1+\Omega)} & \frac{\eta}{f}\\ & -\frac{\tilde{h}\kappa}{f^2(1+\Omega)} & -\frac{\eta\kappa}{f^2(1+\Omega)} & 1-\frac{\kappa^2}{f^2(1+\Omega)} & \frac{\kappa}{f}\\ & -\frac{\tilde{h}}{f} & -\frac{\eta}{f} & -\frac{\kappa}{f} & \Omega\end{pmatrix}, \qquad \Omega=\frac{1}{f}\sqrt{f^2-\tilde{h}^2-\eta^2-\kappa^2}\,. \tag{3.86}$$

Under $g\in SO(7)$, the GB matrix transforms as

$$U(\vec{\pi})\to g\,U(\vec{\pi})\,h(\vec{\pi};g)^T, \tag{3.87}$$

where $h(\vec{\pi};g)$ is block-diagonal in our basis,

$$h(\vec{\pi};g)=\begin{pmatrix} h_6 & 0\\ 0 & 1\end{pmatrix}, \qquad h_6\in SO(6). \tag{3.88}$$

The d_μ and e_μ symbols are defined via[25]

$$iU^\dagger D_\mu U \equiv d_\mu^a X^a + e_\mu^{\hat{a}} T^{\hat{a}}\,, \tag{3.89}$$

where $D_\mu U = \partial_\mu U - iA_\mu^{\hat{a}} T^{\hat{a}} U$. Notice that we took the gauge fields as belonging to the $SO(6)$ subalgebra, since this is the relevant case. Explicitly, for $SU(2)_L \times U(1)_Y$ we have $A_\mu^{\hat{a}} T^{\hat{a}} = \bar{g}\bar{W}_\mu^\alpha T_L^\alpha + \bar{g}'\bar{B}_\mu T_R^3$. If the $U(1)_{\rm DM}$ were also gauged, then $A_\mu^{\hat{a}} T^{\hat{a}} \to A_\mu^{\hat{a}} T^{\hat{a}} + g_D A_{D\mu} T^{56}$, with A_D the associated vector field and g_D its coupling. Under $g \in SO(7)$,

$$d_\mu^a \to (h_6)^a{}_b\, d_\mu^b\,, \qquad e_\mu \equiv e_\mu^{\hat{a}} t^{\hat{a}} \to h_6\,(e_\mu + i\partial_\mu)\, h_6^T\,, \tag{3.90}$$

where h_6 was defined in Eq. (3.88). To leading order in $1/f$, we have

$$d_\mu^a = -\frac{\sqrt{2}}{f}\, D_\mu \pi^a + O(1/f^3), \qquad e_\mu^{\hat{a}} = A_\mu^{\hat{a}} + O(1/f^2)\,, \tag{3.91}$$

where $D_\mu \pi^a = \partial_\mu \pi^a - iA_\mu^{\hat{a}} (t^{\hat{a}})^a{}_b \pi^b$. The fermion covariant derivatives that appear in Eq. (3.27) read

$$D_\mu q_L = \Big(\partial_\mu - i\bar{g}\bar{W}_\mu^\alpha \frac{\sigma^\alpha}{2} - i\bar{g}'\frac{1}{6}\bar{B}_\mu\Big) q_L\,, \qquad D_\mu \Psi = \Big(\partial_\mu - i\frac{2}{3}\bar{g}'\bar{B}_\mu\Big)\Psi\,, \tag{3.92}$$

where $\Psi = t_R, Q_i, S_j$, and in all cases the color $SU(3)$ component is understood.

At the leading order in derivatives, the Lagrangian describing the vector resonances $\rho_\mu \equiv \rho_\mu^{\hat{a}} t^{\hat{a}} \sim \mathbf{15}$ and $a_\mu \equiv a_\mu^a X^a \sim \mathbf{6}$ reads

$$\mathcal{L}_V = -\frac{1}{4}{\rm Tr}\,(\rho_{\mu\nu}\rho^{\mu\nu}) + \frac{f_\rho^2}{2}{\rm Tr}\,(g_\rho \rho_\mu - e_\mu)^2 - \frac{1}{4}{\rm Tr}\,(a_{\mu\nu}a^{\mu\nu}) + \frac{f_a^2}{2\Delta^2}{\rm Tr}\,(g_a a_\mu - \Delta d_\mu)^2\,, \tag{3.93}$$

where $f_{\rho,\,a}$ are decay constants, $g_{\rho,\,a}$ are couplings, and Δ is a dimensionless parameter. The field strengths are given by

$$\rho_{\mu\nu} = \partial_\mu \rho_\nu - \partial_\nu \rho_\mu - ig_\rho\,[\rho_\mu, \rho_\nu]\,, \qquad a_{\mu\nu}^a = \nabla_\mu a_\nu^a - \nabla_\nu a_\mu^a, \quad \nabla_\mu = \partial_\mu - ie_\mu\,. \tag{3.94}$$

In the limit where the external gauge fields are neglected, the masses of the ρ and a read

$$m_\rho^2 = g_\rho^2 f_\rho^2\,, \qquad m_a^2 = \frac{g_a^2 f_a^2}{\Delta^2}\,. \tag{3.95}$$

Neglecting EWSB, only ρ_μ can mix with the $SU(2)_L \times U(1)_Y$ gauge fields. The mass eigenstates are obtained via the rotations

$$\begin{pmatrix}\bar{W}^\alpha \\ \rho_L^\alpha\end{pmatrix} \to \frac{1}{\sqrt{g_\rho^2 + \bar{g}^2}}\begin{pmatrix} g_\rho & -\bar{g} \\ \bar{g} & g_\rho\end{pmatrix}\begin{pmatrix} W^\alpha \\ \rho_L^\alpha\end{pmatrix}, \qquad \begin{pmatrix}\bar{B} \\ \rho_R^3\end{pmatrix} \to \frac{1}{\sqrt{g_\rho^2 + \bar{g}'^{\,2}}}\begin{pmatrix} g_\rho & -\bar{g}' \\ \bar{g}' & g_\rho\end{pmatrix}\begin{pmatrix} B \\ \rho_R^3\end{pmatrix}, \tag{3.96}$$

with W^α and B identified with the SM states. The associated SM couplings are $g = g_\rho \bar{g}/\sqrt{g_\rho^2 + \bar{g}^2}$ and $g' = g_\rho \bar{g}'/\sqrt{g_\rho^2 + \bar{g}'^{\,2}}$.

Now let us consider the case where $U(1)_{\rm DM}$ is gauged. The d_μ and e_μ symbols are computed starting from $D_\mu U = \partial_\mu U - iA_\mu^{\hat{a}} T^{\hat{a}} U$, where

$$A_\mu^{\hat{a}} T^{\hat{a}} = \bar{g}\bar{W}_\mu^\alpha T_L^\alpha + \bar{g}'\bar{B}_\mu T_R^3 + \sqrt{2}\,\bar{g}_D \bar{A}_{D\mu} T^{\rm DM} \tag{3.97}$$

[25] Notice that we define the d_μ and e_μ symbols with opposite sign compared to, e.g., Ref. [110].

when $SU(2)_L \times U(1)_Y \times U(1)_{\rm DM} \subset SO(6)$ are gauged. The normalization of the $U(1)_{\rm DM}$ gauge coupling is chosen in such a way that the χ kinetic term obtained from the two-derivative GB Lagrangian of Eq. (3.15) is $|(\partial_\mu - i\bar{g}_D \bar{A}_{D\mu})\chi|^2$. ρ_μ contains an $SO(4) \times U(1)_{\rm DM}$ singlet ρ_D that mixes with $\bar{A}_D$. The mass matrix and the rotation that diagonalizes it are

$$\frac{f_\rho^2}{2}(\bar{A}_D, \rho_D)\begin{pmatrix} 2\bar{g}_D^2 & -\sqrt{2}\bar{g}_D g_\rho \\ -\sqrt{2}\bar{g}_D g_\rho & g_\rho^2 \end{pmatrix}\begin{pmatrix} \bar{A}_D \\ \rho_D \end{pmatrix}, \quad \begin{pmatrix} \bar{A}_D \\ \rho_D \end{pmatrix} \to \begin{pmatrix} \frac{g_\rho}{\sqrt{g_\rho^2+2\bar{g}_D^2}} & -\frac{\sqrt{2}\bar{g}_D}{\sqrt{g_\rho^2+2\bar{g}_D^2}} \\ \frac{\sqrt{2}\bar{g}_D}{\sqrt{g_\rho^2+2\bar{g}_D^2}} & \frac{g_\rho}{\sqrt{g_\rho^2+2\bar{g}_D^2}} \end{pmatrix}\begin{pmatrix} A_D \\ \rho_D \end{pmatrix}, \tag{3.98}$$

hence the physical dark photon coupling is $g_D = g_\rho \bar{g}_D / \sqrt{g_\rho^2 + 2\bar{g}_D^2}$.

3.B Scalar potential : gauge sector

Integrating out the vector resonances at tree level, we obtain the effective Lagrangian containing the gauge fields $\bar{W}^\alpha, \bar{B}$ and the Higgs,

$$\mathcal{L}_g^{\rm eff} = \frac{1}{2}\Big(g^{\mu\nu} - \frac{p^\mu p^\nu}{p^2}\Big)\Big(2\Pi_{+-}\bar{W}_\mu^+\bar{W}_\nu^+ + \Pi_{33}\bar{W}_\mu^3\bar{W}_\nu^3 + \Pi_{BB}\bar{B}_\mu\bar{B}_\nu + 2\Pi_{3B}\bar{W}_\mu^3\bar{B}_\nu\Big) \tag{3.99}$$

where

$$\Pi_{+-} = \Pi_{33} = \Pi_0 + \frac{\tilde{h}^2}{4f^2}\Pi_1^g\,, \quad \Pi_{BB} = \Pi_B + \frac{\bar{g}'^2}{\bar{g}^2}\frac{\tilde{h}^2}{4f^2}\Pi_1^g\,, \quad \Pi_{3B} = -\frac{\bar{g}'}{\bar{g}}\frac{\tilde{h}^2}{4f^2}\Pi_1^g\,. \tag{3.100}$$

The dynamics of the strong sector resonances are encoded in the momentum-dependent form factors, which read in Euclidean space

$$\Pi_{0(B)} = p^2\left(1 + \frac{\bar{g}^{(\prime)\,2} f_\rho^2}{p^2 + m_\rho^2}\right), \qquad \Pi_1^g = \bar{g}^2\left[f^2 + 2p^2\left(\frac{f_a^2}{p^2+m_a^2} - \frac{f_\rho^2}{p^2+m_\rho^2}\right)\right]. \tag{3.101}$$

The effective potential for the Higgs has the expression

$$V_g(\tilde{h}) = \frac{3}{2}\int\frac{d^4p}{(2\pi)^4}\log\left[\Pi_{+-}^2(\Pi_{33}\Pi_{BB} - \Pi_{3B}^2)\right]. \tag{3.102}$$

Integrating out the dark photon at tree level generates additional contribution to the effective Lagrangian, $\mathcal{L}_g^{\rm eff} + \delta\mathcal{L}_g^{\rm eff}$, where $\mathcal{L}_g^{\rm eff}$ is given in Eq. (3.99), while

$$\delta\mathcal{L}_g^{\rm eff} = \frac{1}{2}\Big(g^{\mu\nu} - \frac{p^\mu p^\nu}{p^2}\Big)\Pi_{AA}\bar{A}_{D\mu}\bar{A}_{D\nu}, \qquad \Pi_{AA} = \Pi_A + \frac{2\bar{g}_D^2}{\bar{g}^2}\frac{\chi^*\chi}{f^2}\,\Pi_1^g, \tag{3.103}$$

with Euclidean-space form factors

$$\Pi_A = p^2\left(1 + \frac{2\bar{g}_D^2 f_\rho^2}{p^2+m_\rho^2}\right), \qquad \Pi_1^g = \bar{g}^2\left[f^2 + 2p^2\left(\frac{f_a^2}{p^2+m_a^2} - \frac{f_\rho^2}{p^2+m_\rho^2}\right)\right]. \tag{3.104}$$

The one-loop effective potential is also modifies $V_g(\tilde{h}) + \delta V_g(\chi)$, where the Higgs-dependent piece is given Eq. (3.102), and

$$\delta V_g(\chi) = \frac{3}{2}\int\frac{d^4p}{(2\pi)^4}\log\left[1 + \frac{\bar{g}_D^2}{\bar{g}^2}\frac{2\chi^*\chi}{f^2}\frac{\Pi_1^g}{\Pi_A}\right]. \tag{3.105}$$

Note that, importantly, the one-loop potential does not contain a Higgs portal term $\sim \lambda\tilde{h}^2\chi^*\chi$.

If the gauging of $U(1)_{\rm DM}$ is the only source of DM shift symmetry breaking, expanding the logarithm in Eq. (3.105) and matching to Eq. (3.46) gives for the χ mass term

$$\mu^2_{\rm DM} = \frac{3\bar{g}_D^2}{16\pi^2\bar{g}^2 f^2}\int_0^\infty dp^2 p^2 \frac{\Pi_1^g}{\Pi_A}\,, \quad \text{(DM shift symmetry broken by gauging)} \tag{3.106}$$

which is in general quadratically UV-divergent, but is automatically rendered finite after the two WSRs that ensure finiteness of $V_g(\tilde{h})$ are imposed, namely $2(f_\rho^2 - f_a^2) = f^2$ and $f_\rho^2 m_\rho^2 = f_a^2 m_a^2$. After the WSRs are used to express f_a, m_a in terms of f_ρ, m_ρ, and f, we find $\Pi_1^g > 0$, which guarantees that $U(1)_{\rm DM}$ is never spontaneously broken. Performing the integral and taking the leading order in $\bar{g}_D^2 f^2/m_\rho^2, \bar{g}_D^2 f_\rho^2/m_\rho^2 \ll 1$ we arrive at

$$\mu^2_{\rm DM} \simeq \frac{3\alpha_D}{2\pi}\frac{f_\rho^2}{f^2}\, m_\rho^2 \log\left(\frac{2f_\rho^2/f^2}{2f_\rho^2/f^2 - 1}\right). \tag{3.107}$$

The results above assume massless dark photon. A Stückelberg mass can be obtained by extending the coset to $SO(7)\times U(1)'/SO(6)$ and gauging the diagonal combination of $U(1)_{\rm DM}\times U(1)'$, namely $\sqrt{2}\,T^{\rm DM} + Z'$. All SM fields are assumed to be uncharged under $U(1)'$. The extended Goldstone matrix is $U = \exp(i\sqrt{2}\pi^a X^a/f)\exp(i\hat{\pi}Z'/f')$ and the two-derivative Lagrangian becomes $\mathcal{L}_\pi + (f'^2/2)\hat{d}_\mu\hat{d}^\mu$, where $\hat{d}_\mu = -(\partial_\mu\hat{\pi} - \bar{g}_D f'\bar{A}_{D\mu})/f'$ to all orders in $1/f'$. The additional piece is precisely the Stückelberg Lagrangian, which gives a mass $m_A = \bar{g}_D f'$ to $\bar{A}_D$. In the effective Lagrangian of Eq. (3.103) we must then replace $\Pi_A \to \Pi_A + m_A^2$, which in turn leads to a suppression of the χ mass: taking for simplicity $f_\rho = f$, Eq. (3.107) becomes

$$\frac{\mu^2_{\rm DM}(m_A^2)}{\mu^2_{\rm DM}(0)}\Big|_{f_\rho = f} = \frac{1 + \frac{y}{2(1-y)}\frac{\log y}{\log 2}}{1 - \frac{y}{2}}\,, \qquad y \equiv \frac{m_A^2}{m_\rho^2}\,. \tag{3.108}$$

Numerically, the suppression is small: for example $\mu^2_{\rm DM}(m_A^2)/\mu^2_{\rm DM}(0) \approx 0.97$ for $m_A/m_\rho = 1/10$. As long as $m_A^2/m_\rho^2, \bar{g}_D^2/g_\rho^2 \ll 1$, after m_A^2 is included in the mass matrix in Eq. (3.98) the diagonalization is still obtained through a rotation of angle $\theta \sim \sqrt{2}\bar{g}_D/g_\rho$.

3.C Scalar potential : fermion sector

Integrating out the fermionic resonances at tree level we obtain an effective Lagrangian containing the top quark, the b_L and the GBs as degrees of freedom,

$$\mathcal{L}_t^{\rm eff} = \Pi_{L_0}\bar{b}_L \not{p} b_L + \Pi_L \bar{t}_L \not{p} t_L + \Pi_R \bar{t}_R \not{p} t_R - \left(\Pi_{LR}\,\bar{t}_L t_R + \text{h.c.}\right), \tag{3.109}$$

In order to proceed, one must specify the couplings between the elementary and composite operators. For example, let us focus on the couplings given in Eq. (3.27). In this scenraio, the left handed top coupling break only the Higgs shift symmetry, while the right handed top coupling break both the Higgs and the DM shift symmetry. This leads to the following form factors

$$\Pi_L = \Pi_{L_0} + \frac{\tilde{h}^2}{2f^2}\Pi_{L_1}\,, \quad \Pi_R = \Pi_{R_0} + \left(\frac{\tilde{h}^2}{f^2} + \frac{2\chi^*\chi}{f^2}\right)\Pi_{R_1}\,, \quad \Pi_{LR} = \frac{\tilde{h}}{\sqrt{2}f}\sqrt{1 - \frac{\tilde{h}^2}{f^2} - \frac{2\chi^*\chi}{f^2}}\;\Pi_1^t\,. \tag{3.110}$$

The momentum-dependent form factors read, in Euclidean space,

$$\begin{aligned}
\Pi_{L_0} &= 1 + \sum_{i=1}^{N_Q} \frac{|\epsilon^i_{qQ}|^2}{p^2 + m^2_{Q_i}}\,, \qquad \Pi_{L_1} = \sum_{j=1}^{N_S} \frac{|\epsilon^j_{qS}|^2}{p^2 + m^2_{S_j}} - \sum_{i=1}^{N_Q} \frac{|\epsilon^i_{qQ}|^2}{p^2 + m^2_{Q_i}}\,, \\
\Pi_{R_0} &= 1 + \sum_{j=1}^{N_S} \frac{|\epsilon^j_{tS}|^2}{p^2 + m^2_{S_j}}\,, \qquad \Pi_{R_1} = \sum_{i=1}^{N_Q} \frac{|\epsilon^i_{tQ}|^2}{p^2 + m^2_{Q_i}} - \sum_{j=1}^{N_S} \frac{|\epsilon^j_{tS}|^2}{p^2 + m^2_{S_j}}\,, \\
\Pi^t_1 &= \sum_{j=1}^{N_S} \frac{\epsilon^{*j}_{tS}\epsilon^j_{qS} m_{S_j}}{p^2 + m^2_{S_j}} - \sum_{i=1}^{N_Q} \frac{\epsilon^{*i}_{tQ}\epsilon^i_{qQ} m_{Q_i}}{p^2 + m^2_{Q_i}}\,.
\end{aligned} \tag{3.111}$$

The effective potential for the GBs reads

$$V_f(\tilde{h}, \chi) = -2N_c \int \frac{d^4p}{(2\pi)^4} \log\left(p^2 \Pi_L \Pi_R + |\Pi_{LR}|^2\right). \tag{3.112}$$

Expanding Eqs. (3.102) and (3.112) to quartic order in the fields and matching with Eq. (3.29), we obtain the expressions of the parameters $\mu_h^2, \lambda_h, \mu^2_{\rm DM}, \lambda_{\rm DM}$ and λ as integrals over the form factors. For the dominant fermion contribution we find

$$\begin{aligned}
\mu^2_{h,f} &= -\frac{N_c}{8\pi^2 f^2} \int_0^\infty dp^2 p^2 \left(\frac{\Pi_{L_1}}{\Pi_{L_0}} + \frac{2\Pi_{R_1}}{\Pi_{R_0}} + \frac{(\Pi^t_1)^2}{p^2 \Pi_{L_0}\Pi_{R_0}}\right), \\
\lambda_{h,f} &= \frac{N_c}{4\pi^2 f^4} \int_{\mu^2_{\rm IR}}^\infty dp^2 p^2 \left[\frac{1}{4}\left(\frac{\Pi_{L_1}}{\Pi_{L_0}} + \frac{2\Pi_{R_1}}{\Pi_{R_0}} + \frac{(\Pi^t_1)^2}{p^2 \Pi_{L_0}\Pi_{R_0}}\right)^2 + \frac{(\Pi^t_1)^2 - p^2 \Pi_{L_1}\Pi_{R_1}}{p^2 \Pi_{L_0}\Pi_{R_0}}\right], \\
\mu^2_{\rm DM} &= -\frac{N_c}{4\pi^2 f^2} \int_0^\infty dp^2 p^2 \frac{\Pi_{R_1}}{\Pi_{R_0}}\,, \qquad \lambda_{\rm DM} = \frac{N_c}{4\pi^2 f^4} \int_0^\infty dp^2 p^2 \frac{\Pi^2_{R_1}}{\Pi^2_{R_0}}\,, \\
\lambda &= \frac{N_c}{8\pi^2 f^4} \int_0^\infty dp^2 p^2 \left[2\frac{\Pi^2_{R_1}}{\Pi^2_{R_0}} + \frac{(\Pi^t_1)^2}{p^2 \Pi_{L_0}\Pi_{R_0}}\left(1 + \frac{\Pi_{R_1}}{\Pi_{R_0}}\right)\right],
\end{aligned} \tag{3.113}$$

where we assumed real mixing parameters ϵ. Notice that the integral for the Higgs quartic $\lambda_{h,f}$ is IR divergent; the same happens for the (small) gauge contribution $\lambda_{h,g}$. The IR divergence signals that the potential is non-analytic at $\tilde{h} = 0$, due to the contribution of the light degrees of freedom (the top quark and SM gauge bosons). To remove this issue, the expansion of the potential in Eq. (3.29) is extended to include an additional term $\Delta V = (\delta_h/2)\tilde{h}^4 \log(\tilde{h}^2/f^2)$, which captures the non-analytic contribution to the Higgs quartic. Then all the coefficients of $V + \Delta V$ are IR-finite, including δ_h. The Higgs VEV $\langle \tilde{h} \rangle = v$ is obtained by solving the equation $\langle \tilde{h} \rangle^2 = -\mu_h^2/[\lambda_h + \delta_h(1 + 2\log(\langle \tilde{h} \rangle^2/f^2))]$, and the Higgs mass is $m_h^2 = (1-\xi)2v^2(\lambda_h + 3\delta_h + 2\delta_h \log \xi)$.

We now summarize our procedure for the parameter scan. From Eq. (3.43), requiring that $0 \leq s^2_{\theta,\phi} \leq 1$ leads to the constraints

$$\frac{m^2_{S_1} - m^2_{Q_1}}{m^2_{Q_2} - m^2_{Q_1}} \leq s^2_{\alpha,\beta} \leq \frac{m^2_{S_2} - m^2_{Q_1}}{m^2_{Q_2} - m^2_{Q_1}}\,. \tag{3.114}$$

These can be satisfied only for $m_{S_2} > m_{Q_1}$, which we therefore assume. Taking into account that Π^t_1 is the only form factor that is sensitive to the signs of the mixing parameters ϵ, and that furthermore the scalar potential is unaffected by $\Pi^t_1 \to -\Pi^t_1$, the angles are restricted to the following ranges

$$\theta, \alpha \in [-\pi/2, \pi/2], \qquad \phi \in [0, \pi/2], \qquad \beta \in [0, \pi]. \tag{3.115}$$

We summarize here the procedure adopted in the parameter scan of the two-layer model with WSRs (the procedure for the scan of the one-layer model is analogous).

1. The following parameters are randomly selected: $\epsilon_t \in [f/10, 8f]$, $m_{S_1,Q_1} \in [0, 6f]$, $m_{S_2,Q_2} \in [m_{Q_1}, 6f]$, $f_\rho \in \left[f/\sqrt{2}, 2f\right]$;

2. The angles α and β are randomly picked, compatibly with the restrictions in Eqs. (3.114) and (3.115). Then ϕ is completely fixed, while the sign of $\sin\theta$ is picked randomly.

3. ϵ_q is fixed by solving the following equation

$$m_t^2 = \left.\frac{\left|\Pi_{LR}(m_t^2)\right|^2}{\Pi_L(m_t^2)\Pi_R(m_t^2)}\right|_{\tilde{h}=v,\,\chi=0}, \tag{3.116}$$

   where the numerical value of the top mass is set to $m_t = m_t^{\overline{MS}}(2\text{ TeV}) = 150$ GeV.

4. m_ρ is fixed by requiring the Higgs VEV to match the observed value, $\langle\tilde{h}\rangle = v \simeq 246$ GeV.

In the two-layer model, the compositeness fraction s_L (s_R) of the left (right) handed top is computed by diagonalizing analytically the fermion mass matrix for $v \to 0$, and taking the projection onto the composite fermions of the normalized eigenvector that corresponds to the physical t_L (t_R). For example, the compositeness fraction of t_R is defined as

$$s_R \equiv \sqrt{\frac{a_2^2+a_3^2}{a_1^2+a_2^2+a_3^2}} \qquad \text{with} \qquad t_R^p = \frac{1}{\sqrt{a_1^2+a_2^2+a_3^2}}\left(a_1 t_R + a_2 S_1 + a_3 S_2\right), \tag{3.117}$$

where t_R^p denotes the mass-eigenstate right-handed top (for $v \to 0$). The compositeness fractions satisfy $0 \le s_{L,R} \le 1$. In the one-layer model, they are identified with the sine of the elementary-composite mixing angles.

In the scenarios where the DM shift symmetry is preserved by the top quark, the following embeddings are used

$$\mathbf{7}_{2/3} \sim \xi_L^{(t)} = \frac{1}{\sqrt{2}}\left(ib_L,\quad b_L,\quad it_L,\quad -t_L,\quad \mathbf{0}_3^T\right)^T, \qquad \mathbf{21}_{2/3} \sim \xi_R^{(t)} = \frac{i\,t_R}{2}\begin{pmatrix} 0 & -1 & & & & \\ 1 & 0 & & & & \\ & & 0 & 1 & & \\ & & -1 & 0 & & \\ & & & & \mathbf{0}_{3\times 3} & \end{pmatrix}, \tag{3.118}$$

where empty entries in the expression of $\xi_R^{(t)}$ are zeros. Since $\mathbf{7} = \mathbf{6} \oplus \mathbf{1}$ and $\mathbf{21} = \mathbf{15} \oplus \mathbf{6}$ under $SO(6)$, in the top sector we expect fermionic resonance multiplets $G \sim \mathbf{15}_{2/3}$, $Q \sim \mathbf{6}_{2/3}$ and $S \sim \mathbf{1}_{2/3}$ under $SO(6) \times U(1)_X$. The decomposition and component expression of Q is given in Eq. (3.26), whereas G decomposes as $\mathbf{15} = [(\mathbf{3},\mathbf{1}) + (\mathbf{1},\mathbf{3})]_0 \oplus (\mathbf{1},\mathbf{1})_0 \oplus (\mathbf{2},\mathbf{2})_{\pm 1}$ under $SU(2)_L \times SU(2)_R \times U(1)_{\rm DM}$, where the $X = 2/3$ charge is understood. In components,

$$G = \frac{1}{2}\begin{pmatrix} 0 & -iT_+^{12} & B_+^{12} - X_+^{12} & -i(B_-^{12} + X_-^{12}) & -\mathcal{B}_- - \mathcal{X}_{5/3\,-} & -i(\mathcal{B}_+ + \mathcal{X}_{5/3\,+}) \\ & 0 & -i(B_+^{12} + X_+^{12}) & -B_-^{12} + X_-^{12} & i(\mathcal{B}_- - \mathcal{X}_{5/3\,-}) & -\mathcal{B}_+ + \mathcal{X}_{5/3\,+} \\ & & 0 & -iT_-^{12} & -\mathcal{T}_- - \mathcal{X}_{2/3\,-} & -i(\mathcal{T}_+ + \mathcal{X}_{2/3\,+}) \\ & & & 0 & -i(\mathcal{T}_- - \mathcal{X}_{2/3\,-}) & \mathcal{T}_+ - \mathcal{X}_{2/3\,+} \\ & & & & 0 & -i\sqrt{2}\,\widetilde{S} \\ & & & & & 0 \end{pmatrix}, \tag{3.119}$$

(3.119)

where the lower triangle is determined by antisymmetry. We have made the definitions $T^{12}_{\pm} \equiv \widetilde{T}_1 \pm \widetilde{T}_2$, $Q^{12}_{\pm} \equiv (\widetilde{Q}_1 \pm \widetilde{Q}_2)/\sqrt{2}$ $(Q = X, B)$ and $\mathcal{Q}_{\pm} \equiv (\mathcal{Q}^{(+)} \pm \mathcal{Q}^{(-)})/\sqrt{2}$ $(\mathcal{Q} = \mathcal{T}, \mathcal{B}, \mathcal{X}_{2/3}, \mathcal{X}_{5/3})$. Here $(\widetilde{X}_i, \widetilde{T}_i, \widetilde{B}_i)^T$ is a $(\mathbf{3},\mathbf{1})_0$ for $i = 1$ and a $(\mathbf{1},\mathbf{3})_0$ for $i = 2$, $\widetilde{S} \sim (\mathbf{1},\mathbf{1})_0$, and the fields with calligraphic names compose the $(\mathbf{2},\mathbf{2})_{\pm 1}$.[26] The elementary-composite mixing Lagrangian for the top sector is

$$\mathcal{L}^{(t)}_{\rm mix} = \epsilon^i_{qS}\bar{\xi}^{(t)A}_L U_{A7} S_{R,i} + \epsilon^j_{qQ}\bar{\xi}^{(t)A}_L U_{Aa} Q^a_{R,j} + \epsilon^j_{tQ}\bar{\xi}^{(t)BA}_R U_{Aa} U_{B7} Q^a_{L,j} + \epsilon^k_{tG}\bar{\xi}^{(t)BA}_R U_{Aa} U_{Bb} G^{ab}_{L,k} + \text{h.c.}, \tag{3.120}$$

where repeated indices are summed. Here $\{i, j, k\}$ count the multiplicities of resonances and therefore run from 1 to $\{N_S, N_Q, N_G\}$, respectively, while A, B are $SO(7)$ indices and a, b are $SO(6)$ indices. Calculability of the one-loop scalar potential is obtained via generalized Weinberg sum rules (WSRs). The minimal field content that gives a completely ultraviolet (UV)-finite one-loop Higgs potential is $N_S = N_Q = N_G = 1$, which we adopt. The embeddings in Eq. (3.118) yield a Higgs potential with "double tuning" structure [131], where parametrically $\Delta^{-1} \sim (v^2/f^2)(\epsilon^t)^2$.

We now describe the embeddings of the bottom quark in the two models discussed in the main text: the one of Sec. 3.4, where the χ shift symmetry is broken by b_R, and the one of Sec. 3.5, where the χ shift symmetry is preserved by the bottom sector.

DM shift symmetry broken by b quark The bottom quark embeddings are

$$\mathbf{7}_{-1/3} \sim \xi^{(b)}_L = \frac{1}{\sqrt{2}}\left(-it_L,\quad t_L,\quad ib_L,\quad b_L,\quad \mathbf{0}^T_3\right)^T, \qquad \mathbf{7}_{-1/3} \sim \xi^{(b)}_R = b_R\left(\mathbf{0}^T_6,\quad 1\right)^T. \tag{3.121}$$

We thus expect resonances $Q^{(b)} \sim \mathbf{6}_{-1/3}$ and $S^{(b)} \sim \mathbf{1}_{-1/3}$ under $SO(6)\times U(1)_X$. The component expression of $Q^{(b)}$ is

$$Q^{(b)} = \frac{1}{\sqrt{2}}\left(iU_{-4/3} - i\widetilde{T}, U_{-4/3} + \widetilde{T}, iU_{-1/3} + i\widetilde{B}, -U_{-1/3} + \widetilde{B}, -i\mathcal{V} + i\mathcal{W}, \mathcal{V} + \mathcal{W}\right)^T, \tag{3.122}$$

where under $(SU(2)_L)^{\rm DM}_Y$ we have $(U_{-1/3}, U_{-4/3})^T \sim \mathbf{2}^0_{-5/6}$, $(\widetilde{T}, \widetilde{B})^T \sim \mathbf{2}^0_{1/6}$ and $\mathcal{V}, \mathcal{W} \sim \mathbf{1}^{\pm 1}_{-1/3}$. The elementary-composite mixing Lagrangian for the bottom sector reads

$$\mathcal{L}^{(b)}_{\rm mix} = (\epsilon^m_{qS^{(b)}}\bar{\xi}^{(b)A}_L S^{(b)}_{R,m} + \epsilon^m_{bS^{(b)}}\bar{\xi}^{(b)A}_R S^{(b)}_{L,m})U_{A7} + (\epsilon^n_{qQ^{(b)}}\bar{\xi}^{(b)A}_L Q^{(b)a}_{R,n} + \epsilon^n_{bQ^{(b)}}\bar{\xi}^{(b)A}_R Q^{(b)a}_{L,n})U_{Aa} + \text{h.c.}, \tag{3.123}$$

where $\{m, n\}$ run from 1 to $\{N_{S^{(b)}}, N_{Q^{(b)}}\}$, respectively. The complete fermionic Lagrangian is $\mathcal{L}_f = (\text{kin. terms}) + (\text{resonance masses}) + \mathcal{L}^{(t)}_{\rm mix} + \mathcal{L}^{(b)}_{\rm mix}$, where the kinetic terms include both those for the elementary fields and the CCWZ ones for the resonances. Integrating out the resonances we obtain an effective Lagrangian for the top and bottom quarks and the GBs, which we use to calculate the one-loop potential for $\tilde{h}$ and χ. In particular, for the DM mass parameter we find

$$\mu^2_{\rm DM} = -\frac{N_c}{4\pi^2 f^2}\int_0^\infty dp^2 p^2 \frac{\Pi^b_{R_1}}{\Pi^b_{R_0}}, \qquad (b_R \text{ loops}) \tag{3.124}$$

[26] Fields with calligraphic names have the same $SO(4)$ quantum numbers as their non-calligraphic versions. For example $\mathcal{X}^{(\pm)}_{5/3}$ transforms as $X_{5/3}$ under $SO(4)$, but has in addition charge ± 1 under $U(1)_{\rm DM}$.

with Euclidean form factors

$$\Pi^b_{R_0} = 1 + \sum_{m=1}^{N_{S^{(b)}}} \frac{|\epsilon^m_{bS^{(b)}}|^2}{p^2 + m^2_{S^{(b)}_m}}\,, \qquad \Pi^b_{R_1} = \sum_{n=1}^{N_{Q^{(b)}}} \frac{|\epsilon^n_{bQ^{(b)}}|^2}{p^2 + m^2_{Q^{(b)}_n}} - \sum_{m=1}^{N_{S^{(b)}}} \frac{|\epsilon^m_{bS^{(b)}}|^2}{p^2 + m^2_{S^{(b)}_m}}\,. \tag{3.125}$$

We introduce $N_{Q^{(b)}} = N_{S^{(b)}} = 1$ resonances and to obtain partial calculability of the bottom-induced potential we impose one set of WSRs, which make the dimensionless couplings UV-finite and reduce to logarithmic the degree of divergence of the mass parameters. The WSRs correspond to the relations $\epsilon^2_{qS^{(b)}} = \epsilon^2_{qQ^{(b)}}$ and $\epsilon^2_{bS^{(b)}} = \epsilon^2_{bQ^{(b)}}$, the latter of which implies from Eq. (3.125) that $\mu^2_{\rm DM}$ vanishes for $m^2_{Q^{(b)}} = m^2_{S^{(b)}}$. Assuming $m_{Q^{(b)}}, m_{S^{(b)}} > 0$ we take as solutions to the sum rules $\epsilon_{qS^{(b)}} = +\epsilon_{qQ^{(b)}}$ and $\epsilon_{bS^{(b)}} = -\epsilon_{bQ^{(b)}}$, in which case λ does not vanish even for $m_{Q^{(b)}} = m_{S^{(b)}}$. We have then the parametric scalings

$$\mu^2_{\rm DM} \simeq a\,\frac{N_c}{16\pi^2}\frac{M^4_{*b}}{f^2}(\epsilon^b_R)^2\,C_{QS}\,, \quad C_{QS} \equiv \frac{m^2_{Q^{(b)}} - m^2_{S^{(b)}}}{M^2_{*b}}\,, \qquad \lambda \simeq b\,\frac{N_c}{16\pi^2}\frac{M^2_{*b}}{f^2}\,y_b^2, \tag{3.126}$$

where $a, b > 0$ are $O(1)$ coefficients and M_{*b}, defined via Eq. (3.14), is identified with $M_{*b} = m_{Q^{(b)}} + m_{S^{(b)}}$, which implies $|C_{QS}| < 1$. An important constraint on this setup comes from tree-level corrections to the $Z\bar{b}_L b_L$ coupling, since the embedding of b_L in a $(\mathbf{2},\mathbf{2})_{-1/3}$ of $SU(2)_L \times SU(2)_R \times U(1)_X$ is not invariant under the P_{LR} custodial symmetry [108]. The corrections scale as

$$\frac{g}{c_w} Z_\mu \bar{b}_L \gamma^\mu (g^{\rm SM}_{b_L} + \delta g_{b_L}) b_L\,, \qquad \delta g_{b_L} \simeq +(\epsilon^b_L)^2\,\frac{v^2}{f^2} \tag{3.127}$$

($g^{\rm SM}_{b_L} = -1/2 + s^2_w/3$), where the sign is fixed to be positive. For comparison, the experimental bound is $-1.7 < 10^3\,\delta g_{b_L} < +1.4$ at 99% CL [166].[27] A large b_L compositeness, namely $\epsilon^b_L \sim 1$ and $\epsilon^b_R \sim y_b f/M_{*b}$, leads to $\mu^2_{\rm DM} \lesssim \lambda v^2$ and therefore very light DM, $m_\chi \approx 4$ GeV $(M_{*b}/8$ TeV$)(1$ TeV$/f)$,[28] but is robustly ruled out by $Z\bar{b}_L b_L$ unless $f \gg$ TeV. Conversely, a large b_R compositeness $\epsilon^b_R \sim 1$, $\epsilon^b_L \sim y_b f/M_{*b}$ easily satisfies the $Z\bar{b}_L b_L$ constraint. This region, however, yields parametric scalings for $\mu^2_{\rm DM}$ and λ that are similar to those already discussed in the case where the DM shift symmetry is broken by t_R couplings. We are thus led to focus on the "intermediate" range $\epsilon^b_L \sim \epsilon^b_R \sim \sqrt{y_b f/M_{*b}}$, where the correction to $Z\bar{b}_L b_L$ is typically moderate, $10^3\,\delta g_{b_L} \sim +\text{few} \times 0.1\,(8\text{ TeV}/M_{*b})\,(1\text{ TeV}/f)$, and the DM potential scales as in Eq. (3.64), where in the (crude) estimate of the DM mass we have taken a typical $C_{QS} \sim 0.2$ for this parameter region.

For illustration a numerical scan of the model parameter space was performed, setting $f = 1$ TeV and requiring that the scalar potential generated by the top and bottom sectors gives the observed Higgs VEV and mass. We chose $m_{Q^{(b)}} > m_{S^{(b)}}$, yielding $0 < C_{QS} < 1$ and $\mu^2_{\rm DM} > 0$, therefore $U(1)_{\rm DM}$ is never spontaneously broken. In addition, we took $\Lambda = 10f$ as UV cutoff for the bottom contributions to $\mu^2_{\rm DM}$ and μ^2_h. The results of the scan are reported in Fig. 3.19, where to approximately account for LHC constraints [167] only points where all resonances are heavier than 1.2 TeV are shown. The distribution of the mixings $\epsilon^b_{L,R}$, shown in the left panel, clearly follows Eq. (3.14) and significantly populates the region $\epsilon^b_L \sim \epsilon^b_R \sim \sqrt{y_b f/M_{*b}} \sim 0.03$ - 0.04, where the parametric scalings in Eq. (3.64) approximately apply. From the right panel, which shows

[27] In this model b_R is embedded in a $(\mathbf{1},\mathbf{1})_{-1/3} \subset \mathbf{7}_{-1/3}$, so the $Z\bar{b}_R b_R$ coupling is protected by P_{LR} and very suppressed. Therefore it makes sense to set $\delta g_{b_R} = 0$ in the electroweak fit. Since δg_{b_L} is weakly correlated with the remaining precision observables, we can then simply quote its one-parameter bound.

[28] We have fixed the numerical value of y_b via $m_b = m_b^{\overline{MS}}(2\text{ TeV}) \simeq 2.5$ GeV.

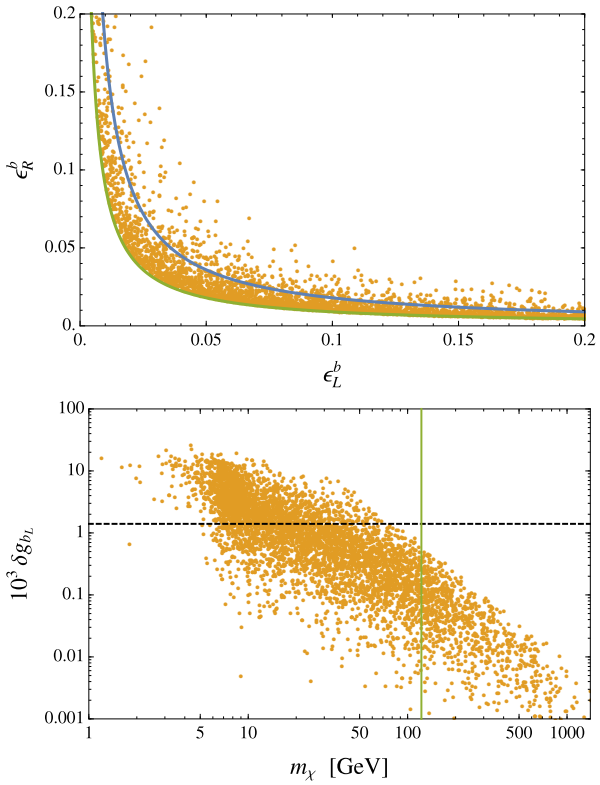

Figure 3.19: *Results of the parameter scan of the model where the DM shift symmetry is broken by b_R, for $f = 1$ TeV. Left panel: distribution of the mixings for the two chiralities of the bottom quark. The blue (green) curve corresponds to the relation $y_b \simeq \epsilon_L^b \epsilon_R^b M_{*b}/f$ with $M_{*b} = 8\,(16)$ TeV. Notice that $M_{*b} = m_{Q^{(b)}} + m_{S^{(b)}}$ is not a physical mass, and can therefore exceed $4\pi f$. Right panel: tree-level correction to the $Z\bar{b}_L b_L$ coupling versus the physical χ mass. The black dashed line indicates the 99% CL experimental upper bound, $10^3\,\delta g_{b_L} < 1.4$, whereas the green vertical line corresponds to the mass for which χ yields the observed DM density by annihilating purely through the derivative Higgs portal.*

the tree-level δg_{b_L} versus the physical χ mass, we read that in the region where χ constitutes all or part of the observed DM, i.e. $m_\chi \geq m_\chi^{(f=1\text{ TeV})} \approx 122$ GeV, the tree-level correction to $Z\bar{b}_L b_L$ is always below the experimental bound.

DM shift symmetry preserved by b quark The right-handed bottom is embedded as

$$\mathbf{21}_{2/3} \sim \xi_R^{(b)} = \frac{b_R}{2\sqrt{2}} \begin{pmatrix} & & 1 & i & \\ & \mathbf{0}_{2\times 2} & -i & 1 & \\ -1 & i & & & \\ -i & -1 & & \mathbf{0}_{2\times 2} & \\ & & & & \mathbf{0}_{3\times 3} \end{pmatrix}, \tag{3.128}$$

where empty entries are zeros. Therefore the embedding of q_L in Eq. (3.118) is sufficient to generate the bottom mass, and an $X = -1/3$ sector needs not be introduced. The Lagrangian that mixes the b_R with the composite resonances reads

$$\widetilde{\mathcal{L}}_{\text{mix}}^{(b)} = \epsilon_{bQ}^j \bar{\xi}_R^{(b)BA} U_{Aa} U_{B7} Q_{L,j}^a + \epsilon_{bG}^k \bar{\xi}_R^{(b)BA} U_{Aa} U_{Bb} G_{L,k}^{ab} + \text{h.c.}, \tag{3.129}$$

and the complete fermionic Lagrangian is $\mathcal{L}_f = (\text{kin. terms}) + (\text{resonance masses}) + \mathcal{L}_{\text{mix}}^{(t)} + \widetilde{\mathcal{L}}_{\text{mix}}^{(b)}$.

As a final remark, we have neglected one-derivative operators built out of fermionic resonances, such as (schematically) $\bar{S}_i \not{d}^a Q_j^a$ and $\bar{Q}_j^a \not{d}^b G_k^{ab}$ in the $X = 2/3$ sector and $\bar{S}_m^{(b)} \not{d}^a Q_n^{(b)a}$ in the $X = -1/3$ sector, which are generically expected to appear in $\mathcal{L}_f$ with $O(1)$ coefficients. Their presence does not affect our discussion, but can have important effects on the resonance phenomenology at high-energy colliders [110].

3.D Details on DM phenomenology

The explicit values of the couplings in Eqs. (3.45, 3.46) are

$$\begin{aligned} a_{hhh} = b_{h\chi\chi} = \frac{\xi}{\sqrt{1-\xi}}\,, \qquad a_{hh\chi\chi} = \frac{\xi^2}{1-\xi}\,, \qquad b_{hh\chi\chi} = \xi\,\frac{1+\xi}{1-\xi}\,, \\ a_{hVV} = d_{h\chi\chi} = d_{hhh} = \sqrt{1-\xi}\,, \qquad d_{hh\chi\chi} = 1-\xi\,. \end{aligned} \tag{3.130}$$

The couplings between the scalars and the top quark in Eq. (3.47) can be easily computed by matching with Eq. (3.109), where the top partners have been integrated out in the original field basis. However, the results of the parameter scan show that the "composite" mass of the lightest singlet, m_{S_1}, can in some cases be as low as few hundred GeV (while the physical mass of the lightest singlet is still above the experimental lower bound of 1 TeV, because it receives a large contribution from the elementary-composite mixing parameters $\sim \epsilon_t$), thus invalidating the simple effective theory approach in this basis. Therefore we proceed as follows: Starting from the UV Lagrangian in Eq. (3.27), after exact, numerical diagonalization of the fermion mass matrices we consider the following terms

$$\begin{aligned} \mathcal{L}_f \;\ni\; & i\bar{t}\not{\partial} t - m_t \bar{t}t\Big(\tilde{c}_{tth}\frac{h}{v} + 2\,\tilde{c}_{tt\chi\chi}\frac{\chi^*\chi}{v^2}\Big) \\ & + \sum_{i=1}^{N_Q}\Big[\overline{\mathcal{Y}}_i\,(i\not{\partial} - m_{Q_i})\,\mathcal{Y}_i + \overline{\mathcal{Z}}_i\,(i\not{\partial} - m_{Q_i})\,\mathcal{Z}_i + \bar{t}(b_L^i P_L + b_R^i P_R)(\mathcal{Y}_i\chi^* + \mathcal{Z}_i\chi) + \text{h.c.}\Big], \end{aligned} \tag{3.131}$$

where we introduced the coefficients $\tilde{c}_{tth}, \tilde{c}_{tt\chi\chi}, b_L^i$ and b_R^i, which are real if CP invariance is imposed. After integrating out the $\mathcal{Y}_i$ and $\mathcal{Z}_i$ and matching to Eq. (3.47), we find that $c_{tth} = \tilde{c}_{tth}$, whereas

$$c_{tt\chi\chi} = \tilde{c}_{tt\chi\chi} - \frac{v^2}{m_t}\sum_{i=1}^{N_Q}\left[\frac{b_L^i b_R^i}{m_{Q_i}} + \frac{m_t}{2m_{Q_i}^2}(b_L^{i\,2} + b_R^{i\,2})\right]. \tag{3.132}$$

We have verified that for parameter choices where the EFT approximation is justified, the values of c_{tth} and $c_{tt\chi\chi}$ obtained from Eq. (3.109) agree with those computed with this semi-numerical method.

The cosmological evolution of the χ number density[29] is described by the Boltzmann equation

$$\frac{dn_\chi}{dt} + 3Hn_\chi = -\langle\sigma v_{\rm rel}\rangle\left[n_\chi^2 - \left(n_\chi^{\rm eq}\right)^2\right], \tag{3.133}$$

where $n_\chi^{\rm eq}$ is the equilibrium number density, H is the time-dependent Hubble parameter and $\langle\sigma v_{\rm rel}\rangle$ is the thermally averaged annihilation cross-section times the relative velocity of two DM particles, whose expression is [91]

$$\langle\sigma v_{\rm rel}\rangle(T) = \frac{1}{16m_\chi^4 T K_2^2(m_\chi/T)}\int_{4m_\chi^2}^{\infty} ds\, s\,\sqrt{s-4m_\chi^2}\,K_1(\sqrt{s}/T)\,\sigma v_{\rm rel}(s)\,, \tag{3.134}$$

[29] Notice that the DM number density is obtained summing over particles and anti-particles, $n_{\rm DM} = 2\,n_\chi$.

where T denotes the temperature and K_1, K_2 are modified Bessel functions of the second kind. Dark matter annihilates dominantly into WW, ZZ, hh and $t\bar{t}$. The corresponding cross sections were calculated analytically in terms of the parameters of the effective Lagrangian in Eq. (3.44), and found to agree with those of Ref. [73] in the limit $c_{tth} = c_{tth}^{\rm nl\sigma m}$, $c_{tt\chi\chi} = c_{tt\chi\chi}^{\rm nl\sigma m}$. Equation (3.50) provides a naive solution of the Boltzmann equation, which is nevertheless useful for a qualitative understanding.

The leading 1-loop corrections to the derivative $\chi\chi^* hh$ coupling in Eq. (3.52) are obtained computing the set of Feynman diagrams depicted in Fig. 3.10, and selecting the logarithmically divergent pieces. For simplicity, we report the result in the limit where the GB masses are neglected. Even though this is a rough approximation for DM annihilation, where the kinematic variables take the values (assuming $m_\chi^2 \gg m_h^2$) $s \sim 4m_\chi^2$ and $t \sim u \sim -m_\chi^2$, it is nevertheless sufficient for the purpose of estimating the theoretical uncertainty on the cross section. In particular, it implies that $s + t + u \simeq 0$. The first class of diagrams in Fig. 3.10, which contain two insertions of the elementary-composite mixings, yield the result in momentum space

$$\frac{iN_c}{8\pi^2 f^4}\Big(\epsilon_t^2 - \frac{\epsilon_q^2}{8}\Big) s \log\Lambda^2 \,. \tag{3.135}$$

Notice that this class of diagrams also yield the $O(p^0)$ coupling λ. The second class of diagrams contain two derivative couplings arising from the e_μ symbol, and give

$$\frac{iN_c}{8\pi^2 f^4}\Big(-\frac{\epsilon_q^2}{8}\Big) 3\, s \log\Lambda^2 \,, \tag{3.136}$$

which can be seen as arising from two ϵ insertions on the internal fermion lines. The contribution of the third class of diagrams turns out to be proportional to the external masses, and thus negligible within our approximations. Lastly, the triangle diagrams composing the fourth class yield

$$\frac{iN_c}{8\pi^2 f^4}(\epsilon_t^2) 3\, s \log\Lambda^2 \,. \tag{3.137}$$

Summing Eqs. (3.135), (3.136) and (3.137) and making the argument of the logarithm dimensionless by inserting m_*^2, we arrive at the final result in Eq. (3.54).

The SI DM-nucleon cross section is given by

$$\sigma_{\rm SI}^{\chi N} = \frac{1}{\pi}\Big(\frac{m_N}{m_\chi + m_N}\Big)^2 \Big[\frac{ZF_p + (A-Z)F_n}{A}\Big]^2 , \tag{3.138}$$

where $m_N = (m_p + m_n)/2$ is the average nucleon mass, and for Xenon $A = 130$, $Z = 54$. The effective couplings of the DM to nucleons can be written as

$$\frac{F_x}{m_x} = \sum_{q=u,d,s} f_{T_q}^x a_q + \frac{2}{27} f_{T_g}^x \Big(\sum_{q=c,b} a_q + k_g^t\Big), \qquad (x = p,\, n) \tag{3.139}$$

where the first term represents the tree-level coupling to the light quarks u, d, s, while the second term parameterizes the coupling to gluons via loops of heavy fermions. For convenience, in the second term we have further singled out the contribution mediated by the top and top partners, k_g^t, from the one coming from the charm and bottom. The former can be easily computed using the low-energy theorem for the GBs,

$$k_g^t = \frac{\lambda v}{m_h^2}\, d_{h\chi\chi} D_h - \frac{1}{2} D_{\chi\chi^*} \tag{3.140}$$

with the definitions

$$\begin{aligned} D_h &\equiv \sqrt{1-\xi}\left(\frac{\partial}{\partial\tilde{h}}\log|\det\mathcal{M}_t(\tilde{h},\chi)|\right)_{\tilde{h}=v,\,\chi=0} = \frac{1}{v}\frac{1-2\xi}{\sqrt{1-\xi}}\,, \\ D_{\chi\chi^*} &\equiv \left(\frac{\partial^2}{\partial\chi\partial\chi^*}\log|\det\mathcal{M}_t(\tilde{h},\chi)|\right)_{\tilde{h}=v,\,\chi=0} = -\frac{1}{f^2(1-\xi)}\,, \end{aligned} \tag{3.141}$$

where $\mathcal{M}_t$ is the field-dependent mass matrix for the top sector. The expression of the coefficients a_q was given in Eq. (3.12). Even though k_g^t receives contributions from the top partners, its final expression depends only on f and is insensitive to the resonance parameters. This cancellation can be traced to the fact that with our choice of fermion embeddings, $q_L, t_R \sim \mathbf{7}$ of $SO(7)$, there is only one $SO(6)$ invariant that generates the top mass [168, 169].[30] We remark that our computation based on Eq. (3.140) is only approximate for the box diagrams that contain $\mathcal{Y}, \mathcal{Z}$ propagators, and could be improved through an exact computation of the $\chi g \to \chi g$ scattering amplitude, see Ref. [170] for an extensive discussion in the similar case of neutralino-nucleon scattering. However, we have checked that for realistic parameter points the contribution of the box diagrams to k_g^t is $\lesssim 10\%$, hence we estimate that the corrections to our approximation would only affect $\sigma_{\rm SI}^{\chi N}$ at the percent level.

The contribution of the light SM quarks is encoded by the coefficients a_q ($q = u, d, c, s, b$) in Eq. (3.139). It is somewhat model-dependent, being determined by the choice of the corresponding embeddings, which we have not specified so far since they do not affect any other aspect of the phenomenology. For concreteness, we assume all left-handed light quarks to be embedded in the **7**, whereas for the right-handed light quarks we take $b_R \sim \mathbf{7}$, leading to a contribution identical to the one of the top sector, and $q_R \sim \mathbf{1}$ ($q = u, d, c, s$), yielding a vanishing coefficient for the $\chi^*\chi\bar{q}q$ contact term. In summary, we have

$$k_g^t = a_b = \frac{\lambda}{m_h^2}(1-2\xi) + \frac{1}{2f^2(1-\xi)}\,, \qquad a_{u,d,c,s} = \frac{\lambda}{m_h^2}(1-\xi). \tag{3.142}$$

For the nuclear matrix elements that appear in Eq. (3.139) we take $f_{T_u}^p = 0.021$, $f_{T_d}^p = 0.041$, $f_{T_u}^n = 0.019$, $f_{T_d}^n = 0.045$, obtained from agreeing determinations of the pion-nucleon sigma term $\sigma_{\pi N}$ from chiral perturbation theory [171] and dispersive methods [172], and $f_{T_s}^{p,n} = 0.043$, based on lattice QCD results [173]. The gluon matrix element is then $f_{T_g}^{p,n} = 1 - \sum_{q=u,d,s} f_{T_q}^{p,n} \simeq 0.89$. For realistic parameters the Higgs exchange dominates and the cross section can be approximated by the simple expression in Eq. (3.56), with $f_N \equiv 2/9 + (7/9)\sum_{q=u,d,s} f_{T_q}^{p,n} \simeq 0.30$.

In the scenario where the χ shift symmetry is broken by b_R, λ is negligible and the cross section takes the form in Eq. (3.65), where $\tilde{f}_N = (2/27) f_{T_g} \approx 0.066$ in case I and $\tilde{f}_N = f_{T_d} + f_{T_s} + (2/27) f_{T_g} \approx 0.15$ in case II.

3.E $U(1)_Y$ - $U(1)_{\rm DM}$ kinetic mixing

In this appendix we show that kinetic mixing of $U(1)_Y$ and $U(1)_{\rm DM}$ (in short, Y-DM kinetic mixing) can vanish exactly in the $SO(7)/SO(6)$ model, thus motivating the choice $\varepsilon = 0$ made throughout our discussion.

As first step, we neglect the explicit $\mathcal{G}$ breaking in the fermion sector and consider the bosonic Lagrangian including the gauging of $SU(2)_L \times U(1)_Y \times U(1)_{\rm DM}$. At $O(p^2)$ this is simply given

[30] Notice that the expression of k_g^t is identical to that obtained in $SO(6)/SO(5)$ when $q_L, t_R \sim \mathbf{6}$ [73].

by Eq. (3.15), and the kinetic mixing operators arise at $O(p^4)$. The four-derivative bosonic Lagrangian was first written down for the $SO(5)/SO(4)$ model in Ref. [174]. To obtain a basis of operators for our model we find it convenient to follow Ref. [175], where the $O(p^4)$ Lagrangian for $SO(5)/SO(4)$ was discussed by parametrizing the GBs with the matrix $\Sigma(\vec{\pi}) = U(\vec{\pi})^2$. This alternative, but equivalent, description is possible for *symmetric* cosets such as $SO(N+1)/SO(N)$, which admit an automorphism (grading) $\mathcal{R}$ of the algebra that flips the sign of only the broken generators, $T^{\hat{a}} \to +T^{\hat{a}}$ and $X^a \to -X^a$. The three building blocks that are used to construct invariant operators, all transforming in the adjoint of $\mathcal{G}$, are

$$V_\mu = (D_\mu \Sigma)\Sigma^{-1}, \qquad A_{\mu\nu} = \partial_\mu A_\nu - \partial_\nu A_\mu - i[A_\mu, A_\nu], \qquad \Sigma A^{\mathcal{R}}_{\mu\nu}\Sigma^{-1}, \tag{3.143}$$

where $A^{\mathcal{R}}_{\mu\nu} \equiv \mathcal{R}(A_{\mu\nu})$ and we formally took the whole of $\mathcal{G}$ to be gauged by $A_\mu = g_{\mathcal{G}} A^A_\mu T^A$, hence the covariant derivative is $D_\mu \Sigma = \partial_\mu \Sigma - i(A_\mu \Sigma - \Sigma A^{\mathcal{R}}_\mu)$. In this formalism, the two-derivative Lagrangian is $\mathcal{L}_\pi = -(f^2/16)\mathrm{Tr}[V_\mu V^\mu]$.

In our model the physical sources are given by Eq. (3.97), which satisfies $A^{\mathcal{R}}_\mu = A_\mu$. By constructing a complete basis for the $O(p^4)$ Lagrangian $\mathcal{L}_4$, we find that Y-DM kinetic mixing is encoded by the operators

$$\mathrm{Tr}[\bar{\mathbf{B}}_{\mu\nu}\bar{\mathbf{F}}^{\mu\nu}_D], \qquad \mathrm{Tr}[\Sigma\bar{\mathbf{B}}_{\mu\nu}\Sigma^{-1}\bar{\mathbf{F}}^{\mu\nu}_D], \tag{3.144}$$

where $\bar{\mathbf{B}}^{\mu\nu} \equiv \bar{g}' \bar{B}^{\mu\nu} T^3_R$ and $\bar{\mathbf{F}}^{\mu\nu}_D \equiv \sqrt{2}\, \bar{g}_D \bar{F}^{\mu\nu}_D T^{\rm DM}$. Both operators in Eq. (3.144) vanish identically. In fact, we have checked that the whole $\mathcal{L}_\pi + \mathcal{L}_4$ is invariant under the parity $P_6 = \mathrm{diag}\,(1,1,1,1,1,-1,1) \in O(7)$. Recalling that $T^{\rm DM}$ generates rotations in the $(5,6)$ plane $[\sqrt{2}\,T^{\rm DM} = \mathrm{diag}\,(\mathbf{0}_{4\times4}, \sigma^2, 0)]$, P_6 is identified with the charge conjugation C_D that we referred to in the main text. The action of P_6 on the $SO(7)$ generators is

$$P_6\, T P_6 = +T, \quad T = \left\{T^\alpha_{L,R}, T^{a5}, X^b\right\} \qquad \text{and} \qquad P_6\, \mathcal{T} P_6 = -\mathcal{T}, \quad \mathcal{T} = \left\{T^{\rm DM}, T^{a6}, X^6\right\} \tag{3.145}$$

where $a = 1, \ldots, 4$ and $b = 1, \ldots, 5$. As a consequence, the GBs and the elementary gauge fields transform as

$$\chi \to -\chi^*, \qquad \bar{A}_D \to -\bar{A}_D\,, \qquad \{h_i, \bar{W}, \bar{B}\} \to +\{h_i, \bar{W}, \bar{B}\} \qquad (i = 1, \ldots, 4), \tag{3.146}$$

which shows that if P_6 is exact, Y-DM kinetic mixing is forbidden. Furthermore, "higher-derivative kinetic mixing" operators (i.e. operators that mix $\bar{B}^{\mu\nu}$ and $\bar{F}^{\mu\nu}_D$, but with the insertion of additional derivatives) also have to be built out of the objects in Eq. (3.143), and are found to vanish. Summarizing our results thus far, the explicit breaking of $SO(7)$ due to the weak gauging does not generate Y-DM kinetic mixing.

As second step, we turn on the explicit $\mathcal{G}$ breaking in the fermion sector. Since $[T^{\rm DM}, P_6] \neq 0$, the SM fermions cannot be simultaneously assigned a nonzero $U(1)_{\rm DM}$ charge and definite P_6 parity. Therefore if the SM fermions were taken to have $Q_{\rm DM} \neq 0$, then fermion loops would generate Y-DM kinetic mixing: for example, this would happen if q_L were embedded in the $(\mathbf{2},\mathbf{2})_{+1} \subset \mathbf{21}_{2/3}$ of $SO(7) \times U(1)_X$ and t_R in the $(\mathbf{1},\mathbf{1})_{+1} \subset \mathbf{7}_{2/3}$. However, for our purposes we must take $Q_{\rm DM} = 0$ for all SM fields, in order for χ to be the lightest $U(1)_{\rm DM}$-charged particle and therefore stable. In this case each elementary fermion can be assigned definite parity (all the fermion embeddings employed in this thesis have in fact $P_6 = +1$), which guarantees that fermion loops do not generate Y-DM kinetic mixing.

Note that the last conclusion can be altered by subleading spurions, if a single elementary fermion couples to operators with different P_6. As a concrete example we can imagine that t_R has,

in addition to the embedding in the $(\mathbf{1},\mathbf{3})_0 \subset \mathbf{21}_{2/3}$ given in Eq. (3.118), a second embedding in the $(\mathbf{1},\mathbf{1})_0 \subset \mathbf{21}_{2/3}$, namely $\xi_R^{\prime(t)} = t_R T^{\rm DM}$. Then it is clear from Eq. (3.145) that the first spurion has $P_6 = +1$ while the second has $P_6 = -1$, so t_R cannot be assigned a definite parity. Nonetheless, P_6 invariance of the fermionic Lagrangian can still be *enforced*, by imposing that each elementary field couples to only even operators (or only odd ones, although we are not interested in that possibility here).

Notice that from Eq. (3.145) it follows that P_6 also acts on the resonances: taking as examples the S, Q and G fermionic multiplets, we have

$$\mathcal{Y} \leftrightarrow -\mathcal{Z}\,, \qquad \widetilde{S} \to -\widetilde{S}, \qquad \{\mathcal{T}^{(+)}, \mathcal{B}^{(+)}, \mathcal{X}^{(+)}_{2/3}, \mathcal{X}^{(+)}_{5/3}\} \leftrightarrow -\{\mathcal{T}^{(-)}, \mathcal{B}^{(-)}, \mathcal{X}^{(-)}_{2/3}, \mathcal{X}^{(-)}_{5/3}\}, \tag{3.147}$$

while all the other components are left invariant. One can similarly derive the transformation properties of the other fermionic resonances and of the vector multiplets, where in particular $\rho_D \to -\rho_D$.

3.F Collected results for phenomenology

The loop function for the $h \to \gamma_D\gamma_D$ decay is, for $m_{\gamma_D} = 0$,

$$F(\tau) = \frac{\tau}{3} A_0(\tau), \quad A_0(\tau) = \frac{3}{\tau^2}[f(\tau) - \tau]\,, \quad f(\tau) = \begin{cases} \arcsin^2\sqrt{\tau}\,, & \tau \le 1\,, \\ -\frac{1}{4}\left[\log\left(\frac{1+\sqrt{1-1/\tau}}{1-\sqrt{1-1/\tau}}\right) - i\pi\right]^2, & \tau > 1\,. \end{cases} \tag{3.148}$$

Note that $A_0(\tau) = 1 + O(\tau)$ for small τ.

Finally we report the thermally averaged cross sections relevant to the region $m_\chi \lesssim m_{\gamma_D} < 2m_\chi$. The one for $\chi\chi^* \to \gamma_D\gamma_D$ is

$$\langle \sigma_{\chi\chi^* \to \gamma_D\gamma_D} v_{\rm rel} \rangle = \frac{2\pi\alpha_D^2}{m_\chi^2} \sqrt{1-R}\, \frac{1 - R + 3R^2/8}{(1-R/2)^2}\,, \qquad R \equiv \frac{m_{\gamma_D}^2}{m_\chi^2}\,, \tag{3.149}$$

whereas

$$\langle \sigma_{\gamma_D\gamma_D \to \chi\chi^*} v_{\rm rel} \rangle = \frac{22\pi\alpha_D^2}{9m_{\gamma_D}^2} (1-\widetilde{R})^{1/2} \left(1 - \frac{24\widetilde{R}}{11} + \frac{16\widetilde{R}^2}{11}\right), \qquad \widetilde{R} \equiv \frac{m_\chi^2}{m_{\gamma_D}^2}\,. \tag{3.150}$$

For the semi-annihilation

$$\langle \sigma_{\gamma_D h \to \chi\chi^*} v_{\rm rel} \rangle = \frac{\alpha_D v^2 m_h (m_{\gamma_D} + m_h)^2}{6 f^4 m_{\gamma_D}^3} \left[1 - \frac{4m_\chi^2}{(m_{\gamma_D} + m_h)^2}\right]^{3/2}, \tag{3.151}$$

while for the inverse process we have

$$\langle \sigma_{\chi\chi^* \to \gamma_D h} v_{\rm rel} \rangle = \frac{\alpha_D v^2 m_h^4 T}{8 f^4 m_\chi^5}\, \beta_{h\gamma_D}\, \frac{1 - (\frac{3}{2}R_{\gamma_D} + 2R_h) + R_h(R_h + 3R_{\gamma_D}) + \frac{1}{2}R_{\gamma_D}(R_{\gamma_D} - R_h)^2}{(1 - R_h - R_{\gamma_D})^4}\,, \tag{3.152}$$

where $\beta_{h\gamma_D} \equiv [1 + (R_h - R_{\gamma_D})^2 - 2(R_h + R_{\gamma_D})]^{1/2}$ and $R_i \equiv m_i^2/(4m_\chi^2)$. Notice the additional factor T/m_χ coming from the p-wave suppression.

Lastly,

$$\langle \sigma_{\gamma_D \chi \to h \chi} v_{\rm rel} \rangle = \frac{\alpha_D v^2 m_h^4 \, G(m_{\gamma_D}, m_h; m_\chi)}{24 f^4 m_\chi m_{\gamma_D}^3} \,, \quad \langle \sigma_{h \chi \to \gamma_D \chi} v_{\rm rel} \rangle = \frac{\alpha_D v^2 m_h m_{\gamma_D}^2 G(m_h, m_{\gamma_D}; m_\chi)}{8 f^4 m_\chi (m_h + 2 m_\chi)^2} \,,$$
$$G(m_1, m_2; m_\chi) = \frac{\left[(m_1^2 - m_2^2)((m_1 + 2m_\chi)^2 - m_2^2)\right]^{3/2}}{(m_1 + m_\chi)^2 [m_\chi (m_1 + 2 m_\chi) - m_2^2]^2} \,. \tag{3.153}$$

Part III

The QCD axion at finite density

4

Motivation and framework

4.1 The strong CP problem

In order to present the *Strong CP Problem* which constitutes the motivation for the Axion, we start by reviewing the vacuum structure of non-abelian gauge theories [176, 177, 178, 179]. We show that due to the vacuum structure and tunneling effects driven by instantons, an additional term must be added to the Lagrangian

$$\mathcal{L} \supset \frac{\theta g^2}{32\pi^2}\epsilon^{\mu\nu\alpha\beta}\mathrm{Tr}F_{\mu\nu}\tilde{F}_{\alpha\beta}\,, \tag{4.1}$$

where θ is a constant and g is the gauge coupling. Next we discuss the effects of instantons on a theory with fermions and the axial anomaly [180, 181, 182]. We conclude by discussing the consequences of the θ term and formulate the Strong CP Problem.

4.1.1 Vacuum structure of non-abelian gauge theories

For simplicity, we focus on $SU(2)$, but the results are generalizable to other non-abelian gauge groups containing an $SU(2)$ subgroup. We note that a more intuitive picture of the vacuum structure emerges when working in the $A_0 = 0$ gauge, which we shall adopt in this section. Under a generic gauge transformation $U(\mathbf{x}) \in SU(2)$

$$A_i \to A_i' = UA_iU^{-1} + \frac{i}{g}U\partial_iU^{-1}\,. \tag{4.2}$$

Any particular gauge configuration in the $A_0 = 0$ is not uniquely defined - gauge equivalent configurations are found by performing time-independent transformations which conserve the gauge fixing condition. We consider gauge configurations that are gauge equivalent to the trivial vacuum $A_i = 0$ for $i =, 1, 2, 3$,

$$A_i = \frac{i}{g}U^{-1}\partial_iU\,. \tag{4.3}$$

Let us assume that $U(\mathbf{x})$ becomes a constant as $\mathbf{x} \to \infty$, which we can set without loss of generality to be the identity $\mathbb{1}$. The topology of $\mathbb{R}^N$ with spatial infinity identified as the same point is equivalent to an N-sphere. In our case $N = 3$, and Eq. (4.3) represents a mapping between a 3-sphere and $SU(2)$ group members. The manifold describing $SU(2)$ is a 3-sphere as well: this could be easily shown from the fact that a generic $SU(2)$ transformation can be written as

$$U(\{c\}) = c_0\mathbb{1} + ic_i\sigma_i\,, \tag{4.4}$$

with the constraint $c_0^2 + c_1^2 + c_2^2 + c_3^2 = 1$. All the mapping from $S^3 \to S^3$ can be collected into equivalency classes. Each equivalency class is comprised of mappings which are *continuously deformable* into each other. All the classes form a group, in this case

$$\pi_3(S^3) = \mathbb{Z}\,, \tag{4.5}$$

namely each class is defined by an integer, known as the winding number. The winding number is given by

$$N[U] = \frac{1}{24\pi^2}\epsilon^{ijk}\int \mathrm{d}^3x\,\mathrm{Tr}[(U^{-1}\partial_i U)\,(U^{-1}\partial_j U)\,(U^{-1}\partial_k U)]\,. \tag{4.6}$$

One can show that for any two configurations $U_1, U_2 \in SU(2)$,

$$N[U_1 \cdot U_2] = N[U_1] + N[U_2]\,, \tag{4.7}$$

as excepted from the group $\mathbb{Z}$. For example, a family of configurations with winding number n is given by

$$U^{(n)} = \exp\left[\frac{n\,x_i\sigma_i}{r}f(r)\right]\,, \tag{4.8}$$

with $f(r)$ any monotonic function with $f(0) = -\pi$ and $f(\infty) = 0$. It is useful to define the gauge variant current

$$j_A^\mu = \frac{g^2}{16\pi^2}\epsilon^{\mu\nu\alpha\beta}\mathrm{Tr}\left[A_\nu F_{\alpha\beta} + \frac{2ig}{3}A_\nu A_\alpha A_\beta\right]\,, \tag{4.9}$$

whose divergence is the gauge invariant expression

$$\partial_\mu J_A^\mu = \frac{g^2}{32\pi^2}\epsilon^{\mu\nu\alpha\beta}F_{\mu\nu}F^{\alpha\beta} \equiv \frac{g^2}{16\pi^2}F_{\mu\nu}\tilde{F}^{\mu\nu}\,. \tag{4.10}$$

The charge associated with this current (which is not conserved since $\partial_\mu J_A^\mu \neq 0$) is

$$Q_A = \int \mathrm{d}^3x\,j_A^0 = \frac{g^2}{16\pi^2}\epsilon^{ijk}\int \mathrm{d}^3x\,\mathrm{Tr}\left[A_i F_{jk} + \frac{2ig}{3}A_i A_j A_k\right]\,.. \tag{4.11}$$

In a vacuum gauge configuration where $F_{jk} = 0$, and A_i is of the form of Eq. (4.3), one immediately finds that $Q_A = N[U]$.

We have shown the existence of degenerate vacua, characterized by a winding number (or topological charge) which are not continuously deformable to each other. In other words, the gauge transformation relating configuration with different winding numbers are *large* in the sense they cannot be constructed from a set of infinitesimal transformation. Thus, we can treat these degenerate minima as being separated by energy barriers. At the classical level each vacuum is stable, but at the quantum level transitions between vacua are possible due to *instantons*: gauge configuration which describe the tunneling process from one degenerate minima to another. Let us consider such a configuration, describing a transition starting from some initial time t_i with winding number N_i, and ending at some final time t_f with winding number N_f. One can show that

$$\int \mathrm{d}^4x\,\partial_\mu J_A^\mu = \int \mathrm{d}^3x\int \mathrm{d}t\,\partial_0 J_A^0 + \int \mathrm{d}t\int \mathrm{d}^3x\,\partial_i J_A^i = N_f - N_i\,, \tag{4.12}$$

where the spatial gradient term vanishes at the boundary under the assumption that $A_i \to 0$ at spatial infinity, leaving only the contribution from the time derivative. The latter is evaluated as the charge at the temporal boundaries, fixed as N_i and N_f at initial and final time, respectively.

The presence of instantons requires a redefinition of the true vacuum state. For example, in the simple 1D double well potential in quantum mechanics, the true ground state of the system becomes the symmetric linear combination $|L\rangle + |R\rangle$, with $|L\rangle, |R\rangle$ the vacua state of each well in the absence of tunneling. A generalization of this occurs in case of infinite degenerate vacua, which can be thought of as a periodic potential. In this case, the vacuum is written as a Bloch wave, and one defines the θ vacuum as

$$|\theta\rangle = \sum_{n=-\infty}^{+\infty} e^{-in\theta} |n\rangle \ , \tag{4.13}$$

with $|n\rangle$ representing a vacuum state with winding number n, which are summed over with the phase factor $e^{in\theta}$. [1]. The defining feature of the θ-vacuum is that is it an eigenstate of the operator T acting as

$$T|n\rangle = |n+1\rangle \ , \tag{4.14}$$

which could be realized simply by performing the gauge transformation of Eq. (4.8) with $n = 1$. One than finds that $T|\theta\rangle = e^{i\theta}|\theta\rangle$. Importantly, θ vacua are eigenstates of the Hamiltonian, and therefore do not overlap at any time

$$\langle\theta'| e^{-iHt} |\theta\rangle = \sum_{n,m} e^{im\theta'} e^{-in\theta} \langle m| e^{-iHt} |n\rangle = \sum_{n,m} e^{im(\theta'-\theta)} e^{i\theta(m-n)} \langle m| e^{-iHt} |n\rangle \tag{4.15}$$

However since

$$\langle m| e^{-iHt} |n\rangle = \langle m| e^{-iHt} TT^\dagger |n\rangle = \langle m| Te^{-iHt} T^\dagger |n\rangle = \langle m-1| e^{-iHt} |n-1\rangle \ , \tag{4.16}$$

where we used the fact that $[H, T] = 0$ since the Hamiltonian is gauge invariant, we can replace $\langle m| e^{-iHt} |n\rangle = \langle m-n| e^{-iHt} |0\rangle$ and relabel the indices to find

$$\langle\theta'| e^{-iHt} |\theta\rangle = \sum_{m,l} e^{im(\theta'-\theta)} e^{i\theta l} \langle l| e^{-iHt} |0\rangle = 2\pi\delta(\theta-\theta') \sum_l e^{i\theta l} \langle l| e^{-iHt} |0\rangle \ . \tag{4.17}$$

The last term can be conveniently written using the path integral formalism as

$$\begin{aligned} \sum_l e^{i\theta l} \langle l| e^{-iHt} |0\rangle &= \sum_l e^{i\theta l} \int [\mathcal{D}A_\mu]_l \exp\left\{ i \int \mathrm{d}^4x \, \mathcal{L}[A_\mu] \right\} \\ &= \int \mathcal{D}A_\mu \exp\left\{ i \int \mathrm{d}^4x \, \mathcal{L}[A_\mu] + \frac{\theta g^2}{16\pi^2} \mathrm{Tr} F_{\mu\nu} \tilde{F}^{\mu\nu} \right\} , \end{aligned} \tag{4.18}$$

where the measure $[\mathcal{D}A_\mu]_l$ integrates over all the configurations which transition from $N_i = 0$ and $N_f = l$. Than we used Eqs. (4.10) and (4.12) the express the topologic charge l as the space time integral of the $F\tilde{F}$ term. Lastly, in the final expression we absorbed the sum of all final winding number in the measure $[\mathcal{D}A_\mu]$, which integrates over all possible winding number changing transitions. Lastly, let us point out that the θ vacuum is invariant under a discrete shift symmetry $\theta \to \theta + 2\pi$.

[1] Note that in the A_0 gauge, each topological sector contains additional internal gauge redundancies, relating different configuration within the same sector. These can be removed using an appropriate gauge condition, see Ref. [179].

4.1.2 Anomalies

One of the important physical effects of instantons emerge when theories beyond pure Yang-Mills are considered, namely when fermions are introduced. Let us consider a theory with N_f fermions in some representation of a non-abelian gauge group

$$\mathcal{L} \supset \frac{\theta_0 g^2}{16\pi^2}\mathrm{Tr}F_{\mu\nu}\tilde{F}^{\mu\nu} + \bar{q}^i i\partial\!\!\!/ q^i - (\bar{q}^i_L M^{ij} q^j_R + \text{h.c}) \tag{4.19}$$

$$= \frac{\theta_0 g^2}{16\pi^2}\mathrm{Tr}F_{\mu\nu}\tilde{F}^{\mu\nu} + \bar{q}^i i\partial\!\!\!/ q^i - (\bar{q}^i[\tilde{M}\cos Q_M]_{ij} q^j + i\bar{q}^i[\tilde{M}\sin Q_M]_{ij}\gamma_5 q^j)\,, \tag{4.20}$$

where the repeated indices are summed $i, j = 1, ..., N_f$. We parameterize $M \equiv \tilde{M}\exp[iQ_M]$, where $\tilde{M}$ and Q_M is a real diagonal N_f-by-N_f matrices in flavor space. The former matrix carries dimensions of mass while the latter is dimensionless and encodes the phase of each diagonal entry. Classically, in the $M \to 0$ limit the theory contains the global symmetry

$$SU(N_f)_L \times SU(N_f)_R \times U(1)_L \times U(1)_R\,. \tag{4.21}$$

Of particular interest is the axial combination $U(1)_A \equiv U(1)_{R-L}$, defined as the transformation

$$q \to e^{i\alpha\gamma_5 Q} q\,, \tag{4.22}$$

where Q is a real diagonal N_f-by-N_f matrix in flavor space and α a real number. Let us use an old trick and allow α to be space-time dependent and performs this transformation (we can always set it to constant at a later point). The Lagrangian shifts at $O(\alpha)$ by

$$\alpha^{-1}\Delta\mathcal{L} = \partial_\mu(\bar{q}\gamma^\mu\gamma^5 Q q) - 2i\bar{q}Q\tilde{M}\cos Q_M\gamma^5 q + 2\bar{q}Q\tilde{M}\sin Q_M q + \frac{g^2}{8\pi^2}\mathrm{Tr}[Q]\mathrm{Tr}F_{\mu\nu}\tilde{F}^{\mu\nu}\,. \tag{4.23}$$

The first term in the right-hand side of Eq. (4.23) is the divergence of the would be conserved current $j^\mu_5 = \bar{q}\gamma^\mu\gamma^5 Q q$ in the limit $M, g \to 0$. The second and third terms represent the explicit breaking of $U(1)_A$ in the theory due to the presence of a mass term. The fourth and final term is the anomaly term, which represent the breaking of the symmetry at the quantum level. Using Fujikawa's method [183], the appearance of the anomaly term could be also understood as the *Jacobian* associated with the chiral transformation of Eq. (4.22), which changes the measure in the path integral.

Since $\Delta\mathcal{L} \neq 0$, $U(1)_A$ is not a symmetry of the Lagrangian, and Eq. (4.22) can be regarded as a field redefinition or equivalently, a change of basis. In the new basis

$$\theta_0 \to \theta_0 + 2\alpha\,\mathrm{Tr}[Q]\,, \tag{4.24}$$

$$Q_M \to Q_M + 2\alpha Q\,. \tag{4.25}$$

It is therefore useful to identify the base-independent and thus physical angle

$$\theta \equiv \theta_0 - \mathrm{Arg}\det M\,, \tag{4.26}$$

where $\mathrm{Arg}\det M = \mathrm{Tr}[Q_M]$ shifts precisely like the θ_0 angle. Note that if we insist that α is space-time dependent, the new basis also contains the derivative term

$$\mathcal{L} \supset -(\partial_\mu\alpha) j^\mu_5\,. \tag{4.27}$$

In light of Eqs. (4.24) and (4.25), the chiral transformation can be used either to completely remove the $F\tilde{F}$ term from the Lagrangian, or to remove all the phases from the mass parameters thus making them real.

The anomalous nature of the $U(1)_A$ and its explicit breaking to due to the presence of instantons lead to the solution of the so called $U(1)$ *problem* [184], which is the absence in the low energy spectrum of a Goldstone boson associated with the $U(1)_A$, usually denoted as η'. See Sec. 4.3 for further discussion.

4.1.3 θ angle measurement

We now include the relevant term in the SM,

$$\mathcal{L}_{\rm SM} \supset \frac{\theta g^2}{16\pi^2} {\rm Tr} G_{\mu\nu}\tilde{G}^{\mu\nu}\,, \tag{4.28}$$

where we explicitly wrote it in terms of the gluon field strength $G_{\mu\nu}$ and use the basis where all the mass parameters in $\mathcal{L}_{\rm SM}$ are real[2]. As shown above, the $G\tilde{G}$ term can be written as a full derivative, see Eqs. (4.9) and (4.10). This implies that the term does not have any effect on the *classical* equation of motion, as well as no effect at the *quantum* level: in momentum space the relevant vertex is proportional to the sum of incoming momenta and vanishes identically due to momentum conservation. One could then naively conclude that the $\theta\, G\tilde{G}$ term leads to no observable effects.

However, the θ angle *does* have physically observable consequences. θ is a pure phase parameter: the $G\tilde{G}$ term is odd under CP (or T), and θ breaks CP invariance unless it is set to 0 or π. Importantly, CP is already violated in the SM by the weak interactions, and the so called CKM matrix contains an $O(1)$ CP violating phase $\delta = \tan^{-1}(\bar{\eta}/\bar{\rho}) \sim 0.38\pi$ [185]. Therefore, it is reasonable to assume that θ is $O(1)$ as well. One notable observable which probes θ is the neutron electric dipole moment, given by [186]

$$d_n \sim 5\times 10^{-16}\,\theta\,{\rm e\,cm}\,. \tag{4.29}$$

A recent bound on the magnitude of d_n [187]

$$|d_n| < 3\times 10^{-26}\,{\rm e\,cm}\ \ (90\%\ {\rm C.L})\,, \tag{4.30}$$

implies that

$$|\theta| < 10^{-10} \lll 1\,. \tag{4.31}$$

The fact that the experimental evidence suggest that $\theta \ll 1$ is known as the *strong CP problem*[3]. Interestingly, the θ angle also appears in a contribution to the so-called vacuum energy

$$\mathcal{L} \supset \Lambda^4_{\rm QCD}\cos\theta\,. \tag{4.32}$$

[2]In principle a *weak* θ term, $\frac{\theta_{\rm w} g^2}{16\pi^2}{\rm Tr} W_{\mu\nu}\tilde{W}^{\mu\nu}$, can be introduced as well. However due to the chiral nature of $SU(2)_L$, $\theta_{\rm w}$ is not physical and can be removed by a vector-like transformation of the fields: first, the term can be removed by a rotation of the left-handed fields only. As discussed above, this transformation would in general generate a shift in the mass terms (or equivalently in this case, the Yukawa couplings with the Higgs field). A similar rotation on the right-handed fields can remove the shift in the mass terms without reintroducing a weak θ term, since the right-handed fields do not carry $SU(2)_L$ quantum numbers.

[3]The strong CP problem can be immediately solved by making one of the quarks, e.g. the up quark, massless. In this case, θ can be absorbed in the phase of the vanishing mass parameter, thus removing it from the theory and making it unphysical. However, experiments and lattice simulations seem to suggest that there are no massless quarks in Nature.

The fact that the contribution appears as a periodic function can be understood as a consequence of the discrete shift symmetry $\theta \to \theta + 2\pi$, which leaves the θ vacuum invariant. Since θ is simply a constant, this sort of term is usually regarded in QFT as an inconsequential constant shift in the vacuum energy, which does not lead to any observable effects in perturbation theory[4]. However, Eq. (4.32) does motivate an interesting question: what if θ was *not* a constant but rather a dynamical field? In light of the potential of Eq. (4.32), the field would than dynamically relax the value of θ to 0! This observation is at the heart of the QCD axion solution to the strong CP problem, which we present in the next section.

4.2 The QCD Axion

We start this section by introducing the Peccei-Quinn (PQ) mechanism [7] behind the QCD axion solution to the strong CP problem. We continue by reviewing the earlier realization of the axion due to Weinberg and Wilczek [8, 9]. In this earlier version, where the axion couples to the SM via interactions that scale like $1/f$ with $f \sim v_{\rm EW}$, these strong interactions lead to observables effects that were excluded by multiple terrestrial experiments. We than present the realizations of the so-called *invisible axion* due to Dine, Fischler, Srednicki and Zhitnitsky (DFSZ) [10, 11] and Kim, Shifman, Vainshtein and Zakharov (KSVZ) [12, 13].

4.2.1 The Peccei-Quinn mechanism

In order to demonstrate the way the PQ mechanism works, let us consider the toy model of the original Ref. [7] with $N_f = 1$

$$\mathcal{L} \supset \frac{\theta g^2}{16\pi^2}\mathrm{Tr}F_{\mu\nu}\tilde{F}^{\mu\nu} - g(\varphi \bar{q}_L q_R + \text{h.c}) + \mu^2|\varphi|^2 - \lambda(|\varphi|^2)^2\,, \tag{4.33}$$

where we introduce a complex scalar field $\varphi(x)$. g is a Yukawa coupling which we take to be real without loss of generality. The scalar potential is the standard Mexican hat potential with real and positive parameters $\mu^2, \lambda > 0$. At the classical level, the Lagrangian is invariant under a chiral $U(1)_{\rm PQ}$ symmetry known as the PQ symmetry

$$q \to e^{i\alpha\gamma^5} q\,, \tag{4.34}$$

$$\varphi \to e^{-2i\alpha}\varphi\,. \tag{4.35}$$

We introduce a non-linear parameterization of $\varphi \equiv \frac{1}{\sqrt{2}}\rho(x)e^{-ia(x)/f_a}$. Under $U(1)_{\rm PQ}$,

$$\rho \to \rho\,, \tag{4.36}$$

$$a \to a + 2\alpha\, f_a\,. \tag{4.37}$$

$a(x)$ is known as the axion field. As we show below, $U(1)_{\rm PQ}$ is spontaneously broken making the axion its Goldstone boson. Let us perform a change of basis by using the chiral rotation $q \to e^{i(a(x)/2f_a)\gamma^5}q$. Using Eqs. (4.24) and (4.25), we find in this basis, the Lagrangian is given by

$$\mathcal{L} \supset \left(\theta + \frac{a}{f_a}\right)\frac{g^2}{16\pi^2}\mathrm{Tr}F_{\mu\nu}\tilde{F}^{\mu\nu} - \frac{g}{\sqrt{2}}\rho\bar{q}q - \frac{\partial_\mu a}{2f}\bar{q}\gamma^\mu\gamma^5 q + \frac{1}{2}\mu^2\rho^2 - \frac{1}{4}\lambda\rho^4\,. \tag{4.38}$$

[4]Note that in the context of general relativity and cosmology, the so-called cosmological constant Λ, which effectively contains quantum contributions from SM fields similar to Eq. (4.32), plays an important role. Its small measured value leads to a fine-tuning problem, even when considering smaller contributions e.g. from $\Lambda_{\rm QCD} \lll M_{\rm PL}$. One can than ask whether it is possible that θ is actually anthropically selected, see e.g. Refs. [188, 189].

At this point we would like to determine the vacuum structure of the scalar sector. The scalar potential is given by (neglecting quantum corrections to the ρ potential due to fermion loops)

$$V(\rho, a) = -\frac{1}{2}\mu^2\rho^2 + \frac{1}{4}\lambda\rho^4 - \Lambda^4 \cos\left(\theta + \frac{a}{f_a}\right) , \tag{4.39}$$

where the last term, which parametrizes the non-perturbative effects[5], explicitly breaks $U(1)_{\rm PQ}$ and the shift symmetry of the axion, making it a pNGB. Note that one implicitly assumes that $\Lambda \ll f_a$ such that the explicit breaking effects can be regarded as a small perturbation (as oppose to the case of η' in QCD). $U(1)_{\rm PQ}$ is spontaneously broken by the VEV of the radial mode

$$\langle\rho\rangle = \frac{\mu}{\sqrt{\lambda}} \equiv f_a \, . \tag{4.40}$$

where f_a is usually referred to as the PQ scale. In the absence of the last term, or more accurately for energies $E \gg \Lambda$, the axion field enjoys the shift symmetry of Eq. (4.37), which can be used to remove the θ term from the Lagrangian. For $E \lesssim \Lambda$, the explicit breaking of $U(1)_{\rm PQ}$ cannot be neglected. The axion than acquires a VEV

$$\langle a\rangle = -\theta f_a \, . \tag{4.41}$$

Expanding the field around its classical value at low energies has the same effect as utilizing the shift symmetry at high energies, namely the disappearance of the θ from the Lagrangian, thus making it unphysical. Note that in this toy model, the fermion and radial mode each acquire a mass which scales like f_a,

$$m_q = \frac{g\, f_a}{\sqrt{2}} \, , \quad m_\rho = \sqrt{2\lambda} f_a \, , \tag{4.42}$$

respectively. The axion mass, on the other hand, depends also on the scale which captures the non-perturbative effects,

$$m_a = \frac{\Lambda^2}{f_a} \ll \Lambda \, , \tag{4.43}$$

where the last inequality is a consequence of the assumption $\Lambda \ll f_a$.

To summarize, the PQ mechanism involves the introduction of an axial symmetry, $U(1)_{\rm PQ}$, spontaneously broken at some scale f_a. Its Goldstone boson, the axion, acts effectively as a dynamical phase for the masses of the $U(1)_{\rm PQ}$ charged fermion fields (or equivalently, a dynamical θ angle). In the notation of the last section, before performing the chiral rotation we have $\mathrm{Arg}\det M = -a(x)/f_a$. The base independent and thus physical combination is given by $\theta + \frac{a}{f_a}$, and the θ angle can always be removed from the Lagrangian by performing an axion field redefinition[6].

[5] Note that in QCD, this term cannot be reliably calculated in perturbation theory since it is dominated by large instantons contributions in the strongly coupled regime. Semi-classical approximations suggest that $\Lambda \sim \Lambda_{\rm QCD} \sim 0.2$ GeV.

[6] In order for the PQ mechanism to work, any other shift symmetry breaking effects must be suppressed *enough* such that the strong experimental bound $\theta < 10^{-10}$ is respected. This leads to the so-called *axion quality problem* [190, 191, 192, 193], which involves additional sources of shift symmetry breaking, e.g. gravity, that may spoil the effectiveness of the PQ mechanism.

4.2.2 Weinberg-Wilczek axion

An early realization of the axion due to Weinberg and Wilczek (WW) [8, 9] unified the PQ symmetry with electroweak symmetry breaking, such that the PQ scale is of the same order as $v_{\rm EW}$. Consider a toy model for the SM with a single generation of quark and the symmetry is

$$SU(2)_c \times SU(2)_L \times U(1)_Y \times U(1)_{\rm PQ}\,. \tag{4.44}$$

We introduce quarks with the following representations

$$q_L : (\mathbf{3},\mathbf{2})_{\frac{1}{6},0}\,,\quad u_R : (\mathbf{3},\mathbf{1})_{\frac{2}{3},\alpha}\quad d_R : (\mathbf{3},\mathbf{1})_{-\frac{1}{3},\beta} \tag{4.45}$$

and two Higgs doublets

$$H_u : (\mathbf{1},\mathbf{2})_{\frac{1}{2},\alpha}\,,\quad H_d : (\mathbf{1},\mathbf{2})_{\frac{1}{2},-\beta}\,. \tag{4.46}$$

The invariant Lagrangian is

$$\begin{aligned}\mathcal{L}_{\rm WW} =& \frac{\theta g^2}{16\pi^2}{\rm Tr}F_{\mu\nu}\tilde{F}^{\mu\nu} + (D_\mu H_u)^\dagger D^\mu H_u + (D_\mu H_d)^\dagger D^\mu H_d \\ & - g_u(\bar{q}_L \tilde{H}_u u_R + {\rm h.c}) - g_d(\bar{q}_L H_d d_R + {\rm h.c}) - V(H_u, H_d)\,.\end{aligned} \tag{4.47}$$

where g_u, g_d are taken to be real without loss of generality. We assume that due to the potential $V(H_u, H_d)$, the scalar fields acquire (real) VEVs

$$\langle H_u\rangle \equiv \frac{1}{\sqrt{2}}(0, v\cos\lambda)^T\,,\quad \langle H_d\rangle \equiv \frac{1}{\sqrt{2}}(0, v\sin\lambda)^T\,, \tag{4.48}$$

where $v \approx 247$ GeV is the electroweak VEV. The symmetry is spontaneously broken $SU(2)_L \times U(1)_Y \times U(1)_{\rm PQ} \to U(1)_{\rm EM}$. According to Goldstone's theorem, we expect to find $5-1=4$ NGBs. However, since three of the broken generators are gauged, in the unitary gauge only a single NGB remains, namely the axion. One can check that given the non-linear parameterization of the neutral GBs

$$H_u = \exp\left[\frac{i\,(a\sin\lambda - \varphi_Y\cos\lambda)}{v\cos\lambda}\right]\langle H_u\rangle\,,\quad H_d = \exp\left[-\frac{i\,(a\cos\lambda + \varphi_Y\sin\lambda)}{v\sin\lambda}\right]\langle H_d\rangle\,, \tag{4.49}$$

the GB denoted by φ_Y is eventually eaten by the Z boson and is removed from the spectrum in the unitary gauge. The only remaining GB is the axion, leading to the following interactions

$$\mathcal{L} \supset \frac{\theta g^2}{16\pi^2}{\rm Tr}G_{\mu\nu}\tilde{G}^{\mu\nu} - m_u(e^{-\frac{i\,a\tan\lambda}{v}}\bar{u}_L u_R + {\rm h.c}) - m_d(e^{-\frac{i\,a\cot\lambda}{v}}\bar{d}_L d_R + {\rm h.c})\,, \tag{4.50}$$

where we defined $m_u \equiv \frac{g_u v\cos\lambda}{\sqrt{2}}$ and $m_d \equiv \frac{g_d v\sin\lambda}{\sqrt{2}}$. We change basis by performing a field redefinition

$$q = (u,d)^T \to \exp\left[\frac{ia}{2v}\begin{pmatrix}\tan\lambda & 0\\ 0 & \cot\lambda\end{pmatrix}\gamma^5\right]q\,. \tag{4.51}$$

In this basis the quark masses are real, the θ angle is shifted, and the quarks interact derivatively with the axion. Since we are considering fields that are charged under another gauged symmetry,

namely electromagnetism, the chiral rotation also generates a $F\tilde{F}$ term which couples the axion to photons, and the Lagrangian is given by

$$\mathcal{L} \supset \left(\theta + \frac{a}{f_a}\right) \frac{g^2}{16\pi^2} \mathrm{Tr} G_{\mu\nu}\tilde{G}^{\mu\nu} + \frac{a}{f_a}\frac{E}{N}\frac{e^2}{16\pi^2} F_{\mu\nu}\tilde{F}^{\mu\nu} \\ - m_u \bar{u}u - m_d \bar{d}d - \frac{\partial_\mu a}{2f_a}(\sin^2\lambda \bar{u}\gamma^\mu\gamma^5 u + \cos^2\lambda \bar{d}\gamma^\mu\gamma^5 d)\,, \tag{4.52}$$

The color and electric anomaly coefficients N and E are given by[7]

$$N = \mathrm{Tr}[Q]\,, \quad E = 3\mathrm{Tr}[QQ_e^2]\,, \tag{4.53}$$

respectively. $Q = \mathrm{Diag}[\tan\lambda, \cot\lambda]$ is the flavor space matrix associate with the chiral rotation and $Q_e = \mathrm{Diag}[2/3, 1/3]$ the electric charges of the up and down quark. We identify the effective PQ scale as $f_a \equiv \frac{v}{N} = \frac{1}{2}v\sin 2\lambda \leq \frac{v}{2}$. We note that Eq. (4.52) is a generic starting point for any axion realization: the basis in which all the quark masses are real and the axion couples to $G\tilde{G}$. The model dependence is introduced through the effective PQ charges, namely in the $F\tilde{F}$ term and in the derivative interactions of the axion. This model is easily generalizable to 2 or 3 generations of quarks. For simplicity, we disregarded the lepton Yukawa which would couple the left-handed doublet ℓ_L and the right-handed singlet e_R through either H_u or H_d in a similar fashion. Importantly, the axion in this realization coupled directly to the SM quarks and leptons. The WW axion is relatively heavy

$$(m_a)_{WW} \sim \frac{\Lambda_{\mathrm{QCD}}^2}{v} \sim 100\ \mathrm{keV}\,, \tag{4.54}$$

and short lived

$$\Gamma(a \to \gamma\gamma) = \frac{\alpha^2}{9\pi^3 v^2}\frac{N^2 m_a^3}{\sin^2 2\lambda} \sim (2\times 10^{-2}\ \mathrm{s})^{-1}\,, \tag{4.55}$$

where for the numerical approximation we take $N = 3$, $\lambda = \pi/4$ and $m_a = 100$ keV. Due to strong interaction between the axion and the SM, this earlier version of the axion was excluded by several experimental results. For example, one bound comes from the decay of $K^+ \to \pi^+ a$ [195, 196]

$$\mathrm{Br}(K^+ \to \pi^+ a) \approx 10^{-6}\tan^2\lambda < 3.8\times 10^{-8} (90\%\ \mathrm{C.L})\,. \tag{4.56}$$

which implies $\tan\lambda < 0.1$. This is however in contradiction to bounds from Quarkonium decay [197]

$$\mathrm{Br}(\Upsilon \to \gamma a) = \mathrm{Br}(\Upsilon \to \mu^+\mu^-) \times \frac{m_b^2}{2\pi\alpha_{\mathrm{EW}} v^2}\cot^2\lambda \approx 1.4\times 10^{-4}\cot^2\lambda < 3\times 10^{-4}\,, \tag{4.57}$$

which implies $\tan\lambda > 0.7$. Additional experimental constrain lead to the exclusion of the WW axion and lead to the development of the invisible axion, the topic of our next section.

4.2.3 The invisible axion

The main lesson from the first axion models is that a large separation $f_a \gg v$ is required in order to evade the experimental bounds. Indeed, a-priori the PQ scale need not be related to electroweak scale but rather to physics at a much higher scale e.g. the GUT scale. This hierarchy suggests that the axion very light and feebly coupled to the SM. This scenario is dubbed *the invisible axion*. Let us shortly present two of the popular axion realizations and discuss their generic properties.

[7] The expressions in Eq. (4.53) are not the most general, and in particular we assume that all the colored fermions are in the fundamental representations of $SU(3)$. For a more general derivation, see Ref. [194].

DFSZ

In the DFSZ axion construction [10, 11] we introduce an $SU(2)_L \times U(1)$ singlet scalar ϕ in additional to the two Higgs doublets

$$H_u : (\mathbf{1},\mathbf{2})_{\frac{1}{2},X_u}\,, \quad H_d : (\mathbf{1},\mathbf{2})_{\frac{1}{2},X_d}\,, \quad \phi : (\mathbf{1},\mathbf{1})_{0,X_\phi}\,. \tag{4.58}$$

Initially the PQ charges as fixed such that $-X_u + X_d = -2X_\phi = 1$. The invariant Lagrangian is now The invariant Lagrangian is

$$\begin{aligned}\mathcal{L}_{\text{DFSZ}} =& \frac{\theta g^2}{16\pi^2}\text{Tr}F_{\mu\nu}\tilde{F}^{\mu\nu} + (D_\mu H_u)^\dagger D^\mu H_u + (D_\mu H_d)^\dagger D^\mu H_d + |\partial_\mu\phi|^2 \\ & - g_u(\bar{q}_L\tilde{H}_u u_R + \text{h.c}) - g_d(\bar{q}_L H_d d_R + \text{h.c}) - V(H_u, H_d, \phi)\,,\end{aligned} \tag{4.59}$$

where the scalar potential is given by the usual Mexican hat potentials, as well as possible mixing terms

$$\begin{aligned}V(H_u, H_d, \phi) \supset & c_1|H_u|^2|H_d|^2 + c_2|H_u|^2|\phi|^2 + c_3|H_d|^2|\phi|^2 + c_4[(H_u^\dagger H_d)\phi^2 + \text{h.c}] \\ & + c_5|H_u^\dagger H_d|^2 + c_6|H_u^\dagger \tilde{H}_d|^2\,.\end{aligned} \tag{4.60}$$

The details of the scalar potential are not important as long as it allows the fields to acquire the following VEVs

$$\langle H_u\rangle \equiv \frac{1}{\sqrt{2}}(0, v\cos\lambda)^T\,, \quad \langle H_d\rangle \equiv \frac{1}{\sqrt{2}}(0, v\sin\lambda)^T\,, \quad \langle\phi\rangle = \frac{1}{\sqrt{2}}f_\phi\,, \tag{4.61}$$

with the added assumption that $v_\phi \gg v$. We parameterize the NBGs as

$$H_u = \exp\left[\frac{i\varphi_u}{v\cos\lambda}\right]\langle H_u\rangle\,, \quad H_d = \exp\left[\frac{i\varphi_d}{v\sin\lambda}\right]\langle H_u\rangle\,, \quad \phi = \exp\left[\frac{i\varphi_\phi}{f_\phi}\right]\langle\phi\rangle\,. \tag{4.62}$$

Note that φ_u, φ_d and φ_ϕ are not independent, but rather linear combination of the two neutral GBs : φ_B which is eaten by the Z boson and the physical axion a. To identify the two physical combinations, we construct the relevant Noether currents in the usual way

$$J_\mu^Y = \frac{1}{2}H_u^\dagger\overset{\leftrightarrow}{\partial_\mu}H_u + \frac{1}{2}H_d^\dagger\overset{\leftrightarrow}{\partial_\mu}H_d = \frac{iv}{2}\partial_\mu(\cos\lambda\varphi_u + \sin\lambda\varphi_d)\,, \tag{4.63}$$

$$J_\mu^{PQ} = X_u H_u^\dagger\overset{\leftrightarrow}{\partial_\mu}H_u + X_d H_d^\dagger\overset{\leftrightarrow}{\partial_\mu}H_d + X_\phi\phi^\dagger\overset{\leftrightarrow}{\partial_\mu}\phi = iv\partial_\mu\left(X_u\cos\lambda\varphi_u + X_d\sin\lambda\varphi_d + \frac{f_\phi}{v}\varphi_\phi\right) \tag{4.64}$$

As before we identify the combination associated with Hypercharge and the orthogonal combination

$$\begin{pmatrix}\varphi_Y \\ \varphi\end{pmatrix} = \begin{pmatrix}\cos\lambda & \sin\lambda \\ -\sin\lambda & \cos\lambda\end{pmatrix}\begin{pmatrix}\varphi_u \\ \varphi_d\end{pmatrix}\,. \tag{4.65}$$

In this basis the currents are given by

$$J_\mu^Y = \frac{iv}{2}\partial_\mu\varphi_Y \tag{4.66}$$

$$J_\mu^{PQ} = iv\partial_\mu\left([X_u\cos^2\lambda + X_d\sin^2\lambda]\varphi_Y + \sin\lambda\cos\lambda\,\varphi + \frac{f_\phi}{v}\varphi_\phi\right) \tag{4.67}$$

It is convenient to remove φ_Y from J_μ^{PQ} by choosing

$$X_d = \cos^2\lambda\,, \quad X_u = -\sin^2\lambda\,. \tag{4.68}$$

Now we can identify the physical axion as the combination

$$a = \sin\alpha\varphi + \cos\alpha\varphi_\phi\,, \tag{4.69}$$

where

$$\tan\alpha \equiv \frac{v\sin\lambda\cos\lambda}{f_\phi}\,. \tag{4.70}$$

To conclude, the physical basis is given by

$$\begin{pmatrix}\varphi_u\\ \varphi_d\\ \varphi_\phi\end{pmatrix} = \begin{pmatrix}c_\lambda & -s_\lambda s_\alpha\\ s_\lambda & +c_\lambda s_\alpha\\ 0 & c_\alpha\end{pmatrix}\begin{pmatrix}\varphi_Y\\ a\end{pmatrix}\,. \tag{4.71}$$

φ_Y is removed in the unitary gauge and we find the following couplings to quarks

$$\begin{aligned}\mathcal{L}_{\text{DFSZ}} \supset & \frac{\theta g^2}{16\pi^2}\text{Tr}F_{\mu\nu}\tilde{F}^{\mu\nu} - m_u\left(\exp\left[\frac{ias_\lambda s_\alpha}{vc_\lambda}\right]\bar{u}_L u_R + \text{h.c}\right)\\ & - m_d\left(\exp\left[\frac{iac_\lambda s_\alpha}{vs_\lambda}\right]\bar{d}_L d_R + \text{h.c}\right)\,,\end{aligned} \tag{4.72}$$

where m_u, m_d are defined as before, see below Eq. (4.50). We change basis by performing a field redefinition

$$q = (u,d)^T \to \exp\left[-\frac{ia}{2v}\begin{pmatrix}\tan\lambda\sin\alpha & 0\\ 0 & \cot\lambda\sin\alpha\end{pmatrix}\gamma^5\right]q\,. \tag{4.73}$$

In this basis the quark masses are real, the θ angle is shifted, and the quarks interact derivatively with the axion

$$\begin{aligned}\mathcal{L} \supset & \left(\theta - \frac{a}{f_a}\right)\frac{g^2}{16\pi^2}\text{Tr}G_{\mu\nu}\tilde{G}^{\mu\nu} - \frac{a}{f_a}\frac{E}{N}\frac{e^2}{16\pi^2}F_{\mu\nu}\tilde{F}^{\mu\nu}\\ & - m_u\bar{u}u - m_d\bar{d}d + \frac{\partial_\mu a}{2f_a}(\sin^2\lambda\bar{u}\gamma^\mu\gamma^5 u + \cos^2\lambda\bar{d}\gamma^\mu\gamma^5 d)\,,\end{aligned} \tag{4.74}$$

where identify $f_a = \frac{v\sin 2\lambda}{2\sin\alpha} = \sqrt{f_\phi^2 + \left(\frac{v\sin 2\lambda}{2}\right)^2} \gg v$. This model essentially reproduces the WW axion Lagrangian of Eq. (4.52) but *without* the added requirement that $f_a \sim v$: it allows for $f_a \gg v$ such that the axion is much lighter, as well as very weakly coupled to the SM. This allows the axion to be *invisible*. As we commented in the previous section, the model dependence is introduced through the effective PQ charges, in particular in the axion-photon coupling and in the last term of the Lagrangian. This model is easily generalizable to 2 or 3 generations of quarks as well. For simplicity, we again disregarded the lepton Yukawa which would couple the left-handed doublet ℓ_L and the right-handed singlet e_R through either H_u or H_d in a similar fashion. Importantly, this sort of setup predicts that the axion interacts with the SM quarks and leptons directly, with an interaction strength which is model-dependent.

KSVZ

Lastly, let us present another simple realization of the invisible axion. The KSVZ axion [12, 13] is completely decoupled from the mechanism of electroweak symmetry breaking, and the minimal model requires a single Dirac fermion Q and a complex scalar ϕ which are electroweak singlets. The SM fermions receive their mass via the usual Higgs mechanism, while the mass of Q is initially forbidden due to $U(1)_{\rm PQ}$ symmetry. The Lagrangian is essentially the same as in the toy model considered in Sec. 4.2.1

$$\mathcal{L}_{\rm KSVZ} \supset \frac{\theta g^2}{16\pi^2}{\rm Tr}F_{\mu\nu}\tilde{F}^{\mu\nu} - g(\phi\bar{Q}_L Q_R + {\rm h.c}) + \mu^2|\phi|^2 - \lambda(|\phi|^2)^2\,, \tag{4.75}$$

After $\phi \equiv \frac{\rho(x)}{\sqrt{2}}e^{ia(x)/f_a}$ acquires a VEV, $\langle\rho\rangle = \frac{\mu}{\sqrt{\lambda}} \equiv f_a$, the remaining GB a is identified as the axion. A chiral rotation can be performed to remove the axion dependence from the quark mass, and the resulting Lagrangian is

$$\mathcal{L} \supset \left(\theta + \frac{a}{f_a}\right)\frac{g^2}{16\pi^2}{\rm Tr}F_{\mu\nu}\tilde{F}^{\mu\nu} - \frac{g}{\sqrt{2}}(f_a+\tilde{\rho})\bar{Q}Q - \frac{\partial_\mu a}{2f}\bar{Q}\gamma^\mu\gamma^5 Q - \frac{1}{4}((f_a+\tilde{\rho})^2 - f_a^2)^2\,, \tag{4.76}$$

where we defined $\rho = f_a + \tilde{\rho}$. The masses of the radial mode $\tilde{\rho}$ and the quark Q scale with $f_a \gg v$

$$m_Q = \frac{g\,f_a}{\sqrt{2}}\,, \quad m_{\tilde{\rho}} = \sqrt{2\lambda}f_a\,. \tag{4.77}$$

Therefore, they can be made heavy such that they effectively decoupled from the low energy theory. In this minimal setup the axion does not couple directly to the SM. As we discuss in Sec. 5.3, the only irreducible interactions between the axion and the SM in this case is due to its mixing with the pions, a mixing which is determined by the parameters of the low energy theory. Lastly we remark that Q can in principle also carry any electrical charge, which would generate a coupling between the axion and photons.

As discussed above, the invisible axion is much lighter [198]

$$m_a = 5.70 \pm 0.07\ {\rm eV}\left(\frac{10^6\ {\rm GeV}}{f_a}\right)\,, \tag{4.78}$$

and long lived

$$\Gamma_{a\to\gamma\gamma} = \frac{g_{a\gamma}^2 m_a^3}{64\pi} = (9.1\times 10^{23}s)^{-1}\left(\frac{m_a}{\rm eV}\right)^5\,, \tag{4.79}$$

where $g_{a\gamma} = \frac{\alpha}{2\pi f_a}\left(\frac{E}{N} - \frac{2}{3}\frac{4+m_u/m_d}{1+m_u/m_d}\right)$ is the coefficient of the operator $\frac{1}{4}aF\tilde{F}$. The numerical result is given for $E/N = 0$. The existence of such a light and long-lived particle leads to various observable effects in cosmology and astrophysics (see e.g. [199, 200]), which presently bound $f_a \gtrsim (10^8 - 10^9)$ GeV. A cosmologically stable axion is a viable dark matter candidate with an extremely rich dark matter phenomenology and non-standard production mechanisms (see Ref. [201] and references therein).

After introducing the actual axion realizations, we proceed to discuss the axion potential at low energies in the next section from a model-independent starting point.

4.3 Axion potential in vacuum

The most general QCD and axion effective Lagrangian below the electroweak scale, at leading order order in fields and derivatives, is given by

$$\mathcal{L} = \mathcal{L}_{\rm QCD} + \mathcal{L}_a \,, \tag{4.80a}$$

$$\mathcal{L}_{\rm QCD} = -\frac{1}{4} G^{\mu\nu} G_{\mu\nu} + i\bar{q}\not{D} q - (\bar{q}_L M q_R + \text{h.c}) \,, \tag{4.80b}$$

$$\mathcal{L}_a = \frac{1}{2}(\partial^\mu a)^2 + \left(\frac{a}{f_a} + \theta\right) \frac{g_s^2}{32\pi^2} G^{\mu\nu}\tilde{G}_{\mu\nu} + \frac{1}{4} a\, g^0_{a\gamma\gamma} F^{\mu\nu}\tilde{F}_{\mu\nu} + \frac{\partial_\mu a}{2f_a} J^\mu_{\rm PQ,0} \,, \tag{4.80c}$$

with implicit flavor and color indices. $J^\mu_{\rm PQ} = \sum_q c^0_q \bar{q}\gamma^\mu\gamma_5 q$ is a model-dependent current associated with a spontaneously broken axial $U(1)_{\rm PQ}$ symmetry, made of the SM matter fields q. The Nambu-Goldstone boson (NGB) of the $U(1)_{\rm PQ}$ is the axion field $a(x)$, with decay constant f_a defined by its coupling to gluons. The axion coupling to photons is given by $g^0_{a\gamma\gamma} = \frac{e^2}{8\pi^2 f_a}\frac{E}{N}$, with E/N the ratio of the electromagnetic (EM) and the color anomalies.

In the free and chiral limit the theory is invariant under the symmetry group

$$SU(3)_c \times SU(N_f)_L \times SU(N_f)_R \times U(1)_B \times U(1)_A \,, \tag{4.81}$$

with the quark representations, for $N_f = 3$ (the number of flavors we consider in this work)

$$q_L : (\mathbf{3}, \mathbf{3}, \mathbf{1})_{+1,+1} \,, \quad q_R : (\mathbf{3}, \mathbf{1}, \mathbf{3})_{+1,-1} \,. \tag{4.82}$$

At low energies, QCD confines and a chiral condensate $\langle \bar{q}_R q_L \rangle$ develops that breaks spontaneously the global symmetries

$$SU(N_f)_L \times SU(N_f)_R \times U(1)_B \times U(1)_A \to SU(N_f)_{R+L} \times U(1)_B \,. \tag{4.83}$$

The low energy degrees of freedom are described by the fluctuations of the condensate, i.e. the NGBs of the broken chiral symmetries [8]

$$\Phi \equiv \exp\left[\frac{i\pi^a \lambda^a}{f_\pi}\right] \exp\left[\frac{i\eta'}{f_{\eta'} N_f}\right] \equiv \Sigma \exp\left[\frac{i\eta'}{f_{\eta'} N_f}\right] \,, \tag{4.84}$$

where λ^a for $a = 1, .., N_f^2 - 1$ are the $SU(N_f)$ generators with the normalization convention $\text{Tr}[\lambda^a \lambda^b] = 2\delta^{ab}$. Under the symmetries in (4.81), Φ transforms as

$$\Phi : (\mathbf{1}, \mathbf{3}, \bar{\mathbf{3}})_{0,+2} \,. \tag{4.85}$$

The explicit breaking of the chiral symmetries by the quark masses can be incorporated in the low-energy theory by promoting the quark mass matrix, $M = \text{Diag}[m_u, m_d, m_s]$, to a spurion with the transformation properties

$$M : (\mathbf{1}, \mathbf{3}, \bar{\mathbf{3}})_{0,+2} \,. \tag{4.86}$$

Under a $U(1)$ axial rotation, the θ angle shifts as $\theta \to \theta + 2N_f\alpha_A$. The $U(1)_A$ is therefore anomalous, explicitly broken by non-perturbative effects associated with incalculable large instantons. Since the shift symmetry of the axion, associated with $U(1)_{\rm PQ}$, can be used to remove

[8] We chose to include the η', even though it is not well described as a NGB (unless in the large N_c limit), to make explicit the similarities with the effective Lagrangian in the CFL phase, see Sec. 6.

the θ angle from the Lagrangian Eq. (4.80), $a \to a - \theta f_a$, the axion can be treated as an actual dynamical spurion for the $U(1)_A$.

The non-perturbative nature of the axial anomaly means that the effective Lagrangian for the η', which shifts under $U(1)_A$ as $\eta' \to \eta' + 2N_f \alpha_A f_{\eta'}$, is not calculable. [9] That would be the case for the axion as well, if not for the fact that one can move to a different basis by performing a local chiral transformation of the quarks in Eq. (4.80),

$$q \to e^{\frac{ia(x)}{2f_a}\gamma_5 Q_a} q\,, \tag{4.87}$$

with Q_a an arbitrary matrix in flavor space which, if $\mathrm{Tr}[Q_a] = 1$, eliminates the axion coupling to gluons. In this basis, the Lagrangian above the QCD confinement scale reads

$$\mathcal{L}_{\rm QCD} = -\frac{1}{4}G^{\mu\nu}G_{\mu\nu} + i\bar{q}\not{D}q - (\bar{q}_L M_a q_R + \text{h.c})\,, \quad M_a \equiv e^{\frac{ia(x)Q_a}{2f_a}} M e^{\frac{ia(x)Q_a}{2f_a}}\,, \tag{4.88a}$$

$$\mathcal{L}_a = \frac{1}{2}(\partial^\mu a)^2 + \frac{1}{4} a\, g_{a\gamma\gamma} F^{\mu\nu}\tilde{F}_{\mu\nu} + \frac{\partial_\mu a}{2f_a} J^\mu_{\rm PQ} \tag{4.88b}$$

$$J^\mu_{\rm PQ} = \sum_q c_q\, \bar{q}\gamma^\mu\gamma_5 q\,, \quad c_q \equiv c_q^0 - [Q_a]_q\,, \quad g_{a\gamma\gamma} = \frac{e^2}{8\pi^2 f_a}\left(\frac{E}{N} - 6\mathrm{Tr}[Q_a Q_e^2]\right) \tag{4.88c}$$

with $Q_e = \mathrm{Diag}[2/3, -1/3, -1/3]$ the flavor-space matrix of electric charges. After such a redefinition of the quark fields, and upon integrating out the heavy η', the axion potential can be related to that of the QCD pions

$$V_0 = b(\mathrm{Tr}[\Sigma^\dagger M_a] + \text{h.c})\,, \tag{4.89}$$

with

$$b = -\frac{m_\pi^2 f_\pi^2}{2(m_u + m_d)}\,, \tag{4.90}$$

where m_π is the neutral pion mass and we neglected $O(\Delta m/m_s)$ terms, $\Delta m \equiv \frac{1}{2}(m_u - m_d)$.

In this $N_f = 2$ approximation, the quark condensates evaluated in the vacuum are $2b = \langle\bar{q}q\rangle_0 \equiv \frac{1}{2}\left\langle \bar{u}u + \bar{d}d\right\rangle_0$, which leads to the Gell-Mann-Oakes-Renner (GOR) relation

$$\langle\bar{q}q\rangle_0(m_u + m_d) = -m_\pi^2 f_\pi^2\,. \tag{4.91}$$

The axion mass can be calculated at leading order by integrating out the chiral NGBs at tree-level, see App. 6.A. The final result for the axion mass reads

$$(m_a^2)_0 = \frac{m_\pi^2 f_\pi^2}{f_a^2}\frac{m_u m_d}{(m_u + m_d)^2}\,, \tag{4.92}$$

where we neglected corrections of order $O(m_{u,d}/m_s)$, since they are numerically of the same order as other next-to-leading order (NLO) corrections (e.g. η' mixing) [14]. We finally note that, as it could not be otherwise, the axion mass is independent of the arbitrarily chosen Q_a. Such a matrix however can be chosen to simplify the calculation of a given observable. For example, choosing $Q_a = \frac{M^{-1}}{\mathrm{Tr}[M^{-1}]}$ removes all the tree-level mixing between the axion and the neutral mesons, thus simplifying e.g. the calculation of the axion mass.

[9] If a perturbative expansion in the number of instantons were possible, the leading effective potential would read $V_0 = b(\mathrm{Tr}[\Phi^\dagger M] + \text{h.c}) - c(e^{-ia/f_a}\det\Phi^\dagger + \text{h.c})$. This will in fact be the case in the CFL phase, see Sec. 6.

4.4 Chemical potential in QFT

Introducing a chemical potential in quantum field theory is a generalization of the procedure in statistical mechanics. One defines a new operator corresponding to the thermodynamic Landau free energy (a.k.a. grand thermodynamic potential density)

$$\hat{\Omega} = \mathcal{H} - \mu_i J_i^0 \,, \tag{4.93}$$

with $\mathcal{H}$ the Hamiltonian density, J_i^0 the conserved charge density associated with a given global symmetry of the system (i.e. the temporal component of the conserved current), and μ_i the corresponding chemical potential. [10] From the path integral representation of the partition function (see e.g. [202]), one arrives at the following prescription: the temporal derivative of each field transforming under the global symmetry in question is shifted by

$$\partial_0 \to \partial_0 + i\mu_i T_i^{\mathcal{R}} \,, \tag{4.94}$$

with $T_i^{\mathcal{R}}$ the generator of the global symmetry in the appropriate representation $\mathcal{R}$. Chemical potential therefore acts as a source for the temporal component of the corresponding conserved current, much like a background gauge field potential. Since it singles out the time direction, the chemical potential breaks the Lorentz symmetry down to its $SO(3)$ subgroup of spatial rotations. Charge conjugation symmetry (C), under which $J_i^0 \to -J_i^0$, is also broken, while parity (P) and time-reserval (T) are preserved – CP and CPT are thus broken. If part of a non-abelian group, a chemical potential also breaks the global symmetry by singling out a specific direction in generator space, namely $\mu_i T_i$, which defines an unbroken $U(1)$ subgroup.

$U(1)$ toy model

A simple toy model that illustrates the main effect of the chemical potential is a complex scalar theory with a global $U(1)$ symmetry [203, 204]. After using the prescription of Eq. (4.94), one finds the following Lagrangian

$$\mathcal{L}(\mu) = \partial_\mu \phi^* \partial^\mu \phi + i\mu(\phi \partial_0 \phi^* - \phi^* \partial_0 \phi) - (m^2 - \mu^2)|\phi|^2 - \lambda |\phi|^4 \,. \tag{4.95}$$

For $m^2 > \mu^2$, the field expectation value is trivial, $\langle \phi \rangle = 0$, and respects the global $U(1)$ symmetry. The two propagating degrees of freedom have different dispersion relations

$$\omega_\phi(\vec{k}) = \sqrt{k^2 + m^2} - \mu \,, \quad \omega_{\phi^*}(\vec{k}) = \sqrt{k^2 + m^2} + \mu \,. \tag{4.96}$$

The appearance of the chemical potential breaks C symmetry, which appears as a $\phi \leftrightarrow \phi^*$ exchange symmetry in the $\mu = 0$ theory – therefore μ can be treated as a spurion transforming as $\mu \to -\mu$.

Above the threshold $|\mu| > m$, the global $U(1)$ is spontaneously broken by the expectation value and the theory describes a Bose-Einstein condensate (BEC) phase. In contrast to the *ideal* ($\lambda = 0$) ultra-relativisitic Bose gas [203], in the *interacting* theory (with $\lambda > 0$) the chemical potential can be larger than m [204], without leading to any inconsistencies. Note, that our

[10] We recall that the grand-canonical density matrix is given by $\hat{\rho} = \exp[-\beta(H - \mu_i Q_i)]$, with $\beta = 1/T$ (T is the temperature), H the Hamiltonian, and Q_i the conserved charge. The partition function is then $Z(\mathcal{V}, T, \mu_i) = \mathrm{Tr}\,\hat{\rho}$, where $\mathcal{V}$ is the volume, eventually taken to infinity. The thermodynamic potential density is $\Omega(T, \mu) = -(T/\mathcal{V}) \ln Z = \rho - \mu_i n_i = -p$, with ρ the energy density, n_i the number density, and p the pressure. The grand-canonical average of an operator $\mathcal{O}$ is then $\langle O \rangle_{T,\mu_i} = \mathrm{Tr}[\mathcal{O}\hat{\rho}]/Z$ (with a slight abuse of notation, when clear we will denote ensemble averages simply by $\langle O \rangle$). Then $n_i = \langle J_i^0 \rangle = -(\partial\Omega/\partial\mu)_T$, while the entropy density is given by $s = -(\partial\Omega/\partial T)_\mu$.

fundamental potential being the Landau free energy Ω, the fixed thermodynamical parameter is μ, which sets the effective energies of the particles in the system due to a coupling to the "particle bath". This allows the flow of particles in and out of the system, implying that the charge density, $n_\phi - n_{\phi^*}$, is a derived quantity set by μ.[11] As we show below, for $|\mu| > m$, the $T = 0$ system contains non vanishing charge density in the form of the BEC. One can interpret this appearance of charge as particles from the "particle bath" being inserted in the ground state of the system.

In the BEC phase, the following parameterization is useful

$$\phi(x) = \frac{1}{\sqrt{2}} e^{i\chi(x)/v}(v + \sigma(x))\,. \tag{4.97}$$

The classical potential is minimized for $v^2 = \frac{\mu^2 - m^2}{\lambda}$, and we find the following Lagrangian

$$\mathcal{L}(\mu) = \frac{1}{2}\left[(\partial_\mu\chi)^2\left(1 + \frac{\sigma}{v}\right)^2 + (\partial_\mu\sigma)^2\right] + \mu v\left(1 + \frac{\sigma}{v}\right)^2 \partial_0\chi - V(\mu)\,, \tag{4.98a}$$

$$V(\mu) = \frac{1}{2}m_\sigma^2\sigma^2 + \lambda v\sigma^3 + \frac{1}{4}\lambda\sigma^4 - \frac{1}{4}\lambda v^4\,, \tag{4.98b}$$

with $m_\sigma^2 = 2\lambda v^2 = 2(\mu^2 - m^2)$. The charge density in the condensed phase is non-vanishing in the limit of zero temperature $\beta \equiv 1/T \to \infty$ and infinite volume $\mathcal{V} \to \infty$,

$$(n_\phi - n_{\phi^*})|_{T=0} = \lim_{\beta,\mathcal{V}\to\infty} \frac{1}{\beta\mathcal{V}}\left(\frac{\partial \ln Z}{\partial\mu}\right)_\beta = -\left(\frac{\partial V}{\partial\mu}\right)\Big|_{\langle\sigma\rangle=0} = \frac{\mu^3}{\lambda}\left(1 - \frac{m^2}{\mu^2}\right)\,, \tag{4.99}$$

where we used the classical ($\hbar \to 0$) result for the generating functional $\ln Z = -\beta\mathcal{V}V(\mu)$ for a homogeneous classical configuration $\langle\sigma\rangle$. By diagonalizing the quadratic field operators in momentum space one finds the dispersion relations for the two propagating degrees of freedom

$$\omega_\pm^2(\vec{k}) = (3\mu^2 - m^2)\left[1 + \frac{k^2}{3\mu^2 - m^2} \pm \sqrt{1 + \left(\frac{2\mu k}{3\mu^2 - m^2}\right)^2}\right]\,, \tag{4.100}$$

which at zero momentum are

$$\omega_-(\vec{0}) = 0\,, \quad \omega_+(\vec{0}) = \sqrt{6\mu^2 - 2m^2}\,. \tag{4.101}$$

As expected, there is one massless excitation, corresponding to the NGB of the spontaneously broken $U(1)$, and one massive excitation, the radial (or Higgs) mode.

4.5 Meson condensation

We review now the importance of a chemical potential in the context of meson condensation in QCD, in particular for the case of two flavors [205, 206, 207, 208], and discuss for the first time its effects on the axion potential. This is a simplified version of the more complicated, but plausibly more realistic, scenario of kaon condensation ($N_f = 3$), to be discussed in Sec. 5.2.

[11] This is in complete analogy to temperature T, with sets the effective energy of particles in the system due to a coupling to a "heat bath". This allows the flow of heat in and out of the system, implying that the entropy of the system is a derived quantity set by T.

For $N_f = 2$, the chiral condensate breaking $SU(2)_L \times SU(2)_R \times U(1)_B \times U(1)_A$ spontaneously to $SU(2) \times U(1)_B$ can be parameterized, in full generality, as

$$\begin{aligned} \langle \bar{q}_R q_L \rangle &\equiv \langle \bar{q}_R q_L \rangle_0 \, e^{i\alpha} \, \Sigma_0 \,, \\ \Sigma_0 = \cos\theta \, \mathbb{1}_2 + i \sin\theta \, \hat{n} \cdot \vec{\sigma} \,, &\quad \hat{n} = (\sin\psi \cos\chi, \sin\psi \sin\chi, \cos\psi) \,, \end{aligned} \tag{4.102}$$

where $-\pi/2 \leq \theta < \pi/2$,[12] and with the sigma field transforming as

$$\Sigma_0 \to L \Sigma_0 R^\dagger \,. \tag{4.103}$$

In Eq. (4.102), we used the fact that a field transforming as a bi-fundamental under $SU(2)_L \times SU(2)_R$ can be written as a radial mode, here frozen to some constant value $\langle \bar{q}_R q_L \rangle_0$, times a 2-by-2 unitary matrix Σ_0, which parameterizes the orientation of the ensemble average in the presence of finite μ, which we call the orientation of the expectation value here. [13]

The phase factor $e^{i\alpha}$ is identified with the direction in field space associated with the anomalous axial $U(1)$. A potential for α is generated by non-perturbative effects, whose minimum is at $\alpha = 0$, which we take from this point on. The angles defined in Eq. (4.102) can be related to expectation values of the usual pion fields (at vanishing chemical potential)

$$\theta \equiv \frac{\langle \Pi \rangle}{f_\pi} \,, \quad \frac{1}{\sqrt{2}} \sin\psi e^{\mp i\chi} = \frac{\langle \pi_\pm \rangle}{\langle \Pi \rangle} \,, \quad \cos\psi = \frac{\langle \pi_3 \rangle}{\langle \Pi \rangle} \,, \tag{4.104}$$

where we defined $\sqrt{\langle \pi_i \pi_i \rangle} \equiv \langle \Pi \rangle$. In Dirac notation

$$\langle \bar{q} q \rangle = \frac{1}{2} \langle \bar{q} q \rangle_0 (\Sigma_0 + \Sigma_0^\dagger) \,, \quad \langle \bar{q} i \gamma_5 q \rangle = \frac{1}{2i} \langle \bar{q} q \rangle_0 (\Sigma_0 - \Sigma_0^\dagger) \,, \tag{4.105}$$

where we denoted $\langle \bar{q}_R q_L \rangle_0 = \langle \bar{q}_L q_R \rangle_0 \equiv \langle \bar{q} q \rangle_0 / 2$. Therefore CP is broken in the ground state if $\Sigma_0 \neq \Sigma_0^\dagger$, that is if $\theta \neq 0$.

We wish to study this system at a non-vanishing chemical potential for isospin

$$\hat{\mu} = \mu (T_L^3 + T_R^3) \,, \tag{4.106}$$

and we shall neglect for the remainder of this section isospin breaking due to the quark masses and electromagnetic interactions, making the choice in Eq. (4.106) completely generic. Such a chemical potential is associated with the σ_3 rotation of the vector $SU(2)_{L+R}$ subgroup. Therefore, according to Eqs. (4.94) and (4.103), we promote the temporal derivative of Σ_0 to

$$\partial_0 \Sigma_0 \to \partial_0 \Sigma_0 + i\mu T_L^3 \Sigma_0 - i\mu \Sigma_0 T_R^3 = \frac{i}{2} \mu [\sigma_3, \Sigma_0] \,. \tag{4.107}$$

Note that changing $\hat{\mu} \to \hat{\mu} + \frac{1}{6} \mathbb{1}_2$ in Eq. (4.106) has no effect on Eq. (4.107) and on the following derivation, therefore in this context the isospin chemical potential can be equivalently associated with the chemical potential for electric charge.[14] The resulting potential for the pions and the axion, the latter entering via the quark mass matrix, $M = m \mathbb{1}_2$ ($m_u = m_d$), as in Eq. (4.88) (with $Q_a = \mathbb{1}_2/2$), is given by

$$V = \frac{f_\pi^2 \mu^2}{16} \mathrm{Tr}[[\sigma_3, \Sigma_0][\sigma_3, \Sigma_0^\dagger]] + \frac{\langle \bar{q} q \rangle_0}{2} \mathrm{Tr}[\Sigma_0 M e^{-\frac{ia}{2f_a}} + \Sigma_0^\dagger M e^{\frac{ia}{2f_a}}] \,, \tag{4.108}$$

[12] The shift $\theta \to \theta + \pi$ can be compensated by shifting $\alpha \to \alpha + \pi$.

[13] $SU(2)_L$ and $SU(2)_R$ are generated by $T_L^a = \frac{1}{2}\sigma^a$ and $T_R^a = \frac{1}{2}\sigma^a$, respectively, where as usual it should be understood that the L and R operators act on different indices and therefore commute.

[14] One can then think of μ as a non-vanishing averaged value for the zero component of the photon field $\mu = \langle A_0 \rangle$, which can be intuitively understood as a classical background electric charge density.

at leading order in m/Λ_χ and μ/Λ_χ, Λ_χ being the cutoff of the chiral Lagrangian. We note that the first term arises from the usual kinetic term, $\frac{1}{4}f_\pi^2\,\mathrm{Tr}[\partial_\mu\Sigma_0\partial^\mu\Sigma_0^\dagger]$, after the replacement (4.107). Using Eq. (4.102) we find

$$V = -\frac{1}{2}\mu^2 f_\pi^2 \sin^2\theta \sin^2\psi - m_\pi^2 f_\pi^2 \cos\theta \cos\left(\frac{a}{2f_a}\right), \tag{4.109}$$

where m_π here is the neutral pion mass in vacuum, i.e. $m_\pi^2 f_\pi^2 = -2m\langle\bar{q}q\rangle_0$. We see that the isospin chemical potential introduces an additional source of explicit symmetry breaking – while leaving unbroken the $U(1)_{L+R}$ symmetry defined by the generator in Eq. (4.106), $\hat{\mu}$ explicitly breaks the shift symmetries associated with the would-be NGBs charged under $U(1)_{L+R}$, i.e. the charged pions. Indeed, as discussed above, $U(1)_{L+R}$ is equivalent to the electric charge. Consequently, the first term in Eq. (4.109) is proportional to the expectation value of the charged pions, $\sin^2\theta\sin^2\psi \propto \langle\pi^+\pi^-\rangle$. Since $\hat{\mu}$ commutes with the $U(1)_{L-R}$ associated with the neutral pion, the neutral NGBs are unaffected by the chemical potential and the potential Eq. (4.109) is minimized at $\langle\pi_3\rangle = 0$ ($\psi = \pi/2$) and $\langle a\rangle = 0$ as in the $\mu = 0$ vacuum.

The minimum of the potential for any value of μ is then found at

$$\cos\theta = \mathrm{Min}\left[1, \frac{m_\pi^2}{\mu^2}\right]. \tag{4.110}$$

For $|\mu| < m_\pi$, the ground state is the trivial one, $\Sigma_0 = 1$, thus its orientation is the same as for $\mu = 0$. For $|\mu| > m_\pi$, pion condensation takes place and the orientation of the expectation value is no longer trivial. We note that in this case χ constitutes a flat direction which, as we confirm later, corresponds to a NGB from the spontaneous breaking of electric charge, $U(1)_{L+R}$. Setting, without loss of generality, $\chi = 0$, we can write the QCD orientation for $|\mu| > m_\pi$ as

$$\Sigma_0 = \begin{pmatrix} \cos\theta & i\sin\theta \\ i\sin\theta & \cos\theta \end{pmatrix}. \tag{4.111}$$

At this point we recall that since $\theta \neq 0$, CP is broken by the expectation value, a result of a sufficiently large explicit breaking of CP by the chemical potential in the *charged* pion sector. Instead, CP-invariance in the *neutral* sector is preserved by the charge chemical potential, which leaves the expectation values in that sector untouched. We see now that only if $\langle\pi_3\rangle \neq 0$ ($\psi \neq \pi/2$) could the axion condense, which requires additionally explicit breaking of isospin, i.e. $m_u \neq m_d$.

Having established the Goldstone boson expectation values at finite-density, let us turn our attention to their fluctuations. Since these are associated with the $SU(2)_L \times SU(2)_R$ generators broken by Σ_0, we define the following rotated generators

$$(T_L^a)_\theta = \xi_0(T_L^a)\xi_0^\dagger\,, \quad (T_R^a)_\theta = \xi_0^\dagger(T_R^a)\xi_0\,, \tag{4.112}$$

where $\xi_0 \equiv \sqrt{\Sigma_0}$. The broken and unbroken generators are then given by

$$X^a = (T_L^a)_\theta - (T_R^a)_\theta\,, \quad T^a = (T_L^a)_\theta + (T_R^a)_\theta\,, \tag{4.113}$$

respectively. The fluctuations around the Σ_0 ground state can be parameterized as

$$\Sigma = \xi_L\Sigma_0\xi_R^\dagger = \exp\left[\frac{i\pi^a(T_L^a)_\theta}{f_\pi}\right]\Sigma_0\exp\left[\frac{i\pi^a(T_R^a)_\theta}{f_\pi}\right] = \xi_0\exp\left[\frac{i\pi^a\sigma^a}{f_\pi}\right]\xi_0\,, \tag{4.114}$$

where, abusing notation, we have written the (pseudo-)NGBs as π^a, like the standard $\theta = 0$ pions. [15]

[15] We note that, given Eq. (4.112) and $T_L^a = \frac{1}{2}\sigma^a$, $T_R^a = \frac{1}{2}\sigma^a$, it follows that $\xi_L = \xi_0\exp\left[\frac{i\pi^a\sigma^a}{2f_\pi}\right]\xi_0^\dagger$ and $\xi_R = \xi_0^\dagger\exp\left[-\frac{i\pi^a\sigma^a}{2f_\pi}\right]\xi_0$.

The dispersion relations for the neutral degrees of freedom, π_0 and the axion, are the same as for vanishing chemical potential. Their masses can be obtained from Eq. (4.108) (with the substitution of Σ_0 by Σ),

$$(m^2_{\pi_0})_\theta = m^2_\pi/\cos\theta\,, \quad (m^2_a)_\theta = (m^2_a)_0\cos\theta\,, \tag{4.115}$$

with $(m^2_a)_0$ the mass of the axion in vacuum, Eq. (4.92), and where we note that for $|\mu| > m_\pi$, $(m^2_{\pi_0})_\theta = \mu^2$. The change of the axion mass for $\theta \neq 0$ simply follows from the fact that, once the mixing with π_3 is eliminated, it has to be proportional to the CP-even combination $\mathrm{Tr}[\Sigma_0 + \Sigma_0^\dagger] \propto \cos\theta$. The increase in the neutral pion mass can be understood as a result of its repulsive interaction with the charged pions. The dispersion relation for the charged pions is very similar to the $U(1)$ toy model of Sec. 4.4. In the uncondensed phase $|\mu| < m_\pi$, their dispersion relations are

$$\omega_{\pi_\pm}(\vec{k}) = \sqrt{m^2_\pi + k^2} \mp \mu\,. \tag{4.116}$$

Indeed, for the charged states $\pi_\pm \equiv \frac{1}{\sqrt{2}}(\pi_1 \mp i\pi_2)$ we recognize the same mass splitting we found in Eq. (4.96). In the condensed phase $|\mu| > m_\pi$, the remaining $U(1)_{L+R}$ symmetry is spontaneously broken. The effective masses of the charged pions are

$$\omega_{\pi_+}(\vec{0}) = 0\,, \quad \omega_{\pi_-}(\vec{0}) = \mu\sqrt{1 + \frac{3m^4_\pi}{\mu^4}}\,. \tag{4.117}$$

As in the $U(1)$ toy model, the condensed phase contains one massless Goldstone mode and one massive radial mode. In this phase, the system has a non-vanishing charge density

$$n_{\pi_+} - n_{\pi_-} = -\left(\frac{\partial V}{\partial\mu}\right)\Big|_{\pi_i = a = 0} = f^2_\pi\mu\left(1 - \frac{m^4_\pi}{\mu^4}\right)\,. \tag{4.118}$$

The effective masses of the pions and the axion are plotted in Fig. 4.1.

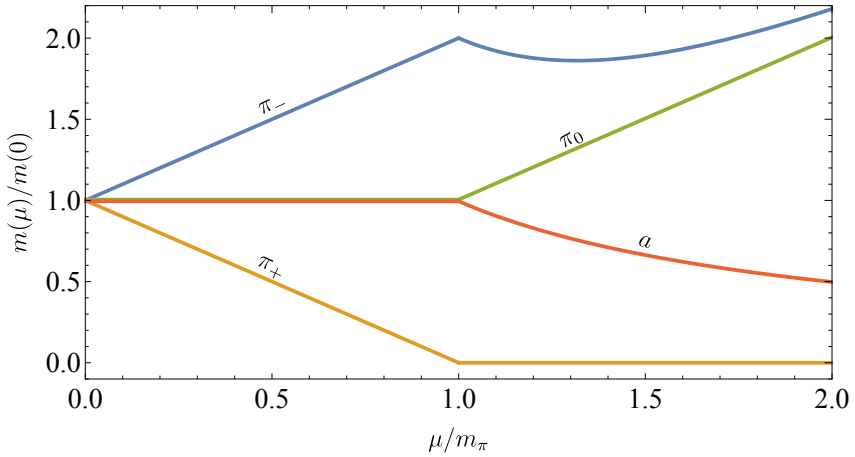

Figure 4.1: *Mass spectrum of the vacuum excitations as a function of μ/m_π. The masses are normalized to their respective $\mu = 0$ value. The charged π_+ and π_- modes (orange and blue curves respectively) evolve similarly as the ϕ and ϕ^* modes in the $U(1)$ toy model: a linear split in masses in the uncondensed phase, continuously transitioning to a massless Goldstone mode and a massive radial mode in the condensed phase. The masses of the neutral modes, π_0 and a (green and red curve respectively) are unaffected by the chemical potential in the uncondensed phase. In the condensed phase, m_{π_0} increase linearly with μ, while the axion becomes lighter as μ increases.*

5

Nuclear densities

In this chapter we study how the properties of the axion, mainly its potential and coupling to nucleons, change in systems at finite baryon density, n. In particular, our focus here is on densities around nuclear saturation, $n \sim n_0$, where a description of QCD in terms of hadrons is still meaningful.

For the axion potential, we identify two main effects: 1) the change in the size and, to some degree, flavor orientation of the quark condensates, as "measured" by the mass of the pions (Sec. 5.1), and 2) kaon condensation (Sec. 5.2), similar to meson condensation, introduced in Sec. 4.5. Both of these effects can be taken into account by a generalization of the axion potential in vacuum, Eq. (4.89), to

$$V(n) = \frac{1}{2}\mathrm{Tr}[\langle \bar{q}q\rangle_n \hat{M}_a + \mathrm{h.c}]\,, \quad \hat{M}_a = \xi_0^\dagger \xi_L^\dagger M_a \xi_R \xi_0^\dagger \tag{5.1}$$

with M_a encoding the dependence on the axion as in Eq. (4.88). $\Sigma_0 = \xi_0^2$ parametrizes the orientation of the QCD ground state that spontaneously breaks $SU(3)_L \times SU(3)_R$ to $SU(3)$ and therefore encodes the effects of kaon condensation. In vacuum, we have $\xi_0 = \mathbb{1}_3$ and the unbroken subgroup is the usual $SU(3)_{L+R}$, while in the kaon-condensed phase, we have $\xi_0 = \xi_0(\theta)$, with θ controlling the size of the kaon condensate which, as explained below, ultimately depends on the baryon density. $\xi_{L,R}$ are the Goldstone matrices, given by

$$\xi_L = e^{i\frac{\pi^a}{2f_\pi}(T_L^a)_\theta} = \xi_0 \exp\left[\frac{i\pi^a\lambda^a}{2f_\pi}\right]\xi_0^\dagger\,, \quad \xi_R = e^{-i\frac{\pi^a}{2f_\pi}(T_R^a)_\theta} = \xi_0^\dagger \exp\left[-\frac{i\pi^a\lambda^a}{2f_\pi}\right]\xi_0\,, \tag{5.2}$$

a generalization to $SU(3)_L \times SU(3)_R$ of those in Eq. (4.114). Finally, the quark condensate $\langle \bar{q}q\rangle_n$ at finite density becomes a matrix in flavor space,

$$\langle \bar{q}q\rangle_n = \mathrm{Diag}[\langle \bar{u}u\rangle_n, \langle \bar{d}d\rangle_n, \langle \bar{s}s\rangle_n]\,, \tag{5.3}$$

The detailed derivation of Eq. (5.1) is given in App. 5.A. The result can also be understood in terms of symmetries: $\hat{M}_a$ is a spurion that has been dressed by the Goldstones and projected into the $SU(3)_{L+R}$ subgroup. Therefore, it transforms as $\hat{M}_a \to V\hat{M}_a V^\dagger$, where V is an $SU(3)_{L+R}$ transformation. $\langle \bar{q}q\rangle_n$ transforms in the same way, since it is the result of a non-vanishing expectation value of the temporal component of the baryonic current, $n = \langle J_B^0\rangle$. [1]

Concerning the couplings of the axion to nucleons, the main effect we consider can be traced to a change at finite baryonic density of the nuclear matrix elements $\langle p|\bar{q}\gamma^\mu\gamma^5 q|p\rangle$ (with p the proton, $q = u, d$) as "measured" by the axial pion-nucleon coupling (Sec. 5.3). These set the size of the

[1] When the quark condensate is trivial, $\langle \bar{q}q\rangle_n \propto \mathbb{1}_3$, we recover $V(n) \propto \mathrm{Tr}[\Sigma^\dagger M_a + \mathrm{h.c}]$. Instead, when the ground state is trivial, $\Sigma_0 = \mathbb{1}_3$, the change in condensates effectively amounts to $m_q \to m_q\langle \bar{q}q\rangle_n/\langle \bar{q}q\rangle_0$.

couplings of protons and neutrons to the axion, as they follow from either its model-dependent UV couplings to light quarks, or from axion-pion mixing. The latter also changes at finite density although, as we explain below, the effect is within known uncertainties.

Before going into the details, several general comments about our treatment of the nuclear medium are in order. To describe the state of the system, we will work directly in terms of baryon densities, n_p and n_n considering only protons and neutrons, respectively. In practice, our independent parameters are the total baryonic density, $n = n_p + n_n$, and the proton fraction, n_p/n. This will be more convenient than introducing the corresponding chemical potentials, because our analysis is limited to linear order in n, i.e. we work in the mean-field or Hartree approximation, where e.g. $n_p \approx \langle \bar{p}\gamma_0 p\rangle_{T,\mu_i}$ (and in fact $n_p \approx \langle \bar{p}p\rangle_{T,\mu_i}$ in the non-relativistic limit) – higher-order corrections generically being beyond perturbative control when relevant. Besides, the relative fraction of protons and neutrons is, as shown below, relevant only in our discussion of kaon condensation. There, the chemical potential for electric charge, μ, will also be required to properly describe the system, along with the condition of charge neutrality.

5.1 Quark condensates

We first discuss how the quark condensate changes at finite baryonic density, since this is the most robust effect from the point of view of perturbative control. We derive the implications for the axion mass, which were first noted in [209]. The change with density of the quark condensates can be calculated utilizing the Hellmann-Feynman theorem [210]

$$\zeta_{\bar{q}q}(n) \equiv \frac{\langle \bar{q}q\rangle_n}{\langle \bar{q}q\rangle_0} = 1 + \frac{1}{\langle \bar{q}q\rangle_0}\frac{\partial \Delta E(n)}{\partial m_q}\,, \quad q = u, d, s\,. \tag{5.4}$$

$\Delta E(n)$ is the energy shift of the QCD ground state due to the finite density background, such that $\Delta E(0) = 0$. It can be decomposed as

$$\Delta E = E^{\text{free}} + E^{\text{int.}}\,, \tag{5.5}$$

where the first term represents the energy shift due to the presence of a non-interacting Fermi gas, while the second term encodes the energy shift due to nuclear interactions. Neglecting these interactions as well as relativistic corrections, we have $\Delta E = \sum_{x=n,p,\ldots} m_x n_x$, and we arrive at the so-called linear approximation for the in-medium condensate

$$\zeta_{\bar{q}q}(n) = 1 + \frac{1}{\langle \bar{q}q\rangle_0}\sum_x n_x \frac{\partial m_x}{\partial m_q}\,, \quad q = u, d, s\,. \tag{5.6}$$

The derivatives $\partial m_x/\partial m_q$ describe the shift in the nucleon mass due to the non-vanishing quark masses. For two nucleons $\{n, p\}$ and three quarks $\{u, d, s\}$, one naively counts six independent shifts. However, due to the $\{p, u\} \leftrightarrow \{n, d\}$ exchange symmetry, only three shifts are independent. Working in the isospin basis for the quark masses, $\bar{m} \equiv \frac{1}{2}(m_u + m_d)$ and $\Delta m \equiv \frac{1}{2}(m_u - m_d)$, the following sigma terms are identified and defined

$$\sigma_{\pi N} \equiv \bar{m}\left(\frac{\partial m_p}{\partial \bar{m}}\right) = \bar{m}\left(\frac{\partial m_n}{\partial \bar{m}}\right)\,, \tag{5.7}$$

$$\tilde{\sigma}_{\pi N} \equiv \Delta m\left(\frac{\partial m_n}{\partial \Delta m}\right) = -\Delta m\left(\frac{\partial m_p}{\partial \Delta m}\right)\,, \tag{5.8}$$

$$\sigma_s \equiv m_s\left(\frac{\partial m_p}{\partial m_s}\right) = m_s\left(\frac{\partial m_n}{\partial m_s}\right)\,, \tag{5.9}$$

such that

$$m_n = M_B + \sigma_{\pi N} + \tilde{\sigma}_{\pi N} + \sigma_s \,, \tag{5.10}$$
$$m_p = M_B + \sigma_{\pi N} - \tilde{\sigma}_{\pi N} + \sigma_s \,. \tag{5.11}$$

with M_B the baryon mass in the chiral limit, $m_q \to 0$. We note that the sigma terms can be expressed in terms of the parameters of the $N_f = 3$ chiral Lagrangian for baryons, see Eq. (5.110) in App. 5.A. The $\sigma_{\pi N}$ and σ_s terms have been extracted from pion-nucleon and kaon-nucleon scattering experiments, as well as from lattice simulations by calculating the mass shifts of the nucleons. There are ongoing efforts aimed at the determination of the precise values of these sigma terms. A summary of latest results [211] shows that their current values are scattered over a fairly wide range, with some tension between experimental and lattice results. In this work we use the conservative estimates $\sigma_{\pi N} = 45 \pm 15$ MeV and $\sigma_s = 30$ MeV. The other sigma term is extracted from the $p-n$ non-electromagnetic mass splitting $2\tilde{\sigma}_{\pi N} = (m_n - m_p)^{\text{non-EM}} = 2 \pm 0.3$ MeV [212]. Using the GOR relation in Eq. (4.91), we rewrite the ratios $\langle \bar{q}q \rangle_n / \langle \bar{q}q \rangle_0$ as

$$\zeta_{\bar{u}u}(n) = 1 - b_1 \frac{n}{n_0} + b_2 \left[2\frac{n_p}{n} - 1 \right] \frac{n}{n_0} \,, \tag{5.12a}$$
$$\zeta_{\bar{d}d}(n) = 1 - b_1 \frac{n}{n_0} - b_2 \left[2\frac{n_p}{n} - 1 \right] \frac{n}{n_0} \,, \tag{5.12b}$$
$$\zeta_{\bar{s}s}(n) = 1 - b_3 \frac{n}{n_0} \,, \tag{5.12c}$$

with

$$b_1 \equiv \frac{\sigma_{\pi N} n_0}{m_\pi^2 f_\pi^2} = 3.5 \times 10^{-1} \left(\frac{\sigma_{\pi N}}{45 \text{ MeV}} \right) , \tag{5.13a}$$
$$b_2 \equiv \frac{\tilde{\sigma}_{\pi N} n_0}{m_\pi^2 f_\pi^2} \frac{\bar{m}}{\Delta m} = -2.2 \times 10^{-2} \left(\frac{\tilde{\sigma}_{\pi N}}{1 \text{ MeV}} \right) , \tag{5.13b}$$
$$b_3 \equiv \frac{\sigma_s n_0}{m_\pi^2 f_\pi^2} \frac{2\bar{m}}{m_s} = 1.7 \times 10^{-2} \left(\frac{\sigma_s}{30 \text{ MeV}} \right) . \tag{5.13c}$$

Clearly the $\langle \bar{s}s \rangle_n$ condensate is only weakly affected by the nucleonic background. Therefore, as in vacuum, its contribution to the axion mass will be subleading, being suppressed by $m_{u,d}/m_s$. Additionally, $\langle \bar{u}u \rangle_n \approx \langle \bar{d}d \rangle_n$ up to the small isospin breaking correction [213], which we neglect. From Eq. (5.1) with $\xi_0 = \mathbb{1}_3$ and after taking care of axion-pion mixing (which we discuss in the context of the axion couplings Sec. 5.3) we reproduce the axion mass at finite density found in [209]

$$(m_a)_n^2 = \frac{m_\pi^2 f_\pi^2}{f_a^2} \frac{m_u m_d}{m_u + m_d} \langle \bar{u}u \rangle_n \approx (m_a)_0^2 \left(1 - b_1 \, \frac{n}{n_0} \right) , \tag{5.14}$$

where m_π here is the neutral pion mass in vacuum, Eq. (4.91). In this regard, we note that at the linear order in density the same correction as the axion enters the neutral pion mass in medium, i.e. $(m_\pi)_n^2 = m_\pi^2 \langle \bar{u}u \rangle_n$. This is why for the remainder of this section, we shall only consider $n < n_c \equiv n_0/b_1 \approx 2.8\, n_0\, (45 \text{ MeV}/\sigma_{\pi N})$, with n_c being the critical density in which one naively expects chiral symmetry restoration in the linear approximation.

At this point, let us turn our attention to the corrections to the linear, non-relativistic approximation we have considered. This will allow us to estimate the densities up to which our leading result is under perturbative control and can therefore be trusted. First, the energy of

a degenerate (zero temperature) ideal Fermi gas receives relativistic corrections. In the fully relativistic limit, the free part of the energy for a fermion x is given by

$$E_x^{\text{free}} = 2\int^{k_f^x} \frac{\mathrm{d}^3k}{(2\pi)^3}\sqrt{k^2+m_x^2} = m_x n_x F(k_f^x/m_x)\,, \tag{5.15}$$

$$F(q) = \frac{3q\sqrt{q^2+1}\,(2q^2+1) - 3\sinh^{-1}(q)}{8q^3} = 1 + \frac{3q^2}{10} + O(q^4)\,, \tag{5.16}$$

where k_f^x is the Fermi momentum, $k_f^x = \sqrt{m_x^2-\mu_x^2}$, which determines the number density,

$$n_x = 2\int^{|\vec{k}|\leq k_f^x} \frac{\mathrm{d}^3k}{(2\pi)^3} = \frac{(k_f^x)^3}{3\pi^2}\,. \tag{5.17}$$

Therefore, relativistic corrections, of $O((k_f^x/m_x)^2)$, become important at large densities. When this happens, corrections to the QCD ground state energy Eq. (5.5) from nucleon interactions become important as well. These are predominantly due to pion exchange, but also from four-baryon contact interactions. It is clear that the latter become important when $n_x/\Lambda_\chi f_\pi^2$ becomes order one. Given Eq. (5.17), this is also the place where ChPT is beyond control, $k_f^x \sim \Lambda_\chi$, e.g. the pion-exchange contribution to the energy is not predictable. In addition, since the cutoff of ChPT Λ_χ is numerically close to $m_p \approx m_n$, relativistic corrections are approximately controlled by the same expansion parameter,

$$\frac{k_f^2}{\Lambda_\chi^2} \approx \frac{(3\pi^2 n/2)^{2/3}}{\Lambda_\chi} \approx (15\,\%)\,\left(\frac{n}{n_0}\right)^{2/3}\,\left(\frac{700\text{ MeV}}{\Lambda_\chi}\right)^2\,, \tag{5.18}$$

where we took $k_f = k_f^p \sim k_f^n$. Ultimately the best way to asses the validity of our linear approximation is to explicitly compute the relevant NLO corrections. The interaction energy $E^{\text{int.}}$ has been calculated by summing the so-called Hugenholtz diagrams, which are connected bubble diagrams describing ground-state to ground-state transitions [214]. The resulting higher-order finite density effects on the quark condensates have been obtained in ChPT for symmetric nuclear matter [215, 216] and pure neutron matter [217, 218]. These authors have indeed found $O(1)$ deviations from the linear approximation for densities somewhat above nuclear saturation. Specifically, nucleon interactions seem to ameliorate the linear decrease of $\langle\bar{u}u\rangle_n \approx \langle\bar{d}d\rangle_n$ in Eq. (5.12), such that already at $n \approx 2n_0$, the condensates are only at approximately 60 % of their vacuum value, as opposed to the 15 % predicted by the linear approximation, and in fact start increasing with density [215]. This then implies that a more realistic prediction of the axion mass in dense symmetric nuclear matter is

$$(m_a)^2_{n\lesssim 2n_0} \gtrsim 0.6\,(m_a)_0^2\,. \tag{5.19}$$

while for larger densities $n \gtrsim 2_0 \sim n_c$ it becomes difficult to trust the results of ChPT.

Therefore, the determination of the quark condensates and the axion mass at densities significantly beyond nuclear saturation remains an open and difficult theoretical problem. Importantly, realistic lattice simulations at finite density are currently not feasible due to so-called sign problem. In addition, at such high densities other issues arise (ultimately related to the problem of perturbativity), such as the "hyperon puzzle", which concerns the appearance, or absence, of hyperons, see e.g. [219] and references therein. In the next section we will focus our attention instead on another effect of strangeness, potentially much more relevant for the fate of the axion at finite density.

5.2 Kaon condensation

In the previous section we assumed that the vacuum of QCD is trivially oriented and CP-preserving, or equivalently that none of the mesons acquire a non-trivial expectation value. This might, however, not be the case in dense matter. It has been hypothesized [220] that above certain baryonic densities it becomes energetically possible for the strangeness changing process of a neutron splitting into a proton and a scalar K^- meson, and vice versa, to take place

$$n \leftrightarrow p^+ + K^- \,, \tag{5.20}$$

The reason being the low in-medium kaon mass, which eventually leads to the formation of a K^- condensate. This process takes place along with, and even becomes favored over, the usual neutron β-decay, $n \to p^+ + e^- + \bar{\nu}_e$, and inverse β-decay, $p^+ + e^- \to n + \nu_e$, because of the high price of occupying the increasingly energetic Fermi surface of the electrons. Because of this fact, also the processes $e^- \leftrightarrow K^- + \nu_e$ and $e^- \leftrightarrow \mu^- + \bar{\nu}_\mu + \nu_e$, $\mu^- \leftrightarrow e^- + \nu_\mu + \bar{\nu}_e$ reach β-equilibrium [221]. On the other hand, the formation of a pion (π^-) condensate ($n \leftrightarrow p^+ + \pi^-$) seems to be disfavored, as we shall discuss below.

Motivated by these arguments, we shall now entertain the possibility of kaon condensation and derive its effects on the axion potential. Several important comments and some caveats are however in order. We consider this scenario because of the thrilling possibility of leading to axion condensation, even though it takes place – if it takes place at all – at densities where a perturbative expansion is questionable, $n \gtrsim 2n_0$. Because of the inherent uncertainties at such densities, our conclusions will be *qualitative* rather than quantitive. Indeed, similar to our discussion at the end of the previous section on the quark condensates and their finite density corrections beyond the linear approximation, kaon condensation cannot be simply described by the leading order terms in ChPT. In particular, nucleon self-interactions and interactions with pions need to be considered in order to capture the full complexity of this strongly interacting system [222] – for instance, the latter are the reason behind the fact that K^- condensation is more likely than π^- condensation. Our working assumption is that all the processes above (neglecting the pions) are in equilibrium, which implies a set of equations relating the chemical potentials of the particle species involved,

$$\mu_\mu = \mu_e = \mu_{K^-} = \mu \,, \quad \mu_p - \mu_n = \mu \,, \tag{5.21}$$

where μ is the chemical potential associated with (positive) electric charge. For convenience, we work directly with muon and electron densities, n_μ and n_e respectively, both of which are determined by μ as they follow from an ideal Fermi gas. The size of the kaon condensate, θ, is determined, as in the simple example of meson condensation discussed in Sec. 4.5, by the minimization of the scalar potential, which of course also determines if the axion condenses or not. Finally, due to the importance of nuclear interactions, the densities of protons and neutron, or equivalently the total baryon density n and the proton fraction n_p/n, are not determined by μ. Instead, we enforce the condition of (electric) charge neutrality $n_{\rm EM} = 0$, and present our results in terms of n and n_p/n.

An additional important final comment regards the implications of kaon condensation on the NS equation of state (EoS). It has been argued that the inclusion of kaon condensation generically leads to a softer EoS [221, 223], which usually cannot sustain a large NS mass. This is in conflict with the most massive NSs observed, with masses around $2M_\odot$ [224, 225]. This is the main reason why kaon condensation is currently considered an "exotic" possibility. However, axion effects can in fact harden the EoS [226] and reopen this window. Also, kaon condensation

is in fact related to another issue, namely the hyperon puzzle [227]. The appearance of hyperons also tends to soften the EoS, resulting in a similar apparent conflict with the observation of massive NSs. Therefore, although the appearance of strangeness seems to be in tension with observations, we think it would be premature to definitively exclude the possibility of kaon condensation at this point, especially in the presence of new physics.

Let us consider then the possibility that kaon condensation occurs in nuclear matter and qualitatively examine its effects on the axion potential. Once the chemical potential for electric charge μ is introduced, the dispersion relations for the $K^\pm$ modes are given by

$$\omega_{K^\pm}(\vec{k}) = \sqrt{\left(m^2_{K^\pm}\right)_n + k^2} \pm \mu\,, \tag{5.22}$$

with the kaon effective in-medium mass

$$\left(m^2_{K^\pm}\right)_n = \frac{1}{f_\pi^2}\left(-\frac{\langle \bar{u}u + \bar{s}s\rangle_n}{2} m_s - \frac{1}{2}(n+n_p)\,\mu\right)\,. \tag{5.23}$$

The first term in Eq. (5.23) is the usual kaon mass to leading order in m_s, with the inclusion of the finite density corrections to the relevant quark condensate, which in the linear approximation are given by

$$-\frac{\langle \bar{u}u + \bar{s}s\rangle_n}{2f_\pi^2}\, m_s = m_K^2\,\left(1 - \frac{1}{2}\left[b_1 - b_2\left(\frac{2\,n_p}{n} - 1\right) + b_3\right]\frac{n}{n_0}\right)\,, \tag{5.24}$$

where $m_K^2 = -m_s\langle \bar{q}q\rangle_0/f_\pi^2$, the neutral kaon mass in vacuum, neglecting $O(m_{u,d}/m_s)$ terms. The second term in Eq. (5.23) is a mass correction induced by the baryonic background, due to the model-independent s-wave interactions of the baryons with the mesons, arising from the baryon kinetic term,

$$(\mathcal{L}_B)_n = i\,\mathrm{Tr}[\bar{B}\gamma^\mu D_\mu B] \supset -\mu\,\mathrm{Tr}[\bar{B}\gamma^0[\hat{Q}_e, B]]\,,\; \hat{Q}_e = \tfrac{1}{2}\left(\xi_0^\dagger\xi_L^\dagger Q_e \xi_L \xi_0 + \xi_0\xi_R^\dagger Q_e \xi_R \xi_0^\dagger\right) \tag{5.25}$$

as it follows from the covariant derivative of ChPT, $D_\mu B = \partial_\mu B + [e_\mu, B]$ with the chiral connection $e_\mu = \frac{1}{2}(\xi_0^\dagger\xi_L^\dagger\partial_\mu\xi_L\xi_0 + \xi_0\xi_R^\dagger\partial_\mu\xi_R\xi_0^\dagger)$, upon introducing the charge chemical potential, $\partial_0 \to \partial_0 + i\mu Q_e$ with $Q_e = \mathrm{Diag}[2/3, -1/3, -1.3]$, see App. 5.A for the details. Note that since $b_2 \ll b_1$, the effective kaon mass decreases with density, and condensation is expected to occur when [2]

$$\omega_{K^-}(0) = (m_{K^\pm})_n - \mu = 0 \tag{5.27}$$

Kaon condensation is introduced by allowing the kaon field to take a non-trivial average value, $\langle\sqrt{2}K^\pm/f_\pi\rangle$, or equivalently, in our notation, reorienting the QCD ground state in medium [221],

$$\Sigma_0 = \begin{pmatrix} \cos\theta & 0 & i\sin\theta \\ 0 & 1 & 0 \\ i\sin\theta & 0 & \cos\theta \end{pmatrix}\,. \tag{5.28}$$

[2] It is illustrative to also consider the pion effective in-medium mass,

$$\left(m^2_{\pi^\pm}\right)_n = \frac{1}{f_\pi^2}\left(-\langle\bar{u}u + \bar{d}d\rangle_n\bar{m} + \frac{1}{2}(n-2n_p)\mu\right)\,, \tag{5.26}$$

since it shows that, due to the second term and contrary to the kaon, the charge pion becomes heavier with increasing density, at least for a neutron rich background $n_p/n < 1/2$ [228]. The argument against pion condensation becomes even stronger when considering higher order terms in ChPT [213], as we discussed at the end of Sec. 5.1 – these additional corrections even make the pion mass increase with density for $n \approx 2n_0$, even in symmetric nuclear matter, $n_p/n = 1/2$.

The ground state orientation is determined by the static Lagrangian after setting all the fluctuations to zero. Neglecting for the time being the axion, we find a similar potential to Eq. (4.109)

$$V(\theta) = -\frac{1}{2}\mu^2 f_\pi^2 \sin^2\theta - f_\pi^2 (m_{K^\pm}^2)_n \cos\theta \,. \tag{5.29}$$

Minimizing $V(\theta)$ leads to the condition

$$\cos\theta = \text{Min}\left[1, \frac{(m_{K^\pm}^2)_n}{\mu^2}\right] , \tag{5.30}$$

which can be used to determined $\theta = \theta(\mu, n, n_p/n)$. The requirement of electrical neutrality, $n_{\rm EM} = -\langle \partial\mathcal{L}/\partial\mu\rangle = 0$, leads to

$$-f_\pi^2 \mu \sin^2\theta + \cos\theta\, n_p - \sin^2(\theta/2)\, n_n - n_e(\mu) - n_\mu(\mu) = 0 \,, \tag{5.31}$$

where we included the lepton charge densities, given by

$$n_l(\mu) = \Theta(|\mu| - m_l)\,\text{Sign}(\mu)\,\frac{(\mu^2 - m_l^2)^{3/2}}{3\pi^2} \,, \quad l = e, \mu \,. \tag{5.32}$$

Solving (numerically) the coupled Eqs. (5.30) and (5.31), one can determine the values of $\{\theta, \mu\}$ as a function of $\{n, n_p/n\}$. In Fig. 5.1 we show the results for θ and μ as a function of baryon density for different values of the proton fraction, while in Fig. 5.3 we plot the region (blue) in the $\{n, n_p/n\}$ plane where $\theta \neq 0$, namely where the system is in the kaon-condensed phase. The evolution for given $\{n, n_p/n\}$ can be understood as follows: for a fixed proton fraction n_p/n, as n increases the amount of positive charge due to the protons increases as well, and more leptons are required to satisfy the neutrality condition, leading to an increase in μ. This increase in μ drives the effective mass of the kaon, Eq. (5.23), further down (on top of the decrease in $\langle \bar{u}u\rangle$ at finite density), until eventually the threshold condition for kaon condensation is met, $\mu = (m_{K^\pm})_n$, and a further increase in the proton density can be compensated by inserting K^- particles in the ground state.

Even though we keep them undetermined, let us briefly comment at this point on how the proton fraction could be determined in terms of the total density. Since the interaction energy of nuclear matter also depends on the proton fraction, $E^{\rm int.} = n\,\epsilon^{\rm int.}(n, n_p)$, one could enforce that the total energy density is minimal with respect to n_p/n, which would lead to the constraint [221],

$$c_4 \sin^2(\theta/2) + \mu \cos^2(\theta/2) + \frac{\partial \epsilon^{\rm int.}(n, n_p)}{\partial(n_p/n)} = 0 \,, \tag{5.33}$$

where $c_4 \equiv (2 b_2 f_\pi^2 m_K^2)/n_0 \sim 49$ MeV.

After determining the ground state orientation, let us examine the consequences on the axion potential. The pseudo-NGB potential, after reintroducing the fluctuations we are mainly interested in, namely the neutral mesons π_0, η and the axion, is given by

$$V(\pi_0, \eta, a) = \frac{f_\pi^2 \mu^2}{4}\text{Tr}[[Q_e, \Sigma][Q_e, \Sigma^\dagger]] + \frac{1}{2}\text{Tr}[\langle \bar{q}q\rangle_n \hat{M}_a + \text{h.c}] \tag{5.34}$$

with $\hat{M}_a$ given in Eq. (5.1) and

$$\Sigma = \xi_L \Sigma_0 \xi_R^\dagger = \xi_0 \exp\left[\frac{i\pi^a \lambda^a}{f_\pi}\right] \xi_0 \,. \tag{5.35}$$

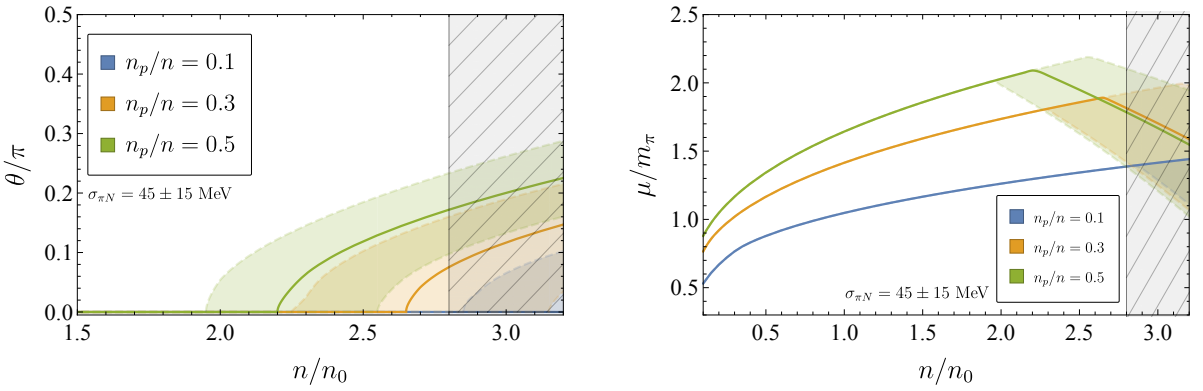

Figure 5.1: *The ground state orientation angle θ (left panel) and the chemical potential μ in units of pion mass (right panel) as function of baryon density n for fixed values of proton fraction n_p/n. The blue, orange and green curves correspond to $n_p/n = 0.1$, 0.3 and 0.5, respectively. The solid curves correspond to the numerical solution using the central value of $\sigma_{\pi N} = 45 \pm 15$ MeV, while the bands are obtained by the corresponding 1σ variation. The gray slashed region corresponds to $n > n_c \approx 2.8\, n_0$ where the quark condensate $\langle \bar{u}u \rangle_n$ changes sign (for the central value of $\sigma_{\pi N}$).*

Note this potential is similar to that discussed in Sec. 4.5 in the context of meson condensation, with the additional relevant feature of the density dependent quark condensates, in particular their decrease with density, $\zeta_{\bar{u}u} \approx \zeta_{\bar{d}d} \approx 1 - b_1(n/n_0)$. The three mass eigenstates, corresponding to mixtures of π_3, η and a, have the following masses in the isospin symmetric limit $\Delta m = 0$ and at leading order in θ and $\bar{m}/m_s$, [3]

$$(m^2_{\pi_0})_{n,\theta} \approx m^2_\pi\, \zeta_{\bar{u}u} \left[1 + \frac{1}{8}\left(\frac{2\mu^2}{m^2_\pi \zeta_{\bar{u}u}} - \frac{m_s}{\bar{m}}\right)\theta^2\right] , \tag{5.36}$$

$$(m^2_{\eta})_{n,\theta} \approx m^2_\eta \left[1 - \frac{1}{4}\left(1 + \frac{\zeta_{\bar{u}u}}{4}\right)\theta^2\right] , \tag{5.37}$$

$$(m^2_{a})_{n,\theta} \approx (m^2_a)_0\, \zeta_{\bar{u}u} \left[1 - \frac{1}{8}\left(1 + \frac{1}{\zeta_{\bar{u}u}}\right)\theta^2\right] . \tag{5.38}$$

with m_π and m_η the masses in vacuum, respectively Eq. (4.91) and $m^2_\eta = -4m_s\langle \bar{q}q \rangle_0 / 3f^2_\pi$ neglecting $O(m_{u,d}/m_s)$ terms. Note that only the neutral pion mass depends on the charge chemical potential, and that such dependence enters along with kaon condensation. The effect of a non-vanishing θ on $(m^2_{\pi_0})_{n,\theta}$ therefore depends on the relative size of $m_s/\bar{m} \approx 27$ and $2\mu^2/(m^2_\pi \zeta_{\bar{u}u})$, which enter with opposite signs. Note in this regard that while we use the leading order result for the quark condensate ratio $\zeta_{\bar{u}u}$, we did not perform an expansion in density. This is because, as we advanced at the beginning of this section and as explicitly shown in Fig. 5.1, when kaon condensation sets is we have $n/n_0 > 1$. Then, when $m_s/\bar{m} > 2\mu^2/m^2_\pi \zeta_{\bar{u}u}$, the coefficient of θ is negative and π_0 becomes lighter as kaon condensation sets in. Such a decrease could potentially lead to an instability and CP violation in the neutral sector. However, in the opposite case, when $m_s/\bar{m} < 2\mu^2/(m^2_\pi \zeta_{\bar{u}u})$, which occurs at larger densities where $\zeta_{\bar{u}u}$ is small and μ/m_π large (see Fig. 5.1), the coefficient of θ is positive and π_0 becomes heavier in the kaon-condensed phase. As opposed to the π_0, the η mass depends only weakly on θ. In Fig. 5.2 we plot the numerical result for $(m^2_{\pi_0})_{n,\theta}$ as a function of density for fixed values of

[3] The calculation of the axion mass is simplified by choosing a particular θ-dependent Q_a matrix which removes the tree-level mixing between the axion and π_0 and η, see App. 5.B for more details.

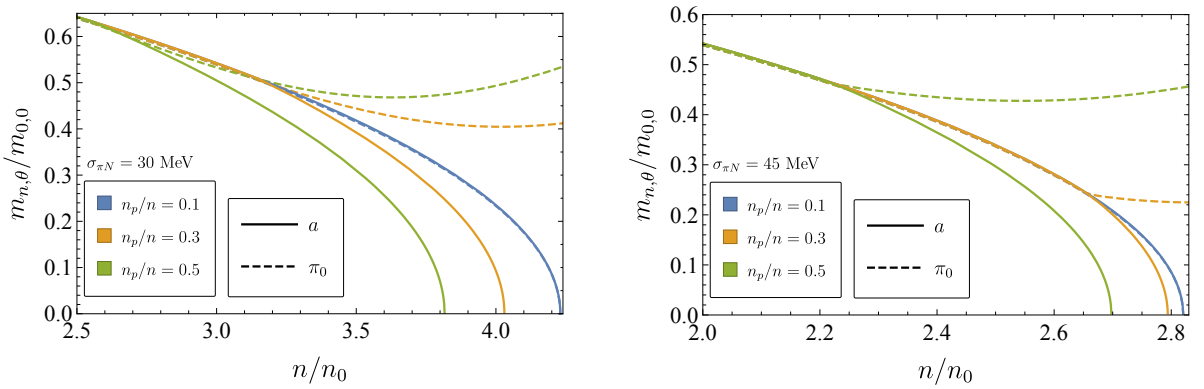

Figure 5.2: *Numerical result for the neutral pion (dashed line) and axion (solid line) masses normalized to their $n = \theta = 0$ values as a function of density n/n_0 for $\sigma_{\pi N} = 30$ MeV (left panel) and $\sigma_{\pi N} = 45$ MeV (right panel). The blue, orange and green curves correspond to fixed values of the proton fraction $n_p/n = 0.1, 0.3$ and 0.5, respectively. We consider densities in the region $n < n_c \equiv n_0/b_1 \approx 2.8 n_0\,(45\ \text{MeV}/\sigma_{\pi N})$ for the corresponding values of $\sigma_{\pi N}$. The effect of kaon condensation is to eventually increase the neutral pion mass, while the axion becomes lighter and even massless at some density below n_c. Above this density the axion field is therefore unstable around $\langle a \rangle = 0$ and axion condensation is expected to occur.*

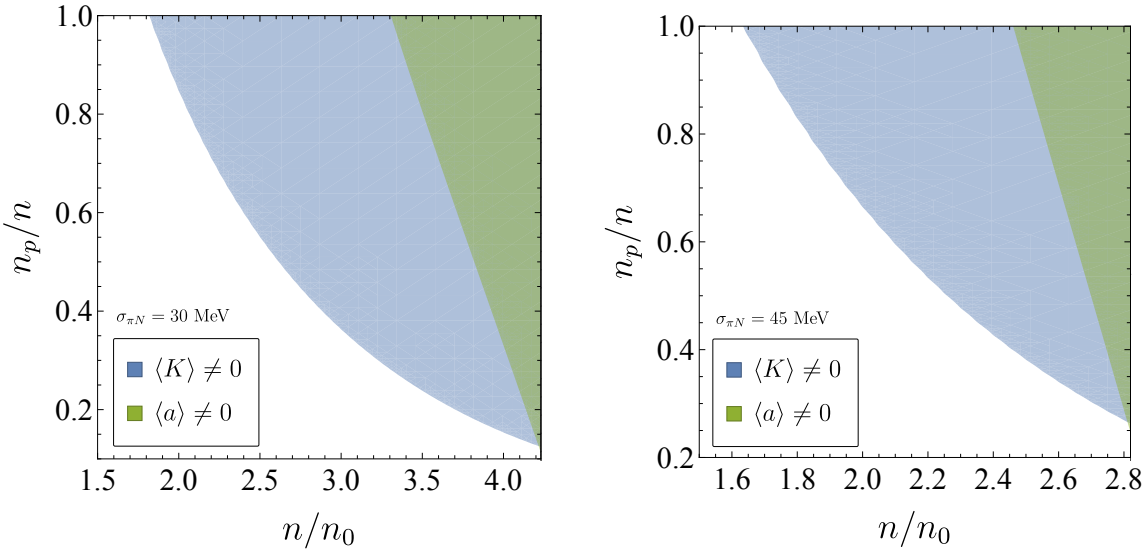

Figure 5.3: *Phase diagram in the plane of baryon density n/n_0 and proton fraction n_p/n based on the numerical solution of Eqs. (5.30) and (5.31) for $\sigma_{\pi N} = 30$ MeV (left panel) and $\sigma_{\pi N} = 45$ MeV (right panel). The blue region marks the kaon-condensed phase, while the green region marks the axion-condensed phase. We consider densities in the region $n < n_c$ for the corresponding values of $\sigma_{\pi N}$.*

proton fraction, using the numerical results for $\theta(n)$ and $\mu(n)$ displayed in Fig. 5.1. We find that the μ^2 contribution leads to an increase in the mass of the neutral pion, similar to the effect of pion condensation in the simplified case discussed in Sec. 4.5. Finally, the axion mass is independent of μ and decreases with the size of the kaon condensate. Interestingly, the negative coefficient of θ^2 is enhanced as density increases, since then $\zeta_{\bar{u}u}$ becomes smaller. As shown in Fig. 5.3, this behavior eventually results in axion condensation at large densities, yet before the quark condensate vanishes. In this phase CP is thus spontaneously broken in the neutral sector.

Lastly, we note that one should be wary of the fact that for the quark condensates we included only density corrections at linear order and disregarded higher order corrections. As discussed at the end of the previous section, for densities $n \sim n_c$, these corrections are in fact important. In this regard, we would like to stress the fact that while our results might not be trustable at the quantitative level, this does not necessarily make an axion-condensed phase less likely. First, let us note that qualitatively we expect $(m_a^2)_{n,\theta}$ to decrease with n even when considering higher-order corrections to $\zeta_{\bar{u}u}(n)$. Second, to further support our claim, let us consider the limit of maximal kaon condensation, i.e. $\theta \to \pi/2$, where

$$(m_a^2)_{n,\pi/2} \approx (m_a^2)_0(\zeta_{\bar{u}u} - \zeta_{\bar{s}s}) \approx -(m_a^2)_0\, b_1\, \frac{n}{n_0}\,. \tag{5.39}$$

If one ignores the density dependence of the condensates by taking $b_1 = 0$, this result is consistent with the naive expectation of a vanishing axion mass for $\cos\theta \to 0$, since $(m_a^2)_\theta \propto \mathrm{Tr}[\Sigma_0 + \Sigma_0^\dagger] \propto \cos\theta$, as we showed in Sec. 4.5. However, as discussed in Sec. 5.1, a background of protons and neutrons makes $\zeta_{\bar{u}u} < \zeta_{\bar{s}s} \approx 1$, in other words $b_1 > 0$, this implies a negative axion mass for large kaon condensates, where it becomes energetically favorable for the axion field to develop a non-vanishing expectation value.

5.3 Axion couplings

Let us now turn our attention to the couplings of the axion to QCD matter at finite density. These couplings are of special importance, as they are a crucial input in the astrophysical axion bounds [200], in particular regarding supernovae and neutron star cooling, see e.g. [229, 230, 231, 232] for recent works on the subject.

In vacuum

These coupling have been precisely calculated including RGE effects [14] and more recently at next-to-next-to-leading order in ChPT [233, 234]. We review here how the couplings to protons and neutrons are derived in ChPT, following closely the discussion in [14]. The relevant part of the low-energy effective Lagrangian for the isospin doublet $N = (p, n)^T$ in the non-relativistic approximation is given by

$$\mathcal{L}_{\pi N}^{(1)} \supset \bar{N} i v_\mu D^\mu N + g_A \bar{N} S^\mu u_\mu N + g_0^i \bar{N} S^\mu \hat{u}_\mu^i N + \dots\,, \tag{5.40}$$

where we omitted mass terms proportional to the axion-dependent quark mass matrix M_a, since there are no linear interactions coming from them if CP is preserved, see the discussion on CP violation at the end of this section. We also omitted higher-order terms in the expansion in (spatial) momenta, $k/\Lambda_\chi \sim k/M_B$. v_μ is the velocity of the non-relativistic fields, which satisfy $v_\mu \gamma^\mu N = N$, while S_μ is the spin operator, $\bar{N} S_\mu N = \frac{1}{2}\bar{N}\gamma_\mu\gamma_5 N = \frac{1}{2}\bar{N}(i\gamma_5\sigma_{\mu\nu}v^\nu)N$. D_μ is the usual covariant derivative of ChPT, $D_\mu N = (\partial_\mu + e_\mu)N$ with the chiral connection $e_\mu = \frac{1}{2}(\xi^\dagger\nabla_\mu\xi + \xi\nabla_\mu\xi^\dagger)$, while the vielbein is $u_\mu = i(\xi\nabla_\mu\xi^\dagger - \xi^\dagger\nabla_\mu\xi)$, where $\xi = \exp[i\pi^a\sigma^a/2f_\pi]$. Here we have introduced the derivative ∇_μ, which contains the external (isospin) axial and vector currents, i.e. $\nabla_\mu\xi = \partial_\mu\xi - i(V_\mu - A_\mu)\xi$ and $\nabla_\mu\xi^\dagger = \partial_\mu\xi^\dagger - i(V_\mu + A_\mu)\xi^\dagger$. [4] Finally, $\hat{u}_\mu^i$ is associated to the (isospin) axial scalar current, $\hat{u}_\mu^i = 2\hat{A}_\mu^i$, [5] where the index $i = (u + d, s)$ runs over iso-scalar quark combinations.

[4] We have also introduced the Goldstone matrix ξ, because when the QCD orientation is trivial, $\xi_L = \xi_R^\dagger = \xi$. Besides, note that in our convention u_μ is twice that used in [14], following the standard in the ChPT literature, see e.g. [235] (however, in this reference the roles of ξ and $\xi^\dagger$ are interchanged with respect to ours).

[5] In case the η' was light, then $\hat{u}_\mu^i \propto \partial_\mu\eta'$.

Because of its UV couplings to the axial currents made out of quarks, Eq. (4.88c), the axion enters Eq. (5.40) as an external axial current, with components in both the iso-vector and iso-scalar directions. Therefore, with the inclusion of the axion, one finds

$$u_\mu = \left(\frac{\partial_\mu \pi_i}{f_\pi}\right)\sigma_i + c_-^{\rm IR}\left(\frac{\partial_\mu a}{f_a}\right)\sigma_3 + O\left(\frac{\pi_i^2 \partial_\mu \pi_j}{f_\pi^3}\right), \tag{5.41}$$

$$\hat{u}_\mu = (c_+^{\rm IR}, c_s^{\rm IR})\left(\frac{\partial_\mu a}{f_a}\right) \tag{5.42}$$

with $c_\pm^{\rm IR} \equiv (c_u^{\rm IR} \pm c_d^{\rm IR})/2$ and where we have written $\hat{u}_\mu$ explicitly as a two-component vector. The couplings $c_{u,d,s}^{\rm IR}$ are related to the UV couplings by

$$c_q^{\rm IR} = C_{qq'}(c_{q'}^0 - [Q_a]_{q'})\,. \tag{5.43}$$

where the matrix $C_{qq'}$ accounts for renormalization group evolution (RGE) [14],

$$C_{qq'} = \begin{cases} 0.975 & q = q' \\ -0.024 & q \neq q' \end{cases}, \tag{5.44}$$

see [14] for a detailed derivation.

We recall from Sec. 4.3 that the c_q^0 are the UV model-dependent couplings of the axion to SM axial quark currents, while the matrix Q_a was introduced in order to remove the $aG\tilde{G}$ term. To further eliminate all axion-pion mixing, we chose a particular rotation matrix Q_a^*, which at zero density (denoted by the "0" subscript) is given by

$$(Q_a^*)_0 = \frac{\mathrm{Diag}[1, z, zw]}{1 + z + zw}\,, \tag{5.45}$$

with [236]

$$z \equiv \frac{m_u}{m_d} = 0.47^{+0.06}_{-0.07}\,, \quad w \equiv \frac{m_d}{m_s} = (17 - 22)^{-1}\,. \tag{5.46}$$

The coefficients g_A and g_0^i in Eq. (5.40) are given by linear combinations of hadronic matrix elements encoding the contribution of a quark q to the spin operator of the proton,

$$g_A = \Delta u - \Delta d\,, \quad g_0^i = (\Delta u + \Delta d, \Delta s)\,, \quad S^\mu \Delta q \equiv \langle p|\bar{q}\gamma^\mu\gamma^5 q|p\rangle\,. \tag{5.47}$$

The axial-vector coupling g_A have been precisely measured in β-decay experiments, while g_0^{ud} and Δs have been be extracted from lattice calculations, where in both cases isospin breaking effects are neglected. Their values at zero density are [236, 14]

$$(g_A)_0 = 1.2723(23)\,, \quad (g_0^{ud})_0 = 0.521(53)\,, \quad (\Delta s)_0 = -0.026(4)\,. \tag{5.48}$$

With this information, the couplings of the axion to nucleons,

$$\frac{\partial_\mu a}{f_a}\left(c_p\, \bar{p}\, S^\mu\, p + c_n\, \bar{n}\, S^\mu\, n\right) \tag{5.49}$$

can be finally extracted from the effective Lagrangian in Eq. (5.40),

$$c_p = +g_A c_-^{\rm IR} + g_0^{ud} c_+^{\rm IR} + \Delta s c_s^{\rm IR}\,, \tag{5.50}$$

$$c_n = -g_A c_-^{\rm IR} + g_0^{ud} c_+^{\rm IR} + \Delta s c_s^{\rm IR}\,. \tag{5.51}$$

This leads for instance to the accurate determination of the model-independent axion couplings, i.e. those of the KSVZ or hadronic axion [12, 13], for which $c_q^0 = 0$,

$$(c_p)_0^{\rm KSVZ} = -0.47(3)\,, \quad (c_n)_0^{\rm KSVZ} = -0.02(3)\,. \tag{5.52}$$

We note in particular that the axion coupling to neutrons in vacuum is suppressed with respect to the naive $O(1)$ expectation due to an accidental cancelation between $z = m_u/m_d \approx 1/2$ and the ratio of matrix elements in vacuum $\Delta u/\Delta d = (g_0^{ud} + g_A)/(g_0^{ud} - g_A) \approx -2$,

$$\left(\frac{c_n}{c_p}\right)_0^{\rm KSVZ} \propto \frac{1 + z(\Delta u/\Delta d)_0}{(\Delta u/\Delta d)_0 + z} \approx 7.6 \times 10^{-2}\,, \tag{5.53}$$

neglecting RGE and other subleading effects such as $m_{u,d}/m_s$ corrections. It is precisely this cancelation that makes c_n sensitive to small variations of the parameters. For example, RGE is naively an $O(10^{-2})$ effect according to Eq. (5.44) – however, because of the accidental cancelation of the axion-neutron coupling in the KSVZ model, it is in fact an $O(1)$ effect, $(c_n)_0^{\rm no\ RGE}/(c_n)_0 \approx 1.5$. As we will be showing in the following, finite density corrections also spoil the cancellation, leading in fact to a much larger effect.

In-medium mixing angles

The mixing angles with the neutral pions change at finite baryon density due to the change in the values of the quark condensates, as discussed in Sec. 5.1. The Q_a^* matrix that diagonalizes such mixings becomes therefore density dependent,

$$(Q_a^*)_n = \frac{\mathrm{Diag}[1, zZ, zZwW]}{1 + zZ + zZwW}\,, \tag{5.54}$$

where we defined

$$Z \equiv \frac{\langle \bar{u}u\rangle_n}{\langle \bar{d}d\rangle_n}\,, \quad W \equiv \frac{\langle \bar{d}d\rangle_n}{\langle \bar{s}s\rangle_n}\,. \tag{5.55}$$

Using Eq. (5.12) for the quark condensates at linear order in density, we find

$$Z = 1 - 2\,b_2 \frac{n - 2n_p}{n_0}\,, \quad W = 1 - \left[b_1 - b_2\left(1 - \frac{2n_p}{n}\right) - b_3\right]\frac{n}{n_0}\,, \tag{5.56}$$

where $b_{1,2,3}$ have been defined in terms of sigma terms in Eq. (5.13). Note that the deviation of Z from unity is small, being proportional to the anomalously small coefficient b_2, while the effects of W will be suppressed by $m_{u,d}/m_s$. However, similar to the RGE effects discussed above, the small density effect from Z gets amplified due to the cancellation structure of $(c_n)_0^{\rm KSVZ}$, while no large enhancement is expected in c_p. Indeed, one finds

$$(\Delta c_n)_n^{Z,W\neq 1}/(c_n)_0^{\rm KSVZ} \approx 40\%\,\frac{n - 2n_p}{n_0}\,, \tag{5.57}$$

$$(\Delta c_p)_n^{Z,W\neq 1}/(c_p)_0^{\rm KSVZ} \approx -2.5\%\,\frac{n - 2n_p}{n_0}\,. \tag{5.58}$$

Note that both the $O(1)$ correction to c_n and the $O(10^{-2})$ correction to c_p fall within the uncertainty range of the KSVZ axion couplings in vacuum given in Eq. (5.52).

In-medium matrix elements

The hadronic matrix elements Δu, Δd and Δs are also density dependent quantities in medium. In particular, the combination $g_A \equiv \Delta u - \Delta d$, which fixes the coupling of the pions to nucleons, is known to get quenched inside nucleons [237]. This was observed from the reduced rates for β-decay in various large nuclei [238], suggesting that in medium $(g_A)_{n_0/2}/(g_A)_0 \approx 0.75$, with $n_0/2$ being the typical baryon density around the surface of such large nuclei.

The in-medium change in the effective axial coupling can be derived from the following higher-order terms in the non-relativistic baryon chiral Lagrangian [239, 240] [6]

$$\mathcal{L}^{(2)}_{\pi N} \supset \frac{\hat{c}_3}{\Lambda_\chi}\bar{N}u^\mu u_\mu N + \left(\frac{\hat{c}_4}{\Lambda_\chi} + \frac{1}{4M}\right)\bar{N}\,[S^\mu, S^\nu]u_\mu u_\nu\, N\,, \tag{5.59}$$

$$\mathcal{L}^{(1)}_{\pi NN} \supset -\frac{c_D}{2f_\pi^2\Lambda_\chi}(\bar{N}N)(\bar{N}\,S^\mu u_\mu\, N)\,. \tag{5.60}$$

The density dependence of g_A was originally calculated in [241] and used recently to explain the apparent discrepancy in β-decay rates in large nuclei [242]. [7] It is given, at leading order in $n/\Lambda_\chi f_\pi^2$ (recall $\Lambda_\chi \sim M_B$), by

$$\frac{(g_A)_n}{(g_A)_0} = 1 + \frac{n}{\Lambda_\chi f_\pi^2}\left[\frac{c_D}{4(g_A)_0} - \frac{I(m_\pi/k_f)}{3}\left(2\hat{c}_4 - \hat{c}_3 + \frac{\Lambda_\chi}{2M_B}\right)\right]\,, \tag{5.61}$$

with

$$I(x) = 1 - 3x^2 + 3x^3\tan^{-1}\left(\frac{1}{x}\right)\,. \tag{5.62}$$

We identify two types of corrections. The terms proportional to $I(m_\pi/k_f)$ arise from (the resummation of) pion-exchange contributions originating in the operators in Eq. (5.59), where $k_f = (3\pi^2 n/2)^{1/3} \approx (270\text{ MeV})\,(n/n_0)^{1/3}$ and we took the limit of vanishing momentum carried by the pion (there is little variation if instead the Fermi gas average value $p_\pi^2 = 6k_f^2/5$ is taken). The contribution proportional to c_D comes instead from the contact term in Eq. (5.60), as it immediately follows from the mean field result $\langle\bar{N}N\rangle = n$. The values of the low energy couplings $\hat{c}_3$, $\hat{c}_4$ and c_D can be extracted from experiments. In this work we use the values provided in [242]

$$c_D = -0.85 \pm 2.15\,, \quad (2\hat{c}_4 - \hat{c}_3) = 9.1 \pm 1.4\,, \tag{5.63}$$

for $\Lambda_\chi = 700$ MeV. The finite density value of axial-vector coupling that follows from Eqs. (5.61) and (5.63) is then

$$\frac{(g_A)_n}{(g_A)_0} \approx 1 - (30 \pm 20)\%\,\frac{n}{n_0}\,. \tag{5.64}$$

Similar to g_A, higher-order operators in ChPT will give rise to a density dependent modification of $g_0^{ud} \equiv \Delta u + \Delta d$ and Δs,

$$\mathcal{L}^{(2)}_{\pi N} \supset \frac{\hat{c}_3^i}{\Lambda_\chi}\bar{N}u^\mu \hat{u}^i_\mu N + \frac{\hat{c}_4^i}{\Lambda_\chi}\bar{N}\,[S^\mu, S^\nu]u_\mu \hat{u}^i_\nu\, N\,, \tag{5.65}$$

$$\mathcal{L}^{(1)}_{\pi NN} \supset -\frac{c_D^i}{2f_\pi^2\Lambda_\chi}(\bar{N}N)(\bar{N}\,S^\mu \hat{u}^i_\mu\, N)\,, \tag{5.66}$$

[6] Note that in the literature these terms usually appear with dimensionful coefficients c_3 and c_4. Here we normalized them to the cutoff of ChPT, $c_i \equiv \hat{c}_i\Lambda_\chi$.

[7] This change in g_A does not only affect the axion but also neutrino dynamics in supernovae (see e.g. [243] for a review on neutrinos in supernovae), which would be interesting to explore.

from where one could derive, analogously to g_A, the density corrections from pion exchange or contact terms. We parametrize our ignorance about the density dependence of the axial-scalar coupling g_0^{ud} by defining κ,

$$\frac{(g_0^{ud})_n}{(g_0^{ud})_0} \equiv 1 + \kappa \frac{n}{n_0}\,, \tag{5.67}$$

and, in light of Eq. (5.64), we will consider the two benchmarks, $\kappa = \pm 0.3$, leading to in-medium quenching, as $(g_A)_n$, or enhancement. Besides, while we could use a similar parametrization for Δs, its contribution to the axion couplings to nucleons is already subleading, since $(\Delta s)_0 = O(10^{-2})$, thus we will neglect it in the following. We stress that it is certainly important to properly compute the density corrections to g_0^{ud} and Δs, a challenging task given the expected uncertainties that would be associated with the determination of the coefficients in Eqs. (5.65) and (5.66). We wish to point out however that we find no reason for the approximate relation $\Delta u/\Delta d \approx -1/z \approx -2$ to hold even if all the relevant finite density corrections are taken into account.

Combining both the finite density effects discussed above, let us write the density dependent axion-nucleon couplings as the obvious generlization of Eq. (5.51),

$$(c_p)_n = +(g_A)_n (c_-^{\rm IR})_n + (g_0^{ud})_n (c_+^{\rm IR})_n + (\Delta s)_n (c_s^{\rm IR})_n\,, \tag{5.68}$$

$$(c_n)_n = -(g_A)_n (c_-^{\rm IR})_n + (g_0^{ud})_n (c_+^{\rm IR})_n + (\Delta s)_n (c_s^{\rm IR})_n\,, \tag{5.69}$$

with

$$(c_q^{\rm IR})_n = C_{qq'} \left(c^0_{q'-} [(Q_a^*)_n]_{q'} \right)\,. \tag{5.70}$$

where we recall that, since $[(Q_a^*)_0]_q/[(Q_a^*)_n]_q \sim b_2(n/n_0) = O(10^{-2})$ for $q = u, d$, the main effect of a baryonic background comes via $(g_A)_n$ (as well as $(g_0^{ud})_n$), a change that affects any type of axion (something fully encoded in the coefficients $(c_\pm^{\rm IR})_n$).

To highlight the main point of this analysis, namely that the couplings of the axion to nucleons significantly change at finite density, we plot in Fig. 5.4 the ratio of the model-independent but density-dependent axion couplings to nucleons (including RGE), normalized to the vacuum values, as a function of n/n_0. As argued above, for such a hadronic axion the finite density effects are most striking, because the accidental suppression of the in-vacuum axion-neutron coupling is gone.

In the left panel, where we take κ positive, the $O(1)$ modification of $(g_A)_n$ and $(g_0^{ud})_n$ translates into an $O(10)$ enhancement of $(c_n)_n^{\rm KSVZ}$ at nuclear-saturation densities. In case of a negative κ, the ratio $\Delta u/\Delta d$ remains similar to its $n = 0$ value, and the accidental cancellation persists even after including in-medium effects leading only to $O(1)$ modification of c_n, although with large uncertainties. For the coupling to protons we find the opposite behaviour: for $\kappa > 0$ the increase in $(g_0^{ud})_n$ compensates for the decrease in $(g_A)_n$, such that the coupling is almost unchanged at saturation density. On the other hand, for $\kappa < 0$, both $(g^0)_n$ and $(g_0^{ud})_n$ decrease, which leads to an $O(1)$ decrease of c_p.

In kaon- and axion-condensed phases

Let us briefly comment on the couplings of the axion when this acquires a non-trivial background value, which is the most interesting potential consequence of kaon condensation. If $\langle a \rangle \neq 0$ in

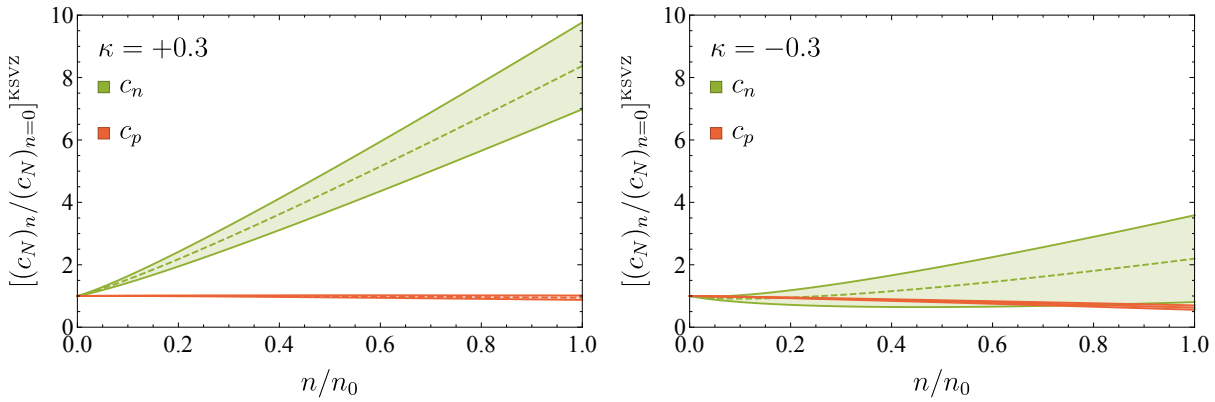

Figure 5.4: *The model-independent axion coupling to neutrons (protons) plotted in green (red) as a function of n/n_0. The couplings are normalized to the zero density values, Eq. (5.52). The bands represent the uncertainty in the couplings due to the coefficients in Eq. (5.63). The density dependence of g_0^{ud} is parameterized by κ, see Eq. (5.67). We consider two benchmark cases, $\kappa = +0.3$ (left panel) and $\kappa = -0.3$ (right panel).*

medium, CP is violated in the neutral scalar sector and the axion acquires scalar-like couplings to nucleons,

$$y_{a\bar{N}N}\, a\bar{N}N, \tag{5.71}$$

see e.g. [244, 245]. While the effects of these couplings certainly deserve further investigation, in particular in the context of dense systems such as neutron stars, we only wish to point out that they are proportional to the quark masses,

$$y_{a\bar{N}N} \sim \langle a\rangle\, \sigma_{\pi N}/f_a^2 \sim \langle a\rangle\, m_{u,d}/f_a^2, \tag{5.72}$$

since in the chiral limit the expectation value of the axion is not physical. [8]

5.A Baryon-ChPT with non-trivial vacuum alignment

We generalize the $N_f = 3$ chiral Lagrangian with baryons for a non-trivial ground state orientation, $\Sigma_0 \neq 1$ with $\Sigma_0^\dagger \Sigma_0 = \mathbb{1}_3$, e.g. in the kaon-condensed phase

$$\Sigma_0(\theta) = \begin{pmatrix} \cos\theta & 0 & i\sin\theta \\ 0 & 1 & 0 \\ i\sin\theta & 0 & \cos\theta \end{pmatrix}. \tag{5.73}$$

We denote $\Sigma_0(\theta/2) \equiv \xi_0(\theta)$ (such that $\xi_0^2 = \Sigma_0$) and drop for brevity the explicit θ-dependence. The standard $SU(3)_L \times SU(3)_R$ generators are given by the Gell-Mann matrices

$$T_L^a = \lambda^a\,, \quad T_R^a = \lambda^a\,. \tag{5.74}$$

It should be understood that the L and R operators act on different indices and therefore commute. We define the following rotated generators

$$(T_L^a)_\theta = \xi_0 (T_L^a) \xi_0^\dagger\,, \quad (T_R^a)_\theta = \xi_0^\dagger (T_R^a) \xi_0\,, \tag{5.75}$$

[8] Axion CP-violating (self-)interactions enable the axion to mediate forces between neutron stars as investigated in [209].

The broken and unbroken generators are given by

$$X^a = (T_L^a)_\theta - (T_R^a)_\theta\,, \quad T^a = (T_L^a)_\theta + (T_R^a)_\theta\,, \tag{5.76}$$

respectively. The fluctuation around the vacuum are parametrized by the Goldstone matrices

$$\xi_L = e^{i\frac{\pi^a}{2f_\pi}(T_L^a)_\theta} = \xi_0 \exp\left[\frac{i\pi^a\lambda^a}{2f_\pi}\right]\xi_0^\dagger\,, \quad \xi_R = e^{-i\frac{\pi^a}{2f_\pi}(T_R^a)_\theta} = \xi_0^\dagger \exp\left[-\frac{i\pi^a\lambda^a}{2f_\pi}\right]\xi_0\,, \tag{5.77}$$

with transformation properties

$$\xi_L \to L\xi_L V_\theta^\dagger\,, \quad \xi_R = R\xi_R V_\theta^\dagger\,, \tag{5.78}$$

with V_θ a NGB-dependent transformation under the unbroken $SU(3)$ subgroup of $SU(3)_L \times SU(3)_R$, the transformations under the latter denoted by L and R respectively. As usual, it is convenient to construct

$$\Sigma = \xi_L\Sigma_0\xi_R^\dagger = \xi_0 \exp\left[\frac{i\pi^a\lambda^a}{f_\pi}\right]\xi_0\,, \tag{5.79}$$

which transforms as $\Sigma \to L\Sigma R^\dagger$. Following standard notation,

$$\pi^a\lambda^a = \sqrt{2}\begin{pmatrix} \frac{\pi_0}{\sqrt{2}} + \frac{\eta}{\sqrt{6}} & \pi^+ & K^+ \\ \pi^- & -\frac{\pi_0}{\sqrt{2}} + \frac{\eta}{\sqrt{6}} & K_0 \\ K^- & \bar{K}_0 & -\sqrt{\frac{2}{3}}\eta \end{pmatrix}. \tag{5.80}$$

We introduce the (θ-rotated) baryon octet as linearly-transforming fields, $\hat{B}^\theta_{L,R}$,

$$\hat{B}_L^\theta \to L\hat{B}_L^\theta L^\dagger\,, \quad \hat{B}_R^\theta = R\hat{B}_R^\theta R^\dagger\,, \tag{5.81}$$

where we use the θ-superscript because the finite-density backgrounds we consider consist of a non-vanishing ensemble of the standard (non-rotated) baryons, given by

$$\hat{B}_L = \xi_0^\dagger\hat{B}_L^\theta\xi_0\,, \quad \hat{B}_R = \xi_0\hat{B}_R^\theta\xi_0^\dagger\,, \tag{5.82}$$

with the usual parameterization

$$B_{L,R} = \begin{pmatrix} \frac{\Sigma_0}{\sqrt{2}} + \frac{\Lambda}{\sqrt{6}} & \Sigma^+ & p \\ \Sigma^- & -\frac{\Sigma_0}{\sqrt{2}} + \frac{\Lambda}{\sqrt{6}} & n \\ \Xi^- & \Xi_0 & -\sqrt{\frac{2}{3}}\Lambda \end{pmatrix}_{L,R}. \tag{5.83}$$

The Lagrangian in this basis is given by

$$\mathcal{L} = \mathcal{L}_\Sigma^0 + \mathcal{L}_B^0 + \mathcal{L}_M + \mathcal{L}_\ell^0\,, \tag{5.84}$$

$$\mathcal{L}_\Sigma^0 = \frac{f_\pi^2}{4}\,\mathrm{Tr}[\partial_\mu\Sigma^\dagger\partial^\mu\Sigma]\,, \tag{5.85}$$

$$\mathcal{L}_B^0 = i\,\mathrm{Tr}[\bar{\hat{B}}_L^\theta\gamma^\mu\partial_\mu\hat{B}_L^\theta] + i\,\mathrm{Tr}[\bar{\hat{B}}_R^\theta\gamma^\mu\partial_\mu\hat{B}_R^\theta] - M_B\,\mathrm{Tr}[\bar{\hat{B}}_L^\theta\Sigma\hat{B}_R^\theta\Sigma^\dagger + \mathrm{h.c}]\,, \tag{5.86}$$

$$\begin{aligned}\mathcal{L}_M = &-\frac{\langle\bar{q}q\rangle_0}{2}\,\mathrm{Tr}[\Sigma^\dagger M] \\ &+ a_1\,\mathrm{Tr}[\bar{\hat{B}}_L^\theta M\hat{B}_R^\theta\Sigma^\dagger] + \bar{a}_1\,\mathrm{Tr}[\bar{\hat{B}}_R^\theta\Sigma^\dagger M\Sigma^\dagger\hat{B}_L^\theta\Sigma] \\ &+ a_2\,\mathrm{Tr}[\bar{\hat{B}}_R^\theta\Sigma^\dagger\hat{B}_L^\theta M] + \bar{a}_2\,\mathrm{Tr}[\bar{\hat{B}}_L^\theta\Sigma\hat{B}_R^\theta\Sigma^\dagger M\Sigma^\dagger] \\ &+ a_3\,\mathrm{Tr}[\bar{\hat{B}}_L^\theta\Sigma\hat{B}_R^\theta\Sigma^\dagger + \bar{\hat{B}}_R^\theta\Sigma^\dagger\hat{B}_L^\theta\Sigma]\,\mathrm{Tr}[\Sigma^\dagger M] + \mathrm{h.c}\,,\end{aligned} \tag{5.87}$$

$$\mathcal{L}_\ell^0 = \sum_{\ell=e,\mu}\bar{\ell}(i\gamma^\mu\partial_\mu - m_\ell)\ell\,. \tag{5.88}$$

where we recall the quark mass matrix spurion transforms as $M \to LMR^\dagger$, we dropped some terms at the same order in derivatives (acting on the Σ matrices) that are irrelevant for our discussion, and we included leptons.

5.A.1 Adding chemical potential

We add chemical potentials for the three mutually commuting abelian symmetries associated with neutron and proton numbers and electric charge (from here on we neglect the other baryons). Under $U(1)_{n,p}$, $\psi \to e^{i\alpha}\psi$ for $\psi = n, p$ respectively, while under $U(1)_{\rm EM}$ electromagnetism,

$$\hat{B}_{L,R} \to e^{i\alpha Q_e}\hat{B}_{L,R}e^{-i\alpha Q_e}\,, \quad \Sigma \to e^{i\alpha Q_e}\Sigma e^{-i\alpha Q_e}\,, \quad \ell \to e^{-i\alpha}\ell\,, \tag{5.89}$$

with

$$Q_e = \frac{1}{3}\begin{pmatrix} 2 & & \\ & -1 & \\ & & -1 \end{pmatrix}. \tag{5.90}$$

Chemical potentials are introducing following the prescription in Eq. (4.94), i.e. by modifying temporal derivatives as

$$\partial_0\Sigma \to \partial_0\Sigma + i[\hat{\mu}, \Sigma]\,, \tag{5.91}$$

$$\partial_0\hat{B}_{L,R} \to \partial_0\hat{B}_{L,R} + i[\hat{\mu}, \hat{B}_{L,R}] + i\hat{\mu}_{n,p}\hat{B}_{L,R}\,, \tag{5.92}$$

$$\partial_0\ell \to \partial_0\ell - i\mu\ell\,, \tag{5.93}$$

where we denoted

$$\hat{\mu} = \mu\, Q_e\,, \quad \hat{\mu}_{n,p} = \mathrm{Diag}[\mu_p - \mu, \mu_n, 0]\,. \tag{5.94}$$

We then get the following additional terms to the Lagrangian (5.84)

$$\mathcal{L}^\mu_\Sigma = \mathcal{L}^0_\Sigma + \frac{f_\pi^2}{4}\left(\mathrm{Tr}[2i\partial_0\Sigma[\hat{\mu}, \Sigma^\dagger]] - \mathrm{Tr}[[\hat{\mu}, \Sigma][\hat{\mu}, \Sigma^\dagger]]\right), \tag{5.95}$$

$$\begin{aligned}\mathcal{L}^\mu_B = \mathcal{L}^0_B &- \left(\mathrm{Tr}[\bar{\hat{B}}^\theta_L\gamma^0[\hat{\mu}, \hat{B}^\theta_L]] + \mathrm{Tr}[\bar{\hat{B}}^\theta_R\gamma^0[\hat{\mu}, \hat{B}^\theta_R]]\right)\\ &- \left(\mathrm{Tr}[\bar{\hat{B}}^\theta_L\gamma^0\hat{\mu}_{n,p}\hat{B}^\theta_L] + \mathrm{Tr}[\bar{\hat{B}}^\theta_R\gamma^0\hat{\mu}_{n,p}\hat{B}^\theta_R]\right),\end{aligned} \tag{5.96}$$

$$\mathcal{L}^\mu_\ell = \mathcal{L}^0_\ell + \mu\sum_{\ell=e,\mu}\bar{\ell}\gamma^0\ell\,. \tag{5.97}$$

5.A.2 Non-linear field basis

It is usually most convenient to work in a field basis for the baryons in which these only transform under the non-linearly realized unbroken $SU(3)$ subgroup of $SU(3)_L \times SU(3)_R$,

$$B^\theta_L \to V_\theta B^\theta_L V^\dagger_\theta\,, \quad B^\theta_R = V_\theta B^\theta_R V^\dagger_\theta\,, \tag{5.98}$$

with the dressed fields

$$B^\theta_R = \xi^\dagger_R\hat{B}^\theta_R\xi_R\,, \quad B^\theta_L = \xi^\dagger_L\hat{B}^\theta_L\xi_L\,. \tag{5.99}$$

In this basis there are no non-derivative interactions of the mesons with the baryons from the mass terms in Eq. (5.87). Besides, in complete analogy to Eq. (5.82), the standard (non-rotated) baryons are given by

$$B_L = \xi_0^\dagger B_L^\theta \xi_0 \,, \quad B_R = \xi_0 B_R^\theta \xi_0^\dagger \,. \tag{5.100}$$

In terms of such fields, which we recall make up the finite-density background, the baryon Lagrangian is given by

$$\mathcal{L}_B^\mu = i\,\mathrm{Tr}[\bar{B}\gamma^\mu D_\mu B] - M_B\,\mathrm{Tr}[\bar{B}B] - \mu\,\mathrm{Tr}[\bar{B}\gamma^0[\hat{Q}_e, B]] - \mathrm{Tr}[\bar{B}\gamma^0\hat{\mu}_{u,d}B]\,, \tag{5.101}$$

where the baryon covariant derivative is given by $D_\mu B = \partial_\mu B + [e_\mu, B]$, with

$$e_\mu \equiv \frac{1}{2}\left(\xi_0^\dagger (e_L)_\mu \xi_0 + \xi_0 (e_R)_\mu \xi_0^\dagger\right) \,, \quad (e_L)_\mu \equiv i\xi_L^\dagger \partial_\mu \xi_L \,, \;\; (e_R)_\mu \equiv i\xi_R^\dagger \partial_\mu \xi_R \,, \tag{5.102}$$

and

$$\hat{Q}_e \equiv \frac{1}{2}\left(\xi_0^\dagger \xi_L^\dagger Q_e \xi_L \xi_0 + \xi_0 \xi_R^\dagger Q_e \xi_R \xi_0^\dagger\right) \,, \tag{5.103}$$

reproducing Eq. (5.25). The part of the Lagragian proportional to the quark mass matrix reads

$$\begin{aligned}\mathcal{L}_M = &-\frac{\langle\bar{q}q\rangle_0}{2}\,\mathrm{Tr}[\hat{M}] + a_1\,\mathrm{Tr}[\bar{B}_L\hat{M}B_R] + \bar{a}_1\,\mathrm{Tr}[\bar{B}_R\hat{M}B_L] \\ &+ a_2\,\mathrm{Tr}[\bar{B}_R B_L\hat{M}] + \bar{a}_2\,\mathrm{Tr}[\bar{B}_L B_R\hat{M}] + a_3\,\mathrm{Tr}[\bar{B}_L B_R + \bar{B}_R B_L]\,\mathrm{Tr}[\hat{M}] + \mathrm{h.c}\,.\end{aligned}$$

where we defined the dressed mass matrix

$$\hat{M} \equiv \xi_0^\dagger \xi_L^\dagger M \xi_R \xi_0^\dagger \,, \tag{5.104}$$

as in Eq. (5.1). From $\mathcal{L}_M$ in this form it becomes apparent that the $L \leftrightarrow R$ exchange symmetry of QCD implies $a_{1,2} = \bar{a}_{1,2}$, which allows us to write

$$\mathcal{L}_M = -\frac{1}{2}\mathrm{Tr}[\langle\bar{q}q\rangle_n(\hat{M} + \hat{M}^\dagger)] \,, \tag{5.105}$$

$$\langle\bar{q}q\rangle_n \equiv \langle\bar{q}q\rangle_0 \mathbb{1}_3 - 2a_1 B\bar{B} - 2a_2\bar{B}B - 2a_3\,\mathrm{Tr}[\bar{B}B]\mathbb{1}_3 \,. \tag{5.106}$$

From this expression one can derive the density-dependent quark condensate of Eq. (5.12), since in the non-relativistic limit $\bar{B}B = \bar{B}\gamma_0 B$ and in the mean-field approximation we can treat the baryons as fixed classical background fields, thus

$$\bar{p}p = \bar{p}\gamma_0 p \to \langle\bar{p}\gamma_0 p\rangle = n_p \tag{5.107}$$

and likewise for the neutron. Besides, note that the baryon masses m_n and m_p are given in terms of $\{\sigma_{\pi N}, \tilde{\sigma}_{\pi N}, \sigma_s\}$ in Eqs. (5.10) and (5.11) respectively. One can then relate the coefficients $\{a_1, a_2, a_3\}$ of the baryon chiral Lagrangian to the sigma terms

$$\sigma_{\pi N} = -2\bar{m}(a_1 + 2a_3) \,, \tag{5.108}$$

$$\tilde{\sigma}_{\pi N} = 2\Delta m\, a_1 \,, \tag{5.109}$$

$$\sigma_s = -2m_s(a_2 + a_3) \,. \tag{5.110}$$

Finally, we recall that at zero temperature all the states with $E(p) = \sqrt{p^2 + m_\psi^2} < \mu_\psi$ are occupied, such that

$$n_\psi = \langle \bar{\psi}(x)\gamma_0\psi(x)\rangle = g_\psi \int_0^{E(p)<\mu_\psi} \frac{\mathrm{d}^3 p}{(2\pi)^3} = \frac{g_\psi}{6\pi^2}(\mu_\psi^2 - m_\psi^2)^{3/2}\,, \tag{5.111}$$

with g_ψ counting the internal degrees of freedom, e.g. $g_\psi = 2$ for a fermion. In Sec. 5.1 we fixed the values of $\{n, n_p\}$ by implicitly fixing the values of $\{\mu_p, \mu_n\}$

$$\mu_p = \sqrt{(3\pi^2 n_p)^{2/3} + m_p^2}\,, \tag{5.112}$$

$$\mu_n = \sqrt{(3\pi^2 n_n)^{2/3} + m_n^2}\,. \tag{5.113}$$

Note that one can fix $\{n, n_p\}$ while still keeping the charge chemical potential μ free by choosing the appropriate value of μ_p, namely if $\mu \to \mu + \delta\mu$, then $\mu_p \to \mu_p - \delta\mu$.

5.B Axion mass in Kaon-condensed phase

Tree-level mixing with the mesons in the kaon-condensed phase are removed when the matrix Q_a satisfies the following condition

$$\{\langle \bar{q}q\rangle_n, \xi_0 M Q_a \xi_0 + \xi_0^\dagger M Q_a \xi_0^\dagger\} \propto \mathbb{1}_3\,. \tag{5.114}$$

If $\mathrm{Re}(\Sigma_0)$ is a diagonal matrix, such that $[\mathrm{Re}(\Sigma_0), \langle \bar{q}q\rangle_n] = 0$, the Q_a matrix given by

$$(Q_a)_n^\theta = \frac{X_n^\theta}{\mathrm{Tr} X_n^\theta}\,, \quad X_n^\theta = M^{-1}\left(\xi_0 \frac{\langle \bar{q}q\rangle_n^{-1}}{\mathrm{Re}(\Sigma_0)}\xi_0^\dagger + \xi_0^\dagger \frac{\langle \bar{q}q\rangle_n^{-1}}{\mathrm{Re}(\Sigma_0)}\xi_0\right)\,, \tag{5.115}$$

satisfies 5.114. Plugging Eq. (5.115) in Eq. (5.1), we find the axion mass

$$(m_a^2)_{\theta,n} = -\frac{1}{2f_a^2}\mathrm{Tr}\left[\langle \bar{q}q\rangle_n \left(\xi_0 M (Q_a^\theta)^2 \xi_0 + \xi_0^\dagger M (Q_a^\theta)^2 \xi_0^\dagger\right)\right]\,. \tag{5.116}$$

6

CFL densities

In this chapter we make a jump to asymptotically large baryon densities, or equivalently large quark chemical potentials, $\mu_q \gg \Lambda_\chi$ ($\mu_q \equiv \mu_u = \mu_d = \mu_s$). At such high densities, two quark around the highly energetic Fermi surface interact weakly via tree-level gluon exchange, interactions which can be effectively parametrized below the Fermi momentum by 4-Fermi operators. Such operators, when in the attractive color $\bar{\mathbf{3}}$ channel, become relevant for back-to-back scattering as one approaches the Fermi surface (see e.g. [246, 247]), leading to the formation of diquark pairs and ultimately to color superconductivity [248, 249, 250, 251], see also [252] for a comprehensive review. Such a diquark pairing manifests itself in the form of a diquark condensate $\langle q_L C q_L \rangle$, which leads to the color-flavor-locked symmetry breaking pattern

$$SU(3)_c \times SU(N_f)_L \times SU(N_f)_R \times U(1)_B \times U(1)_A \to SU(N_f)_{L+R+c}\,. \tag{6.1}$$

The condensates are given by [252]

$$\langle q_L^{ia} C q_L^{jb} \rangle = \left(\epsilon^{abc}\epsilon^{ijk}\langle \Delta_L^{\bar{3}}\rangle_{kc} + \langle \Delta_L^{6}\rangle^{ij,ab}\right)\frac{3\sqrt{2}\pi}{g_s}\frac{\mu_q^2}{2\pi}\,, \tag{6.2}$$

$$\langle q_R^{\bar{i}a} C q_R^{\bar{j}b} \rangle = \left(\epsilon^{abc}\epsilon^{\bar{i}\bar{j}\bar{k}}\langle \Delta_R^{\bar{3}}\rangle_{\bar{k}c} + \langle \Delta_R^{6}\rangle^{\bar{i}\bar{j},ab}\right)\frac{3\sqrt{2}\pi}{g_s}\frac{\mu_q^2}{2\pi}\,, \tag{6.3}$$

where i, j, k are $SU(3)_L$ indices, $\bar{i}, \bar{j}, \bar{k}$ are $SU(3)_R$ indices, and a, b, c are $SU(3)_c$ indices, upper (lower) if in the (anti-)fundamental. The representations under the unbroken symmetries in (6.1) of the scalar field matrices above are

$$\Delta_L^{\bar{3}} : (\bar{\mathbf{3}}, \bar{\mathbf{3}}, \mathbf{1})_{+2,+2}\,, \quad \Delta_L^{6} : (\mathbf{6}, \mathbf{6}, \mathbf{1})_{+2,+2}\,, \tag{6.4}$$

$$\Delta_R^{\bar{3}} : (\bar{\mathbf{3}}, \mathbf{1}, \bar{\mathbf{3}})_{+2,-2}\,, \quad \Delta_R^{6} : (\mathbf{6}, \mathbf{1}, \mathbf{6})_{+2,-2}\,, \tag{6.5}$$

while their expectation values, proportional to the gap parameters Δ_3 and Δ_6, are

$$\langle \Delta_L^{\bar{3}}\rangle_{kc} = \delta_{kc}\Delta_3\,, \quad \langle \Delta_L^{6}\rangle^{ij,ab} = (\delta^{ia}\delta^{jb} + \delta^{ja}\delta^{ib})\Delta_6\,, \tag{6.6}$$

$$\langle \Delta_R^{\bar{3}}\rangle_{\bar{k}c} = -\delta_{\bar{k}c}\Delta_3\,, \quad \langle \Delta_R^{6}\rangle^{\bar{i}\bar{j},ab} = -(\delta^{\bar{i}a}\delta^{\bar{j}b} + \delta^{\bar{j}a}\delta^{\bar{i}b})\Delta_6\,. \tag{6.7}$$

We parametrize the low-energy fluctuations of the ground state, i.e. the NGBs associated with the symmetry breaking pattern (6.1) as

$$\Delta_L^{\bar{3}} = \xi_L^\dagger \langle \Delta_L^{\bar{3}} \rangle \exp\left[2i\left(\frac{\eta'}{f_{\eta'}} + \frac{H}{f_H}\right)\right], \tag{6.8}$$

$$\Delta_R^{\bar{3}} = \xi_R^\dagger \langle \Delta_R^{\bar{3}} \rangle \exp\left[2i\left(-\frac{\eta'}{f_{\eta'}} + \frac{H}{f_H}\right)\right], \tag{6.9}$$

$$\Delta_L^{6} = \xi_L^T \langle \Delta_L^{6} \rangle \xi_L \exp\left[2i\left(\frac{\eta'}{f_{\eta'}} + \frac{H}{f_H}\right)\right], \tag{6.10}$$

$$\Delta_R^{6} = \xi_R^T \langle \Delta_R^{6} \rangle \xi_R \exp\left[2i\left(-\frac{\eta'}{f_{\eta'}} + \frac{H}{f_H}\right)\right], \tag{6.11}$$

where

$$\xi_L = \xi_R^\dagger = \exp\left[\frac{i\pi^a \lambda^a}{2f_\pi}\right]. \tag{6.12}$$

The η' and H are the NGBs associated with the spontaneous breaking of $U(1)_A$ and $U(1)_B$, respectively. The NGBs associated with the breaking of color have been removed, since they are "eaten" by the gluons (unitary gauge). The rest of the NGBs, formally equivalent to those of the standard QCD chiral Lagrangian, are contained in the $\xi_{L,R}$ matrices, which are used to construct the following linearly-transforming color-neutral Goldstone matrix

$$\Sigma \equiv \xi_L \xi_R^\dagger : (\mathbf{1}, \mathbf{3}, \bar{\mathbf{3}})_{0,0}\,, \tag{6.13}$$

similarly as we did in vacuum, $\mu_q = 0$, see Sec. 4.3.

6.1 Kinetic terms

The kinetic terms in the CFL phase are given by

$$\mathcal{L}_{\text{kin.}}^{\text{CFL}} = \frac{f_\pi^2}{4}\eta_\Sigma^{\mu\nu}\text{Tr}[D_\mu \Sigma D_\nu \Sigma^\dagger] + \frac{1}{2}\eta_{\eta'}^{\mu\nu}\partial_\mu\eta'\partial_\nu\eta' + \frac{1}{2}\eta_H^{\mu\nu}\partial_\mu H \partial_\nu H\,, \tag{6.14}$$

with

$$\eta_\varphi^{\mu\nu} = \text{Diag}[1, -v_\varphi^2, -v_\varphi^2, -v_\varphi^2]\,, \quad \varphi = \Sigma, \eta', H\,. \tag{6.15}$$

We recall that the introduction of chemical potential breaks Lorentz symmetry down to spatial rotations, and the low-energy excitations, even if massless, propagate sub-luminally. These velocities, as well as the decay constants, can be calculated by matching the UV microscopic theory [253] to the effective low-energy theory [254, 255], [1]

$$f_\pi^2 = \frac{21 - 8\ln 2}{18}\frac{\mu_q^2}{2\pi^2}\,, \quad f_{\eta',H}^2 = 18\frac{\mu_q^2}{2\pi^2}\,, \quad v_{\Sigma,\eta',H}^2 = 1/3\,. \tag{6.16}$$

The Σ field gets a dynamically induced chemical potential due to the non-vanishing quark masses [257]

$$D_0\Sigma = \partial_0\Sigma + i\mu_L^{\text{eff}}\Sigma - i\Sigma\mu_R^{\text{eff}}\,, \tag{6.17}$$

[1] As mentioned above, the gluons, with electric and magnetic masses $m_D^2 = g_s^2 f_\pi^2$ and $m_M^2 = v_\varphi^2 m_D^2$ respectively, are heavy and integrated out [256].

with

$$\mu_L^{\text{eff}} = (\mu_R^{\text{eff}})^\dagger = \frac{MM^\dagger}{2\mu_q}\,. \tag{6.18}$$

Note that even if we choose a basis in which the axion enters the CFL effective Lagrangian via an axion-dependent quark mass matrix M_a, as in Eq. (4.88), it will not appear in such an effective chemical potential, since we can restrict ourselves to diagonal Q_a matrices. In any case, for the analysis of the axion potential in the CFL phase, it will be more convenient to work in a basis where the axion is coupled to gluons, since a perturbative instanton expansion exists, being the gluons heavy and weakly coupled.

6.2 Mass terms

Given the spurionic transformation properties of the quark mass M in Eq. (4.86), the leading order terms preserving the global symmetries in (6.1) are

$$V_M^{\text{CFL}} = A_1 \epsilon^{ijk}\epsilon_{\bar{i}\bar{j}\bar{k}} \left([\Delta_L^{\bar{3}\dagger}\Delta_R^{\bar{3}}]_i{}^{\bar{i}} M_j{}^{\bar{j}} M_k{}^{\bar{k}} + \text{h.c}\right) - \frac{A_2}{2}\left([\Delta_L^{6\dagger}\Delta_R^{6}]^{ij}_{\bar{i}\bar{j}} M_i{}^{\bar{i}} M_j{}^{\bar{j}} + \text{h.c}\right). \tag{6.19}$$

Note that this potential respects $U(1)_A$ and it is generated perturbatively. Contrary to QCD in vacuum, the axial symmetry thus dictates that the leading order terms in the scalar potential are $O(M^2)$. Using Eqs. (6.6) - (6.11) one finds [254] [2]

$$\begin{aligned} V_M^{\text{CFL}} =& -A_1\Delta_3^2\left[e^{-4i\eta'/f_{\eta'}}\left(\text{Tr}[\Sigma^\dagger M]\text{Tr}[\Sigma^\dagger M] - \text{Tr}[\Sigma^\dagger M\Sigma^\dagger M]\right) + \text{h.c}\right] \\ &+ A_2\Delta_6^2\left[e^{-4i\eta'/f_{\eta'}}\left(\text{Tr}[\Sigma^\dagger M]\text{Tr}[\Sigma^\dagger M] + \text{Tr}[\Sigma^\dagger M\Sigma^\dagger M]\right) + \text{h.c}\right]. \end{aligned} \tag{6.20}$$

The coefficients can be computed by appropriately matching to the UV theory [254, 255, 258],

$$A_1 = 2A_2 = \frac{3}{4\pi^2}\,. \tag{6.21}$$

Importantly, these two coefficients enter with opposite signs in Eq. (6.19). This is due to the fact that while the color $\bar{\mathbf{3}}$ channel is attractive and lowers the total energy of the system, the color $\mathbf{6}$ channel is repulsive and increases it. As a result, one finds that $\Delta_6 = 0$ at the classical level. However, since $\langle\Delta_{L,R}^6\rangle$ does not break any additional symmetries compared to $\langle\Delta_{L,R}^{\bar{3}}\rangle$, there is nothing preventing it from being generated at the quantum level in the presence of a non-vanishing Δ_3. Indeed, a perturbative calculation yields [259]

$$\Delta_6^2 = \alpha_s\frac{\ln^2 2}{162\pi}\Delta_3^2\,, \tag{6.22}$$

where $\alpha_s = g_s^2/4\pi$. Δ_3 itself can be calculated using the so-called gap equation, in particular in the CFL phase with $N_f = 3$ [252]

$$\Delta_3 = 512\pi^4(2/3)^{5/2}e^{-\frac{\pi^2+4}{8}}2^{-1/3}\,\frac{\mu_q}{g_s^5}\exp\left(-\frac{3\pi^2}{\sqrt{2}g_s}\right). \tag{6.23}$$

[2] The first term in Eq. (6.19) can also be written as $-2A_1\Delta_3^2(e^{4i\eta'/f_{\eta'}}\,\text{Tr}[\tilde{M}\Sigma] + \text{h.c})$, where $\tilde{M} = \det[M]M^{-1} = (\bar{m}m_s, \bar{m}m_s, \bar{m}^2)$.

The reason for considering the contribution of the condensate Δ_6 to the potential, even though it is suppressed with respect to Δ_3, comes from the hierarchy in the quark masses. Indeed, one finds e.g. contributions from both condensates to the masses of the mesons, of order [260],

$$\Delta_3 m_{u,d}^2 \sim \Delta_6 m_s^2 \,. \tag{6.24}$$

The similarity of these two contributions, along with the fact that the coefficients of the respective operators (in Eq. (6.21)) come with opposite signs, can lead to non-trivial vacuum structures, as we review below.

Finally, we note that although at $O(MM^\dagger)$ there exist other operators which could be considered along with those in Eq. (6.19), $\mathrm{Tr}[M\Sigma^\dagger M^\dagger \Sigma]$ and $\mathrm{Tr}[M\Sigma^\dagger]\,\mathrm{Tr}[M^\dagger\Sigma]$, these are not generated at the order we are interested in [254].

6.3 Non-perturbative terms

Instantons explicitly break the $U(1)$ axial symmetry of QCD, also in the CFL phase [261]. At leading order in the gap parameters, one finds the following term generated via a single t'-Hooft vertex

$$V_{\text{1-inst.}}^{\text{CFL}} = A_3 \left([\Delta_L^{\bar{3}\dagger} \Delta_R^{\bar{3}}]_i{}^{\bar{i}} [M^\dagger]^i{}_{\bar{i}} + \text{h.c} \right) = -A_3 \Delta_3^2 \,\mathrm{Tr}[e^{-4i\eta'/f_{\eta'}} \Sigma M^\dagger + \text{h.c}] \,. \tag{6.25}$$

The coefficient A_3 can be calculated reliably at large chemical potentials due to the screening of gluons for instantons of size $\rho \gtrsim 1/\mu_q \ll 1/\Lambda_{\text{QCD}}$, where $\Lambda_{\text{QCD}} \approx 250$ MeV is the QCD scale parameter,

$$A_3 = c\,(6\pi)^3 \,\frac{\Lambda_{\text{QCD}}^9}{3\alpha_s^7 \mu_q^8} \,, \tag{6.26}$$

with $c = 0.155$ [261, 252]. Given that the operator in Eq. (6.25) matches the leading term in the meson potential of the chiral Lagrangian at zero density, Eq. (4.89), its coefficient can be mapped to the value of the standard quark condensate in the CFL phase

$$\frac{\langle \bar{q}q \rangle_n^{\text{CFL}}}{\langle \bar{q}q \rangle_0} = \frac{A_3 \Delta_3^2}{\langle \bar{q}q \rangle_0} \sim 1 \times 10^{-5} \left(\frac{\Delta_3}{50 \text{ MeV}} \right)^2 \left(\frac{\pi}{\alpha_s} \right)^7 \left(\frac{500 \text{ MeV}}{\mu_q} \right)^8 \left(\frac{\Lambda_{\text{QCD}}}{250 \text{ MeV}} \right)^9 \,, \tag{6.27}$$

where we set the chemical potential to a value expected to be realized in the core of a NS, noting that α_s is to be evaluated at the scale μ_q and that Δ_3 depends on both α_s and μ_q. Due to the limited reliability of the perturbative result at such chemical potentials (see the discussion below), as well as to the strong dependence on Λ_{QCD}, it is clear that one cannot make a robust prediction regarding the value of the quark condensate at realistic densities, yet a strong suppression of $\langle \bar{q}q \rangle$ remains the most plausible outcome.

A higher-order operator that contributes to the mass of the η' in the chiral limit appears at the two-instanton level,

$$V_{\text{2-inst.}}^{\text{CFL}} = \frac{1}{\Lambda^2} \left(\det[\Delta_L^{\bar{3}\dagger} \Delta_R^{\bar{3}}] + \text{h.c} \right) = -\frac{2\Delta_3^6}{\Lambda^2} \cos\left(\frac{12\eta'}{f_{\eta'}} \right) \,. \tag{6.28}$$

Note this term matches the would-be leading potential for the standard η' in vacuum, see footnote 9.

Before moving to the discussion of the axion potential in the CFL phase, let us note that the matching procedure by which the coefficients of the effective CFL Lagrangian are extracted from the microscopic theory relies on perturbative calculations that have been found to be under control for $g_s \lesssim 0.8$ [262]. Such a small coupling corresponds to very high quark chemical potentials, $\mu_q \gtrsim 10^8$ MeV, which in turn implies baryon densities that are five orders of magnitude higher than those expected at the cores of dense NSs, where $\mu_q \sim 500$ MeV. Still, a quantitative but more importantly a qualitative understanding of the CFL phase and of the corresponding axion potential provides a solid ground from which to extrapolate to lower chemical potentials and thus to realistic densities. In fact, the qualitative features and basic symmetry structure of the CFL phase should hold down to $\mu \sim m_s^2/\Delta_3 \approx 180$ MeV $(50$ MeV$/\Delta_3)$ [252].

6.4 Axion potential

In view of the previous discussion, in the following we examine the different axion potentials that arise by considering different hierarchies between the coefficients of the CFL operators.

Non-perturbative dominance

In this case we assume that the non-perturbative contributions to the potential dominate over the mass terms, that is $V^{\rm CFL}_{\text{1-inst.}}, V^{\rm CFL}_{\text{2-inst.}} \gg V^{\rm CFL}_M$. Nevertheless, we still consider there exists a weak-coupling expansion, in the sense that the one-instanton contribution dominates over the two-instanton one, that is

$$e^{-S_I} \gg e^{-2S_I} \sim e^{-S_{II}}\,, \tag{6.29}$$

with S_I, S_{II} the action of the one- and two-instanton solutions, respectively. Given that the CFL operators in Eq. (6.19) are of order $V^{\rm CFL}_M \sim \bar{m} m_s \Delta_3^2$, where here and in the following we neglect $\Delta m = \frac{1}{2}(m_u - m_d)$, our hierarchy of potentials implies $\bar{m} A_3 \gg \Delta_3^4/\Lambda^2 \gg \bar{m} m_s$. In this case the potential, including the axion, reads

$$V^{\rm CFL}_{\text{1+2-inst.}} = -A_3 \Delta_3^2 \,\mathrm{Tr}[e^{i(a/f_a + 4\eta'/f_{\eta'})}\Sigma^\dagger M + \text{h.c}] + \frac{\Delta_3^6}{\Lambda^2}(e^{i(2a/f_a + 12\eta'/f_{\eta'})} + \text{h.c})\,. \tag{6.30}$$

After a field redefinition $\eta' \to \eta' - (f_{\eta'}/4f_a)a$, this is found to be the same as in the vacuum chiral Lagrangian with a light η', which is minimized at the trivial vacuum, $\langle \eta' \rangle = \langle a \rangle = 0$ in particular. The axion mass can be calculated by integrating out the mesons as we in zero density. The details of this derivation can be found in App. 6.A. We find that the axion mass is suppressed with respect to its vacuum value by

$$\frac{(m_a^2)^{\rm NP}_{\rm CFL}}{(m_a^2)_0} = \frac{8\Delta_3^6}{(m_\pi^2 f_\pi^2)_0 \Lambda^2} \sim 3 \times 10^{-3} \left(\frac{\Delta_3}{50\ \text{MeV}}\right)^6 \left(\frac{500\ \text{MeV}}{\Lambda}\right)^2\,. \tag{6.31}$$

Perturbative dominance

Let us now consider the hierarchy $V^{\rm CFL}_M \gg V^{\rm CFL}_{\text{1-inst.}} \gg V^{\rm CFL}_{\text{2-inst.}}$. One should first note that if the instanton terms are set to zero, the axion is massless, as can be immediately seen by using the basis defined by $Q_a = 0$ in Eq. (4.88); we use such a basis in the following. We write the potential in terms of the variables

$$\langle 4\eta'/f_{\eta'} \rangle \equiv \alpha\,, \quad \langle a/f_a \rangle \equiv \beta\,, \tag{6.32}$$

and use the ansatz [260]

$$\langle\Sigma\rangle = \mathrm{Diag}[e^{-i\varphi}, e^{-i\varphi}, e^{2i\varphi}] \begin{pmatrix} 1 & 0 & 0 \\ 0 & \cos\theta & i\sin\theta \\ 0 & i\sin\theta & \cos\theta \end{pmatrix} , \tag{6.33}$$

where the angles φ and θ correspond to the expectation values $\langle\eta/\sqrt{3}f_\pi\rangle$ and $\langle K_0/f_\pi\rangle$, respectively. In this basis the meson potential is given by

$$V^{\mathrm{CFL}}_{\mathrm{pert.,LO}} = -\frac{f_\pi^2 m_s^4}{8\mu_q^2}\sin^2\theta - 4A_1\Delta_3^2\bar{m}m_s(\cos\theta+1)\cos(\alpha-\varphi)\,, \tag{6.34a}$$

$$V^{\mathrm{CFL}}_{\mathrm{pert.,NLO}} = -4A_1\Delta_3^2\bar{m}^2\cos\theta\cos(\alpha+2\varphi) + 4A_2\Delta_6^2 m_s^2\cos^2\theta\cos(\alpha-4\varphi)\,, \tag{6.34b}$$

$$V^{\mathrm{CFL}}_{\text{1-inst.}} = -2A_3\Delta_3^2 m_s\cos\theta\cos(\alpha+\beta+2\varphi)\,. \tag{6.34c}$$

where we separated LO terms of $O(\bar{m}m_s\Delta_3^2)$, from NLO terms of $O(\bar{m}^2\Delta_3^2 \sim m_s^2\Delta_6^2)$, and instanton-generated terms. [3] Minizing the LO potential $V^{\mathrm{CFL}}_{\mathrm{pert.,LO}}$ with respect to φ and θ yields

$$\varphi = \alpha \tag{6.35}$$

$$\cos\theta = \mathrm{Min}\left[1, \frac{16A_1\Delta_3^2\bar{m}}{m_s^3}\left(\frac{\mu_q}{f_\pi}\right)^2\right] \tag{6.36}$$

The solution $\varphi = \alpha$ implies that the minimization of the NLO potential $V^{\mathrm{CFL}}_{\mathrm{pert.,NLO}}$ with respect to α is found at

$$\cos 3\alpha = \mathrm{Sign}[A_1\Delta_3^2\bar{m}^2 - A_2\Delta_6^2 m_s^2\cos\theta]\,. \tag{6.37}$$

Eqs. (6.36) and (6.37) match the the results of [260]. Lastly, the instanton potential is minimized with respect to β at

$$\cos\beta = \mathrm{Sign}\left[\cos(3\alpha)\right]\,. \tag{6.38}$$

Therefore, one finds that the the axion is aligned with the η', such that

$$\langle a/f_a\rangle = \begin{cases} 0\,, & A_1\Delta_3^2\bar{m}^2 > A_2\Delta_6^2 m_s^2\cos\theta \\ \pi\,, & A_1\Delta_3^2\bar{m}^2 < A_2\Delta_6^2 m_s^2\cos\theta \end{cases}\,, \tag{6.39}$$

while the axion mass, neglecting mixing with η' and normalized to its vacuum value, is given by

$$\frac{(m_a^2)_{\mathrm{CFL}}}{(m_a^2)_0} = \frac{8A_3\Delta_3^2 m_s\cos\theta}{(m_\pi^2 f_\pi^2)_0} \sim 7\times10^{-4}\left(\frac{\Delta_3}{50\text{ MeV}}\right)^2\left(\frac{A_3}{4\times10^{-4}\text{ MeV}}\right)\left(\frac{\cos\theta}{1}\right)\,. \tag{6.40}$$

where we evaluated A_3 in Eq. (6.26) at $\mu_q = 1$GeV, $\Lambda_{\mathrm{QCD}} = 250$ MeV and $\alpha_s = \pi$. We therefore find that the axion can develop a non-vanishing expectation value in the CFL phase also, when the kaon condensate is large. Up to uncertainties associated with the value of A_3, the axion is significantly lighter than in vacuum.

[3] We should note at this point that we did not include the neutral pion π_0 in our analysis because the corresponding first term in Eq. (6.34a), which destabilizes the potential at the origin of field space for K^0, vanishes for π_0.

6.A Axion mass calculation with instantons

We calculate the axion mass by integrating out the neutral pions $\{\pi_0, \eta, \eta'\}$ in the $N_f = 3$ chiral Lagrangian, from the potential

$$V_0 = b(\mathrm{Tr}[\Sigma^\dagger M] + \mathrm{h.c}) - c(e^{-i(a/f_a + \eta'/f_{\eta'})} + \mathrm{h.c})\,, \tag{6.41}$$

where in vacuum b is given in Eq. (4.90) and effectively $c \to \infty$, while $b = -A_3\Delta_3^2$ and $c = \Delta_3^6/\Lambda^2$ in the CFL phase when instantons dominate. Note that the η' is normalized differently in the CFL phase. This procedure produces the correct leading order result for the axion mass but neglects (some of) the subleading corrections. In the generic basis of Eq. (4.88), the potential then reads

$$\begin{aligned} V =& 2bm_u \cos\left(\frac{Q_u a}{f_a} - \frac{\frac{\eta}{\sqrt{3}} + \pi_0}{f_\pi} - \frac{\eta'}{3f_{\eta'}}\right) + 2bm_d \cos\left(\frac{Q_d a}{f_a} + \frac{\pi_0 - \frac{\eta}{\sqrt{3}}}{f_\pi} - \frac{\eta'}{3f_{\eta'}}\right) \\ &+ 2bm_s \cos\left(\frac{Q_s a}{f_a} + \frac{2\eta}{\sqrt{3}f_\pi} - \frac{\eta'}{3f_{\eta'}}\right) - 2c\cos\left(\frac{\eta'}{f_{\eta'}} - \frac{(\mathrm{Tr}[Q_a] - 1)\, a}{f_a}\right), \end{aligned} \tag{6.42}$$

with $Q_a = \mathrm{Diag}[Q_u, Q_d, Q_s]$. We integrate π_0 out by using its equation of motion at linear order in the fields

$$\pi_0 = \frac{(m_u Q_u - m_d Q_d)}{(m_d + m_u)}\left(\frac{f_\pi}{f_a} a\right) + \frac{(m_d - m_u)}{3\,(m_d + m_u)}\left(\sqrt{3}\eta + \frac{f_\pi}{f_{\eta'}}\eta'\right). \tag{6.43}$$

Next we similarly integrate η out

$$\begin{aligned} \eta =& \frac{\sqrt{3}\,(-m_d m_s Q_s + m_d m_u\,(Q_d + Q_u) - m_s m_u Q_s)}{2\,(m_d m_s + m_u m_d + m_s m_u)}\left(\frac{f_\pi}{f_a} a\right) \\ &+ \frac{(m_d\,(m_s - 2m_u) + m_s m_u)}{2\sqrt{3}\,(m_d m_s + m_u m_d + m_s m_u)}\left(\frac{f_\pi}{f_{\eta'}}\eta'\right). \end{aligned} \tag{6.44}$$

Finally, we integrate out η'

$$\eta' = \frac{-bm_d m_s m_u \mathrm{Tr}[Q_a] + c\,(m_d m_s + m_u m_d + m_s m_u)\,(\mathrm{Tr}[Q_a] - 1)}{-bm_d m_s m_u + c\,(m_d m_s + m_u m_d + m_s m_u)}\left(\frac{f_{\eta'}}{f_a} a\right). \tag{6.45}$$

The potential is minimized around $\langle a\rangle = \langle \pi_0\rangle = \langle \eta\rangle = \langle \eta'\rangle = 0$ and we find the following axion mass

$$m_a^2 = \frac{-2bc\, m_u m_d}{f_a^2 (m_u + m_d)\left(c\left[1 + \frac{m_u m_d}{m_s(m_u + m_d)}\right] - b\left[\frac{m_d m_u}{m_u + m_d}\right]\right)}. \tag{6.46}$$

Once we have diagonalized the mass matrix, one could be concerned with the effect of the $O(f_\pi/f_a)$ kinetic mixing which is generically induced by the derivative couplings of the axion. Let us explictly show that this does not affect the leading order results for the axion mass. Our starting point, without loss of generality, is the following Lagrangian

$$\mathcal{L} = \frac{1}{2} m_\pi^2 \begin{pmatrix} \vec{\pi} & a \end{pmatrix} \begin{pmatrix} b & 0 \\ 0 & c\xi^2 \end{pmatrix} \begin{pmatrix} \vec{\pi} \\ a \end{pmatrix} + \frac{1}{2} \begin{pmatrix} \partial_\mu \vec{\pi} & \partial_\mu a \end{pmatrix} \begin{pmatrix} 1 & \xi \vec{d} \\ \xi \vec{d}^{\,T} & 1 \end{pmatrix} \begin{pmatrix} \partial^\mu \vec{\pi} \\ \partial^\mu a \end{pmatrix}, \tag{6.47}$$

where $b = \text{Diag}[b_1, .., b_n]$ is an $n \times n$ diagonal matrix of $O(1)$ numbers, $\vec{d}$ is a vector of n $O(1)$ numbers, c is an $O(1)$ number, and $\xi \equiv f_\pi / f_a$ is our expansion parameter. Let start by performing the orthogonal rotation R_1 in the meson subspace, such that

$$R_1 \vec{d} = (0, \dots, |d|). \tag{6.48}$$

We rewrite the Lagrangian in this basis

$$\begin{aligned}\mathcal{L} =& \frac{1}{2} m_\pi^2 \begin{pmatrix} \vec{\pi} & a \end{pmatrix} \begin{pmatrix} R_1 b R_1^T & 0 \\ 0 & c\xi^2 \end{pmatrix} \begin{pmatrix} \vec{\pi} \\ a \end{pmatrix} \\ &+ \frac{1}{2} \begin{pmatrix} \partial_\mu \pi_1 & ... & \partial_\mu \pi_n & \partial_\mu a \end{pmatrix} \begin{pmatrix} 1 & & & \\ & \ddots & & \\ & & 1 & |d|\xi \\ & & |d|\xi & 1 \end{pmatrix} \begin{pmatrix} \partial^\mu \pi_1 \\ \vdots \\ \partial^\mu \pi_n \\ \partial^\mu a \end{pmatrix} . \end{aligned} \tag{6.49}$$

We diagonalize and canonically normalize the lower 2×2 block in the second term by rotating and rescaling the fields

$$\begin{pmatrix} \pi_n \\ a \end{pmatrix} = \underbrace{\frac{1}{\sqrt{2}} \begin{pmatrix} 1 & 1 \\ -1 & 1 \end{pmatrix}}_{\equiv R_2} \underbrace{\begin{pmatrix} \frac{1}{\sqrt{1-|d|\xi}} & 0 \\ 0 & \frac{1}{\sqrt{1+|d|\xi}} \end{pmatrix}}_{\equiv T} \begin{pmatrix} \bar{\pi}_n \\ \bar{a} \end{pmatrix} . \tag{6.50}$$

Our mass matrix in the new basis now reads

$$m_\pi^2 T R_2^T \begin{pmatrix} [R_1 b R_1^T]_{nn} & 0 \\ 0 & c\xi^2 \end{pmatrix} R_2 T \, . \tag{6.51}$$

T can be expanded $T = \mathbb{1} + \frac{1}{2}|d|\xi\sigma_3 + O(\xi^2)$. At leading order $T = \mathbb{1}$ and the mass matrix can be re-diagonalized by performing the inverse orthogonal rotation R_2^{-1}, bringing it back to the diagonal form of Eq. (6.47). One concludes that the axion mass does not receive any leading order correction due to the kinetic mixing.

7

Observables

We briefly discuss in this section the potentially observable consequences of a non-vanishing axion condensate in NSs, where the largest baryonic densities among the stars are found. We defer to future work a more in-depth analysis of the corresponding phenomenology [226], as well as the study of the implications of the change in the axion-nucleon couplings with density, the latter particularly relevant for supernovae and NS cooling.

For simplicity, let us consider the following toy model, namely a stepwise radius-dependent axion potential

$$V(a,r) = \begin{cases} f_a^2 (m_a^2)_{\rm in} \left[\cos(a/f_a) - 1\right] & r < r_c \\ -f_a^2 (m_a^2)_{\rm out} \left[\cos(a/f_a) - 1\right] & r > r_c \end{cases}, \quad f_a^2 (m_a^2)_{\rm out} \sim m_\pi^2 f_\pi^2 \,, \tag{7.1}$$

where m_π and f_π are the vacuum values and we have fixed the constants such that in the decoupling limit $f_a \to \infty$, the potential vanishes. The potential grossly captures the effect of matter on the axion potential, i.e. at a critical radius r_c, which is of the order of the NS radius R, the axion field gets destabilized and the minimum of the potential is located at $\langle a/f_a \rangle = \pi$. The field equation can be solved numerically and one finds the intuitive result based on energy conservation, i.e. for the axion to get sourced the gain in potential energy needs to be enough to compensate for the gradient energy that comes with the change in field value, $\Delta V \sim (\Delta a/R)^2$, which occurs when the object is large enough compared to the de Broglie wavelength of the field inside the object [209], namely

$$(m_a)_{\rm in}^{-1} \lesssim r_c \sim R \,. \tag{7.2}$$

Let us assume this is the case for the rest of the discussion, keeping in mind that the axion mass decreases with baryon density and that in vacuum $(m_a)_{\rm out}^{-1} \sim 16\,{\rm km}\,(f_a/10^{18}{\rm GeV})$. The typical field configuration of the sourced axion is roughly

$$\frac{a(r)}{\pi f_a} = \begin{cases} 1 \,, & r < r_c \\ \frac{r_c}{r} e^{-(m_a)_{\rm out}(r - r_c)} \,, & r > r_c \end{cases} . \tag{7.3}$$

In Fig. 7.1 we depict the typical field configurations of the axion sourcing, highlighting in grey the possible observable implication, to be discussed in turn below.

7.1 Free (vacuum) energy

The first potentially observable implication is associated with the shift in potential energy density inside the NS,

$$\Delta V \sim -2 f_a^2 (m_a^2)_{\rm in}, \tag{7.4}$$

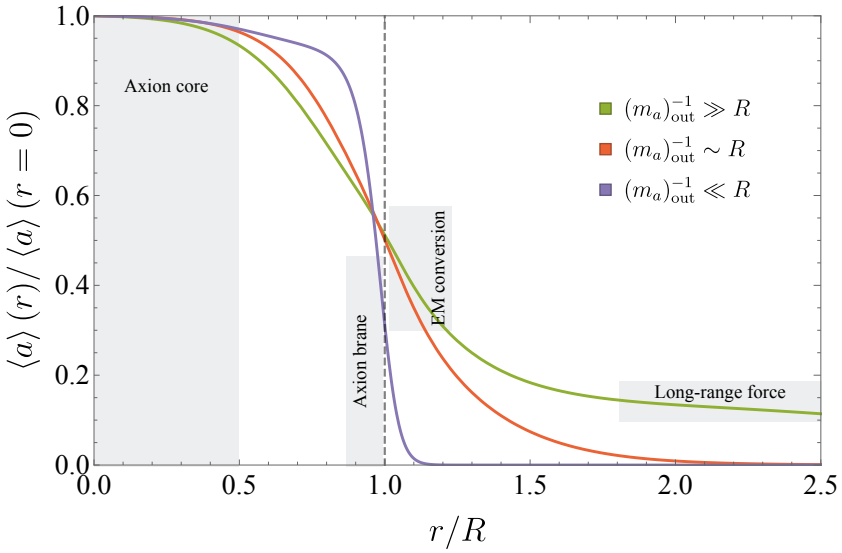

Figure 7.1: *Sketch of the typical field configurations of a sourced axion field, see the discussion in the main text.*

as a result of the axion sourcing. This effect is independent of the field configuration outside the core of the NS, namely it is independent of $(m_a^2)_{\rm out}$. Such an energy density shift can be of considerable size compared to the energy density inside a NS, $\rho_0 \approx m_n n_0 \approx (190\ \text{MeV})^4$. Indeed, if the axion is sourced at relatively low baryon densities, as in the kaon condensed phase (Sec. 5.2), one expects $\Delta V \sim m_\pi^2 f_\pi^2$, which is indeed not significantly below ρ_0 or the energy change due to kaon condensation, of $O(m_K^2 f_\pi^2)$. Instead, if axion sourcing happens in the CFL phase (Sec. 6), this effect is expected to be suppressed by a few orders of magnitude, see Eq. (6.40), and therefore likely negligible.

A NS with a core of "vacuum energy" was considered as a generic scenario in [263, 264], in the context of exotic QCD phases. It was found that the energy shift inside the NS leads to a significant change in the mass-radius relation of NSs, as well as to changes of the so-called chirp mass, one of main the gravitational wave observables of compact binary mergers. One could then, in a similar fashion, consider axion condensation as a possible source for such a potential energy shift.

7.2 Axion brane

Another interesting implication of axion condensation concerns the generation of a brane of energy density inside the NS. In particular, if the condition

$$(m_a)^{-1}_{\rm out} \ll R\,, \tag{7.5}$$

is met, the exponentially suppression of the axion field outside the NS is very rapid, a change that contributes to the energy density of the system in the form of a gradient energy

$$(\vec{\nabla} a)^2 \sim \left(\frac{\Delta a}{\Delta r}\right)^2 \sim f_a^2 (m_a)^2_{\rm out} \sim m_\pi^2 f_\pi^2\,. \tag{7.6}$$

One can think of such an abrupt change in field values as a localized (spherical) brane of energy density. The effect of such a brane has in fact not been considered in previous studies of NS

structure. Such a brane would appear as an effective discontinuity in the temporal and radial components of the metric, which because of Einstein's field equations (known as the Tolman-Oppenheimer-Volkoff equations), imply a discontinuity in the pressure and enclosed mass of the star.

7.3 Axion-EM conversion

Next we consider the interplay between the EM fields of rotating NSs (i.e. pulsars), which are the strongest found in the Universe, and the axion, in particular when

$$(m_a)^{-1}_{\rm out} \gtrsim R\,, \tag{7.7}$$

such that the sourced axion field is still non-negligible in the close surroundings of the NS.

The axion and the classical EM fields form a coupled system, as seen from the generalized form of the Maxwell equations

$$\vec{\nabla}\cdot\mathbf{E} = g_{a\gamma\gamma}\,\mathbf{B}\cdot(\vec{\nabla}a)\,, \tag{7.8a}$$

$$\vec{\nabla}\times\mathbf{B} = \frac{\partial\mathbf{E}}{\partial t} + g_{a\gamma\gamma}\left[\mathbf{E}\times\vec{\nabla}a - \mathbf{B}\dot{a}\right]\,, \tag{7.8b}$$

$$\Box a = g_{a\gamma\gamma}(\mathbf{E}\cdot\mathbf{B}) - \frac{\partial V}{\partial a} = g_{a\gamma\gamma}(\mathbf{E}\cdot\mathbf{B}) - (m_a^2)_{\rm out}a + O(a^2)\,, \tag{7.8c}$$

where the last line is the axion equation of motion. The interplay between the axion and the EM field of pulsars has been actively investigated before, see e.g. [265, 266, 267, 268] for recent works on the subject, although the effects we consider here, associated with a large classical axion field configuration also sourced by the NS, are novel. Assuming the conventional rotating dipole model, one finds that at the surface of the NS

$$B_{\rm dipole}(R) \sim B_* \sim 10^{14}\,{\rm G} \sim \ {\rm MeV}^2\,, \tag{7.9}$$

$$E_{\rm dipole}(R) \sim R\Omega B_* \sim 10^{-3}\left(\frac{R}{10\,{\rm km}}\right)\left(\frac{\Omega}{100\,{\rm Hz}}\right)B_*\,, \tag{7.10}$$

with Ω the angular velocity of the NS. Even with such large EM fields, we may still neglect the effects of the axion-photon coupling on the axion dynamics, since

$$\frac{g_{a\gamma\gamma}(\mathbf{E}\cdot\mathbf{B})}{(m_a^2)_{\rm out}\langle a(R)\rangle} \sim \frac{\alpha_{\rm EM}R\Omega B_*^2}{m_\pi^2 f_\pi^2} \sim 10^{-13}\left(\frac{R}{10\,{\rm km}}\right)\left(\frac{\Omega}{100\,{\rm Hz}}\right)\left(\frac{B_*}{10^{14}\,{\rm G}}\right)^2\,, \tag{7.11}$$

where we used $(m_a^2)_{\rm out} \sim m_\pi^2(f_\pi/f_a)^2$, $\langle a(R)\rangle \sim f_a$ and $g_{a\gamma\gamma} \sim \alpha_{\rm EM}/f_a$. While we can safely assume that the back-reaction of the EM fields on the axion is negligible, it is also important to note that the value of $\langle a(R)\rangle$ decreases exponentially outside the NS, see Eq. (7.3), such that one could well imagine a situation where the effect of the $g_{a\gamma\gamma}(\mathbf{E}\cdot\mathbf{B})$ term is in fact comparable to the axion mass term. In this case the back-reaction of the EM fields would have to be taken into account, which is beyond the scope of this work.

We thus treat the axion field as a rigid source of additional EM fields, which can be simply estimated as

$$\Delta E \sim g_{a\gamma\gamma}B_*\langle a(R)\rangle \sim \alpha_{\rm EM}B_*\,, \tag{7.12}$$

$$\Delta B \sim g_{a\gamma\gamma}R\Omega B_*\langle a(R)\rangle \sim \alpha_{\rm EM}R\Omega B_*\,. \tag{7.13}$$

While the magnetic field receives a small correction $\Delta B/B \sim \alpha_{\rm EM} R\Omega \ll 1$, for the electric field

$$\frac{\Delta E}{E} \sim \frac{\alpha_{\rm EM}}{R\Omega} \sim 2\left(\frac{10\,\text{km}}{R}\right)\left(\frac{100\,\text{Hz}}{\Omega}\right), \tag{7.14}$$

thus leading to an $O(1)$ enhancement around the surface of the NS. We note that since this correction is large, one could be concerned about whether the system can be treated perturbatively. This is in fact the case, since the higher order terms scale like

$$E \sim R\Omega B_*(1+\alpha_{\rm EM}^2+\dots)+\alpha_{\rm EM}B_*(1+\alpha_{\rm EM}^2+\dots). \tag{7.15}$$

This means that, apart from the leading $O(\alpha_{\rm EM}B_*)$ correction, further contributions are subleading.

An additional sensitive observable is the dipole radiation output P that is responsible for the spin-down of rotating NSs. In this case we find that $\Delta P/P \sim \alpha_{\rm EM}^2 \ll 1$, namely there is no appreciable addition to the radiated energy due to the axion field.

7.4 Long-range force

Lastly, we can consider the case

$$(m_a)_{\rm out}^{-1} \gg R\,, \tag{7.16}$$

even though we note that from our previous analysis of the QCD axion at finite density, we expect this regime not to be realized since $(m_a)_{\rm out}^{-1} \lesssim (m_a)_{\rm in}^{-1} \lesssim R$, where the last condition follows from the requirement of the axion being actually sourced, Eq. (7.2). Therefore we expect the hierarchy $(m_a)_{\rm in}^{-1} \lesssim R \ll (m_a)_{\rm out}^{-1}$ to arise only in non-standard scenarios, such as the one considered in [209]. If that is indeed the case, the long tails of the axion field configuration lead to a long range force between the NSs, generated by the Yukawa-like potential

$$V \sim \frac{Q_{\rm eff}}{r} e^{-(m_a)_{\rm out} r}\,, \tag{7.17}$$

where $Q_{\rm eff} = 4\pi f_a R$ plays the role of the effective charge. This could lead to a deformation of the merger wave-form predicted by general relativity in case of NS with opposite-sign charges. A more dramatic effect would be found in the case of a repulsive force from same-sign charges, since in this case at some critical distance the axion force would dominate gravity, which could lead to halt in the merger process [209]. The presence of the axion field can also lead to an additional mechanism of energy loss in NS mergers, in the form of the scalar equivalent of Larmor radiation [269].

Part IV

Conclusions

In this thesis, we studied the phenomenology of Goldstone bosons which appear in well-motivated extension of the standard model. In particular, in Part II we studied realizations of composite dark matter in non-minimal composite Higgs models. These models offer a solution to the hierarchy problem and contain compelling dark matter candidates. Generically, non-renormalizable interactions play an important role in the phenomenology of composite dark matter [73]. In particular, we saw that the annihilation cross section at the early universe is sensitive both to the normal Higgs portal coupling, as well as to a *derivative* portal coupling. The latter is an irreducible feature of dark matter in this paradigm, which arises due to the self-interactions among the Higgs and the dark matter, both of which are realized as Nambu-Goldstone bosons of a spontaneously broken global symmetry.

We first study in Chapter 2 the phenomenology of composite dark matter within a minimal extension of Little Higgs with T-Parity, which consistently realizes the *collective breaking* mechanism without introducing massless fermions. Importantly, the shift symmetry of the singlet dark matter is broken by the its couplings to the top quark. Although the scalar potential is not calculable, some conservative assumptions can be made. In particular, in light of the IR contribution to the portal couplings, it seems likely that the expected portal coupling λ is of the same order as the Higgs quartic $\lambda_h \sim O(0.1)$, putting this model within reach of present direct detection experiments. The model can evade direct detection only by allowing the portal coupling to be much smaller than its expected value, possibly due to some cancellation with the UV contributions. Depending on the UV completion, this cancellation can be a consequence of fine tuning or due to some symmetry which protects the portal coupling.

We are able to test our conclusion from the previous model in an extension of the minimal composite Higgs, the $SO(7)/SO(6)$ model which was the focus of Chapter 3. The first scenario in Sec. 3.3 represents a similar setup, where the dark matter shift symmetry is broken by its coupling with the top quark. The $SO(7)/SO(6)$ model can be partially UV completed by the introduction of resonances, and the implementation of the so-called Weinberg sum rules renders the scalar potential finite and calculable. The model which contains a single layer of resonances turns out the be extremely predictive, with $\lambda \sim \lambda_h/2$ and $m_\chi \sim m_h/2$, which is ruled out by direct detection. By introducing a second layer of resonances, the model has the freedom to deviate from the 1-layer case. As expected, a large deviation that allows $m_\chi \gg m_h$ and $\lambda \ll \lambda_h$ is achieved at the price of some additional tuning. The irreducible tuning of $2\xi \sim 6\%$ (due to LHC bounds requiring $f \geq 1.4$ TeV) must be lowered to $\sim 1\%$ in order to produce a model which evades current direct detection bounds.

The additional tuning can be avoided if the suppression of the portal coupling is actually a result of a symmetry, namely the dark matter shift symmetry. By making the explicit breaking of the DM less severe, the portal coupling is naturally expected to become suppressed. Interestingly, as discussed in Sec. 3.1, if the portal coupling is negligible, the correct relic abundance is produced due to the derivative interactions with the natural values of $f \sim 1$ TeV and $m_\chi \sim 100$ GeV. This type of dark matter is extremely hard to detect in direct detection experiments, since the scattering cross section scales with $|t|/f^2 \sim (100\text{ MeV})^2/(1\text{ TeV}) \sim 10^{-8}$, with t the usual Mandelstam variable. Thus, it seems that a model in which $\lambda \ll \lambda_h$ is also theoretically appealing.

We studied two scenarios in which the suppression above naturally occurs. In Sec. 3.4 the dark matter shift symmetry is broken only by the (smaller) bottom Yukawa. The portal coupling is negligible in this case, $\lambda \propto y_b^2$, and the direct detection cross section, now dominated by the

contact terms $|\chi|^2\bar{b}b$, is expected to be within reach of direct detection experiments in the near future. A second and perhaps more appealing possibility is explored in Sec. 3.5, where the shift symmetry is broken only by the weak gauging of $U(1)_{\rm DM}$. Using a gauged symmetry as a stabilizing symmetry (assuming it is not spontaneously broken) is a robust stabilizing mechanism; it avoids some of the pitfalls of global stabilizing symmetries, i.e. additional sources of explicit symmetry breaking, both at the classical level and at the quantum level. In this scenario, the portal coupling vanishes at 1 loop due to a collective breaking mechanism. Since the coupling to SM fermions respect the dark matter shift symmetry, the contact terms are absent as well, making the direct detection cross section extremely suppressed.

The dark sector, containing a complex scalar and a dark photon, can only be probed indirectly. If the dark photon is massless, the annihilation cross section of dark matter to SM particles in dense objects, like galaxies, is enhanced due to the Sommerfeld effect, potentially excluding a large part of the parameter space due to indirect detection bounds. As a cross check, the effect of a dark photon can be probed also at the cosmological scale using the CMB indirect measurement of the relativistic degree of freedom $\Delta N_{\rm eff}$. We find that the next generation of CBM measurements will have the required sensitivity to probe the contribution of this dark photon to the energy of the universe. If the dark photon is massive, we find that it can comprise some of the dark matter in the region or parameter space where it is stable. Indirect detection via dark matter annihilation in galaxies remains, in the case of a massive dark photon, the main prospect for future detection of dark matter.

The collider phenomenology of composite Higgs models was examined in the various model and scenarios presented above. Generically, the colored top partners (or more generally, resonances) can be singly produced through weak processes or doubly produced through strong processes. The latter production mechanism is the only mechanism relevant for the resonances charged under the dark matter stabilizing symmetry. Current dedicated LHC searches, as well as recasting SUSY searches with similar signatures as a result or R-Parity, put a lower bound on the masses of the colored fermionic resonances at the TeV scale. Sensitivity is expected to increase in the future as the production cross sections become larger. Another interesting aspect is the possibility of probing the derivative interaction between the Higgs and the dark matter through an off-shell Higgs in future colliders [270].

Composite Higgs model are well-motivated frameworks which allows for the exploration of non-minimal dark matter scenarios. After a systematic exploration of the various shift breaking sources, we found a compelling non-minimal scenario where dark matter interacts only derivatively with the Higgs. Such dark matter can be consistent with the measured present-day abundance, as well as with the fact that dark matter has not yet been directly detected. Near future experiments will be able to probe some of its parameter space.

In Part III we studied the properties of the QCD axion at finite density. The axion is a prediction of the Peccei-Quinn mechanism designed to solve the strong CP problem. The axion emerges as the Goldstone boson of a spontaneously broken and anomalous $U(1)$ symmetry. The axion effectively serves as a dynamical θ angle, whose value is set to 0 due to instanton induced potential in vacuum. In Sec. 5 we investigate the properties of the axion is nuclear matter composed of neutrons and protons. We used the perturbative description given by chiral perturbation theory to single out two sources of density dependence for the axion potential in the nuclear phase. First, we discuss the effect of the quark condensates

$\langle\bar{q}q\rangle$, which are density dependent, in Sec. 5.1. Using the so-called linear approximation for $\langle\bar{q}q\rangle_n$, one generically finds that chiral symmetry is restored around $(2-3)n_0$, which in turn implies the axion becomes massless. However, it is well known that the linear approximation, which neglects the nuclear interactions, breaks down at around n_0. Using existing state of the art calculations of $\langle\bar{q}q\rangle$, one finds that the axion experiences a mild reduction of mass inside nuclear medium, namely $(m_a)^2_{n\lesssim 2n_0} \gtrsim 0.6\,(m_a)^2_0$. The second effect we considered in Sec. 5.2 is the onset of kaon condensation, equivalent to the reorientation of the QCD ground state in medium. This condensation is predicted to appear at higher densities, $(3-5)n_0$, where the perturbative description is no longer valid, limiting the discussion to a qualitative one. We find that the combination of the kaon condensation and the reduction of the quark condensate leads to a destabilization of the axion field around the origin, even before the naive restoration of chiral symmetry occurs. This could lead to a sourcing of the axion field by a large dense object like a neutron star. The discussion on the observable effects of such sourcing is postponed to Sec. 7.

We also examined the couplings of the axion the nucleons in dense nuclear matter. These are particularly important due to experimental bounds on the axion derived from the cooling of SN1987A. The cooling process occurs in the dense collapsed core and depends directly on these couplings. The couplings are in general density dependent, due to the density dependence of the axion-pion mixing angles and the hadronic matrix elements. The former can be calculated within perturbation theory, while the latter must be deduced from experiment. In particular, according to experiment one combination of matrix elements $g_A \equiv \Delta u - \Delta d$ appears to be quenched in large nuclei. After taking all these effects into consideration, we find that generically the in medium couplings receive at least $O(1)$ corrections in medium. A large correction may appear if the orthogonal linear combination $g_0^{ud} \equiv \Delta u + \Delta d$ increases in high densities. In this case, the accidental cancelation of the axion coupling to neutrons in vacuum is spoiled in medium, which could lead to an $O(10)$ enhancement of the coupling.

Next we considered the axion in the color superconducting phase, also known as the color-flavor locking (CFL) phase. This phase of matter is hypothesized to appears at very large densities, and a perturbative description is applicable for densities above $(10-100)n_0$. The densities reached in the core of a neutron star is expected to be $(3-6)n_0$, but phenomenological models suggest that some of the qualitative features of the CFL phase remain in these densities as well. After reviewing the various terms present in this phase in Secs. 6.1-6.3, we examine the axion potential in the CFL phase in Sec. 6.4. We considered two possible scenarios. In the first, the non-perturbative terms dominate over the perturbatively generated terms. In this case, the form of the potential is similar to that in vacuum, with the exception that due to the weak coupling, the perturbative expansion in number of instantons is assumed to be valid. One can than calculate the axion mass and find that it is much smaller compared to its vacuum value by a factor of $\sim 10^{-3}$. In the second scenario we assumed that the non-perturbative terms are negligible. In this case, it has already been shown that an η' condensate may occur under certain circumstances. However, as we show, in the presence of the suppressed non-perturbative effects the η' and the axion unavoidably mix. Thus, an η' condensation would trigger an axion condensation, i.e. it would destabilize the axion around the origin.

Interestingly, we find that in both the nuclear and CFL phase, there is a mechanism which could lead to the destabilization of the axion around the origin. If the size of the region in which the axion is destabilized is comparable to the Compton wave length of the axion, it can be sourced by the object e.g. a neutron star. We briefly review the potential observables effects of such a sourc-

ing in Sec. 7. In particular we consider the effect of vacuum energy inside (Sec. 7.1), the gradient energy which can appear as a thin brane (Sec. 7.1), the interplay between the axion and the strong electromagnetic fields outside the neutron star (Sec. 7.3) and lastly we mention the scenario in which the axion sourcing leads to long range forces (Sec. 7.4). The latter scenario is however less likely in our minimal setup, since we predict that the Compton wave length outside the object is smaller than inside, such that the range of the force is at most the size of the object itself.

The study of the in medium properties of the axion is an exciting and largely uncharted territory, and there are many directions for future research. On the theoretical side, one can hope to try and describe the axion in the densities of interest, namely $(2-6)n_0$, using phenomenological models e.g. the Nambu-Jona-Lasinio (NJL) model. Another compelling direction is the application of this study to other new particles which couple to QCD, e.g. the relaxion. Lastly, the possible observable implications of an axion sourcing in a neutron star deserves a careful examination. We expect to learn a great deal about the local properties of neutron stars through their collisions, which are already observable in gravitational wave detectors, with more events expected in the next generation of gravitational wave experiments.

Acknowledgements

I am very grateful to my supervisor, Andreas Weiler, for allowing me to pursue my interests in physics in the last 4.5 years and for his supportive mentorship. The professional and personal guidance he provided through the countless hours of discussions, whether in the office or over a bowl of spicy soup, was invaluable and helped me become a better physicist. His enthusiastic attitude was a constant source of inspiration.

As the first member of T75, I am honored to have had the privilege of watching the group form over the years and become an active research group. I had the pleasure of collaborating over the years with Ennio Salvioni, Javi Serra, Max Ruhdorfer, Stefan Stelzl and Konstantin Springmann. I would like to thank them and all the past and present members of the group for the fantastic atmosphere which allowed all of us to do what we love and have fun in the process.

I thank my parents, Asia and Lev, for 33 years of unrelenting support. They gave me the opportunity, the tools and the values which allowed me to reach this point and realize my potential. I thank my sister Dana for her help and guidance through the years.

Last but not least, I would like to thank my wife Tal. You were there before physics, and you were always there for me for the last ten years. Through all the hard times, I could always rely on you and you never failed to give with your unconditional love and support. I could not have asked for a better partner in life and a better mother to our children Nevo and Tavor. I love you all.

Bibliography

[1] Georges Aad et al. "Observation of a new particle in the search for the Standard Model Higgs boson with the ATLAS detector at the LHC". In: *Phys. Lett.* B716 (2012), pp. 1–29. DOI: 10.1016/j.physletb.2012.08.020. arXiv: 1207.7214 [hep-ex].

[2] Serguei Chatrchyan et al. "Observation of a New Boson at a Mass of 125 GeV with the CMS Experiment at the LHC". In: *Phys. Lett. B* 716 (2012), pp. 30–61. DOI: 10.1016/j.physletb.2012.08.021. arXiv: 1207.7235 [hep-ex].

[3] Benjamin W. Lee, C. Quigg, and H.B. Thacker. "The Strength of Weak Interactions at Very High-Energies and the Higgs Boson Mass". In: *Phys. Rev. Lett.* 38 (1977), pp. 883–885. DOI: 10.1103/PhysRevLett.38.883.

[4] Benjamin W. Lee, C. Quigg, and H.B. Thacker. "Weak Interactions at Very High-Energies: The Role of the Higgs Boson Mass". In: *Phys. Rev. D* 16 (1977), p. 1519. DOI: 10.1103/PhysRevD.16.1519.

[5] Sidney R. Coleman, J. Wess, and Bruno Zumino. "Structure of phenomenological Lagrangians. 1." In: *Phys. Rev.* 177 (1969), pp. 2239–2247. DOI: 10.1103/PhysRev.177.2239.

[6] Curtis G. Callan Jr., Sidney R. Coleman, J. Wess, and Bruno Zumino. "Structure of phenomenological Lagrangians. 2." In: *Phys. Rev.* 177 (1969), pp. 2247–2250. DOI: 10.1103/PhysRev.177.2247.

[7] R. D. Peccei and Helen R. Quinn. "CP Conservation in the Presence of Instantons". In: *Phys. Rev. Lett.* 38 (1977). [,328(1977)], pp. 1440–1443. DOI: 10.1103/PhysRevLett.38.1440.

[8] Steven Weinberg. "A New Light Boson?" In: *Phys. Rev. Lett.* 40 (1978), pp. 223–226. DOI: 10.1103/PhysRevLett.40.223.

[9] Frank Wilczek. "Problem of Strong P and T Invariance in the Presence of Instantons". In: *Phys. Rev. Lett.* 40 (1978), pp. 279–282. DOI: 10.1103/PhysRevLett.40.279.

[10] Michael Dine, Willy Fischler, and Mark Srednicki. "A Simple Solution to the Strong CP Problem with a Harmless Axion". In: *Phys. Lett.* 104B (1981), pp. 199–202. DOI: 10.1016/0370-2693(81)90590-6.

[11] A. R. Zhitnitsky. "On Possible Suppression of the Axion Hadron Interactions. (In Russian)". In: *Sov. J. Nucl. Phys.* 31 (1980). [Yad. Fiz.31,497(1980)], p. 260.

[12] Jihn E. Kim. "Weak Interaction Singlet and Strong CP Invariance". In: *Phys. Rev. Lett.* 43 (1979), p. 103. DOI: 10.1103/PhysRevLett.43.103.

[13] Mikhail A. Shifman, A. I. Vainshtein, and Valentin I. Zakharov. "Can Confinement Ensure Natural CP Invariance of Strong Interactions?" In: *Nucl. Phys.* B166 (1980), pp. 493–506. DOI: 10.1016/0550-3213(80)90209-6.

[14] Giovanni Grilli di Cortona, Edward Hardy, Javier Pardo Vega, and Giovanni Villadoro. "The QCD axion, precisely". In: *JHEP* 01 (2016), p. 034. DOI: 10.1007/JHEP01(2016)034. arXiv: 1511.02867 [hep-ph].

[15] Georg Raffelt and David Seckel. “Bounds on Exotic Particle Interactions from SN 1987a”. In: *Phys. Rev. Lett.* 60 (1988), p. 1793. DOI: 10.1103/PhysRevLett.60.1793.

[16] Reuven Balkin, Gilad Perez, and Andreas Weiler. “Little composite dark matter”. In: *Eur. Phys. J. C* 78.2 (2018), p. 104. DOI: 10.1140/epjc/s10052-018-5552-3. arXiv: 1707.09980 [hep-ph].

[17] Reuven Balkin, Maximilian Ruhdorfer, Ennio Salvioni, and Andreas Weiler. “Charged Composite Scalar Dark Matter”. In: *JHEP* 11 (2017), p. 094. DOI: 10.1007/JHEP11(2017)094. arXiv: 1707.07685 [hep-ph].

[18] Reuven Balkin, Maximilian Ruhdorfer, Ennio Salvioni, and Andreas Weiler. “Dark matter shifts away from direct detection”. In: *JCAP* 11 (2018), p. 050. DOI: 10.1088/1475-7516/2018/11/050. arXiv: 1809.09106 [hep-ph].

[19] Reuven Balkin, Javi Serra, Konstantin Springmann, and Andreas Weiler. “The QCD axion at finite density”. In: *JHEP* 07 (2020), p. 221. DOI: 10.1007/JHEP07(2020)221. arXiv: 2003.04903 [hep-ph].

[20] M. Tanabashi et al. “"Tests of Conservation Laws" in Review of Particle Physics”. In: *Phys. Rev. D* 98.3 (2018), p. 030001. DOI: 10.1103/PhysRevD.98.030001.

[21] V. Agrawal, Stephen M. Barr, John F. Donoghue, and D. Seckel. “Viable range of the mass scale of the standard model”. In: *Phys. Rev. D* 57 (1998), pp. 5480–5492. DOI: 10.1103/PhysRevD.57.5480. arXiv: hep-ph/9707380.

[22] Lawrence J. Hall and Yasunori Nomura. “Evidence for the Multiverse in the Standard Model and Beyond”. In: *Phys. Rev. D* 78 (2008), p. 035001. DOI: 10.1103/PhysRevD.78.035001. arXiv: 0712.2454 [hep-ph].

[23] S.M. Barr and Almas Khan. “Anthropic tuning of the weak scale and of m(u) / m(d) in two-Higgs-doublet models”. In: *Phys. Rev. D* 76 (2007), p. 045002. DOI: 10.1103/PhysRevD.76.045002. arXiv: hep-ph/0703219.

[24] Steven Weinberg. “Anthropic Bound on the Cosmological Constant”. In: *Phys. Rev. Lett.* 59 (1987), p. 2607. DOI: 10.1103/PhysRevLett.59.2607.

[25] Peter W. Graham, David E. Kaplan, and Surjeet Rajendran. “Cosmological Relaxation of the Electroweak Scale”. In: *Phys. Rev. Lett.* 115.22 (2015), p. 221801. DOI: 10.1103/PhysRevLett.115.221801. arXiv: 1504.07551 [hep-ph].

[26] Stephen P. Martin. “A Supersymmetry primer”. In: (1997). [Adv. Ser. Direct. High Energy Phys.18,1(1998)]. DOI: 10.1142/9789812839657_0001,10.1142/9789814307505_0001. arXiv: hep-ph/9709356 [hep-ph].

[27] Howard Georgi and A. Pais. “Vacuum Symmetry and the PseudoGoldstone Phenomenon”. In: *Phys. Rev.* D12 (1975), p. 508. DOI: 10.1103/PhysRevD.12.508.

[28] David B. Kaplan and Howard Georgi. “SU(2) x U(1) Breaking by Vacuum Misalignment”. In: *Phys. Lett.* B136 (1984), p. 183. DOI: 10.1016/0370-2693(84)91177-8.

[29] Giuliano Panico and Andrea Wulzer. “The Composite Nambu-Goldstone Higgs”. In: (2015). arXiv: 1506.01961 [hep-ph].

[30] Sidney R. Coleman and Erick J. Weinberg. “Radiative Corrections as the Origin of Spontaneous Symmetry Breaking”. In: *Phys. Rev.* D7 (1973), pp. 1888–1910. DOI: 10.1103/PhysRevD.7.1888.

[31] Kenneth D. Lane. "An Introduction to technicolor". In: *Theoretical Advanced Study Institute (TASI 93) in Elementary Particle Physics: The Building Blocks of Creation - From Microfermius to Megaparsecs*. June 1993, pp. 381–408. DOI: 10.1142/9789814503785_0010. arXiv: hep-ph/9401324.

[32] N. Arkani-Hamed, A. G. Cohen, E. Katz, and A. E. Nelson. "The Littlest Higgs". In: *JHEP* 07 (2002), p. 034. DOI: 10.1088/1126-6708/2002/07/034. arXiv: hep-ph/0206021 [hep-ph].

[33] N. Arkani-Hamed et al. "The Minimal moose for a little Higgs". In: *JHEP* 08 (2002), p. 021. DOI: 10.1088/1126-6708/2002/08/021. arXiv: hep-ph/0206020 [hep-ph].

[34] Ian Low, Witold Skiba, and David Tucker-Smith. "Little Higgses from an antisymmetric condensate". In: *Phys. Rev.* D66 (2002), p. 072001. DOI: 10.1103/PhysRevD.66.072001. arXiv: hep-ph/0207243 [hep-ph].

[35] Spencer Chang and Jay G. Wacker. "Little Higgs and custodial SU(2)". In: *Phys. Rev.* D69 (2004), p. 035002. DOI: 10.1103/PhysRevD.69.035002. arXiv: hep-ph/0303001 [hep-ph].

[36] Witold Skiba and John Terning. "A Simple model of two little Higgses". In: *Phys. Rev.* D68 (2003), p. 075001. DOI: 10.1103/PhysRevD.68.075001. arXiv: hep-ph/0305302 [hep-ph].

[37] Spencer Chang. "A 'Littlest Higgs' model with custodial SU(2) symmetry". In: *JHEP* 12 (2003), p. 057. DOI: 10.1088/1126-6708/2003/12/057. arXiv: hep-ph/0306034 [hep-ph].

[38] Martin Schmaltz, Daniel Stolarski, and Jesse Thaler. "The Bestest Little Higgs". In: *JHEP* 09 (2010), p. 018. DOI: 10.1007/JHEP09(2010)018. arXiv: 1006.1356 [hep-ph].

[39] Csaba Csaki et al. "Big corrections from a little Higgs". In: *Phys. Rev.* D67 (2003), p. 115002. DOI: 10.1103/PhysRevD.67.115002. arXiv: hep-ph/0211124 [hep-ph].

[40] Csaba Csaki et al. "Variations of little Higgs models and their electroweak constraints". In: *Phys. Rev.* D68 (2003), p. 035009. DOI: 10.1103/PhysRevD.68.035009. arXiv: hep-ph/0303236 [hep-ph].

[41] JoAnne L. Hewett, Frank J. Petriello, and Thomas G. Rizzo. "Constraining the littlest Higgs". In: *JHEP* 10 (2003), p. 062. DOI: 10.1088/1126-6708/2003/10/062. arXiv: hep-ph/0211218 [hep-ph].

[42] Tao Han, Heather E. Logan, Bob McElrath, and Lian-Tao Wang. "Phenomenology of the little Higgs model". In: *Phys. Rev.* D67 (2003), p. 095004. DOI: 10.1103/PhysRevD.67.095004. arXiv: hep-ph/0301040 [hep-ph].

[43] Thomas Gregoire, David Tucker-Smith, and Jay G. Wacker. "What precision electroweak physics says about the SU(6) / Sp(6) little Higgs". In: *Phys. Rev.* D69 (2004), p. 115008. DOI: 10.1103/PhysRevD.69.115008. arXiv: hep-ph/0305275 [hep-ph].

[44] Roberto Casalbuoni, Aldo Deandrea, and Micaela Oertel. "Little Higgs models and precision electroweak data". In: *JHEP* 02 (2004), p. 032. DOI: 10.1088/1126-6708/2004/02/032. arXiv: hep-ph/0311038 [hep-ph].

[45] Can Kilic and Rakhi Mahbubani. "Precision electroweak observables in the minimal moose little Higgs model". In: *JHEP* 07 (2004), p. 013. DOI: 10.1088/1126-6708/2004/07/013. arXiv: hep-ph/0312053 [hep-ph].

[46] W. Kilian and J. Reuter. "The Low-energy structure of little Higgs models". In: *Phys. Rev.* D70 (2004), p. 015004. DOI: 10.1103/PhysRevD.70.015004. arXiv: hep-ph/0311095 [hep-ph].

[47] Hsin-Chia Cheng and Ian Low. "TeV symmetry and the little hierarchy problem". In: *JHEP* 09 (2003), p. 051. DOI: 10.1088/1126-6708/2003/09/051. arXiv: hep-ph/0308199 [hep-ph].

[48] Hsin-Chia Cheng and Ian Low. "Little hierarchy, little Higgses, and a little symmetry". In: *JHEP* 08 (2004), p. 061. DOI: 10.1088/1126-6708/2004/08/061. arXiv: hep-ph/0405243 [hep-ph].

[49] Ian Low. "T parity and the littlest Higgs". In: *JHEP* 10 (2004), p. 067. DOI: 10.1088/1126-6708/2004/10/067. arXiv: hep-ph/0409025 [hep-ph].

[50] Jay Hubisz, Patrick Meade, Andrew Noble, and Maxim Perelstein. "Electroweak precision constraints on the littlest Higgs model with T parity". In: *JHEP* 01 (2006), p. 135. DOI: 10.1088/1126-6708/2006/01/135. arXiv: hep-ph/0506042 [hep-ph].

[51] Kaustubh Agashe, Roberto Contino, and Alex Pomarol. "The Minimal composite Higgs model". In: *Nucl. Phys. B* 719 (2005), pp. 165–187. DOI: 10.1016/j.nuclphysb.2005.04.035. arXiv: hep-ph/0412089.

[52] David B. Kaplan. "Flavor at SSC energies: A New mechanism for dynamically generated fermion masses". In: *Nucl. Phys. B* 365 (1991), pp. 259–278. DOI: 10.1016/S0550-3213(05)80021-5.

[53] M. Bando et al. "Is rho Meson a Dynamical Gauge Boson of Hidden Local Symmetry?" In: *Phys. Rev. Lett.* 54 (1985), p. 1215. DOI: 10.1103/PhysRevLett.54.1215.

[54] Masako Bando, Taichiro Kugo, and Koichi Yamawaki. "Nonlinear Realization and Hidden Local Symmetries". In: *Phys. Rept.* 164 (1988), pp. 217–314. DOI: 10.1016/0370-1573(88)90019-1.

[55] Steven Weinberg. "Precise relations between the spectra of vector and axial vector mesons". In: *Phys. Rev. Lett.* 18 (1967), pp. 507–509. DOI: 10.1103/PhysRevLett.18.507.

[56] F. Zwicky. "On the Masses of Nebulae and of Clusters of Nebulae". In: *Astrophys. J.* 86 (Oct. 1937), p. 217. DOI: 10.1086/143864.

[57] S. M. Faber and R. E. Jackson. "Velocity dispersions and mass to light ratios for elliptical galaxies". In: *Astrophys. J.* 204 (1976), p. 668. DOI: 10.1086/154215.

[58] A. N. Taylor et al. "Gravitational lens magnification and the mass of abell 1689". In: *Astrophys. J.* 501 (1998), p. 539. DOI: 10.1086/305827. arXiv: astro-ph/9801158 [astro-ph].

[59] Wayne Hu. "Concepts in CMB anisotropy formation". In: *Lect. Notes Phys.* 470 (1996), p. 207. arXiv: astro-ph/9511130 [astro-ph].

[60] G. Hinshaw et al. "Nine-Year Wilkinson Microwave Anisotropy Probe (WMAP) Observations: Cosmological Parameter Results". In: *Astrophys. J. Suppl.* 208 (2013), p. 19. DOI: 10.1088/0067-0049/208/2/19. arXiv: 1212.5226 [astro-ph.CO].

[61] Volker Springel et al. "Simulating the joint evolution of quasars, galaxies and their large-scale distribution". In: *Nature* 435 (2005), pp. 629–636. DOI: 10.1038/nature03597. arXiv: astro-ph/0504097 [astro-ph].

[62] N. Aghanim et al. "Planck 2018 results. VI. Cosmological parameters". In: (July 2018). arXiv: 1807.06209 [astro-ph.CO].

[63] Ya. B. Zel'dovich and I. D. Novikov. "The Hypothesis of Cores Retarded during Expansion and the Hot Cosmological Model". In: *Soviet Astronomy, Vol. 10, p.602* 10 (Feb. 1967), p. 602.

[64] B. J. Carr and S. W. Hawking. "Black Holes in the Early Universe". In: *Monthly Notices of the Royal Astronomical Society* 168.2 (Aug. 1974), pp. 399–415. ISSN: 0035-8711. DOI: 10.1093/mnras/168.2.399. eprint: https://academic.oup.com/mnras/article-pdf/168/2/399/8079885/mnras168-0399.pdf. URL: https://doi.org/10.1093/mnras/168.2.399.

[65] Wayne Hu, Rennan Barkana, and Andrei Gruzinov. "Cold and fuzzy dark matter". In: *Phys. Rev. Lett.* 85 (2000), pp. 1158–1161. DOI: 10.1103/PhysRevLett.85.1158. arXiv: astro-ph/0003365.

[66] Benjamin W. Lee and Steven Weinberg. "Cosmological Lower Bound on Heavy Neutrino Masses". In: *Phys. Rev. Lett.* 39 (1977). Ed. by M.A. Srednicki, pp. 165–168. DOI: 10.1103/PhysRevLett.39.165.

[67] M. Tanabashi et al. ""Neutrinos in Cosmology" in Review of Particle Physics". In: *Phys. Rev. D* 98.3 (2018), p. 030001. DOI: 10.1103/PhysRevD.98.030001.

[68] Ben Gripaios, Alex Pomarol, Francesco Riva, and Javi Serra. "Beyond the Minimal Composite Higgs Model". In: *JHEP* 04 (2009), p. 070. DOI: 10.1088/1126-6708/2009/04/070. arXiv: 0902.1483 [hep-ph].

[69] Renata Kallosh, Andrei D. Linde, Dmitri A. Linde, and Leonard Susskind. "Gravity and global symmetries". In: *Phys. Rev. D* 52 (1995), pp. 912–935. DOI: 10.1103/PhysRevD.52.912. arXiv: hep-th/9502069.

[70] Nima Arkani-Hamed, Lubos Motl, Alberto Nicolis, and Cumrun Vafa. "The String landscape, black holes and gravity as the weakest force". In: *JHEP* 06 (2007), p. 060. DOI: 10.1088/1126-6708/2007/06/060. arXiv: hep-th/0601001.

[71] Tom Banks, Matt Johnson, and Assaf Shomer. "A Note on Gauge Theories Coupled to Gravity". In: *JHEP* 09 (2006), p. 049. DOI: 10.1088/1126-6708/2006/09/049. arXiv: hep-th/0606277.

[72] Edward W. Kolb and Michael S. Turner. "The Early Universe". In: *Front. Phys.* 69 (1990), pp. 1–547.

[73] Michele Frigerio, Alex Pomarol, Francesco Riva, and Alfredo Urbano. "Composite Scalar Dark Matter". In: *JHEP* 07 (2012), p. 015. DOI: 10.1007/JHEP07(2012)015. arXiv: 1204.2808 [hep-ph].

[74] Kim Griest and David Seckel. "Three exceptions in the calculation of relic abundances". In: *Phys. Rev. D* 43 (1991), pp. 3191–3203. DOI: 10.1103/PhysRevD.43.3191.

[75] Francesco D'Eramo and Jesse Thaler. "Semi-annihilation of Dark Matter". In: *JHEP* 06 (2010), p. 109. DOI: 10.1007/JHEP06(2010)109. arXiv: 1003.5912 [hep-ph].

[76] Duccio Pappadopulo and Alessandro Vichi. "T-parity, its problems and their solution". In: *JHEP* 03 (2011), p. 072. DOI: 10.1007/JHEP03(2011)072. arXiv: 1007.4807 [hep-ph].

[77] Csaba Csaki, Johannes Heinonen, Maxim Perelstein, and Christian Spethmann. "A Weakly Coupled Ultraviolet Completion of the Littlest Higgs with T-parity". In: *Phys. Rev.* D79 (2009), p. 035014. DOI: 10.1103/PhysRevD.79.035014. arXiv: 0804.0622 [hep-ph].

[78] Tom Brown, Claudia Frugiuele, and Thomas Gregoire. "UV friendly T-parity in the SU(6)/Sp(6) little Higgs model". In: *JHEP* 06 (2011), p. 108. DOI: 10.1007/JHEP06(2011)108. arXiv: 1012.2060 [hep-ph].

[79] CMS Collaboration. "Search for single production of vector-like quarks decaying to a Z boson and a top or a bottom quark in proton-proton collisions at 13 TeV". In: (2017).

[80] The ATLAS collaboration. "Search for new phenomena in $t\bar{t}$ final states with additional heavy-flavour jets in pp collisions at $\sqrt{s} = 13$ TeV with the ATLAS detector". In: (2016).

[81] Archana Anandakrishnan et al. "Odd Top Partners at the LHC". In: (2015). arXiv: 1506.05130 [hep-ph].

[82] Mikael Chala. "Direct bounds on heavy toplike quarks with standard and exotic decays". In: *Phys. Rev.* D96.1 (2017), p. 015028. DOI: 10.1103/PhysRevD.96.015028. arXiv: 1705.03013 [hep-ph].

[83] CMS Collaboration. "Search for new physics in the all-hadronic final state with the MT2 variable". In: (2017).

[84] Christoph Borschensky et al. "Squark and gluino production cross sections in pp collisions at $\sqrt{s} = 13$, 14, 33 and 100 TeV". In: *Eur. Phys. J.* C74.12 (2014), p. 3174. DOI: 10.1140/epjc/s10052-014-3174-y. arXiv: 1407.5066 [hep-ph].

[85] M. Aliev et al. "HATHOR: HAdronic Top and Heavy quarks crOss section calculatoR". In: *Comput. Phys. Commun.* 182 (2011), pp. 1034–1046. DOI: 10.1016/j.cpc.2010.12.040. arXiv: 1007.1327 [hep-ph].

[86] Jorge de Blas et al. "Electroweak precision observables and Higgs-boson signal strengths in the Standard Model and beyond: present and future". In: *JHEP* 12 (2016), p. 135. DOI: 10.1007/JHEP12(2016)135. arXiv: 1608.01509 [hep-ph].

[87] Andreas Birkedal, Andrew Noble, Maxim Perelstein, and Andrew Spray. "Little Higgs dark matter". In: *Phys. Rev.* D74 (2006), p. 035002. DOI: 10.1103/PhysRevD.74.035002. arXiv: hep-ph/0603077 [hep-ph].

[88] Oliver Fischer and Jochum J. van der Bij. "The scalar Singlet-Triplet Dark Matter Model". In: *JCAP* 1401.01 (2014), p. 032. DOI: 10.1088/1475-7516/2014/01/032. arXiv: 1311.1077 [hep-ph].

[89] Georges Aad et al. "Search for direct production of charginos, neutralinos and sleptons in final states with two leptons and missing transverse momentum in pp collisions at $\sqrt{s} = 8$ TeV with the ATLAS detector". In: *JHEP* 05 (2014), p. 071. DOI: 10.1007/JHEP05(2014)071. arXiv: 1403.5294 [hep-ex].

[90] *Search for electroweak production of supersymmetric particles in the two and three lepton final state at $\sqrt{s} = 13$ TeV with the ATLAS detector*. Tech. rep. ATLAS-CONF-2017-039. Geneva: CERN, June 2017. URL: https://cds.cern.ch/record/2267406.

[91] Paolo Gondolo and Graciela Gelmini. "Cosmic abundances of stable particles: Improved analysis". In: *Nucl. Phys.* B360 (1991), pp. 145–179. DOI: 10.1016/0550-3213(91)90438-4.

[92] P. A. R. Ade et al. "Planck 2013 results. XVI. Cosmological parameters". In: *Astron. Astrophys.* 571 (2014), A16. DOI: 10.1051/0004-6361/201321591. arXiv: 1303.5076 [astro-ph.CO].

[93] David Marzocca and Alfredo Urbano. "Composite Dark Matter and LHC Interplay". In: *JHEP* 07 (2014), p. 107. DOI: 10.1007/JHEP07(2014)107. arXiv: 1404.7419 [hep-ph].

[94] Vanda Silveira and A. Zee. "SCALAR PHANTOMS". In: *Phys. Lett.* 161B (1985), pp. 136–140. DOI: 10.1016/0370-2693(85)90624-0.

[95] John McDonald. "Gauge singlet scalars as cold dark matter". In: *Phys. Rev.* D50 (1994), pp. 3637–3649. DOI: 10.1103/PhysRevD.50.3637. arXiv: hep-ph/0702143 [HEP-PH].

[96] C. P. Burgess, Maxim Pospelov, and Tonnis ter Veldhuis. "The Minimal model of non-baryonic dark matter: A Singlet scalar". In: *Nucl. Phys.* B619 (2001), pp. 709–728. DOI: 10.1016/S0550-3213(01)00513-2. arXiv: hep-ph/0011335 [hep-ph].

[97] Sebastian Bruggisser, Francesco Riva, and Alfredo Urbano. "Strongly Interacting Light Dark Matter". In: (2016). arXiv: 1607.02474 [hep-ph].

[98] Adam Alloul et al. "FeynRules 2.0 - A complete toolbox for tree-level phenomenology". In: *Comput. Phys. Commun.* 185 (2014), pp. 2250–2300. DOI: 10.1016/j.cpc.2014.04.012. arXiv: 1310.1921 [hep-ph].

[99] G. Bélanger, F. Boudjema, A. Pukhov, and A. Semenov. "micrOMEGAs4.1: two dark matter candidates". In: *Comput. Phys. Commun.* 192 (2015), pp. 322–329. DOI: 10.1016/j.cpc.2015.03.003. arXiv: 1407.6129 [hep-ph].

[100] E. Aprile et al. "First Dark Matter Search Results from the XENON1T Experiment". In: (2017). arXiv: 1705.06655 [astro-ph.CO].

[101] E. Aprile et al. "Physics reach of the XENON1T dark matter experiment". In: *JCAP* 1604.04 (2016), p. 027. DOI: 10.1088/1475-7516/2016/04/027. arXiv: 1512.07501 [physics.ins-det].

[102] G.F. Giudice, C. Grojean, A. Pomarol, and R. Rattazzi. "The Strongly-Interacting Light Higgs". In: *JHEP* 06 (2007), p. 045. DOI: 10.1088/1126-6708/2007/06/045. arXiv: hep-ph/0703164.

[103] Geneviève Bélanger et al. "micrOMEGAs5.0 : Freeze-in". In: *Comput. Phys. Commun.* 231 (2018), pp. 173–186. DOI: 10.1016/j.cpc.2018.04.027. arXiv: 1801.03509 [hep-ph].

[104] Gary Steigman, Basudeb Dasgupta, and John F. Beacom. "Precise Relic WIMP Abundance and its Impact on Searches for Dark Matter Annihilation". In: *Phys. Rev. D* 86 (2012), p. 023506. DOI: 10.1103/PhysRevD.86.023506. arXiv: 1204.3622 [hep-ph].

[105] Andrea Thamm, Riccardo Torre, and Andrea Wulzer. "Future tests of Higgs compositeness: direct vs indirect". In: *JHEP* 07 (2015), p. 100. DOI: 10.1007/JHEP07(2015)100. arXiv: 1502.01701 [hep-ph].

[106] Csaba Csaki, Adam Falkowski, and Andreas Weiler. "The Flavor of the Composite Pseudo-Goldstone Higgs". In: *JHEP* 09 (2008), p. 008. DOI: 10.1088/1126-6708/2008/09/008. arXiv: 0804.1954 [hep-ph].

[107] Naoki Yamatsu. "Finite-Dimensional Lie Algebras and Their Representations for Unified Model Building". In: (Nov. 2015). arXiv: 1511.08771 [hep-ph].

[108] Kaustubh Agashe, Roberto Contino, Leandro Da Rold, and Alex Pomarol. "A Custodial symmetry for $Zb\bar{b}$". In: *Phys. Lett. B* 641 (2006), pp. 62–66. DOI: 10.1016/j.physletb.2006.08.005. arXiv: hep-ph/0605341.

[109] Vardan Khachatryan et al. "Searches for invisible decays of the Higgs boson in pp collisions at $\sqrt{s} = 7$, 8, and 13 TeV". In: *JHEP* 02 (2017), p. 135. DOI: 10.1007/JHEP02(2017)135. arXiv: 1610.09218 [hep-ex].

[110] Andrea De Simone, Oleksii Matsedonskyi, Riccardo Rattazzi, and Andrea Wulzer. "A First Top Partner Hunter's Guide". In: *JHEP* 04 (2013), p. 004. DOI: 10.1007/JHEP04(2013)004. arXiv: 1211.5663 [hep-ph].

[111] David Marzocca, Marco Serone, and Jing Shu. "General Composite Higgs Models". In: *JHEP* 08 (2012), p. 013. DOI: 10.1007/JHEP08(2012)013. arXiv: 1205.0770 [hep-ph].

[112] Alex Pomarol and Francesco Riva. "The Composite Higgs and Light Resonance Connection". In: *JHEP* 08 (2012), p. 135. DOI: 10.1007/JHEP08(2012)135. arXiv: 1205.6434 [hep-ph].

[113] Christophe Grojean, Oleksii Matsedonskyi, and Giuliano Panico. "Light top partners and precision physics". In: *JHEP* 10 (2013), p. 160. DOI: 10.1007/JHEP10(2013)160. arXiv: 1306.4655 [hep-ph].

[114] Csaba Csaki, Teng Ma, and Jing Shu. "Maximally Symmetric Composite Higgs Models". In: *Phys. Rev. Lett.* 119.13 (2017), p. 131803. DOI: 10.1103/PhysRevLett.119.131803. arXiv: 1702.00405 [hep-ph].

[115] J. Alberto Casas, David G. Cerdeño, Jesus M. Moreno, and Javier Quilis. "Reopening the Higgs portal for single scalar dark matter". In: *JHEP* 05 (2017), p. 036. DOI: 10.1007/JHEP05(2017)036. arXiv: 1701.08134 [hep-ph].

[116] Oleksii Matsedonskyi, Giuliano Panico, and Andrea Wulzer. "Light Top Partners for a Light Composite Higgs". In: *JHEP* 01 (2013), p. 164. DOI: 10.1007/JHEP01(2013)164. arXiv: 1204.6333 [hep-ph].

[117] Riccardo Barbieri and G.F. Giudice. "Upper Bounds on Supersymmetric Particle Masses". In: *Nucl. Phys. B* 306 (1988), pp. 63–76. DOI: 10.1016/0550-3213(88)90171-X.

[118] Giuliano Panico and Andrea Wulzer. "The Discrete Composite Higgs Model". In: *JHEP* 09 (2011), p. 135. DOI: 10.1007/JHEP09(2011)135. arXiv: 1106.2719 [hep-ph].

[119] P.A.R. Ade et al. "Planck 2015 results. XIII. Cosmological parameters". In: *Astron. Astrophys.* 594 (2016), A13. DOI: 10.1051/0004-6361/201525830. arXiv: 1502.01589 [astro-ph.CO].

[120] Nayara Fonseca, Renata Zukanovich Funchal, Andre Lessa, and Laura Lopez-Honorez. "Dark Matter Constraints on Composite Higgs Models". In: *JHEP* 06 (2015), p. 154. DOI: 10.1007/JHEP06(2015)154. arXiv: 1501.05957 [hep-ph].

[121] D.S. Akerib et al. "Results from a search for dark matter in the complete LUX exposure". In: *Phys. Rev. Lett.* 118.2 (2017), p. 021303. DOI: 10.1103/PhysRevLett.118.021303. arXiv: 1608.07648 [astro-ph.CO].

[122] James M. Cline, Kimmo Kainulainen, Pat Scott, and Christoph Weniger. "Update on scalar singlet dark matter". In: *Phys. Rev.* D88 (2013). [Erratum: Phys. Rev.D92,no.3,039906(2015)], p. 055025. DOI: 10.1103/PhysRevD.92.039906,10.1103/PhysRevD.88.055025. arXiv: 1306.4710 [hep-ph].

[123] G. Belanger, F. Boudjema, A. Pukhov, and A. Semenov. "micrOMEGAs 3: A program for calculating dark matter observables". In: *Comput. Phys. Commun.* 185 (2014), pp. 960–985. DOI: 10.1016/j.cpc.2013.10.016. arXiv: 1305.0237 [hep-ph].

[124] O. Adriani et al. "PAMELA results on the cosmic-ray antiproton flux from 60 MeV to 180 GeV in kinetic energy". In: *Phys. Rev. Lett.* 105 (2010), p. 121101. DOI: 10.1103/PhysRevLett.105.121101. arXiv: 1007.0821 [astro-ph.HE].

[125] Carmelo Evoli, Daniele Gaggero, and Dario Grasso. "Secondary antiprotons as a Galactic Dark Matter probe". In: *JCAP* 12 (2015), p. 039. DOI: 10.1088/1475-7516/2015/12/039. arXiv: 1504.05175 [astro-ph.HE].

[126] Alessandro Cuoco, Michael Krämer, and Michael Korsmeier. "Novel Dark Matter Constraints from Antiprotons in Light of AMS-02". In: *Phys. Rev. Lett.* 118.19 (2017), p. 191102. DOI: 10.1103/PhysRevLett.118.191102. arXiv: 1610.03071 [astro-ph.HE].

[127] Ming-Yang Cui, Qiang Yuan, Yue-Lin Sming Tsai, and Yi-Zhong Fan. "Possible dark matter annihilation signal in the AMS-02 antiproton data". In: *Phys. Rev. Lett.* 118.19 (2017), p. 191101. DOI: 10.1103/PhysRevLett.118.191101. arXiv: 1610.03840 [astro-ph.HE].

[128] M. Aguilar et al. "Antiproton Flux, Antiproton-to-Proton Flux Ratio, and Properties of Elementary Particle Fluxes in Primary Cosmic Rays Measured with the Alpha Magnetic Spectrometer on the International Space Station". In: *Phys. Rev. Lett.* 117.9 (2016), p. 091103. DOI: 10.1103/PhysRevLett.117.091103.

[129] A. Albert et al. "Searching for Dark Matter Annihilation in Recently Discovered Milky Way Satellites with Fermi-LAT". In: *Astrophys. J.* 834.2 (2017), p. 110. DOI: 10.3847/1538-4357/834/2/110. arXiv: 1611.03184 [astro-ph.HE].

[130] Gauthier Durieux, Christophe Grojean, Jiayin Gu, and Kechen Wang. "The leptonic future of the Higgs". In: *JHEP* 09 (2017), p. 014. DOI: 10.1007/JHEP09(2017)014. arXiv: 1704.02333 [hep-ph].

[131] Giuliano Panico, Michele Redi, Andrea Tesi, and Andrea Wulzer. "On the Tuning and the Mass of the Composite Higgs". In: *JHEP* 03 (2013), p. 051. DOI: 10.1007/JHEP03(2013)051. arXiv: 1210.7114 [hep-ph].

[132] Roberto Contino, Thomas Kramer, Minho Son, and Raman Sundrum. "Warped/composite phenomenology simplified". In: *JHEP* 05 (2007), p. 074. DOI: 10.1088/1126-6708/2007/05/074. arXiv: hep-ph/0612180.

[133] Roberto Contino and Geraldine Servant. "Discovering the top partners at the LHC using same-sign dilepton final states". In: *JHEP* 06 (2008), p. 026. DOI: 10.1088/1126-6708/2008/06/026. arXiv: 0801.1679 [hep-ph].

[134] Jan Mrazek and Andrea Wulzer. "A Strong Sector at the LHC: Top Partners in Same-Sign Dileptons". In: *Phys. Rev. D* 81 (2010), p. 075006. DOI: 10.1103/PhysRevD.81.075006. arXiv: 0909.3977 [hep-ph].

[135] Javi Serra. "Beyond the Minimal Top Partner Decay". In: *JHEP* 09 (2015), p. 176. DOI: 10.1007/JHEP09(2015)176. arXiv: 1506.05110 [hep-ph].

[136] "Search for heavy vector-like quarks decaying to same-sign dileptons". In: (Mar. 2017).

[137] Sabine Kraml, Ursula Laa, Luca Panizzi, and Hugo Prager. "Scalar versus fermionic top partner interpretations of $t\bar{t} + E_T^{\mathrm{miss}}$ searches at the LHC". In: *JHEP* 11 (2016), p. 107. DOI: 10.1007/JHEP11(2016)107. arXiv: 1607.02050 [hep-ph].

[138] *G. Salam and A. Weiler, "Collider Reach," http://collider-reach.web.cern.ch/collider-reach/.*

[139] Albert M Sirunyan et al. "Search for new phenomena with the M_{T2} variable in the all-hadronic final state produced in proton–proton collisions at $\sqrt{s} = 13$ TeV". In: *Eur. Phys. J. C* 77.10 (2017), p. 710. DOI: 10.1140/epjc/s10052-017-5267-x. arXiv: 1705.04650 [hep-ex].

[140] B.J. Mount et al. “LUX-ZEPLIN (LZ) Technical Design Report”. In: (Mar. 2017). arXiv: 1703.09144 [physics.ins-det].

[141] E. Aprile et al. “Dark Matter Search Results from a One Ton-Year Exposure of XENON1T”. In: *Phys. Rev. Lett.* 121.11 (2018), p. 111302. DOI: 10.1103/PhysRevLett.121.111302. arXiv: 1805.12562 [astro-ph.CO].

[142] “Search for invisible decays of the Higgs boson produced through vector boson fusion at $\sqrt{s} = 13$ TeV”. In: (Mar. 2018).

[143] “Projections for measurements of Higgs boson cross sections, branching ratios and coupling parameters with the ATLAS detector at a HL-LHC”. In: (Oct. 2013).

[144] M. Ackermann et al. “Searching for Dark Matter Annihilation from Milky Way Dwarf Spheroidal Galaxies with Six Years of Fermi Large Area Telescope Data”. In: *Phys. Rev. Lett.* 115.23 (2015), p. 231301. DOI: 10.1103/PhysRevLett.115.231301. arXiv: 1503.02641 [astro-ph.HE].

[145] Paolo Gondolo, Junji Hisano, and Kenji Kadota. “The Effect of quark interactions on dark matter kinetic decoupling and the mass of the smallest dark halos”. In: *Phys. Rev. D* 86 (2012), p. 083523. DOI: 10.1103/PhysRevD.86.083523. arXiv: 1205.1914 [hep-ph].

[146] Lotty Ackerman, Matthew R. Buckley, Sean M. Carroll, and Marc Kamionkowski. “Dark Matter and Dark Radiation”. In: (Oct. 2008). Ed. by Hans Volker Klapdor-Kleingrothaus and Irina V. Krivosheina, pp. 277–286. DOI: 10.1103/PhysRevD.79.023519. arXiv: 0810.5126 [hep-ph].

[147] K.N. Abazajian et al. “Neutrino Physics from the Cosmic Microwave Background and Large Scale Structure”. In: *Astropart. Phys.* 63 (2015), pp. 66–80. DOI: 10.1016/j.astropartphys.2014.05.014. arXiv: 1309.5383 [astro-ph.CO].

[148] Ryan Cooke et al. “Precision measures of the primordial abundance of deuterium”. In: *Astrophys. J.* 781.1 (2014), p. 31. DOI: 10.1088/0004-637X/781/1/31. arXiv: 1308.3240 [astro-ph.CO].

[149] Jonathan L. Feng, Manoj Kaplinghat, Huitzu Tu, and Hai-Bo Yu. “Hidden Charged Dark Matter”. In: *JCAP* 07 (2009), p. 004. DOI: 10.1088/1475-7516/2009/07/004. arXiv: 0905.3039 [hep-ph].

[150] A. Sommerfeld. “Über die Beugung und Bremsung der Elektronen”. In: *Annalen der Physik* 403.3 (1931), pp. 257–330. DOI: 10.1002/andp.19314030302. eprint: https://onlinelibrary.wiley.com/doi/pdf/10.1002/andp.19314030302. URL: https://onlinelibrary.wiley.com/doi/abs/10.1002/andp.19314030302.

[151] Jonathan L. Feng, Manoj Kaplinghat, and Hai-Bo Yu. “Sommerfeld Enhancements for Thermal Relic Dark Matter”. In: *Phys. Rev. D* 82 (2010), p. 083525. DOI: 10.1103/PhysRevD.82.083525. arXiv: 1005.4678 [hep-ph].

[152] Til Piffl et al. “The RAVE survey: the Galactic escape speed and the mass of the Milky Way”. In: *Astron. Astrophys.* 562 (2014), A91. DOI: 10.1051/0004-6361/201322531. arXiv: 1309.4293 [astro-ph.GA].

[153] Marco Cirelli et al. “Dark Matter’s secret liaisons: phenomenology of a dark U(1) sector with bound states”. In: *JCAP* 05 (2017), p. 036. DOI: 10.1088/1475-7516/2017/05/036. arXiv: 1612.07295 [hep-ph].

[154] Benedict von Harling and Kalliopi Petraki. “Bound-state formation for thermal relic dark matter and unitarity”. In: *JCAP* 12 (2014), p. 033. DOI: 10.1088/1475-7516/2014/12/033. arXiv: 1407.7874 [hep-ph].

[155] David A. Buote, Tesla E. Jeltema, Claude R. Canizares, and Gordon P. Garmire. "Chandra evidence for a flattened, triaxial dark matter halo in the elliptical galaxy ngc 720". In: *Astrophys. J.* 577 (2002), pp. 183–196. DOI: 10.1086/342158. arXiv: astro-ph/0205469.

[156] Prateek Agrawal, Francis-Yan Cyr-Racine, Lisa Randall, and Jakub Scholtz. "Make Dark Matter Charged Again". In: *JCAP* 05 (2017), p. 022. DOI: 10.1088/1475-7516/2017/05/022. arXiv: 1610.04611 [hep-ph].

[157] Felix Kahlhoefer, Kai Schmidt-Hoberg, Mads T. Frandsen, and Subir Sarkar. "Colliding clusters and dark matter self-interactions". In: *Mon. Not. Roy. Astron. Soc.* 437.3 (2014), pp. 2865–2881. DOI: 10.1093/mnras/stt2097. arXiv: 1308.3419 [astro-ph.CO].

[158] Sean Tulin and Hai-Bo Yu. "Dark Matter Self-interactions and Small Scale Structure". In: *Phys. Rept.* 730 (2018), pp. 1–57. DOI: 10.1016/j.physrep.2017.11.004. arXiv: 1705.02358 [hep-ph].

[159] Roberta Diamanti et al. "Cold dark matter plus not-so-clumpy dark relics". In: *JCAP* 06 (2017), p. 008. DOI: 10.1088/1475-7516/2017/06/008. arXiv: 1701.03128 [astro-ph.CO].

[160] Kalliopi Petraki, Marieke Postma, and Jordy de Vries. "Radiative bound-state-formation cross-sections for dark matter interacting via a Yukawa potential". In: *JHEP* 04 (2017), p. 077. DOI: 10.1007/JHEP04(2017)077. arXiv: 1611.01394 [hep-ph].

[161] Philip J. Humphrey et al. "A Census of Baryons and Dark Matter in an Isolated, Milky Way-sized Elliptical Galaxy". In: *Astrophys. J.* 729 (2011), p. 53. DOI: 10.1088/0004-637X/729/1/53. arXiv: 1010.6078 [astro-ph.CO].

[162] Matthew Reece. "Photon Masses in the Landscape and the Swampland". In: *JHEP* 07 (2019), p. 181. DOI: 10.1007/JHEP07(2019)181. arXiv: 1808.09966 [hep-th].

[163] Nathaniel Craig and Isabel Garcia Garcia. "Rescuing Massive Photons from the Swampland". In: *JHEP* 11 (2018), p. 067. DOI: 10.1007/JHEP11(2018)067. arXiv: 1810.05647 [hep-th].

[164] Geneviève Bélanger et al. "micrOMEGAs5.0 : Freeze-in". In: *Comput. Phys. Commun.* 231 (2018), pp. 173–186. DOI: 10.1016/j.cpc.2018.04.027. arXiv: 1801.03509 [hep-ph].

[165] Genevieve Belanger and Jong-Chul Park. "Assisted freeze-out". In: *JCAP* 03 (2012), p. 038. DOI: 10.1088/1475-7516/2012/03/038. arXiv: 1112.4491 [hep-ph].

[166] Diptimoy Ghosh, Matteo Salvarezza, and Fabrizio Senia. "Extending the Analysis of Electroweak Precision Constraints in Composite Higgs Models". In: *Nucl. Phys. B* 914 (2017), pp. 346–387. DOI: 10.1016/j.nuclphysb.2016.11.013. arXiv: 1511.08235 [hep-ph].

[167] M. Aaboud et al. "Search for pair production of heavy vector-like quarks decaying to high-p_T W bosons and b quarks in the lepton-plus-jets final state in pp collisions at $\sqrt{s} = 13$ TeV with the ATLAS detector". In: *JHEP* 10 (2017), p. 141. DOI: 10.1007/JHEP10(2017)141. arXiv: 1707.03347 [hep-ex].

[168] Aleksandr Azatov and Jamison Galloway. "Light Custodians and Higgs Physics in Composite Models". In: *Phys. Rev. D* 85 (2012), p. 055013. DOI: 10.1103/PhysRevD.85.055013. arXiv: 1110.5646 [hep-ph].

[169] Marc Montull, Francesco Riva, Ennio Salvioni, and Riccardo Torre. "Higgs Couplings in Composite Models". In: *Phys. Rev. D* 88 (2013), p. 095006. DOI: 10.1103/PhysRevD.88.095006. arXiv: 1308.0559 [hep-ph].

[170] Manuel Drees and Mihoko Nojiri. "Neutralino - nucleon scattering revisited". In: *Phys. Rev. D* 48 (1993), pp. 3483–3501. DOI: 10.1103/PhysRevD.48.3483. arXiv: hep-ph/9307208.

[171] J.M. Alarcon, J. Martin Camalich, and J.A. Oller. "The chiral representation of the πN scattering amplitude and the pion-nucleon sigma term". In: *Phys. Rev. D* 85 (2012), p. 051503. DOI: 10.1103/PhysRevD.85.051503. arXiv: 1110.3797 [hep-ph].

[172] Martin Hoferichter, J. Ruiz de Elvira, Bastian Kubis, and Ulf-G. Meißner. "High-Precision Determination of the Pion-Nucleon σ Term from Roy-Steiner Equations". In: *Phys. Rev. Lett.* 115 (2015), p. 092301. DOI: 10.1103/PhysRevLett.115.092301. arXiv: 1506.04142 [hep-ph].

[173] Parikshit Junnarkar and Andre Walker-Loud. "Scalar strange content of the nucleon from lattice QCD". In: *Phys. Rev. D* 87 (2013), p. 114510. DOI: 10.1103/PhysRevD.87.114510. arXiv: 1301.1114 [hep-lat].

[174] Roberto Contino, David Marzocca, Duccio Pappadopulo, and Riccardo Rattazzi. "On the effect of resonances in composite Higgs phenomenology". In: *JHEP* 10 (2011), p. 081. DOI: 10.1007/JHEP10(2011)081. arXiv: 1109.1570 [hep-ph].

[175] Rodrigo Alonso et al. "Sigma Decomposition". In: *JHEP* 12 (2014), p. 034. DOI: 10.1007/JHEP12(2014)034. arXiv: 1409.1589 [hep-ph].

[176] R. Jackiw and C. Rebbi. "Vacuum Periodicity in a Yang-Mills Quantum Theory". In: *Phys. Rev. Lett.* 37 (1976). Ed. by J.C. Taylor, pp. 172–175. DOI: 10.1103/PhysRevLett.37.172.

[177] Jr. Callan Curtis G., R.F. Dashen, and David J. Gross. "The Structure of the Gauge Theory Vacuum". In: *Phys. Lett. B* 63 (1976). Ed. by J.C. Taylor, pp. 334–340. DOI: 10.1016/0370-2693(76)90277-X.

[178] Claude W. Bernard and Erick J. Weinberg. "The Interpretation of Pseudoparticles in Physical Gauges". In: *Phys. Rev. D* 15 (1977), p. 3656. DOI: 10.1103/PhysRevD.15.3656.

[179] Erick J. Weinberg. *Classical solutions in quantum field theory: Solitons and Instantons in High Energy Physics*. Cambridge Monographs on Mathematical Physics. Cambridge University Press, Sept. 2012. ISBN: 978-0-521-11463-9, 978-1-139-57461-7, 978-0-521-11463-9, 978-1-107-43805-7. DOI: 10.1017/CBO9781139017787.

[180] J.S. Bell and R. Jackiw. "A PCAC puzzle: $\pi^0 \to \gamma\gamma$ in the σ model". In: *Nuovo Cim. A* 60 (1969), pp. 47–61. DOI: 10.1007/BF02823296.

[181] Stephen L. Adler. "Axial vector vertex in spinor electrodynamics". In: *Phys. Rev.* 177 (1969), pp. 2426–2438. DOI: 10.1103/PhysRev.177.2426.

[182] William A. Bardeen. "Anomalous Ward identities in spinor field theories". In: *Phys. Rev.* 184 (1969), pp. 1848–1857. DOI: 10.1103/PhysRev.184.1848.

[183] Kazuo Fujikawa. "Path Integral Measure for Gauge Invariant Fermion Theories". In: *Phys. Rev. Lett.* 42 (1979), pp. 1195–1198. DOI: 10.1103/PhysRevLett.42.1195.

[184] Gerard 't Hooft. "How Instantons Solve the U(1) Problem". In: *Phys. Rept.* 142 (1986), pp. 357–387. DOI: 10.1016/0370-1573(86)90117-1.

[185] M. Tanabashi et al. ""CKM Quark-Mixing Matrix" in Review of Particle Physics". In: *Phys. Rev. D* 98.3 (2018), p. 030001. DOI: 10.1103/PhysRevD.98.030001.

[186] R. J. Crewther, P. Di Vecchia, G. Veneziano, and Edward Witten. "Chiral Estimate of the Electric Dipole Moment of the Neutron in Quantum Chromodynamics". In: *Phys. Lett.* 88B (1979). [Erratum: Phys. Lett.91B,487(1980)], p. 123. DOI: 10.1016/0370-2693(80)91025-4,10.1016/0370-2693(79)90128-X.

[187] J. M. Pendlebury et al. “Revised experimental upper limit on the electric dipole moment of the neutron”. In: *Phys. Rev.* D92.9 (2015), p. 092003. DOI: 10.1103/PhysRevD.92.092003. arXiv: 1509.04411 [hep-ex].

[188] Nemanja Kaloper and John Terning. “Landscaping the Strong CP Problem”. In: *JHEP* 03 (2019), p. 032. DOI: 10.1007/JHEP03(2019)032. arXiv: 1710.01740 [hep-th].

[189] Michael Dine, Laurel Stephenson Haskins, Lorenzo Ubaldi, and Di Xu. “Some Remarks on Anthropic Approaches to the Strong CP Problem”. In: *JHEP* 05 (2018), p. 171. DOI: 10.1007/JHEP05(2018)171. arXiv: 1801.03466 [hep-th].

[190] Marc Kamionkowski and John March-Russell. “Planck scale physics and the Peccei-Quinn mechanism”. In: *Phys. Lett. B* 282 (1992), pp. 137–141. DOI: 10.1016/0370-2693(92)90492-M. arXiv: hep-th/9202003.

[191] Stephen M. Barr and D. Seckel. “Planck scale corrections to axion models”. In: *Phys. Rev. D* 46 (1992), pp. 539–549. DOI: 10.1103/PhysRevD.46.539.

[192] S. Ghigna, Maurizio Lusignoli, and M. Roncadelli. “Instability of the invisible axion”. In: *Phys. Lett. B* 283 (1992), pp. 278–281. DOI: 10.1016/0370-2693(92)90019-Z.

[193] Richard Holman et al. “Solutions to the strong CP problem in a world with gravity”. In: *Phys. Lett. B* 282 (1992), pp. 132–136. DOI: 10.1016/0370-2693(92)90491-L. arXiv: hep-ph/9203206.

[194] Mark Srednicki. “Axion Couplings to Matter. 1. CP Conserving Parts”. In: *Nucl. Phys. B* 260 (1985), pp. 689–700. DOI: 10.1016/0550-3213(85)90054-9.

[195] William A. Bardeen, R.D. Peccei, and T. Yanagida. “CONSTRAINTS ON VARIANT AXION MODELS”. In: *Nucl. Phys. B* 279 (1987), pp. 401–428. DOI: 10.1016/0550-3213(87)90003-4.

[196] Y. Asano et al. “Search for a Rare Decay Mode K+ —> pi+ Neutrino anti-neutrino and Axion”. In: (Oct. 1981). Ed. by R.J. Cence, E. Ma, and A. Roberts, pp. 411–414. DOI: 10.1016/0370-2693(81)91172-2.

[197] S. Yamada. “Search for New Particles”. In: *Conf. Proc. C* 830804 (1983), p. 525.

[198] M. Tanabashi et al. “"Axions and Other Similar Particles" in Review of Particle Physics”. In: *Phys. Rev. D* 98.3 (2018), p. 030001. DOI: 10.1103/PhysRevD.98.030001.

[199] Davide Cadamuro, Steen Hannestad, Georg Raffelt, and Javier Redondo. “Cosmological bounds on sub-MeV mass axions”. In: *JCAP* 02 (2011), p. 003. DOI: 10.1088/1475-7516/2011/02/003. arXiv: 1011.3694 [hep-ph].

[200] Georg G. Raffelt. “Astrophysical axion bounds”. In: *Lect. Notes Phys.* 741 (2008). [,51(2006)], pp. 51–71. DOI: 10.1007/978-3-540-73518-2_3. arXiv: hep-ph/0611350 [hep-ph].

[201] Leanne D. Duffy and Karl van Bibber. “Axions as Dark Matter Particles”. In: *New J. Phys.* 11 (2009), p. 105008. DOI: 10.1088/1367-2630/11/10/105008. arXiv: 0904.3346 [hep-ph].

[202] J. I. Kapusta and Charles Gale. *Finite-temperature field theory: Principles and applications*. Cambridge Monographs on Mathematical Physics. Cambridge University Press, 2011. ISBN: 9780521173223, 9780521820820, 9780511222801. DOI: 10.1017/CBO9780511535130.

[203] Howard E. Haber and H. Arthur Weldon. “Thermodynamics of an Ultrarelativistic Bose Gas”. In: *Phys. Rev. Lett.* 46 (1981), p. 1497. DOI: 10.1103/PhysRevLett.46.1497.

[204] Joseph I. Kapusta. "Bose-Einstein Condensation, Spontaneous Symmetry Breaking, and Gauge Theories". In: *Phys. Rev.* D24 (1981), pp. 426–439. DOI: 10.1103/PhysRevD.24.426.

[205] D. T. Son and Misha A. Stephanov. "QCD at finite isospin density". In: *Phys. Rev. Lett.* 86 (2001), pp. 592–595. DOI: 10.1103/PhysRevLett.86.592. arXiv: hep-ph/0005225 [hep-ph].

[206] J. B. Kogut and D. Toublan. "QCD at small nonzero quark chemical potentials". In: *Phys. Rev.* D64 (2001), p. 034007. DOI: 10.1103/PhysRevD.64.034007. arXiv: hep-ph/0103271 [hep-ph].

[207] Andrea Mammarella and Massimo Mannarelli. "Intriguing aspects of meson condensation". In: *Phys. Rev.* D92.8 (2015), p. 085025. DOI: 10.1103/PhysRevD.92.085025. arXiv: 1507.02934 [hep-ph].

[208] Massimo Mannarelli. "Meson condensation". In: (2019). arXiv: 1908.02042 [hep-ph].

[209] Anson Hook and Junwu Huang. "Probing axions with neutron star inspirals and other stellar processes". In: *JHEP* 06 (2018), p. 036. DOI: 10.1007/JHEP06(2018)036. arXiv: 1708.08464 [hep-ph].

[210] Thomas D. Cohen, R. J. Furnstahl, and David K. Griegel. "Quark and gluon condensates in nuclear matter". In: *Phys. Rev.* C45 (1992), pp. 1881–1893. DOI: 10.1103/PhysRevC.45.1881.

[211] Philipp Gubler and Daisuke Satow. "Recent Progress in QCD Condensate Evaluations and Sum Rules". In: *Prog. Part. Nucl. Phys.* 106 (2019), pp. 1–67. DOI: 10.1016/j.ppnp.2019.02.005. arXiv: 1812.00385 [hep-ph].

[212] J. Gasser and H. Leutwyler. "Chiral Perturbation Theory to One Loop". In: *Annals Phys.* 158 (1984), p. 142. DOI: 10.1016/0003-4916(84)90242-2.

[213] Ulf G. Meissner, Jose A. Oller, and Andreas Wirzba. "In-medium chiral perturbation theory beyond the mean field approximation". In: *Annals Phys.* 297 (2002), pp. 27–66. DOI: 10.1006/aphy.2002.6244. arXiv: nucl-th/0109026 [nucl-th].

[214] Norbert Kaiser, S. Fritsch, and W. Weise. "Chiral dynamics and nuclear matter". In: *Nucl. Phys.* A697 (2002), pp. 255–276. DOI: 10.1016/S0375-9474(01)01231-3. arXiv: nucl-th/0105057 [nucl-th].

[215] N. Kaiser, P. de Homont, and W. Weise. "In-medium chiral condensate beyond linear density approximation". In: *Phys. Rev.* C77 (2008), p. 025204. DOI: 10.1103/PhysRevC.77.025204. arXiv: 0711.3154 [nucl-th].

[216] Soichiro Goda and D. Jido. "Chiral condensate at finite density using the chiral Ward identity". In: *Phys. Rev.* C88.6 (2013), p. 065204. DOI: 10.1103/PhysRevC.88.065204. arXiv: 1308.2660 [nucl-th].

[217] N. Kaiser and W. Weise. "Chiral condensate in neutron matter". In: *Phys. Lett.* B671 (2009), pp. 25–29. DOI: 10.1016/j.physletb.2008.11.071. arXiv: 0808.0856 [nucl-th].

[218] T. Krger et al. "The chiral condensate in neutron matter". In: *Phys. Lett.* B726 (2013), pp. 412–416. DOI: 10.1016/j.physletb.2013.08.022. arXiv: 1307.2110 [nucl-th].

[219] Wolfram Weise. "Dense Baryonic Matter and Strangeness in Neutron Stars". In: *8th International Conference on Quarks and Nuclear Physics (QNP2018) Tsukuba, Japan, November 13-17, 2018*. 2019. arXiv: 1905.03955 [nucl-th].

[220] D. B. Kaplan and A. E. Nelson. "Kaon Condensation in Dense Matter". In: *Nucl. Phys.* A479 (1988), p. 273c. DOI: 10.1016/0375-9474(88)90442-3.

[221] Vesteinn Thorsson, Madappa Prakash, and James M. Lattimer. "Composition, structure and evolution of neutron stars with kaon condensates". In: *Nucl. Phys.* A572 (1994). [Erratum: Nucl. Phys.A574,851(1994)], pp. 693–731. DOI: 10.1016/0375-9474(94)90962-8,10.1016/0375-9474(94)90407-3. arXiv: nucl-th/9305006 [nucl-th].

[222] Angels Ramos, Jurgen Schaffner-Bielich, and Jochen Wambach. "Kaon condensation in neutron stars". In: *Lect. Notes Phys.* 578 (2001). [,175(2000)], pp. 175–202. arXiv: nucl-th/0011003 [nucl-th].

[223] Norman K. Glendenning and Jurgen Schaffner-Bielich. "First order kaon condensate". In: *Phys. Rev.* C60 (1999), p. 025803. DOI: 10.1103/PhysRevC.60.025803. arXiv: astro-ph/9810290 [astro-ph].

[224] John Antoniadis et al. "A Massive Pulsar in a Compact Relativistic Binary". In: *Science* 340 (2013), p. 6131. DOI: 10.1126/science.1233232. arXiv: 1304.6875 [astro-ph.HE].

[225] H. Thankful Cromartie et al. "Relativistic Shapiro delay measurements of an extremely massive millisecond pulsar". In: *Nat. Astron.* 4.1 (2019), pp. 72–76. DOI: 10.1038/s41550-019-0880-2. arXiv: 1904.06759 [astro-ph.HE].

[226] Reuven Balkin, Javi Serra, Konstantin Springman, and Andreas Weiler. "To Appear".

[227] Haris Djapo, Bernd-Jochen Schaefer, and Jochen Wambach. "On the appearance of hyperons in neutron stars". In: *Phys. Rev.* C81 (2010), p. 035803. DOI: 10.1103/PhysRevC.81.035803. arXiv: 0811.2939 [nucl-th].

[228] Takumi Muto and Toshitaka Tatsumi. "Theoretical aspects of kaon condensation in neutron matter". In: *Phys. Lett.* B283 (1992), pp. 165–170. DOI: 10.1016/0370-2693(92)90001-K.

[229] Jae Hyeok Chang, Rouven Essig, and Samuel D. McDermott. "Supernova 1987A Constraints on Sub-GeV Dark Sectors, Millicharged Particles, the QCD Axion, and an Axion-like Particle". In: *JHEP* 09 (2018), p. 051. DOI: 10.1007/JHEP09(2018)051. arXiv: 1803.00993 [hep-ph].

[230] Pierluca Carenza et al. "Improved axion emissivity from a supernova via nucleon-nucleon bremsstrahlung". In: *JCAP* 1910.10 (2019), p. 016. DOI: 10.1088/1475-7516/2019/10/016. arXiv: 1906.11844 [hep-ph].

[231] Nitsan Bar, Kfir Blum, and Guido D'amico. "Is there a supernova bound on axions?" In: (). arXiv: 1907.05020 [hep-ph].

[232] A. Y. Potekhin and G. Chabrier. "Magnetic neutron star cooling and microphysics". In: *Astron. Astrophys.* 609 (2018), A74. DOI: 10.1051/0004-6361/201731866. arXiv: 1711.07662 [astro-ph.HE].

[233] Thomas Vonk, Feng-Kun Guo, and Ulf-G. Meißner. "Precision calculation of the axion-nucleon coupling in chiral perturbation theory". In: (2020). arXiv: 2001.05327 [hep-ph].

[234] Zhen-Yan Lu et al. "QCD θ-vacuum energy and axion properties". In: (2020). arXiv: 2003.01625 [hep-ph].

[235] V. Bernard, Norbert Kaiser, and Ulf-G. Meissner. "Chiral dynamics in nucleons and nuclei". In: *Int. J. Mod. Phys.* E4 (1995), pp. 193–346. DOI: 10.1142/S0218301395000092. arXiv: hep-ph/9501384 [hep-ph].

[236] M. Tanabashi et al. "Review of Particle Physics". In: *Phys. Rev.* D98.3 (2018), p. 030001. DOI: 10.1103/PhysRevD.98.030001.

[237] I. S. Towner. "Quenching of spin matrix elements in nuclei". In: *Phys. Rept.* 155 (1987), pp. 263–377. DOI: 10.1016/0370-1573(87)90138-4.

[238] B. A. Brown and B. H. Wildenthal. "Experimental and Theoretical Gamow-Teller Beta-Decay Observables for the sd-Shell Nuclei". In: *Atom. Data Nucl. Data Tabl.* 33 (1985), pp. 347–404. DOI: 10.1016/0092-640X(85)90009-9.

[239] D. R. Entem and R. Machleidt. "Chiral 2pi exchange at order four and peripheral NN scattering". In: *Phys. Rev.* C66 (2002), p. 014002. DOI: 10.1103/PhysRevC.66.014002. arXiv: nucl-th/0202039 [nucl-th].

[240] E. Epelbaum et al. "Three nucleon forces from chiral effective field theory". In: *Phys. Rev.* C66 (2002), p. 064001. DOI: 10.1103/PhysRevC.66.064001. arXiv: nucl-th/0208023 [nucl-th].

[241] J. Menendez, D. Gazit, and A. Schwenk. "Chiral two-body currents in nuclei: Gamow-Teller transitions and neutrinoless double-beta decay". In: *Phys. Rev. Lett.* 107 (2011), p. 062501. DOI: 10.1103/PhysRevLett.107.062501. arXiv: 1103.3622 [nucl-th].

[242] P. Gysbers et al. "Discrepancy between experimental and theoretical β-decay rates resolved from first principles". In: *Nature Phys.* 15.5 (2019), pp. 428–431. DOI: 10.1038/s41567-019-0450-7. arXiv: 1903.00047 [nucl-th].

[243] H. Th. Janka. "Neutrino Emission from Supernovae". In: (2017). DOI: 10.1007/978-3-319-21846-5_4. arXiv: 1702.08713 [astro-ph.HE].

[244] J. E. Moody and Frank Wilczek. "New macroscopic forces?" In: *Phys. Rev.* D30 (1984), p. 130. DOI: 10.1103/PhysRevD.30.130.

[245] Georg Raffelt. "Limits on a CP-violating scalar axion-nucleon interaction". In: *Phys. Rev.* D86 (2012), p. 015001. DOI: 10.1103/PhysRevD.86.015001. arXiv: 1205.1776 [hep-ph].

[246] Joseph Polchinski. "Effective field theory and the Fermi surface". In: *Proceedings, Theoretical Advanced Study Institute (TASI 92): From Black Holes and Strings to Particles: Boulder, USA, June 1-26, 1992*. 1992, pp. 0235–276. arXiv: hep-th/9210046 [hep-th].

[247] David B. Kaplan. "Five lectures on effective field theory". In: 2005. arXiv: nucl-th/0510023 [nucl-th].

[248] Mark G. Alford, Krishna Rajagopal, and Frank Wilczek. "QCD at finite baryon density: Nucleon droplets and color superconductivity". In: *Phys.Lett.B* 422 (1998), pp. 247–256. DOI: 10.1016/S0370-2693(98)00051-3. arXiv: hep-ph/9711395.

[249] R. Rapp, Thomas Schäfer, Edward V. Shuryak, and M. Velkovsky. "Diquark Bose condensates in high density matter and instantons". In: *Phys.Rev.Lett.* 81 (1998), pp. 53–56. DOI: 10.1103/PhysRevLett.81.53. arXiv: hep-ph/9711396.

[250] Mark G. Alford, Krishna Rajagopal, and Frank Wilczek. "Color flavor locking and chiral symmetry breaking in high density QCD". In: *Nucl. Phys.* B537 (1999), pp. 443–458. DOI: 10.1016/S0550-3213(98)00668-3. arXiv: hep-ph/9804403 [hep-ph].

[251] D. T. Son. "Superconductivity by long range color magnetic interaction in high density quark matter". In: *Phys. Rev.* D59 (1999), p. 094019. DOI: 10.1103/PhysRevD.59.094019. arXiv: hep-ph/9812287 [hep-ph].

[252] Mark G. Alford, Andreas Schmitt, Krishna Rajagopal, and Thomas Schäfer. "Color superconductivity in dense quark matter". In: *Rev. Mod. Phys.* 80 (2008), pp. 1455–1515. DOI: 10.1103/RevModPhys.80.1455. arXiv: 0709.4635 [hep-ph].

[253] Deog Ki Hong. "An Effective field theory of QCD at high density". In: *Phys. Lett.* B473 (2000), pp. 118–125. DOI: 10.1016/S0370-2693(99)01472-0. arXiv: hep-ph/9812510 [hep-ph].

[254] D. T. Son and Misha A. Stephanov. "Inverse meson mass ordering in color flavor locking phase of high density QCD". In: *Phys. Rev.* D61 (2000), p. 074012. DOI: 10.1103/PhysRevD.61.074012. arXiv: hep-ph/9910491 [hep-ph].

[255] D. T. Son and Misha A. Stephanov. "Inverse meson mass ordering in color flavor locking phase of high density QCD: Erratum". In: *Phys. Rev.* D62 (2000), p. 059902. DOI: 10.1103/PhysRevD.62.059902. arXiv: hep-ph/0004095 [hep-ph].

[256] R. Casalbuoni and Raoul Gatto. "Effective theory for color flavor locking in high density QCD". In: *Phys. Lett.* B464 (1999), pp. 111–116. DOI: 10.1016/S0370-2693(99)01032-1. arXiv: hep-ph/9908227 [hep-ph].

[257] Paulo F. Bedaque and Thomas Schäfer. "High density quark matter under stress". In: *Nucl. Phys.* A697 (2002), pp. 802–822. DOI: 10.1016/S0375-9474(01)01272-6. arXiv: hep-ph/0105150 [hep-ph].

[258] Thomas Schäfer. "Mass terms in effective theories of high density quark matter". In: *Phys. Rev.* D65 (2002), p. 074006. DOI: 10.1103/PhysRevD.65.074006. arXiv: hep-ph/0109052 [hep-ph].

[259] Thomas Schäfer. "Patterns of symmetry breaking in QCD at high baryon density". In: *Nucl. Phys.* B575 (2000), pp. 269–284. DOI: 10.1016/S0550-3213(00)00063-8. arXiv: hep-ph/9909574 [hep-ph].

[260] Andrei Kryjevski, David B. Kaplan, and Thomas Schäfer. "New phases in CFL quark matter". In: *Phys. Rev.* D71 (2005), p. 034004. DOI: 10.1103/PhysRevD.71.034004. arXiv: hep-ph/0404290 [hep-ph].

[261] Thomas Schäfer. "Instanton effects in QCD at high baryon density". In: *Phys. Rev.* D65 (2002), p. 094033. DOI: 10.1103/PhysRevD.65.094033. arXiv: hep-ph/0201189 [hep-ph].

[262] Krishna Rajagopal and Eugene Shuster. "On the applicability of weak coupling results in high density QCD". In: *Phys. Rev.* D62 (2000), p. 085007. DOI: 10.1103/PhysRevD.62.085007. arXiv: hep-ph/0004074 [hep-ph].

[263] Brando Bellazzini et al. "Cosmological and Astrophysical Probes of Vacuum Energy". In: *JHEP* 06 (2016), p. 104. DOI: 10.1007/JHEP06(2016)104. arXiv: 1502.04702 [astro-ph.CO].

[264] Csaba Csáki et al. "Neutron Star Mergers Chirp About Vacuum Energy". In: *JHEP* 09 (2018), p. 087. DOI: 10.1007/JHEP09(2018)087. arXiv: 1802.04813 [astro-ph.HE].

[265] B. Garbrecht and J. I. McDonald. "Axion configurations around pulsars". In: *JCAP* 1807.07 (2018), p. 044. DOI: 10.1088/1475-7516/2018/07/044. arXiv: 1804.04224 [astro-ph.CO].

[266] Jean-François Fortin and Kuver Sinha. "Constraining Axion-Like-Particles with Hard X-ray Emission from Magnetars". In: *JHEP* 06 (2018), p. 048. DOI: 10.1007/JHEP06(2018)048. arXiv: 1804.01992 [hep-ph].

[267] Francesca V. Day and Jamie I. McDonald. "Axion superradiance in rotating neutron stars". In: *JCAP* 1910.10 (2019), p. 051. DOI: 10.1088/1475-7516/2019/10/051. arXiv: 1904.08341 [hep-ph].

[268] Malte Buschmann, Raymond T. Co, Christopher Dessert, and Benjamin R. Safdi. "X-ray Search for Axions from Nearby Isolated Neutron Stars". In: (2019). arXiv: 1910.04164 [hep-ph].

[269] Junwu Huang et al. "Prospects for axion searches with Advanced LIGO through binary mergers". In: *Phys. Rev.* D99.6 (2019), p. 063013. DOI: 10.1103/PhysRevD.99.063013. arXiv: 1807.02133 [hep-ph].

[270] Maximilian Ruhdorfer, Ennio Salvioni, and Andreas Weiler. "A Global View of the Off-Shell Higgs Portal". In: *SciPost Phys.* 8 (2020), p. 027. DOI: 10.21468/SciPostPhys.8.2.027. arXiv: 1910.04170 [hep-ph].